GAS FORCES DURING THE RAPID OPENING OF DISC VALVES

A Thesis Presented For The Degree Of

Doctor of Philosophy

by

WILLIAM W. HALLAM BSc

Department of Dynamics and Control
Mechanical Engineering Group
University of Strathclyde
Glasgow G1 1XW

NOVEMBER 1981

CONTENTS

CHAPTER IV/

PAGE NO.

ABSTRACT

It is hoped that the research here outlined will give an additional understanding of the performance of "valves" under dynamic conditions and supplement existing steady state or continuous flow analysis as outlined by Wambsganss [1]*, MacLaren [2] etc.

The study describes tests carried out on disc valves in which the valve seat was withdrawn from the valve while a pressure difference existed across the valve. Simultaneous measurements were made of the force on the valve, the pressure in the plenum chamber and the displacement of the seat from the valve. Dynamic force measurements are compared with values of force measured during steady continuous flow conditions (static flow) at selected values of pressure difference and displacement of the valve from its seat. The comparison may, therefore, be considered as relating the force on the valve during dynamic withdrawal of the seat from the valve to the steady state force on the valve at corresponding pressures and displacements during steady continuous flow through the valve. It is shown that during the early part of the withdrawal, there are significant differences between the force on the valve and the steady state force. These differences are accentuated by the pressure difference across the valve and the rate at which the valve is opened.

This study also deals at some length with the instrumentation used/

---

* Numerals in brackets refer to corresponding items in REFERENCES

used and problems encountered.

From the work by Chan [3] on the behaviour of inviscid incompressible fluids, a computer program has been developed for the steady continuous flow condition of the disc valves under study. This program is based on two-dimensional or axisymmetric potential fluid flow and uses the Finite Element method. The method employs the velocity potential ϕ as the primary unknown and 8-node quadrilateral elements of arbitrary shape to represent the region of flow under study. This method is equally applicable to both confined and free surface flow problems. The method first computes a solution for the velocity potential throughout the entire flow domain and then calculates secondary unknowns, e.g. velocity, pressure and force distributions. For free surface flow problems, it also predicts the free surface location, and the contraction or discharge coefficient.

Quantitative comparisons between this approach and experimental work previously outlined are also made and the quality of comparison is found to be good.

INTRODUCTION

INTRODUCTION

Currently there exists relatively little information on the experimental and theoretical behaviour of incompressible fluids as they issue from commonly encountered "nozzle shapes" in use today. These nozzles can be found in countless engineering projects such as those involved in the fields of fuel injection, jet propulsion, compressor technology, or in machinery used to monitor flow and/or direct the efflux in a carefully controlled manner.

As technological advances continue, the design of increasingly sophisticated devices will at times require a better knowledge of the detailed flow behaviour in the neighbourhood of the nozzle. Until quite recently no-one had presented results applicable to any but the simplest two-dimensional or axisymmetric nozzle configurations. The reason that the analysis of these flows from nozzles using confined or free surface boundary conditions and/or curvilinear interior profiles has been largely ignored, is undoubtedly due to the difficulties that must be overcome in accurately applying any of the previously existing numerical methods to such geometries.

A review of past research in the field of theoretical analysis of two-dimensional or axisymmetric, inviscid, irrotational jet efflux from nozzles and orifices only underlines the current incomplete state of understanding of these flows, in spite of contributions by Von Mises [7] and Larock [9] in the field of two-dimensional flow and by Trefftz [11], Southwell and Vaisey [5], Rouse and Abul-Fetouh [6], Garabedian [10], Hunt [8] and Jeppson [4] in the field of axisymmetric flow.

The/

The numerical methods employed by these investigators have previously only been used to analyse problems having simple geometric boundaries; also most of these methods suffer from accuracy problems as Hunt has pointed out. Furthermore, these methods merely use simple trial-and-error procedures to locate the free surface.

Based on the increasing demand for such questions to be answered and the existing techniques which are available, a more versatile and powerful method for the analysis of jet efflux problems is needed. It is believed that the Finite Element Method is well suited to solve such problems, since the basic concepts of this method have already been found to possess general applicability to a wide range of field problems.

Various experimentors have carried out work mainly in the fields of structural and continuum mechanics [30,31], but use of the Finite Element approach has now been extended to cover such diverse fields as ground water and seepage flow [33,34], torsion or temperature distribution in an axisymmetric pressure vessel [32], heat conduction [12], confined two-dimensional potential flow [13], viscous, incompressible unsteady fluid flow [40] and slow viscous compressible and incompressible flow [41].

One of the most important experimental contributions, a study of flow around a disc valve, was given by Schrenk [45]. He showed (among other things) that flow leaving a valve seat could generally be of two types. That is when the lift is low the flow adheres to the seating surface because of the low pressure region there (condition A) and when the valve is raised flow condition A occurs until a critical lift is reached. After this the flow suddenly changes to flow condition B where the flow no longer adheres to/

to the seating surface but separates forming a radial jet at an angle to the valve seat.

An analogous system for flow potentials in electrical engineering is used in the study of an electrostatic field about a high tension lead through a transformer tank [46].

The goal of the present study is two-fold. Firstly, to relate the experimental force on a disc type valve during dynamic withdrawal of the seat from the valve, to the quasi-steady state force on the valve at corresponding pressures and displacements during steady continuous flow through the valve [36]. These tests were carried out with conditions relevant to those obtained in a compressor.

Secondly, to derive a theoretical technique, (a review of "simple" mathematical models of valves in reciprocating compressors is listed in REFERENCES [42]) which will predict the quasi-steady state forces on a disc valve for an irrotational flow condition based on ideal fluid theory. (This theoretical technique can be modified to consider more realistic flow conditions but is limited to cases where a functional exists).

This will allow a direct comparison to be drawn between experimental and theoretical steady-state results.

The Finite Element Method should have the following properties if it is to be truly useful:

1. The method should be able to analyse axisymmetric and two-dimensional flows, with either confined or free surfaces.
2. The method ought to be versatile enough so that problems involving complicated boundary shapes can be analysed without any particular difficulties.

3./

3. The method should use, for fluid flow problems involving a free-surface, a rational, analytical algorithm for adjusting the free-surface co-ordinates.

Solution techniques possessing these features were developed by combining the use of a straightforward variational principle with the finite element concept and the Ritz technique. In the problem formulation, a functional which is characteristic of the problem is formed first. In this study the velocity potential function was chosen as the primary unknown and quadri-lateral elements of arbitrary shape were used to represent the flow region under consideration. This formulation yields a system of linear simultaneous algebraic equations with values of velocity potential at the nodal points of each quadri-lateral as unknowns. The entire system of equations is solved by Gaussian elimination and the secondary unknowns, such as velocities and pressures are subsequently evaluated. The free-surface location if required is then found by an iterative scheme.

A flow diagram showing the overall method of approach is shown in FIG. 1.

Proceeding through the flow diagram, CHAPTER I is devoted to the description of the experimental test rig and equipment, followed by CHAPTER III which includes development of the measuring techniques; the calibration, static and dynamic procedures and the method used in analysing the experimental results which are subsequently recorded in CHAPTER IV.

The theoretical model, CHAPTER II, consists of definitions, basic equations, variational principle, finite element analysis, Ritz technique and includes an algorithm for the prediction of a free-surface profile. CHAPTER V includes the problem formulation for

two-/

EXPERIMENTAL / ANALYTICAL.

METHOD OF APPROACH.

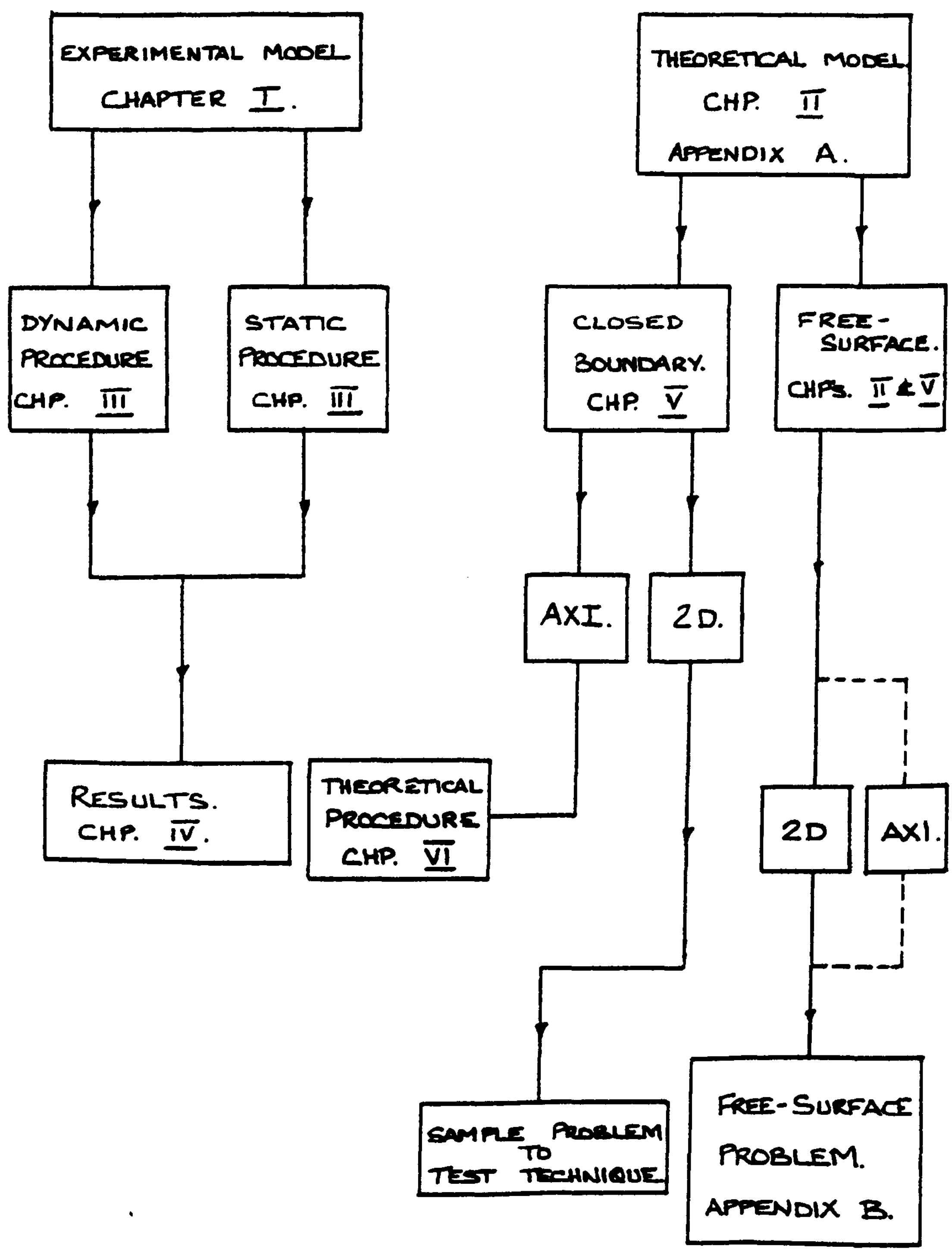

FIGURE 1.

two-dimensional and axisymmetric flow cases, which when using the axisymmetric formulation in combination with the theoretical procedure, CHAPTER VI, enables direct comparison to be drawn between the experimental and theoretical steady-state forces.

APPENDIX A includes the derivation of element matrices and APPENDIX B compares free-surface profiles with previous experimentors' results.

The computer program and operating procedure is shown in APPENDIX C.

NOMENCLATURE

a	=	Orifice area.
a_i	=	Algebraic difference of two points in the x-direction.
A	=	Area or pipe area.
A_1, A_2, A_3	=	Areas of sub-triangles in a triangle.
A^m	=	Area of a triangle.
b_i	=	Algebraic difference of two points in the y-direction (or in the r direction for axisymmetric problems).
B	=	The entire boundary curve.
C	=	The portion of the line boundary on which normal velocity components are specified.
C_c	=	Contraction coefficient.
C_d	=	Discharge coefficient.
C_p	=	Pressure coefficient.
d	=	Width.
e	=	A subscript used to indicate calculation for a quadrilateral element e.
E	=	Kinetic energy for the entire flow region.
F	=	Integrand of an integral.
g	=	Constant of gravitational acceleration.
h	=	Height above a selected datum.
H	=	Total head
i, j	=	Subscripts used to designate points "i" and "j".
$I(\phi)$	=	Functional. It is an expression related to the energy of the fluid motion.
$I^e(\phi)/$		

$I^e(\phi)$	=	The functional for a quadrilateral element e.
L	=	Length.
m	=	A subscript used to indicate calculation for a triangular element m.
n, s	=	Natural co-ordinates, i.e. the outward normal direction and the tangential direction respectively.
N	=	Total number of finite elements.
P	=	Pressure.
P_{atm}	=	Atmospheric pressure.
q	=	Speed or magnitude of velocity.
q_d	=	Downstream asymptotic speed.
q_n	=	Velocity component in the n-direction.
$(q_n)^a$	=	Specified normal velocity component.
q_s	=	Velocity component in the s-direction.
$(q_s)^a$	=	Specified tangential velocity component.
q_u	=	Upstream pressure.
Q	=	Discharge.
r	=	Radial co-ordinate.
R	=	Radius.
S_k	=	Slope of any point on a streamline.
S^e_{ij}	=	Element matrix for element e in two-dimensions.
SA^e_{ij}	=	Element matrix for element e in axisymmetric flow.
SL^e_i	=	Load matrix for element e in two-dimensions.
SLA^e_i	=	Load matrix for element e in axisymmetric flow problems.
t	=	Time
T^m_i, $\hat{T}^m_i$	=	Arrays expressing the geometric properties of a triangular element m.

u/

u	=	Velocity component in the x-direction.
v	=	Velocity component in the y-direction.
v_x	=	Velocity component in the radial direction.
$\vec{V}$	=	Velocity vector.
w	=	Velocity component in the Z-direction.
x, y, z	=	Rectangular cartesian co-ordinates.
X, Y, Z	=	Body force components in the x, y and z directions respectively.
y_o	=	Width of slot opening.
y_u	=	Upstream width of a slot.
y'	=	Derivative of y with respect to r.
α	=	Acute angle between the rigid wall and the vertical axis.
Γ'	=	The portion of surface boundary on which normal velocity components are specified.
∇	=	Vector operator.
∇^2	=	Laplace operator.
γ_i	=	Co-ordinate functions.
ϵ	=	An infinitesimal amount.
ϕ	=	Velocity potential function.
ϕ_i	=	Velocity potential at nodal point i.
$(\phi,_n)^a$	=	Specified normal velocity components
ρ	=	Fluid density.
ψ	=	Stream function.
Ω	=	Body force potential for a unit mass.
$\varepsilon_1, \varepsilon_2, \varepsilon_3$	=	Area co-ordinates of a point in a triangle.
χ_i	=	Array of co-ordinate functions.

In addition to the above notation, partial derivatives of a function are defined as:

$$\phi,_x \;,\; \phi,_y \;,\; \phi,_{xx} \;,\; \phi,_{yy} \;,\; \text{etc.}$$

CHAPTER I

EXPERIMENTAL MODEL

CHAPTER I

EXPERIMENTAL MODEL

1. Basic Description

2. Test Equipment
   (a) Piezoelectric Measuring Instruments
   (b) Quartz Force Transducer
   (c) Quartz Pressure Transducer
   (d) Charge Amplifiers
   (e) Cables
   (f) Displacement Sensor
   (g) Storage Oscilloscope
   (h) Power Supply
   (i) Solenoid Valve

3. Rig Components
   (a) Plenum Chamber
   (b) Valve/Seat Assembly
   (c) Lift-Off Mechanism
   (d) Back-Off Circuit

This chapter starts with the basic description of the experimental test rig used in this study. It then goes on to explain in particular, the various electrical test equipment used. Finally, the various components comprising the rig are detailed and the reasons appertaining to their choice, also any problems encountered and where possible, the means used to alleviate these difficulties.

A diagram showing how the electrical test equipment was connected, is shown in FIG. 2.

1. Basic Description

As shown in FIG. 3 and PHOTOGRAPH 1, a plenum chamber was formed behind the valve seat, the other end of the plenum being closed to the atmosphere. A pressure transducer was introduced into the plenum chamber and monitored by a pressure gauge. The pressure transducer was inserted flush with the bore of the plenum chamber to avoid velocity effects on pressure measurement. The plenum was held vertically in a metal framework by an electro-mechanical actuator and could be centralised by means of three roller bearings. An air inlet is also formed at the opposite end to the valve seat. To obtain adequate frequency response in the force measurements, a quartz crystal transducer was chosen. It is well known, however, that a force transducer performs the function of an accelerometer very adequately, since both are basically the same instrument. For this reason, it was decided to hold the valve stationary by means of the relatively stiff force transducer and withdraw the seat from the valve. The equipment was mounted on a cast iron block to minimise interference effects due to acceleration of/

DIAGRAMMATIC ARRANGEMENT OF ELECTRICAL TEST EQUIPMENT.

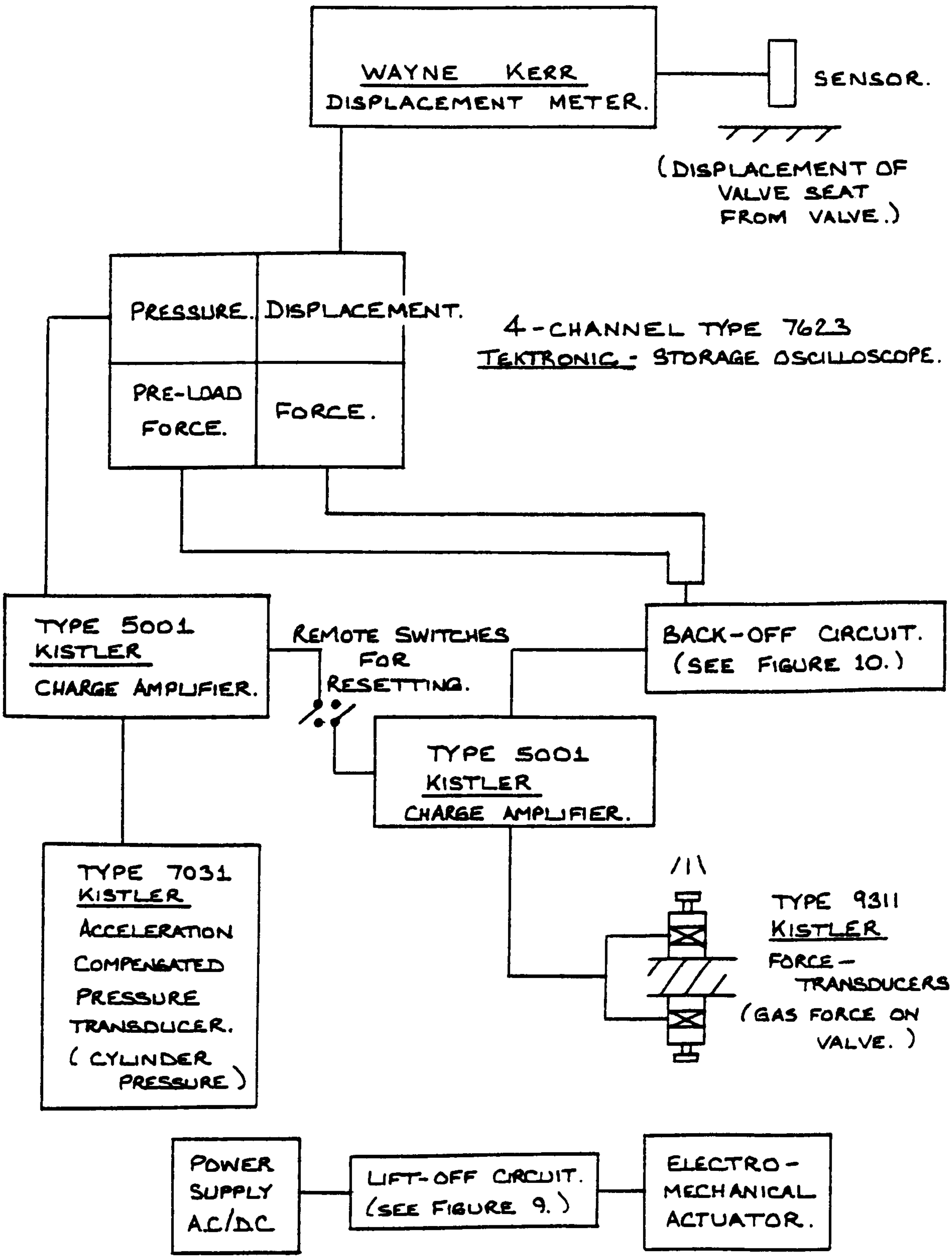

FIGURE 2.

DIAGRAMMATIC ARRANGEMENT OF TEST RIG.

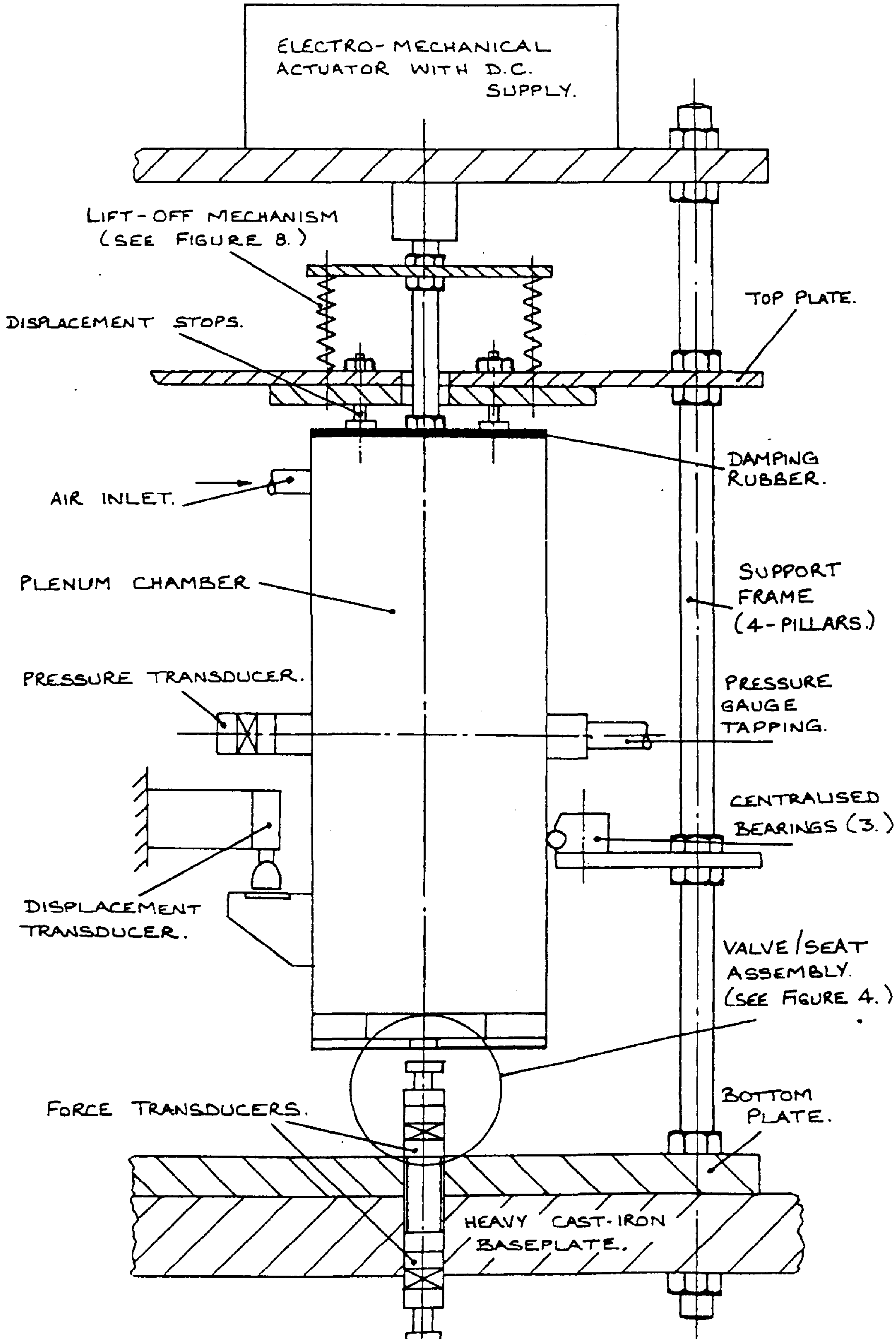

FIGURE 3

of the transducer mounting. Nevertheless, some vibration was experienced following impact of the plenum cylinder on its stop after the seat was withdrawn from the valve, with a consequent deterioration in the signal/noise ratio of the force measurement. To minimise this effect, a force transducer with identical characteristics was mounted on the underside of the cast iron transducer mounting block. The signals from the two transducers were taken to a common input of a charge amplifier. The signal due to acceleration from the two force transducers thus led to cancellation, except at very high frequencies beyond the apparent range of interest. The lack of cancellation at high frequencies was due to a phase shift between the transducer outputs, probably due to the slight differences in their characteristics. The dynamic pressure measurement in the plenum chamber was also subject to acceleration interference, therefore, an acceleration compensated pressure transducer was utilised at this location. It was also found necessary to shield the force transducers against variations in ambient temperature due, for example, to the air stream from the valve. This became apparent as tests proceeded and it was found that temperature sensitivity of transducers is extremely important when small signals are being measured.

The plenum chamber was withdrawn from the valve by means of an electro-mechanical actuator assisted by two springs. The initial force between the valve and the seat (pre-load) and the rate of withdrawal, could be adjusted by means of rheostats in the "lift-off" circuit (CHAPTER I, Section 3c). This pre-load was necessary to ensure triggering of the oscilloscope by the signal from the force transducer, but could not be too large or flooding of an oscilloscope/

oscilloscope amplifier would result. A Wayne Kerr capacitive type displacement meter and sensor were used to determine the displacement of the plenum chamber. A further circuit was incorporated into the rig to enable a datum value of force to be determined (see "Back-Off" CHAPTER I, Section 3d).

Readings of pressure in the plenum chamber, force on the valve and displacement of plenum chamber, were recorded on a Tektronix 7000 series storage oscilloscope for photographic records to be taken.

In order that the static and dynamic test results might be totally comparable, the continuous flow or "static" tests were carried out in the same apparatus.

2. Test Equipment (FIG. 2)

(a) Piezoelectric Measuring Instruments

When rapidly changing mechanical variables such as pressures, forces, accelerations etc., have to be measured and recorded as accurately as possible, particular use is made of piezoelectric measuring systems. The piezoelectric transducer essentially consists of discs or rods of quartz cut out and assembled into a column, which is usually pre-loaded with a spring sleeve. The column now emits a charge signal when it is strained and this signal is directly proportional to the force causing the strain.

The application of these transducers is confined to measuring dynamic and quasi-static processes. This is due to the fact that the transducer will discharge and seek its own initial zero/

zero once a steady state condition has been reached. The discharging time constant (T = R.C, C being the entire capacitance of the transducer cable and amplifier input), precludes the transducers use in long term control operations. However, using a modern type of charge amplifier, the transducers can be used to measure events covering a few minutes, provided that great care is taken to ensure that transducers and leads remain dry and clean. These parts should be stored in a dessicator when not in use.

The quartz used in transducers is silicon dioxide and although its output is low, it is extremely stable. Other valuable properties are:

a) High pressure resistance.

b) High temperature resistance.

c) High insulation resistance.

d) High linearity with no hysteresis.

In order to avoid impurities in the crystals, the quartz used today is artificially grown.

Specific piezoelectric transducers used in this study will now be discussed.

(b) Quartz Force Transducer

The actual force measuring element in a force transducer consists of a quartz loaded washer which is inserted between two special nuts and is pre-loaded by means of an extension bolt. The quartz crystal axis is arranged longitudinally and under the application of a force, an electrostatic charge is generated on the force application faces. The magnitude of this charge is solely dependant on the applied force. The voltage generated is governed by/

by the geometrical dimensions of the quartz washers and is equal to:

$$V = \frac{Q}{C}$$

where Q is the charge and C is the transducer capacitance. Hence, the capacitances of the connecting cable and amplifier input must be taken into account. Because of their design, these force transducers are very rigid and have a correspondingly high resonant frequency (in the region of 50 kHz). Two of these transducers were used in this current work, these being Type 9311 Kistler transducers with the following important specifications:

i) Maximum measuring range ± 500 kp.

ii) Resonant frequency 75 kHz.

iii) Working temperature range -40, $+120^{\circ}$C.

(c) Quartz Pressure Transducer

The quartz crystal axis in a pressure transducer is arranged transversely and under the action of a pressure force the crystal sets up an electrostatic charge on the surface at right angles to the force. The magnitude of this charge is dependent on the geometrical dimensions of the quartz and thus, by adopting a suitable shape of the quartz elements, it is possible to achieve a higher yield than that produced by the longitudinal effect.

Certain types of pressure transducers are acceleration compensated as in this study and this is achieved using a quartz crystal accelerometer built into the pressure transducer. The charge signal produced by acceleration, due to the mass of the diaphragm part of the pressure transducer, is compensated by a signal of inverse polarity resulting from the quartz accelerometer.

It/

It can be seen from PHOTOGRAPHS 2 and 3 that all the acceleration effect is not removed even when using acceleration compensated transducers, but the signal quality is greatly improved. The transducer used was a Type 7031 Kistler acceleration compensated transducer and had the following specifications:

i) Pressure measuring range 0 - 250 atmospheres (1 at = 1kp/cm^2)

ii) Resonant frequency 80 kHz.

iii) Working temperature range -150, +240°C.

These transducers are in turn connected to charge amplifiers.

(d) Charge Amplifiers

The charge amplifiers used were mains operated DC amplifiers of very high input impedance, with capacitive negative feedback intended to convert the electric charge from a piezo-electric transducer into a proportional voltage on the low impedance amplifier output. They were Type 5001 Kistler charge amplifiers and had the facility of long, medium and short time constants. They could also be operated remotely as in this study. The operating range, i.e. mechanical units per volt of output voltage, could be varied and the controls were so designed that, when the amplifier was set to a particular transducer sensitivity, a direct and simple proportionality was achieved between output voltage and mechanical input to the transducer (i.e. pressure or force).

(e) Cables

The cables used to connect the transducer to the charge amplifier must have an extremely high, insulation resistance and must/

must not disturb the charge signals when moved. Their capacitance must also be as small as possible.

(f) Displacement Sensor

A Wayne Kerr meter and sensor were used where the probe provides read outs of small displacements by measuring the electrical capacitance between the sensor and test surface. When connected to an oscilloscope it illustrates a change in displacement by a change of position of a trace on the screen.

(g) Storage Oscilloscope

A 4 channel Type 7623 Tektronix storage oscilloscope was used which consisted of 4 amplifiers with variable gains enabling signals obtained from the transducers to have adequate resolution. The oscilloscope also had variable time-bases. Many other facets were available on this unit and the controls used to facilitate satisfactory completion of these tests are discussed in CHAPTER III, Experimental Procedure.

(h) Power Supply

The power supply required for the electro-mechanical actuator is a device which changes mains AC input to DC output, thereby enabling the actuator to operate in the mode of either opening or closing the valve.

(i) Solenoid Valve

A solenoid valve was positioned on the air inlet line to interrupt the flow for "no-flow" datum readings. It was a mains AC operated unit and was necessary because of the very limited time available/

available to complete a test due to the charge amplifier time constant.

3. Rig Components

(a) Plenum Chamber (FIG. 4 and PHOTOGRAPH 4)

Since this study was primarily concerned with conditions relevant to those obtained in a compressor, it was desirable to have the valve opening as quickly as possible. Preliminary investigations also showed that the difference between static and dynamic lift forces are accentuated at faster opening times. However, in the initial stages of these experiments a brass cylinder was used, since this was readily available, but it was found that the fastest opening time that could be achieved was of the order of 15 ms and this was therefore replaced by a lightweight cylinder.

A plastic cylinder was chosen and additional attachments were made as light as practically possible. This design achieved a range of opening times of the order 7 - 70 ms.

The plastic cylinder had one end sealed to the atmosphere. Attached to this end was a layer of rubber to dampen the impact when the cylinder reached its "maximum" displacement. At the opposite end of the cylinder, a female perspex insert was firmly secured to the cylinder, so designed as to enable brass male inserts of varying bores to be inserted. Brass was used since these gave a good seal between valve and valve seat. In this study the 6.35 mm bore ($\frac{1}{4}$") insert is only reported. Also at this end, a perspex attachment was fixed by means of jubilee clips to the side of the cylinder. This attachment had a metal insert to enable the Wayne Kerr displacement/

PLENUM CHAMBER (PLASTIC)

N.T.S.
FOR CLARITY.

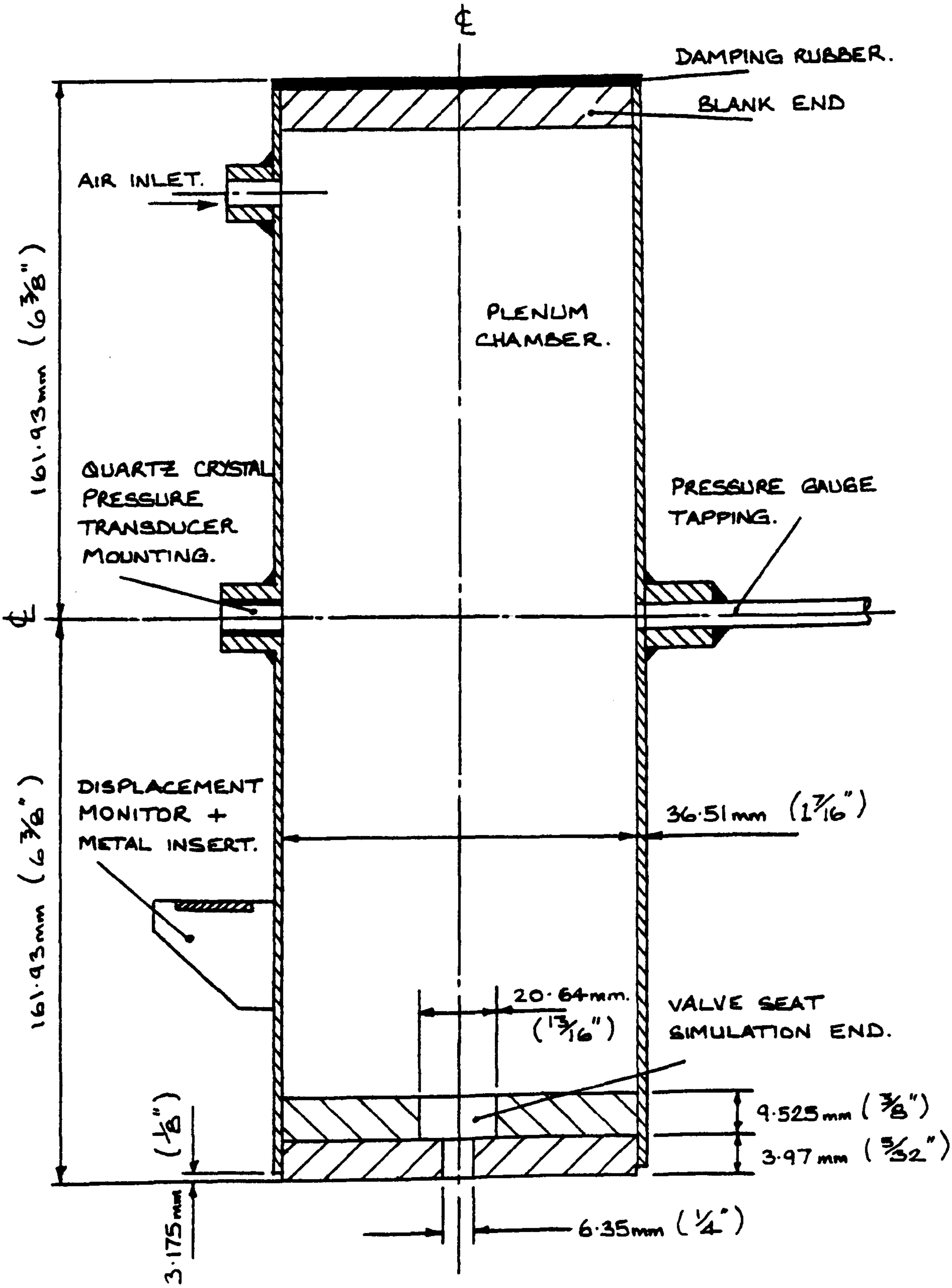

FIGURE 4

displacement sensor to monitor the displacement of the plenum chamber with respect to the valve when the chamber was withdrawn from the valve. It should be noted that a metal insert is required to enable the capacitive type displacement sensor to function adequately. Three plastic bosses were also attached to the chamber, these enabling a compensated quartz crystal pressure transducer, a pressure gauge and an air supply to be attached.

The plenum chamber was attached at the upper end to the lift-off mechanism by a screwed rod and at the lower end, three roller bearings were present to allow centralisation of the valve seat on the valve.

N.B. All recorded results in this report were carried out on the plastic plenum chamber assembly.

(b) Valve/Seat Assembly

The final valve/seat assembly used in these experiments is shown in FIG.5 and PHOTOGRAPH 5, and the dimensions of the valves and valve seat used in FIG. 6.

Brief Background

Three different valve arrangements (FIG. 6(a), (b) & (c)) and two types of cylinder, were used at different stages of this research, each one being modified for a particular reason.

In the first series of tests, the brass plenum chamber was used in conjunction with a type "A" brass valve. At this stage of the study it became apparent that the valve and hence, the force transducers were very susceptible to temperature variations caused by air flowing onto and around the valve and transducer. This was indicated/

VALVE / SEAT ASSEMBLY.

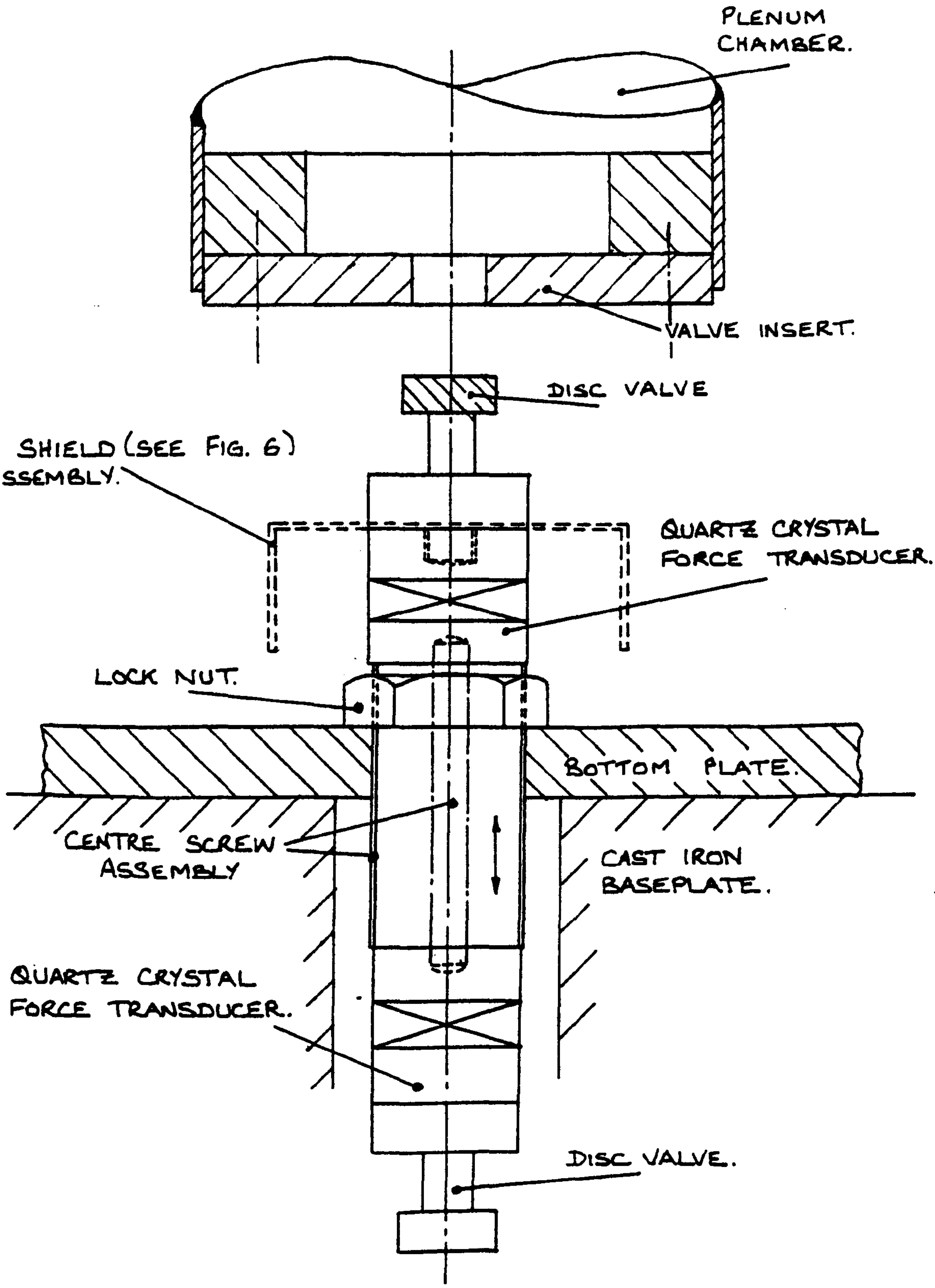

FIGURE 5.

VALVE/SEAT COMPONENTS.

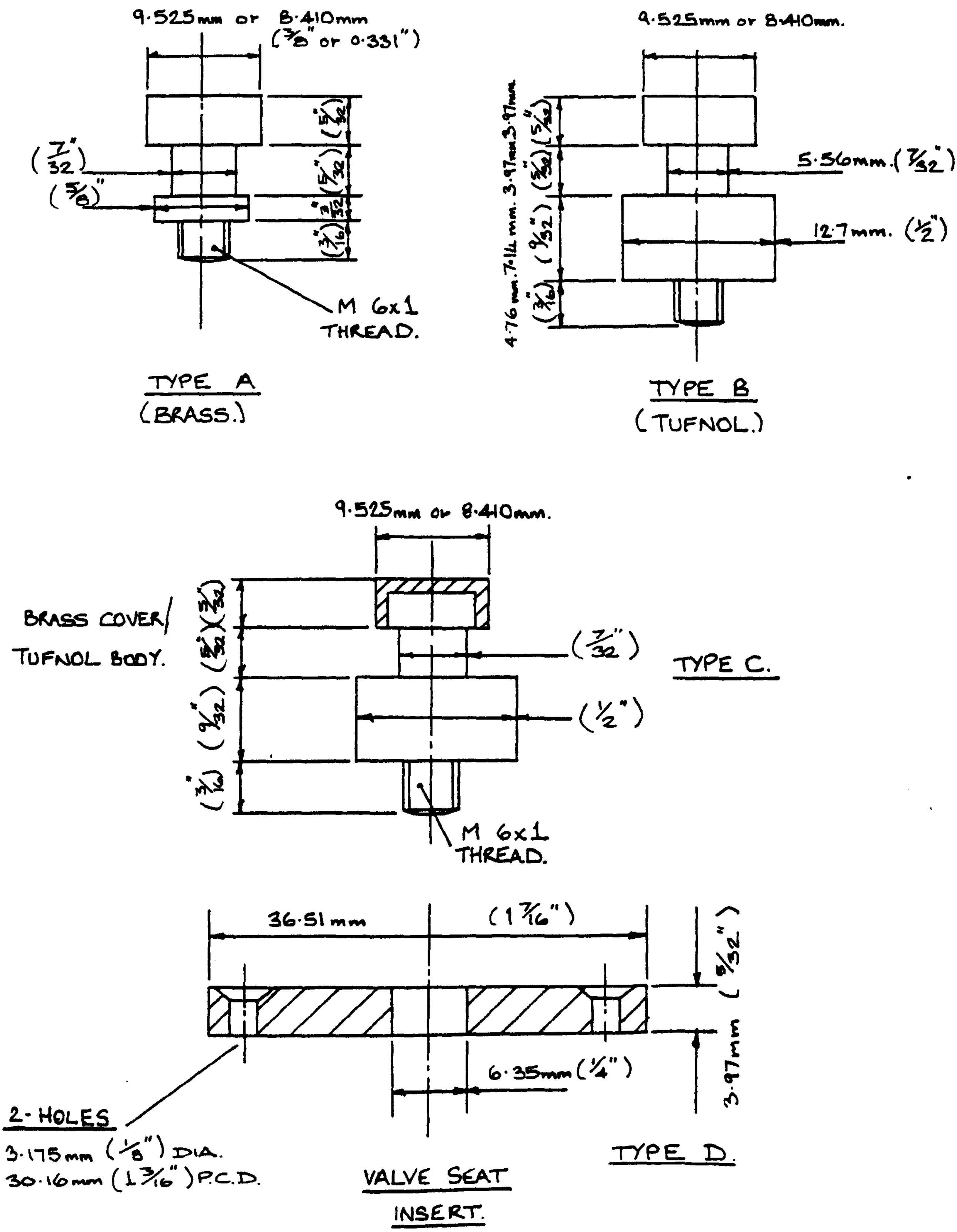

FIGURE 6.

indicated by "drift" on the oscilloscope. To overcome this problem a tufnol valve of type "B" was introduced and this apparently helped in overcoming temperature drift problems, but caused an increase in leakage flow when the valve was closed due to poor surface finish of the valve. Finally, a brass faced tufnol valve of type "C" was tried. This was the most successful in overcoming the temperature drift problem and was further improved by covering the force transducer in contact with the air by a plastic shield filled with insulating material. In conjunction with this valve, the original brass cylinder was replaced by the plastic cylinder as previously described.

The valve seat used during all these experiments was brass of type "D".

Assembly

The valve/seat assembly was as shown in FIG. 5 The centre screw enabled the valve to be raised or lowered and securely locked into position. On the underside of the "centre screw" another transducer and disc valve of similar characteristics and dimensions was attached. (As previously mentioned to eliminate acceleration effects).

In the following sections the main points that have arisen in this chapter regarding problems in implementation will be discussed. These can be effectively broken into two broad areas, these being:

Problems due to: I) Temperature Variations and

II) Acceleration Effects.

I) Temperature Variations/

I) Temperature Variations

Since small signals were being measured, temperature drift was very apparent. That is, any changes in temperature of the transducer affected the output signal from the transducer via the charge amplifier and therefore gave incorrect readings. This would be depicted on the oscilloscope by a sloped line. These changes in temperature occurred from various sources, these being (a) handling of the transducer and (b) conduction and/or convection from other materials in contact with it.

In the case of the pressure transducer, only handling presented a problem and this was eliminated by allowing the transducer to reach thermal equilibrium with its surroundings (i.e. a sufficient time lapse after handling).

The main problems arose with the force transducers and in particular the top one, this being in contact with the air supply. When the cylinder was in the "up" position with air flowing, this blew directly on the face of the disc valve, thereby cooling the valve. This, in turn, cooled the force transducer. To overcome this the valve was made of tufnol instead of brass. As previously mentioned, a brass facing was however retained to give adequate sealing properties when the valve was closed. Also, since air was flowing around the disc valve to the transducer, it was decided that insulation was necessary also in this region. The transducer was wrapped in plastic foam sheet and the whole then covered by a plastic shield which deflected the stream of air away from the transducer (see FIG. 7). The cast iron block was also completely insulated by covering it with foam sheet and finally, the surrounding area blocked off to eliminate any casual draughts.

II) Acceleration Effects/

INSULATION OF VALVE / TRANSDUCER ASSEMBLY.

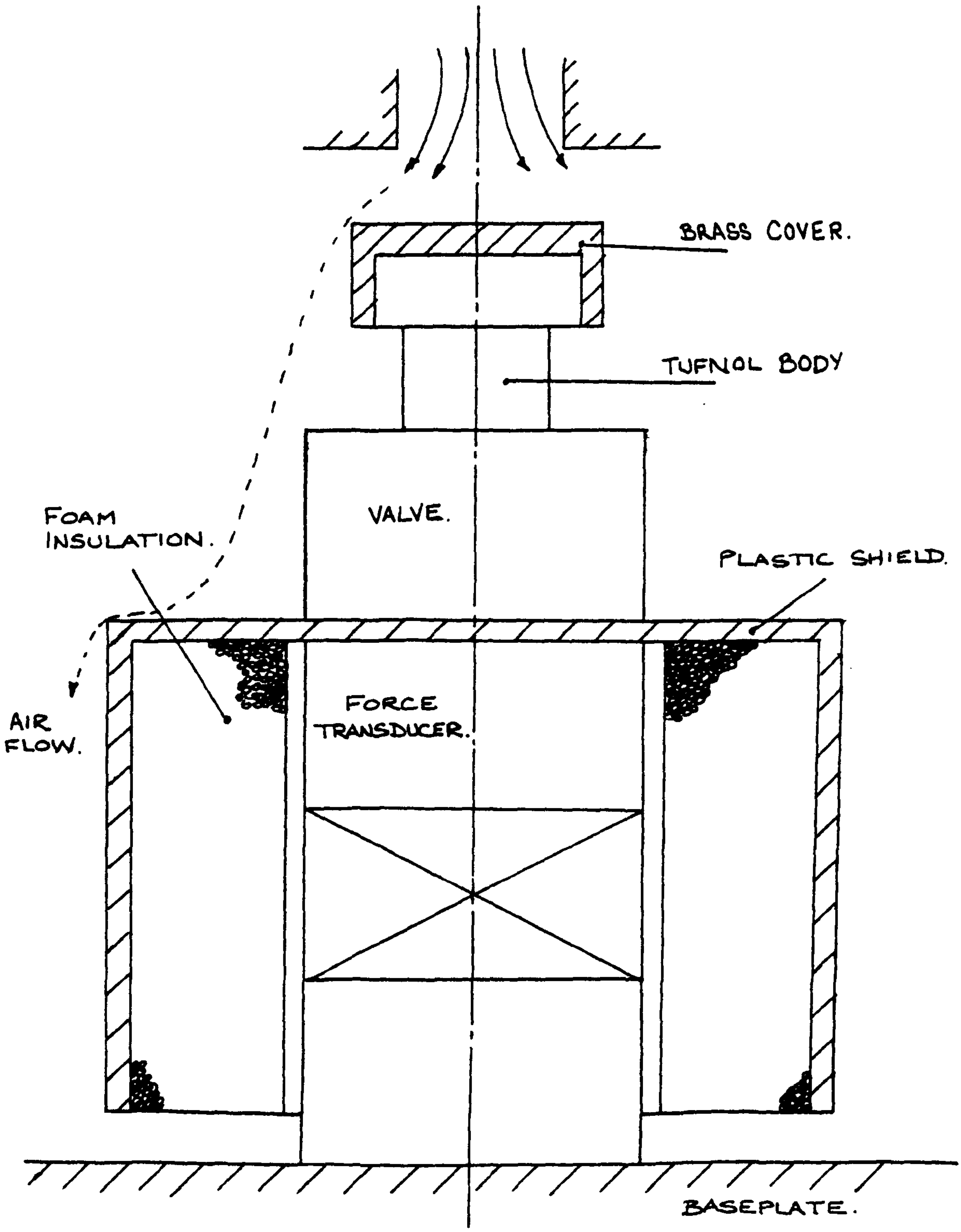

FIGURE 7.

II) Acceleration Effects

When transducers are accelerated, inertia forces are generated due to their mass. These forces can be large and may blanket the actual signal that is required. To overcome this problem:

1. The pressure transducer was acceleration compensated. And
2. Two force transducers were used in conjunction.

When using two force transducers during the tests, as shown in FIG. 4, the primary acceleration was eliminated by securing the transducers firmly to the heavy cast iron block. The force transducers were physically connected together by means of the centre screw so that they suffered the same acceleration force but with one receiving this acceleration in the mode of compression, while the other experienced tension. These signals were then added together via a charge amplifier and the resulting signal displayed on the oscilloscope.

To show, in fact, that this did eliminate acceleration effects, an experimental rig was assembled as shown in FIG. 8. It consisted of a small rigid frame enabling either one or two force transducers (back to back) to be attached to it. The frame was connected to an electro-mechanical actuator and this was then wired to a power oscillator. The outputs from the force transducer(s) were connected to a charge amplifier and so to an oscilloscope.

Setting a constant power level and firstly using one force transducer, a frequency level was set causing the transducer to oscillate at this frequency. A note of the corresponding amplitude displayed on the oscilloscope was then recorded and the test repeated/

TRANSDUCER(S) - BACK TO BACK TEST RIG.

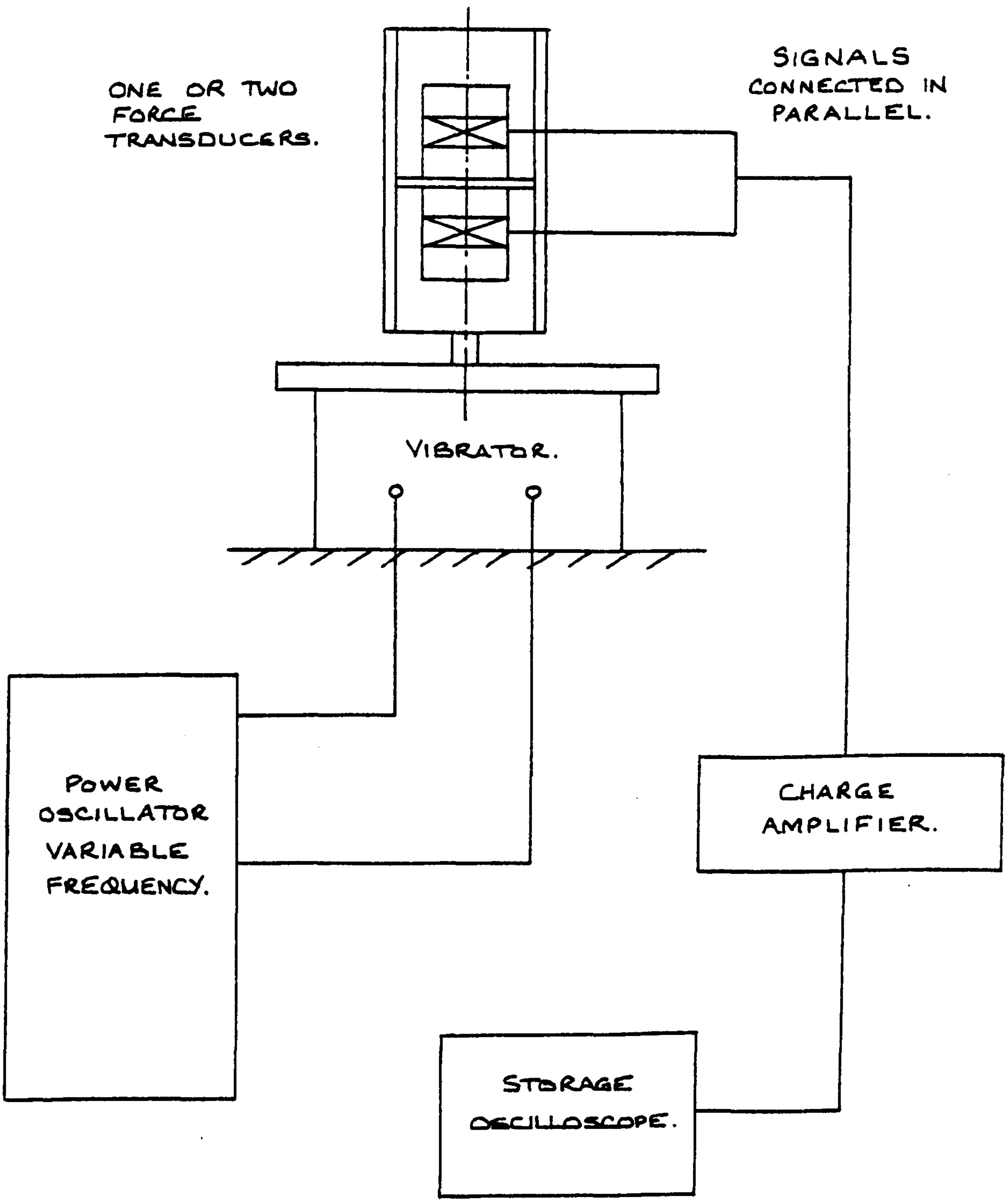

FIGURE 8.

repeated using two force transducers back to back and connected in parallel to the charge amplifier. The results obtained are shown in TABLE 1. As can be seen from these results, there is considerable attenuation of acceleration at all frequencies covered, but more so at lower frequencies. The difference at high frequencies could be attributed to the fact that no two transducers have identical characteristics and this may be the cause of a phase shift observed between the transducer outputs at high frequencies.

On the basis of these results, two transducers were assembled into the main test rig as shown in FIG.3 . With the valve closed, the "lift-off" mechanism was operated without air being pressurised in the cylinder ("no air" test). There was no visible acceleration displayed on the oscilloscope before the cylinder struck the stop and even the shock of hitting the stop was reduced to manageable proportions in terms of the force transducer output (see PHOTOGRAPH 6). For more information on "no air" tests, see CHAPTER III, Section 3c.

On the basis of these results, two transducers were used in carrying out the main experimental work.

(c) Lift-Off Mechanism

The lift-off mechanism, which had the function of removing the valve seat from the valve and which also determined the value of the pre-load for adequate triggering, was an electro-mechanical assembly. The mechanical mechanism being shown in FIG. 9 and PHOTOGRAPH 7 and the electrical circuitry in FIG.10

A screwed rod was attached to an electro-mechanical actuator, coil with DC supply, with a cross spar to which were attached/

TABLE 1

Amplitude/Attenuation Results

FREQUENCY (cycles/sec)	AMPLITUDE (mV) 1-TRANSDUCER	AMPLITUDE (mV) 2-TRANSDUCERS	ATTENUATION OF ACCELERATION SIGNAL
1 kc/s	800	14	60:1
10 kc/s	600	50	12:1
10 kc/s balanced	600	30	20:1
30 kc/s	64	6.5	10:1

NOTE: Balanced refers to the sensitivities of the two transducers being adjusted till attenuation value was at its lowest.

In other cases sensitivites were set as makers instructions.

LIFT-OFF MECHANISM.
(SHOWN WITH VALVE OPEN.)

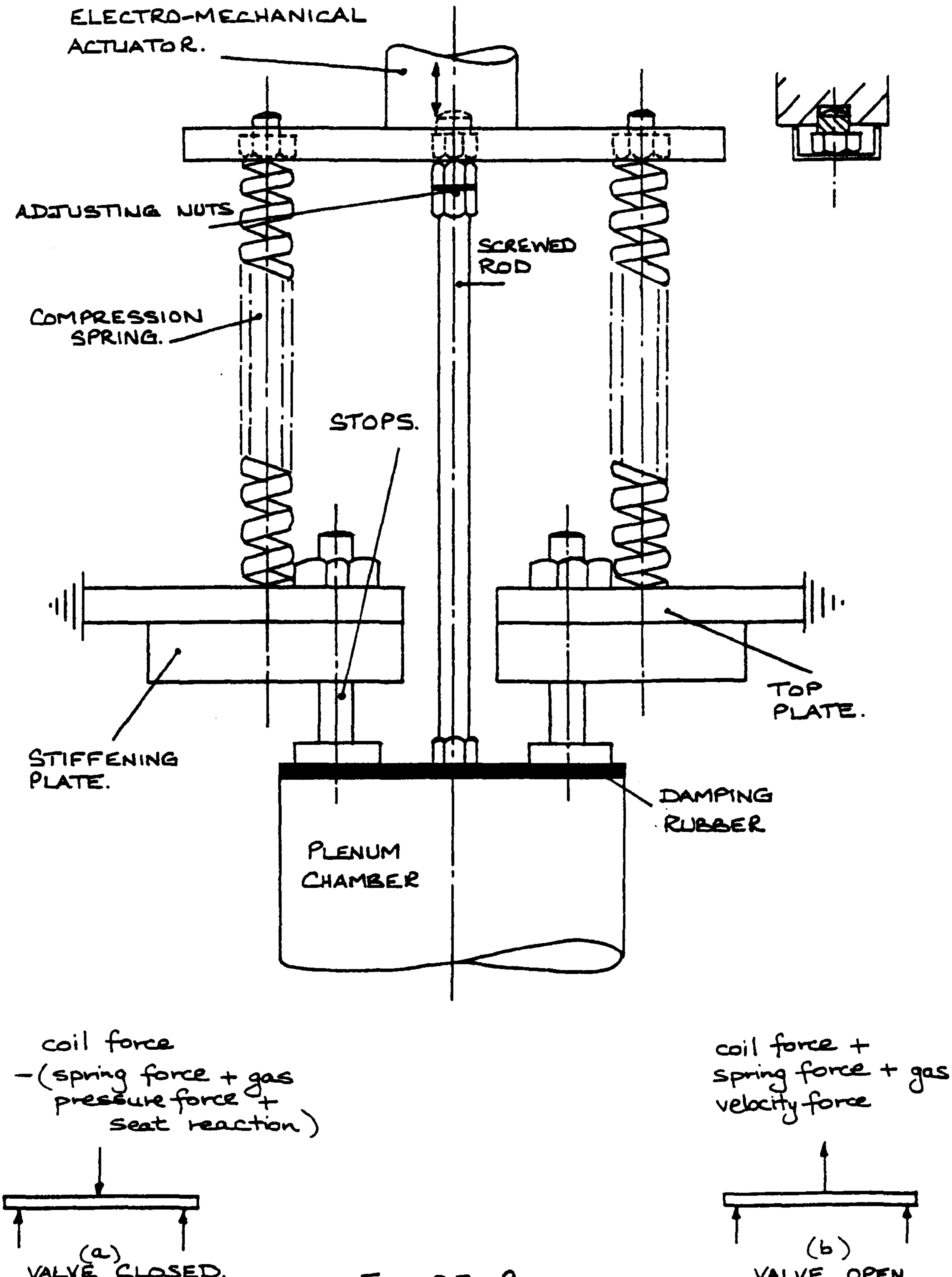

FIGURE 9.

LIFT-OFF CIRCUIT.

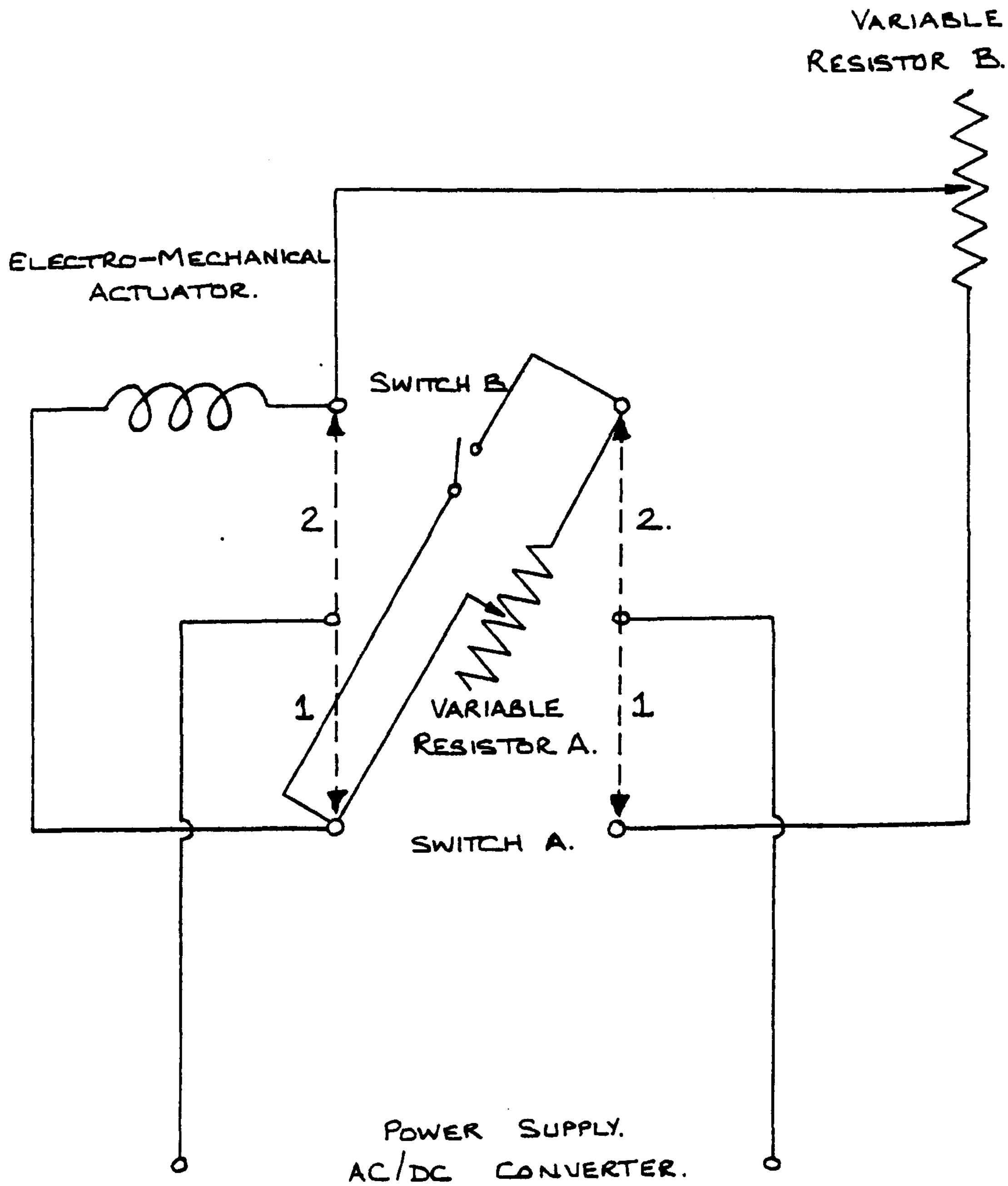

FIGURE 10.

attached two springs. The compression in these springs could be adjusted manually as required by means of the adjusting nuts. The screwed rod in turn was attached to the top end of the plenum chamber to enable the disc valve to be opened or closed. A stiffening plate was attached to the underside of the top plate to help to remove transients caused by the plenum chamber striking this surface on opening of the valve. The springs being in compression tended to lift the valve seat from the valve.

The necessary conditions for satisfactory operation of the valve seat mechanism were as follows:

a) A range of pull-off times whose minimum value was as small as possible, to simulate as nearly as possible the rise times of compressor valves (opening or pull-off time).

b) A pre-load force between the valve and valve seat sufficient to give an adequate seal and to ensure triggering of the oscilloscope on removal of the seat from the valve. Sealing being necessary to give a correct impulsive start to the gas flow. This force, however, should not be so large as to flood the oscilloscope amplifier when set to a gain suitable for recording the variation in gas force on the valve.

To meet these conditions, the coil circuitry was arranged as shown in FIG. 10 Operation of switch A reversed the polarity of the DC supply. In position 2, the coil force held the valve closed against the spring force. When switch A was thrown to position 1, the coil force assisted the springs thus applying maximum force to the opening operation. Both opening and holding down forces could be regulated by adjustment of resistors A and B. For minimum opening times, switch B was closed to short out resistor A. For very/

very long opening times, the circuitry could be varied to allow opening under spring action alone, or even with a residual hold on force, less than the spring force.

(d) Back-Off Circuit

When the oscilloscope was set to a gain suitable for measuring gas force variation during valve opening, it was found that zero force was off screen. The "back-off" circuit is a means of enabling a datum value of force to be determined and recorded. This is achieved by the circuit shown in FIG. 11. The circuit consists of a potentiometer, a 4 volt battery and a combination of switches. When switch A is open and switches B and C are in position 1, the force signal via the charge amplifier is displayed directly on the oscilloscope. When switch C is in position 2 and switch A is closed, one side of the battery is earthed and a measure of the potentiometer voltage can be determined by operating switch B from position 1 to 2. This then gives a measure of the pre-determined voltage set on the potentiometer. When switch C is in position 1, switch A closed and switch B in position 2, this set voltage is added to the signal being transmitted from the charge amplifier. If, then, the valve is open, but no gas is flowing, the charge amplifier signal is that corresponding to zero force on the force transducer. This is off screen using "normal" switch settings, but with switches set as described, a datum signal may be brought on screen, separated from zero force by a known voltage, i.e. by a known force. Values of gas force with respect to this datum may then be determined. The sequence of events in recording the force is explained fully in CHAPTER III Experimental Procedure.

BACK – OFF CIRCUIT.

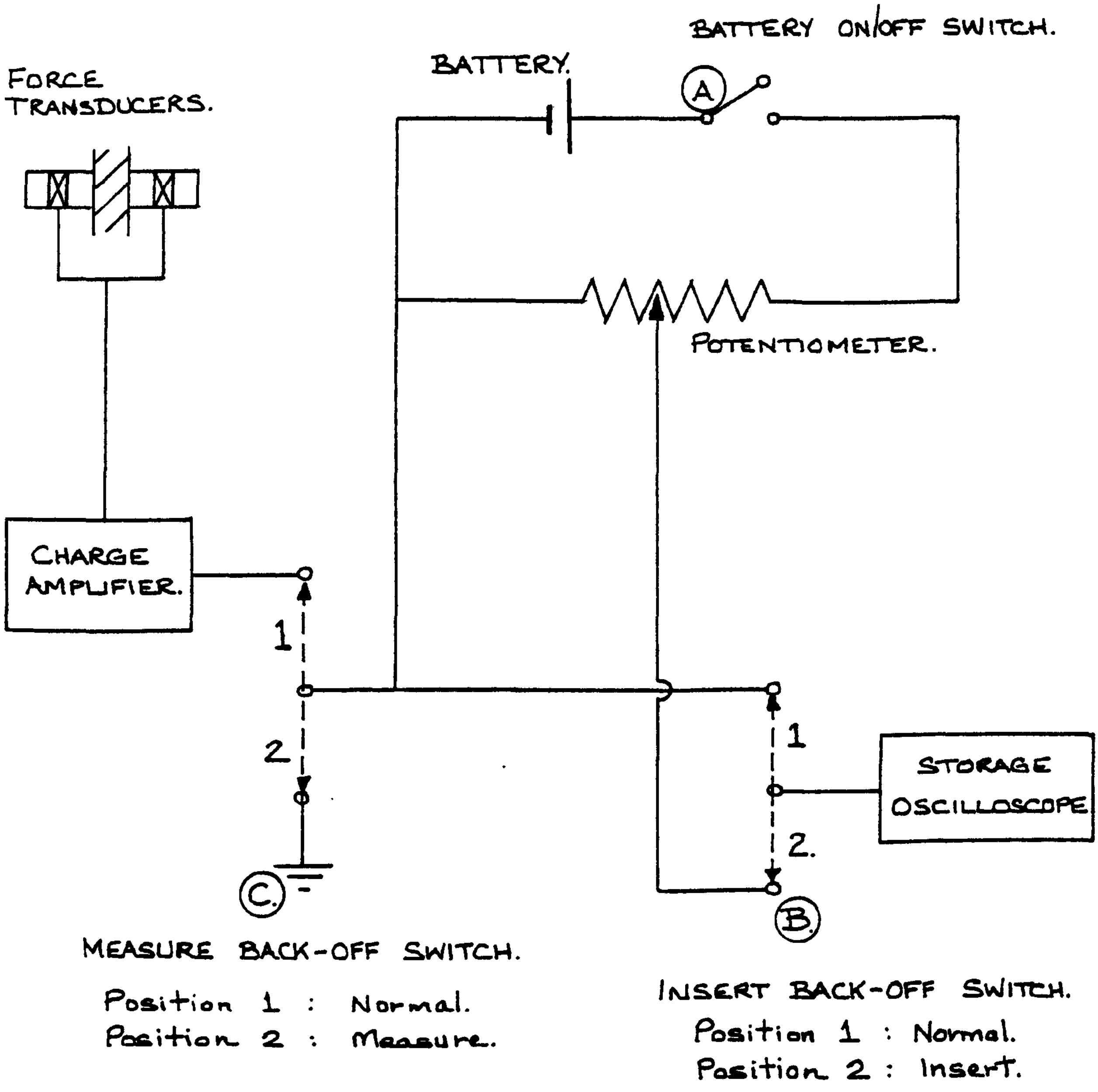

FIGURE 11.

CHAPTER II

MATHEMATICAL MODEL

CHAPTER II

MATHEMATICAL MODEL

In this chapter the fundamental theory on which the mathematical model is based will be presented. This includes the relevant definitions and equations based on cartesian and polar co-ordinate systems, the variational principle, some basic concepts of finite element analysis and the Ritz technique. Two dimensional equations are also included for completeness, since axi-symmetric flow is an extension of two-dimensional flow.

1. Some Definitions and Basic Equations

The following definitions and equations, which can be found in most standard text books, e.g. Vallentine [14], Prandtl [15] and Binder [16], are relevant to the present study and are summarised here for convenience of reference.

Steady Flow

A flow whose physical properties such as velocity $\vec{V}$ (or components u, v and w for three-dimensional flow), fluid density ρ, and pressure p, at every point in the flow domain do not change with time.

Ideal Flow

A fluid which is both incompressible and inviscid is called an ideal fluid. "Incompressible" means that the fluid occupies a definite volume and is unaffected by changes in pressure. "Inviscid" implies the fluid has zero coefficient of viscosity and hence offers no resistance to shearing deformations.

Streamline

A continuous line drawn through the flow so that it has the direction/

direction of the velocity vector $\vec{V}$ at every point on the line. Consequently, no fluid may pass across a streamline. A streamline is mathematically defined by:

$$u.dy - v.dx = 0 \quad \text{for two-dimensional flow} \qquad (2.1a)$$

or as

$$v_x.dr - v_r.dx = 0 \quad \text{for axi-symmetric flow} \qquad (2.1b)$$

in which u and v are the velocity components in the x and y directions and v_x and v_r are the velocity components in the axial and radial directions, respectively.

Free Streamline

A streamline on which the pressure is a constant. For instance, the streamline on the interface of fluid and air of flow issuing from a slot or orifice is a free streamline.

Equipotential Line

A line on which the fluid particles have the same velocity potential. Flow passes an equipotential line at right angles to all points on the line.

Flow Net

A mesh which is composed of two orthogonal sets of lines, streamlines and equipotential lines.

Stream Function ψ

A mathematical device used to describe the form of any particular flow, which when:

i. set equal to constants, results in different streamline in two-dimensional flow, or annular stream surfaces in axi-symmetric flow.

ii./

ii. partially differentiated, yields velocity components, i.e.

$$u = \frac{\partial \psi}{\partial y} \quad , \quad v = -\frac{\partial \psi}{\partial x} \quad \text{for two-dimensional flow} \quad (2.2a)$$

and $$v_x = \frac{1}{r}\cdot\frac{\partial \psi}{\partial r} \quad , \quad v_r = -\frac{1}{r}\cdot\frac{\partial \psi}{\partial x} \quad \text{for axi-symmetric flow} \quad (2.2b)$$

iii. taking the difference between two stream functions yields the flow rate between two lines in two-dimensional flow and in axi-symmetric flow, the flow rate is $dQ = 2\pi . d\psi$ in which $d\psi$ is the difference between two adjacent stream surfaces.

Velocity Potential Function ϕ

Another mathematical device, a useful complementary function for ψ , used to describe a flow pattern, which when:

i. set equal to constants, results in velocity potential lines in two-dimensional flow, or velocity potential surfaces in axi-symmetric flow.

ii. differentiated with respect to distance in any particular direction yields the velocity in that direction, i.e.

$$u = \frac{\partial \phi}{\partial x} \quad , \quad v = \frac{\partial \phi}{\partial y} \quad \text{for two-dimensional flow} \quad (2.3a)$$

$$v_x = \frac{\partial \phi}{\partial x} \quad , \quad v_r = \frac{\partial \phi}{\partial r} \quad \text{for axi-symmetric flow} \quad (2.3b)$$

It is worth remembering that the stream function ψ exists for both two-dimensional and axi-symmetric flow, regardless of whether or not the flow is rotational, while the velocity potential function exists only for irrotational flow.

Velocity Expressions in Natural Co-ordinate System

In terms of the natural co-ordinates s and n, which are

the/

the direction of flow along a streamline and the outward normal direction to the streamline, the velocity at a point is given by:

$$q = \frac{d\phi}{ds} \tag{2.4a}$$

or

$$q = \frac{d\psi}{dn} \tag{2.4b}$$

Irrotational Flow

A flow is irrotational if none of the particles in the flow region suffers rotation, that is, the average of the angular velocities of two mutually perpendicular linear elements of a particle is zero in any plane containing these elements. Mathematically, the irrotationality condition can be expressed as:

$$\frac{\partial v}{\partial x} - \frac{\partial u}{\partial y} = 0 \quad \text{for two-dimensional flow} \tag{2.5a}$$

or

$$\frac{\partial v_x}{\partial r} - \frac{\partial v_r}{\partial x} = 0 \quad \text{for axi-symmetric flow} \tag{2.5b}$$

upon substituting equations (2.2a) and (2.2b) into equations (2.5a) and (2.5b) respectively, one obtains:

$$\nabla^2\psi = 0 \quad \text{for two-dimensional flow} \tag{2.6a}$$

where

$$\nabla^2\psi = \frac{\partial^2\psi}{\partial x^2} + \frac{\partial^2\psi}{\partial y^2} = 0 \tag{2.6b}$$

and

$$\frac{\partial^2\psi}{\partial x^2} - \frac{1}{r}\cdot\frac{\partial\psi}{\partial r} + \frac{\partial^2\psi}{\partial r^2} = 0 \quad \text{for axi-symmetric flow} \tag{2.6c}$$

Equations of Continuity

The continuity equation simply expresses the law of conservation of mass. When derived in terms of the conventional x, y and z rectangular Cartesian co-ordinate system, the continuity relation/

relation may be expressed as [17] pp 55-56

$$\frac{\partial \rho}{\partial t} + \frac{\partial(\rho.u)}{\partial x} + \frac{\partial(\rho.v)}{\partial y} + \frac{\partial(\rho.w)}{\partial z} = 0 \qquad (2.7)$$

for any kind of fluid real or ideal.

For an ideal fluid the time rate of change of density following a fluid particle, $\frac{\partial \rho}{\partial t}$, is zero and equation (2.7) simplifies to:

$$\frac{\partial u}{\partial x} + \frac{\partial v}{\partial y} + \frac{\partial w}{\partial z} = 0 \qquad (2.8)$$

This equation can be specialised to give:

$$\frac{\partial u}{\partial x} + \frac{\partial v}{\partial y} = 0 \quad \text{for two-dimensional flow} \qquad (2.9a)$$

and $$\frac{\partial v_x}{\partial x} + \frac{1}{r}\frac{\partial}{\partial r}(v_r.\,r) = 0 \quad \text{for axisymmetric flow} \qquad (2.9b)$$

Upon substituting equations (2.3a) and (2.3b) into equations (2.9a) and (2.9b) respectively, one derives the Laplace equations:

$$\nabla^2 \phi = 0 \quad \text{for two-dimensional flow} \qquad (2.10a)$$

where $$\nabla^2 \phi = \frac{\partial^2 \phi}{\partial x^2} + \frac{\partial^2 \phi}{\partial y^2} = 0 \qquad (2.10b)$$

and $$\frac{\partial^2 \phi}{\partial x^2} + \frac{1}{r}\frac{\partial \phi}{\partial r} + \frac{\partial^2 \phi}{\partial r^2} = 0 \quad \text{for axi-symmetric flow} \qquad (2.10c)$$

<u>Equations of Motion for a Non-Viscous Fluid</u>

Applying Newton's second law to a small fluid element dV, while considering both body forces and surface forces and taking a limit dV $\to$ 0, yields Euler's equation of motion for a non-viscous fluid in the scalar form:

X -/

$$X - \frac{1}{\rho}\frac{\partial p}{\partial x} = \frac{\partial u}{\partial t} + \frac{\partial u}{\partial x}.u + \frac{\partial u}{\partial y}.v + \frac{\partial u}{\partial z}.w \qquad (2.11a)$$

$$Y - \frac{1}{\rho}\frac{\partial p}{\partial y} = \frac{\partial v}{\partial t} + \frac{\partial v}{\partial x}.u + \frac{\partial v}{\partial y}.v + \frac{\partial v}{\partial z}.w \qquad (2.11b)$$

$$Z - \frac{1}{\rho}\frac{\partial p}{\partial Z} = \frac{\partial w}{\partial t} + \frac{\partial w}{\partial x}.u + \frac{\partial w}{\partial y}.v + \frac{\partial w}{\partial z}.w \qquad (2.11c)$$

The right hand side represents the total acceleration components, $\frac{du}{dt}$, $\frac{dv}{dt}$ and $\frac{dw}{dt}$, respectively, p is the pressure at the point under consideration, X, Y and Z are body force components given by:

$$X = -\frac{\partial \Omega}{\partial x}, \quad Y = -\frac{\partial \Omega}{\partial y}, \quad Z = -\frac{\partial \Omega}{\partial z}$$

and $\Omega = gh$ is the body force potential, with respect to some selected datum level, of a unit mass located at a height h above the datum. Upon integrating equations (2.11) along a streamline and simplifying, one obtains the Bernoulli equation:

$$\frac{q^2}{2} + \frac{p}{\rho} + gh = \bar{H} \qquad (2.12a)$$

where $\bar{H}$ is constant along a streamline and q^2 is the square of the speed, i.e.:

$$q^2 = u^2 + v^2 + w^2$$

In addition, if the flow is irrotational, equation (2.12a) becomes:

$$\frac{q^2}{2} + \frac{p}{\rho} + gh = H \qquad (2.12b)$$

where H is a constant for any point in the flow.

<u>Kinetic Energy E for Irrotational Flow of an Incompressible Fluid</u>

The kinetic energy for incompressible fluid is [18]:

$$E = \frac{\rho}{2}\iiint_{V} q^2 \, dV \qquad (2.13a)$$

or/

or
$$E = \frac{\rho}{2}\iiint_{\forall} (\nabla\phi)(\nabla\phi)\,.\,d\forall \qquad (2.13b)$$

for an irrotational flow and by using GREEN'S THEOREM:

$$\iiint_{\forall} (\nabla\phi)(\nabla\phi)\; d\forall = -\iiint_{\forall} \phi.\nabla^2\,\phi.d\forall + \iint_{\Gamma} \phi\,\frac{\partial\phi}{\partial n}\,dA$$

and the fact that $\nabla^2\,\phi = 0$, the kinetic energy for an irrotational flow can be written as:

$$E = \frac{\rho}{2}\iiint_{\forall} q^2 \cdot d\forall = \iint_{\Gamma} \phi\,\frac{\partial\phi}{\partial n}\,dA \qquad (2.14a)$$

as shown in [14] pp 47-48 and [29] p 293, or for two-dimensional flow, as:

$$E = \frac{\rho}{2}\iint_{A} q^2 \cdot dA = \frac{\rho}{2}\cdot\oint_{c} \phi\,\frac{\partial\phi}{\partial n}\cdot ds \qquad (2.14b)$$

Equations (2.14) imply that the kinetic energy in the entire flow region is equal to the work done by the impulsive pressure in starting the motion from rest [18] p 93.

Pressure Coefficient Cp

The pressure coefficient Cp may be defined mathematically as:

$$Cp = \frac{P - Patm}{\frac{1}{2}\cdot\rho\cdot q_d^{\,2}} \qquad (2.15a)$$

where q_d is the asymptotic speed and Patm is the atmospheric pressure. Upon applying the Bernoulli equation (2.12b) to equation (2.15a) and simplifying for the case g = 0, one achieves the result:

$$Cp = 1 - \left(\frac{q}{q_d}\right)^2 \qquad (2.15b)$$

where/

where q represents the speed at the point under consideration.

2. Variational Principle

For many boundary value problems, two equivalent alternative formulations exist. In the first, a partial differential equation is written and its direct solution is attempted. In the second, the aim is to find a function (or functions) minimising a functional which is characteristic of the problem under consideration. In the past two decades since the advent of high speed digital computers, the latter approach has been quite extensively used in the fields of structural and continuum mechanics. Important variational principles such as least work, minimum strain energy, minimum potential energy, minimum complementary energy and Reissner's variation theorem of elasticity, have been well developed in the past and are documented in standard text books (see, for instance, the books by Wang [19], Langhaar [20], Sokolnikoff [21]). However, similar variational principles applicable to fluid-mechanics problems have not yet been so well developed, in fact, calculus of variations has only been infrequently used in this field. In the past, most use has been made in the "classical sense" for parameter optimisation. For example, shapes producing minimum drag, bodies inducing maximum lift and designs for optimum thrust are all problems involving the optimisation of various parameters appearing in functionals. Nevertheless, owing to the availability of large digital computers, the use of variational principles to solve the basic equations of motion for fluid flow is increasing gradually, even though these equations are essentially non-linear (this holds regardless of whether or not viscosity and compressibility/

compressibility effects are included) and the formulation of these problems is not easy in general.

Although not so well documented in standard texts, most variational principles applicable to fluid-mechanics problems can be found in recently published papers, due to the successful research in the area by Garabedian and Spencer [22] and others (see Whalen's Survey on these principles [23]). Some of the better known principles appearing in Whalen's report include: (1) The principle for incompressible laminar flows presented by Delleur and Sooky [24], (2) Eckart's principle [25], based on a Lagrangian co-ordinate system, for the Lagrangian equations of the motion of an incompressible frictionless fluid, and (3) The principle introduced by Bateman [26], based on the local pressure function, for subsonic flow fields. A more general principle for the flow of a viscous incompressible fluid, which includes the convective terms and covers both time dependent and time independent phenomena, has been recently presented by Lemieux, Unny and Dubey [27].

Among the forementioned variational principles for fluid flows, none is especially suitable for the present study due to either the complexity of application or the lack of relevance to the flows under consideration, that is, irrotational flows of an ideal fluid.

Following a brief review and introduction to some basic ideas of the calculus of variations, variational principles for such flows, either two-dimensional or axi-symmetric, will be developed with derivations leading to their equivalent partial differential equations and associated boundary conditions.

Brief Review on Calculus of Variations/

Brief Review on Calculus of Variations

A fundamental problem in differential calculus is extremising (maximising or minimising) a function f(x) for a range of the independent variable x. The problem in variational calculus is also extremisation; however, it is concerned chiefly with the extremisation of a functional, hence the determination of functions rather than points. The two branches are related in that both are concerned with an extremum; one deals with number spaces and the other deals with function spaces (Courant and Hilbert [28]).

In variational problems a functional which is characteristic of the problem is first formed in terms of a function (or functions). Then variations of this functional are investigated with a view to extremising the functional. In some cases this approach results in a closed form, exact solution. But usually the problem must be solved by an approximate method. One such method is the Rayleigh-Ritz method. This approach, however, is still preferable to the direct application of finite difference techniques to solve the differential equation with its associated boundary conditions, because the functional can often be used to ensure convergence of the approximate solution.

A simple example of variational calculus is the problem of finding the plane curve joining two points (x_1, y_1) and (x_2, y_2) which has the shortest length. The solution sought here is the function y(x) describing the curve of shortest length; the corresponding functional is the length of the curve given by:

$$I(y) = \int_{x_1}^{x_2} \sqrt{1 + \left(\frac{dy}{dx}\right)^2}\, dx$$

Using/

Using method of variation of calculus implies that of all the curves:

$$Y(x) = y(x) + \varepsilon n(x)$$

which pass through the given end points, the shortest one y(x) must be selected. The problem thus reduces to finding the function y(x) that makes the integral I(y) a minimum.

Generally, in order to minimise the integral

$$I(y) = \int_{x_1}^{x_2} F(x, y, y') \, dx \qquad (2.16a)$$

where $y' = \frac{dy}{dx}$, the function y(x) must satisfy the boundary conditions and the Euler differential equation ([28] pp 184-187):

$$\frac{\partial F}{\partial y} - \frac{d}{dx} \cdot \left(\frac{\partial F}{\partial y'}\right) = 0 \qquad (2.16b)$$

The previous result can be extended to several dependent and independent variables. For example, in order to minimise the integral:

$$I(\phi) = \iint_A F(x, y, \phi, \phi_{,x}, \phi_{,y}) \, dx . dy \qquad (2.17a)$$

in which $\phi_{,x}$ and $\phi_{,y}$ are the partial derivatives of ϕ with respect to x and y respectively, the function ϕ must satisfy the Euler differential equation:

$$\frac{\partial F}{\partial \phi} - \frac{\partial}{\partial x} \left(\frac{\partial F}{\partial \phi_{,x}}\right) - \frac{\partial}{\partial y} \left(\frac{\partial F}{\partial \phi_{,y}}\right) = 0 \qquad (2.17b)$$

in addition to the boundary conditions ([28], pp 191-193)

Of/

Of all irrotational motions of an ideal fluid described by velocity potential functions ϕ_n and which satisfy specified values on the boundaries, the actual state satisfying continuity and specified normal velocity boundary conditions $(\phi,n)^a$ is such that the integral:

$$I(\phi) = \frac{\rho}{2}\iiint_{V}\left[(\phi,x)^2 + (\phi,y)^2 + (\phi,z)^2\right] dV - \rho\iint_{\Gamma}\phi\,.(\phi,n)^a\, dA \tag{2.18}$$

is a minimum, where V is the entire flow region and Γ is the portion of the surface on which the normal velocity components $(\phi,n)^a$ are specified.

Equation (2.18) is an expression related to the energy of the fluid motion since the first term is the kinetic energy and the second term represents twice the amount of the work done by the impulsive pressure in starting motion from rest (see equation (2.14)).

This equation can be simplified to give:

$$I(\phi) = \frac{\rho}{2}\iint_{A}\left[(\phi,x)^2 + (\phi,y)^2\right] dx.dy - \rho.\oint_{c}.\phi.(\phi,n)^a\, ds \tag{2.19a}$$

for two-dimensional flow, and

$$I(\phi) = \rho.\pi\iint_{A}\left[\phi,x^2 + \phi,r^2\right]\, r.dr.dx - 2.\rho.\pi\oint_{c}.\phi.(\phi,n)^a\, r.ds \tag{2.19b}$$

for axi-symmetric flow.

Again A represents the entire flow region under study (for axi-symmetric flow, A is a meridian plane) and c is the portion of the boundary on which normal velocity components are specified.

Next/

Next it will be shown that equations (2.19) are equivalent to their corresponding partial differential equations and associated natural boundary conditions. Equation (2.19a) will be treated first and will then be followed by operations on equation (2.19b).

Two-Dimensional Functional

By adding an infinitesimal increment $\delta\phi$ to the function ϕ, equation (2.19a) can be written as:

$$I(\phi + \delta\phi) = \frac{\varrho}{2} \iint_A \left\{ [\phi,x + (\delta\phi),x]^2 + [\phi,y + (\delta\phi),y]^2 \right\} dx.dy$$

$$- \varrho \oint_c (\phi + \delta\phi)(\phi,n)^a . ds$$

$$= \frac{\varrho}{2} \iint_A \left[(\phi,x)^2 + (\phi,y)^2\right] dx.dy - \varrho \oint_c \phi.(\phi,n)^a . ds$$

$$+ \varrho \iint_A \left[\phi,x\ (\delta\phi),x + \phi,y\ (\delta\phi),y\right] dx.dy - \varrho \oint_c \delta\phi.(\phi,n)^a\ ds$$

$$+ \frac{\varrho}{2} \iint_A \left[(\delta\phi),x^2 + (\delta\phi),y^2\right] dx.dy$$

$$= I(\phi) + \delta I(\phi) + \text{higher order terms}$$

To minimise $I(\phi)$, a necessary condition is the vanishing of the first variation of $I(\phi)$, which is $\delta I(\phi)$. The requirement is therefore:

$$\iint_A \left[\phi,x.(\delta\phi),x + \phi,y.(\delta\phi),y\right] dx.dy - \oint_c \delta\phi.(\phi,n)^a . ds = 0$$

This equation, upon integrating by parts and rearranging, becomes:

$$\iint_A (\phi,xx + \phi,yy)\ \delta\phi.dx.dy - \oint_c \phi,x.\delta\phi.dy + \oint_c \phi,y.\delta\phi.dx$$

$$+ \oint_c (\phi,n)^a . \delta\phi.ds = 0$$

The/

The second and third terms in the previous equation are equivalent to an integration along a curve as shown by using the co-ordinate transformation depicted in FIG. 12 where:

$$n = x.\cos\Theta + y.\sin\Theta$$

$$s = -x.\sin\Theta + y.\cos\Theta$$

$$dx = -\sin\Theta . ds$$

$$dy = \cos\Theta . ds$$

By doing so, the previous equation becomes:

$$\iint_A (\phi,xx + \phi,yy)\ \delta\phi.dx.dy - \oint_c \left[\phi,n - (\phi,n)^a\right]\delta\phi.ds = 0$$

Since $\delta\phi$ is arbitrary and non-zero, it follows that:

$$\phi,xx + \phi,yy = 0 \quad \text{in the flow region A} \qquad (2.20)$$

with $\phi,n = (\phi,n)^a$ or $q_n = (q_n)^a$ on c

which is equivalent to a minimisation of the functional $I(\phi)$.

<u>Axi-symmetrical Functional</u>

To derive the partial differential equation with its associated boundary condition for axi-symmetric flow from equation (2.19b) the same procedure will be followed, except that cylindrical co-ordinates x and r must be used in place of the co-ordinates x and y. Given an infinitesimal increment $\delta\phi$ to ϕ, equation (2.19b) becomes:

$$I(\phi + \delta\phi) = \rho.\pi\iint_A\left\{\left[\phi,x + (\delta\phi),x\right]^2 + \left[\phi,r + (\delta\phi),r\right]^2\right\} r.dr.dx$$

$$- 2.\rho.\pi.\oint_c (\phi + \delta\phi)(\phi,n)^a\ r\ ds$$

Imposing the requirement that the first variation of $\delta I(\phi)$

must/

COORDINATE TRANSFORMATION.

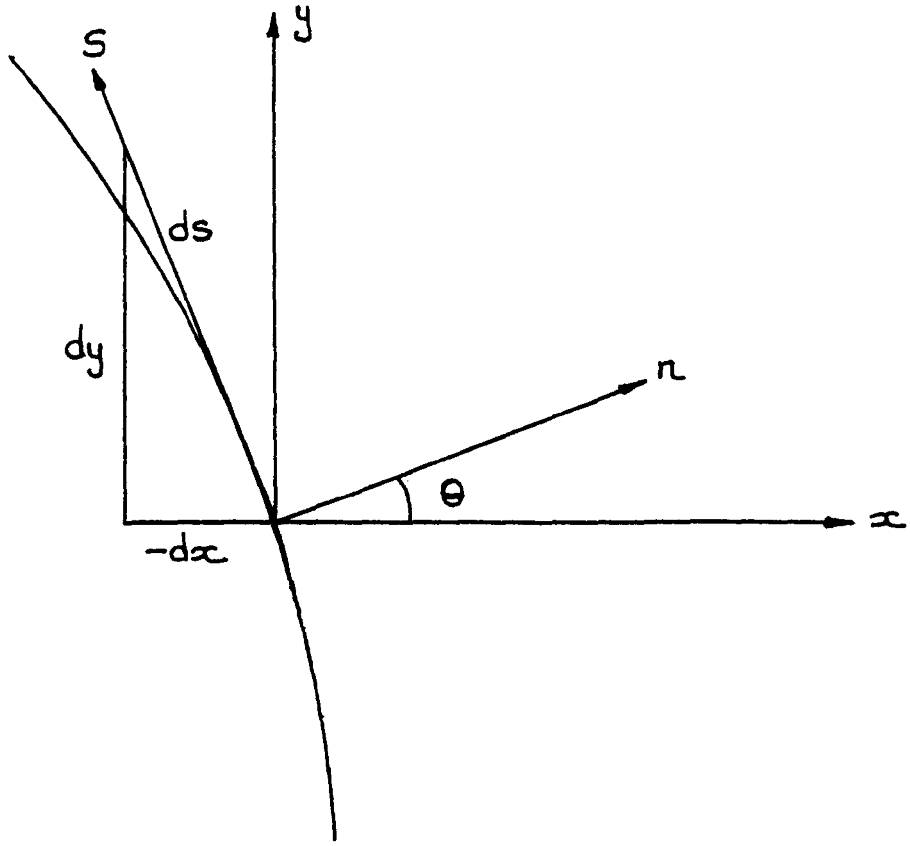

FIGURE 12.

must vanish, yields:

$$\iint_A \left[\phi_{,x} \, (\delta\phi)_{,x} + \phi_{,r} \, (\delta\phi)_{,r} \right] r . dr . dx - \oint_c \delta\phi \, (\phi_{,n})^a \, r . ds = 0$$

Integrating by parts and performing a co-ordinate transformation then yields a line integral and the previous equation becomes:

$$\iint_A \left[r\phi_{,xx} + \phi_{,r} + r\phi_{,rr} \right] \delta\phi . dr . dx - \oint_c \delta\phi_{,n} - \{\phi_{,n} - (\phi_{,n})^a \left.\right] r . d\phi . ds = 0$$

Again, since $\delta\phi$ is arbitrary and not equal to zero, the necessary conditions for the above equation to be valid are that the terms in brackets must simultaneously be equal to zero, or:

$$\phi_{,xx} + \frac{1}{r}\phi_{,r} + \phi_{,rr} = 0 \quad \text{in the flow region A} \qquad (2.21)$$

with $\phi_{,n} = (\phi_{,n})^a$ or $q_n = (q_n)^a$ on c

Equation (2.20) and equation (2.21) could also have been obtained directly by applying the Euler differential equation (2.17b) to equations (2.19)

When the stream function ψ is alternatively used as the primary unknown, the corresponding functionals would be:

$$I(\psi) = \frac{\rho}{2}\iint_A \left[(\psi_{,x})^2 + (\psi_{,y})^2 \right] dx . dy - \rho . \oint_c \psi . (\psi_{,n})^a ds \qquad (2.22a)$$

for two-dimensional flow, and

$$I(\psi) = \rho . \pi \iint_A \left[(\psi_{,x})^2 + (\psi_{,r})^2 \right] \frac{1}{r} \, dr . dx - 2 . \rho . \pi \oint_c \psi \, (\tfrac{1}{r}\psi_{,n})^a \, ds$$

(2.22b)

for axi-symmetric flow.

Equation (2.22a) is equivalent to:

$\psi_{,xx}$/

$$\psi_{,xx} + \psi_{,yy} = 0 \quad \text{in } A \tag{2.23}$$

with $\psi_{,n} = (\psi_{,n})^a$ or $q_s = (q_s)^a$ on C

while for axi-symmetric flow, equation (2.22b) is equivalent to:

$$\psi_{,xx} - \frac{1}{r} \cdot \psi_{,r} + \psi_{,rr} = 0 \quad \text{in } A \tag{2.24}$$

with $\frac{1}{r}\ \psi_{,n} = (\frac{1}{r} \cdot \psi_{,n})^a$ or $q_s = (q_s)^a$ on C

Equation (2.22a) is just as useful as equation (2.19a) in two-dimensional analysis. However, for axi-symmetric analysis, equation (2.22b) is not so useful as equation (2.19b) because the radial co-ordinate r appears in the denominator of the first integral of equation (2.22b). To evaluate this integral, it is necessary to resort to numerical integration.

3. Finite Element Analysis and the Ritz Technique

The development of finite element analysis techniques originated from the classical approaches to structural analysis (Turner, Clough, et al. [30]). Following the rapid development of large digital computers in the past two decades, this method was extensively investigated in the area of structural and continuum mechanics, (Zienkiewicz and Cheung [31]) and then was applied to other branches of fluid problems (e.g. Zienkiewicz and Cheung [32], Zienkiewicz, Mayer and Cheung [33], Finn [34]). The finite element method has several outstanding advantages. These are the following:

i. Non-homogeneous and anisotropic configurations can be treated with relative simplicity.

ii. The elements can be graded in shape and size to follow boundaries of arbitrary shape.

iii./

iii. Once a computer program has been developed, problems of the same kind can be solved simply by supplying the computer with appropriate data.

The finite element method, when applied to fluid flow problems, generally consists of the following steps:

i. The entire flow region under study is divided into a series of subregions or elements assumed to be interconnected at a finite number of nodal points, thus a problem originally possessing an infinite number of degrees of freedom is made finite. In the finite element approach, both free surface and curved solid boundaries can be accounted for. Although this discretisation would make a curved boundary appear to have some singular points, the velocities at these points are kept finite because of the approximate nature of the solution.

ii. A certain simple function pattern, depending on the nodal values of the unknown function, is specified. In this study, the function pattern chosen is the velocity potential. This function pattern is then used to formulate a functional which is characteristic of the problems under study.

iii. All the elements are assembled with boundary conditions taken into account and the Ritz technique is applied to obtain a system of simultaneous equations. This system of equations is then solved to obtain the nodal unknowns.

iv. Finally, all the related physical properties, such as velocity, pressure and force on boundaries, are evaluated from the known nodal values.

Ritz Technique 37 /

Ritz Technique [37]

One general method for obtaining solutions to problems expressed in variational form is known as the Ritz method. Actually, the finite element method is a special case of the Ritz method where the interpolation functions obey certain continuity requirements.

The Ritz method consists of assuming the form of the unknown solution in terms of known functions (trial functions) with unknown adjustable parameters. (The trial functions are sometimes called co-ordinate functions). From the family of trial functions we select the function which renders the functional stationary. The procedure is then to substitute the trial functions into the functional and thereby express the functional in terms of the adjustable parameters. The functional is then differentiated with respect to each parameter and the resulting equation is set to zero. If there are n unknown parameters, there will be n simultaneous equations to be solved for these parameters. By this means, the approximate solution is chosen from the family of assumed solutions.

The procedure does nothing more than give us the "best" solution from the family of assumed solutions. Clearly, then, the accuracy of the approximate solution depends on the choice of trial functions.

Often a family of trial functions is constructed from polynomials of successively increasing degree. In this study, polynomials of degree two have been chosen.

Generally in this technique, we require that the trial functions be defined over the whole solution domain and that they satisfy at least some and usually all of the boundary conditions, whereas/

whereas in the finite element method, the trial functions chosen are not defined over the whole solution domain and they do not have to satisfy boundary conditions, but only certain continuity conditions. Because the Ritz method uses functions defined over the whole domain, it can be used only for domains of relatively simple geometric shape. In the finite element method the same geometric limitations exist, but only for the elements. Since elements with simple shapes can be assembled to represent exceedingly complex geometries, the finite element method is a far more versatile tool than the Ritz method.

For example, considering only a two-dimensional domain, the technique leads to a relative minimisation procedure of the functional

$$I(\phi) = \iint_A F(x,\ y,\ \phi,\ \phi,x,\ \phi,y)\ dx.dy$$

by selecting an appropriate trial family of solutions

$$\phi n = \sum_{i=1}^{n} \phi i \,.\, \gamma i\ (x,\ y)$$

where ϕi and γi are the undetermined parameters and the co-ordinate functions respectively. As before, the relative minimisation is accomplished by setting the first partial derivatives of the functional $I(\phi)$, with respect to the undetermined parameters equal to zero. Application of this procedure results in a system of symmetric linear equations which enables one to obtain the "best" approximation to the true solution out of all the possibilities offered by the trial family.

4. Fluid Flow With a Free Surface/

4. Fluid Flow With a Free Surface

Fluid flow problems involving a free surface are more difficult to analyse because the free surface location is initially unknown and two boundary conditions are to be satisfied concurrently. Analysis is much simpler with an initially known boundary since only one boundary condition, concerning either the normal velocity component or the velocity potential function itself, has to be imposed. The two boundary conditions to be specified on a free surface are:

i. The normal velocity component is zero.

ii. The pressure should be constant, as it is exposed to the atmosphere.

This requirement will lead to the specification of velocity potential values at all nodal points on the free surface according to the following reasoning.

By the Bernoulli equation, equation (2.12b), for any two points on the free surface there exists:

$$\frac{1}{2} \cdot q_i^{\;2} + \frac{P_i}{\rho} + gy_i = \frac{1}{2} \cdot q_d^{\;2} + \frac{P_d}{\rho} + gy_d$$

where "i" represents any point on the free surface and "d" designates the reference point, which, for convenience, is chosen as the far downstream point on the free surface. Gravity is acting downwards and y is measured upwards from a chosen datum. Since, in this work the fluid density ρ is assumed to be constant, the requirement of constant pressure leads to a cancellation of the pressure terms and the above equation becomes:

$$\frac{1}{2}\, q_i^{\;2} + gy_i = \frac{1}{2}\, q_d^{\;2} + gy_d$$

hence:/

hence: $$q_i = \sqrt{q_d^2 - 2g\,(y_i - y_d)} \qquad (2.25a)$$

Equation (2.25a) states that the flow speed at any point i on the free surface can be calculated from a knowledge of the reference speed and the difference in y-co-ordinates between these two points. Assuming that the speed between two adjacent nodal points i and j varies linearly, as shown in FIG. 13, one obtains:

$$q = q_j + \frac{(q_i - q_j)}{s} \cdot s$$

(Note: This assumption is consistent with the approximate velocity potential, which is a second order polynomial).

Since equation (2.4a) states that $q = \frac{\partial \phi}{\partial s}$, ϕ on the free surface must be:

$$\phi = \int q \cdot ds = q_j \cdot s + \frac{(q_i - q_j)}{2\Delta s} \cdot s^2 + c$$

By substituting $\phi_{s=0} = \phi_j$ and $\phi_{s=\Delta s} = \phi_i$ into the above equation, the relationship between the values ϕ_i and ϕ_j of two adjacent nodal points is found to be:

$$\phi_j = \phi_i - \frac{(q_i + q_j)}{2} \cdot \Delta s \qquad (2.26a)$$

where q_i and q_j are given by equation (2.25a).

If gravitational effects are neglected (i.e. $g = 0$), equations (2.25a) and (2.26a) become, respectively:

$$q_i = q_d \quad \text{i.e. constant velocity along the free streamline} \qquad (2.25b)$$

and $$\phi_j = \phi_i - (q_d \cdot \Delta s) \qquad (2.26b)$$

Equations (2.26) show how nodal values of ϕ must be specified on the free surface to satisfy the constant pressure requirement.

This/

LINEAR VARIATION OF SPEED BETWEEN TWO ADJACENT POINTS ON THE FREE-SURFACE

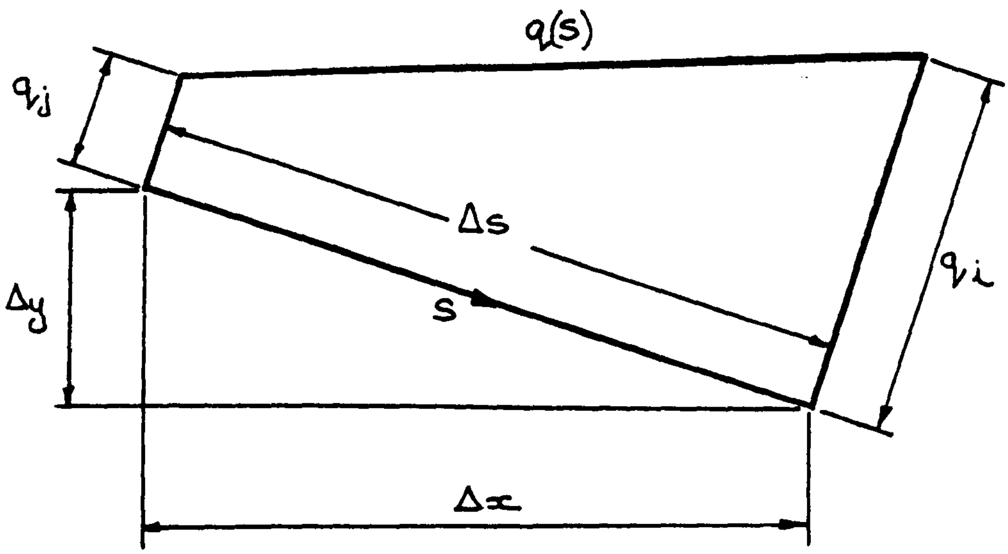

FIGURE 13.

This is a Neumann type problem incorporating Neumann boundary conditions in terms of $\frac{d\phi}{dn}$. On the boundaries, $\frac{\partial \phi}{\partial n} = 0$, or $\frac{\partial \phi}{\partial n} \neq 0$, and non-unique boundary conditions arise. For this reason, when the solution domain is discretised and the element equations formulated and assembled, the system matrix is non-singular. A suitable solution procedure is therefore required to remove this non-singularity [37].

To overcome this difficulty, a value of ϕ is specified for one arbitrarily selected node. (In the present work, a value of 100 was assigned to the nodal point furthest from the orifice). This is essentially the imposition of a Dirichlet boundary condition at this node, with the effect, when incorporated in the computer program, of removing the singularity.

With the singularity removed, the nodal values to be specified on the free surface are computed according to equations (2.26a) or (2.26b), proceeding upstream to the node at the lip. The solution then proceeds as usual

To satisfy the zero normal velocity requirement, the free surface location must be a streamline. This goal is achieved approximately by fitting a series of curves, each of which is chosen to be a second order polynomial, passing through three consecutive nodal points. Each curve has slopes at these three nodal points equal to the values defined by the computed velocity components, as shown in FIG. 14.

In this way, the difference in y-ordinates between two corner nodes of a quadrilateral element is given by:

$$\Delta y_i = (s_i + s_{i+1} + s_{i+2}) . \Delta x_i / 6 \tag{2.27a}$$

where/

SKETCH SHOWING HOW THE FREE-SURFACE LOCATION SHOULD BE ADJUSTED.

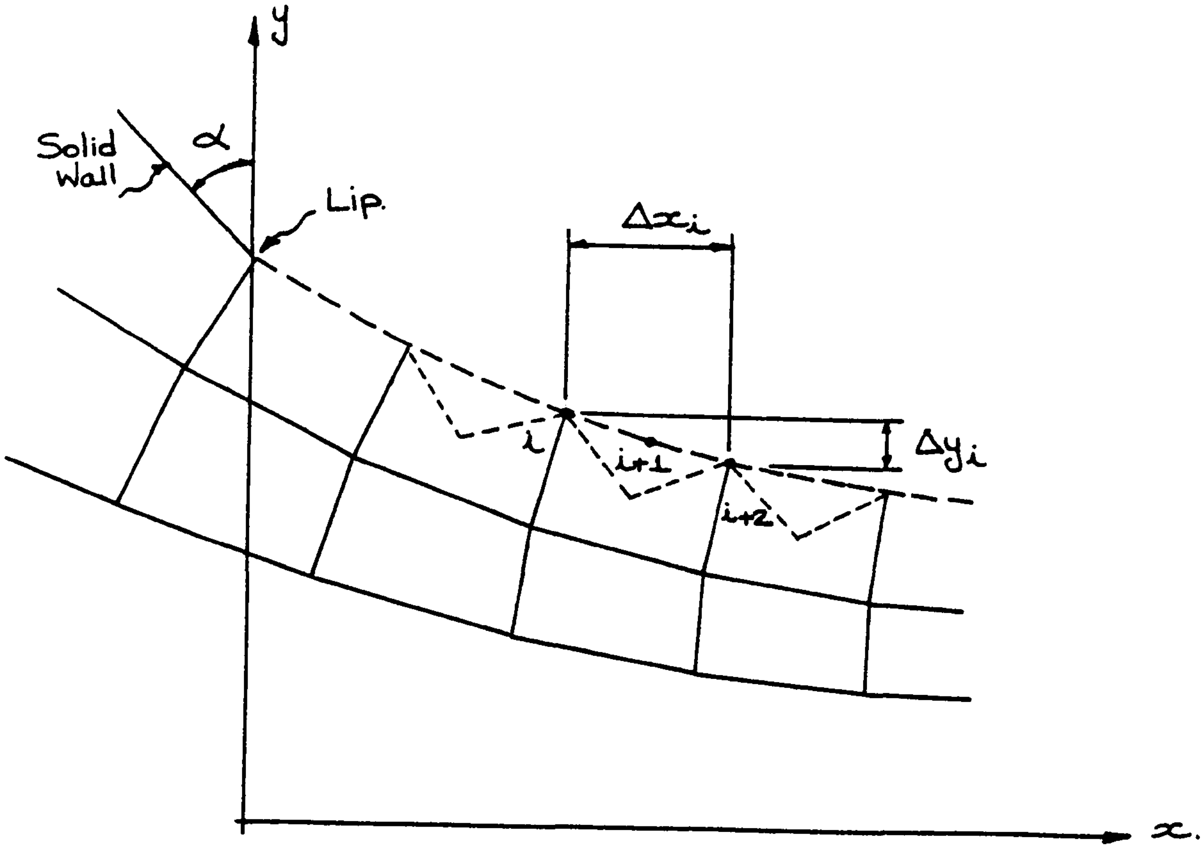

DIAGRAM SHOWN, USES A NOZZLE AS AN EXAMPLE.

FIGURE 14.

where $\quad sk = \frac{Vk}{Uk} \quad (k = i, i + 1, i + 2)$

and $\quad Vk =$ local velocity in y direction

$\quad Uk =$ local velocity in x direction.

With Δy_i known for each quadrilateral element, the locations of all the corner nodes can be determined sequentially, starting from the node at the lip. In the case where the local slope of the lip is vertical or close to vertical, equation (2.27a) can no longer be applied to estimate Δy_i. This occurs because $s_i = V_i/U_i$ may be excessively large when U_i is very small. Hence, a modified equation for this particular curve segment must be used, that is:

$$y_i = 6.\Delta x_i/(s_1 + 4s_2 + s_3) \tag{2.27b}$$

where s_i is equal to $-\tan\alpha$, α being the acute angle between the wall and the y axis and $s_2 = U_2/V_2$, $s_3 = U_3/V_3$, respectively. This equation is obtained by expressing x as a second order polynomial in y and then fitting a curve having slopes s_1, s_2 and s_3 at three nodal points.

The two requirements are incorporated in the computer program and satisfied alternatively by an iterative scheme. For a particular problem, the solution sequence begins with an assumed initial free surface location, with its values specified in accordance with equation (2.26) to satisfy the constant pressure requirement and leaving the requirement of zero normal velocity component initially unsatisfied.

The assumed free surface location is simply a convenient broken line and no special care is required in its selection. However,/

However, experience shows that it is a little better to assume a lower initial free surface to accelerate the convergence. The entire system of equations is solved first, then the velocity components for each node on the free surface are calculated by considering only the contributions from those triangles having one side in common with the free surface, as endorsed by broken lines in FIG. 13. This scheme was chosen because it saves computation time and also achieves higher accuracy.

This is so since the velocities so evaluated are based on the velocity potential values on and close to the free surface. The curve fitting scheme described by equation (2.27), is then applied to find a new free surface satisfying the zero normal velocity condition to conclude the computation cycle. With this "improved" free surface location (in the overall sense) the above procedures are repeated until a prescribed error criterion is satisfied.

Examples incorporating free surface procedure are shown in APPENDIX B.

CHAPTER III

EXPERIMENTAL PROCEDURE

CHAPTER III

EXPERIMENTAL PROCEDURE

1. Introduction

2. Development of Measurement Techniques

3. (a) Calibration Procedure

   (b) Static Procedure

   (c) Dynamic Procedure

4. Method of Analysing Experimental Results

1. Introduction

Tests carried out in this report are a continuation of the work carried out by Brown and Lough [35] on the response of disc valves to rapid pressure changes as applied in a shock tube. The present investigation is concerned with conditions more relevant to those obtained in a compressor [36]. It consists of dynamic and force measurements on disc valves. The "static" method of analysis (adopted in this work) has been widely accepted by many researchers, among them Wambsganss [1] and MacLaren [2]. The "dynamic" method reported here is believed to be new and it is hoped that this investigation will add to existing information on the many types of automatic valves.

The Chapter begins with the background of development techniques used prior to those finally reported in this study and the reasons appertaining to their discontinuation. It then goes on to explain in detail the experimental procedures used in carrying out the static and dynamic tests and the corresponding calibration tests. Finally, the method used in analysing the experimental results obtained (photographs) is discussed briefly.

During these tests, two different sizes of disc valves were used, these being:

a. 6.35 mm bore valve seat ($\frac{1}{4}$")/9.525 mm O/D disc valve ($\frac{3}{8}$").

b. 6.35 mm bore valve seat ($\frac{1}{4}$")/8.41 mm O/D disc valve (0.331").

The first of these valve sizes (9.525 mm O/D) was arbitrarily chosen, the latter being sized in line with Danfoss* practice.

The/

---

* Company name.

The tests carried out on these two sizes of disc valves were identical as were the procedures used in obtaining the results.

Also during the early experimental phase, values of throat pressure were determined for various upstream pressures and displacements. These were required to enable the upstream velocity to be calculated for subsequent determination of static forces on the valve. The first set of these tests were carried out at Strathclyde University, using the 6.35 mm ($\frac{1}{4}$") bore/9.525 mm ($\frac{3}{8}$") O/D valve and secondly, (since leaving University), tests on the 6.35 mm ($\frac{1}{4}$") bore/8.410 mm (0.331") O/D valve were carried out courtesy of Sperry Gyroscope, England.

2. Development of Measurement Techniques

As can be seen from the flow chart in FIG. 15, the object is to compare force measurements in dynamic conditions with forces on the valve at corresponding pressures and displacements during steady continuous flow through the valve (FIG. 16).

The static tests were relatively simple to carry out, providing adequate pressures and displacements were set and are described in full at a later stage.

In the case of the dynamic tests, many problems were encountered. The main problem being in obtaining an adequate record/

record of pressure, displacement and force values simultaneously on the oscilloscope. This required that an initial or final condition of these parameters should be known. In the case of pressure, the initial condition with the valve closed and the cylinder pressurised, was determined by a pressure gauge and this was taken to represent the initial output of a Kistler pressure transducer. When the valve was opened, a subsequent drop in pressure was recorded on the oscilloscope from the Kistler pressure transducer. The final and intermediate values could thus be determined by using the transducer calibration.

In the case of the displacement, the initial value was zero and the final value 1.524 mm (60 thou), therefore, all intermediate values could be determined.

For dynamic force, however, the initial and final values are not so easily determinable. The range of force was between final zero force and gas shut off and initial force including a pre-load/

DEVELOPMENT OF EXPERIMENTAL MEASUREMENT TECHNIQUES.

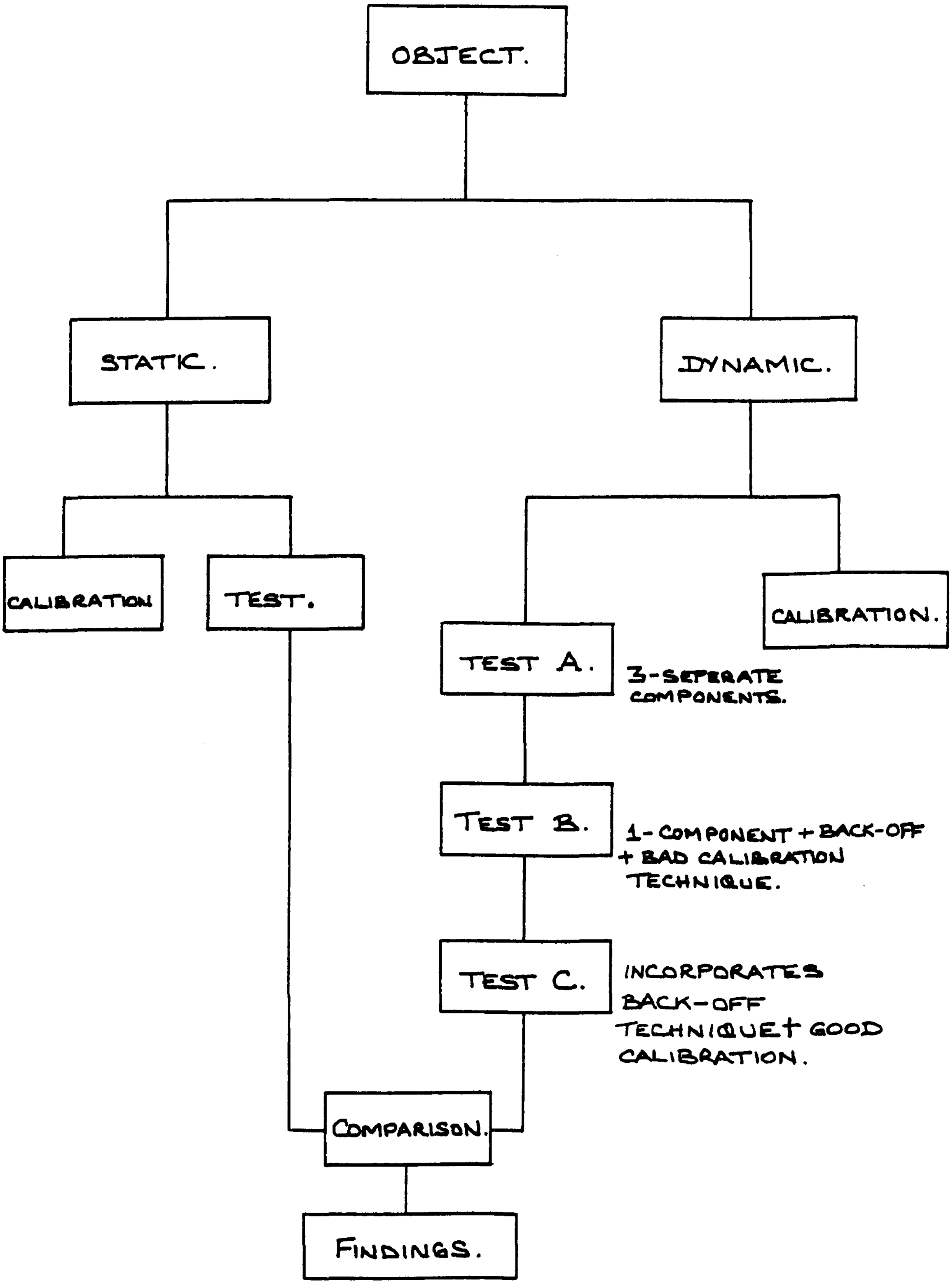

FIGURE 15.

TYPICAL DYNAMIC RECORDING.

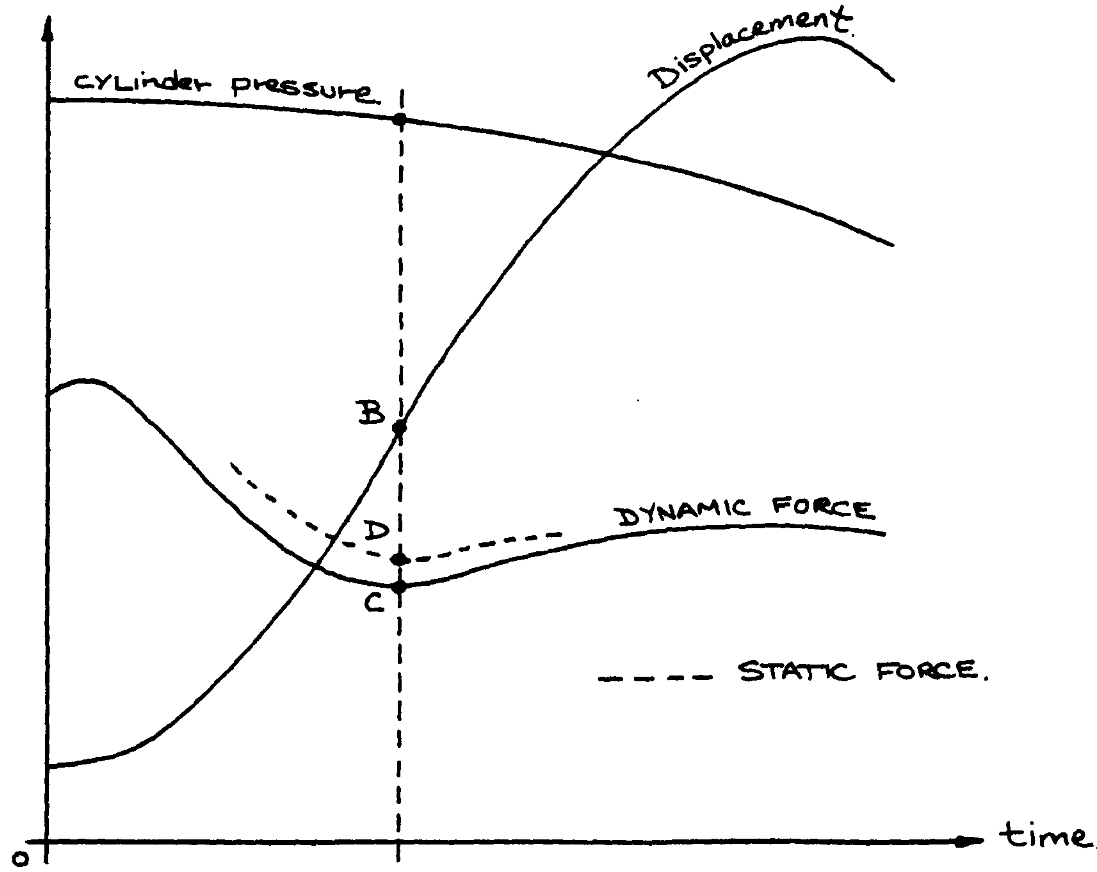

FIGURE 16

pre-load sufficient to seal the valve. To give reasonable resolution of the force trace during valve opening, the oscilloscope gain had to be high. This meant in practice that the initial force including pre-load was off-screen upwards, while final force with no gas was off-screen downwards. A technique was therefore required to enable a datum value of force to be displayed on the oscilloscope.

The first attempt was to do the dynamic tests in three separate parts as shown in FIG. 15 (TEST A). The three parts resulted in three separate photographs (FIG. 17) these showing:

A. Opening of valve.

B. Steadying off of dynamic force with gas flowing.

C. Drop to zero force from steadying off value of dynamic force (i.e. gas shut off).

Graphical combination of the three photographs gave the overall drop in dynamic force to zero and this, with the transducer calibration, allowed calculation of intermediate forces.

However, this method was open to error, since the time to complete this series of photographs was of the order of one minute and the signals recorded were therefore susceptible to temperature drift in the charge amplifier and transducer. The method was therefore discontinued and the back-off technique introduced (TEST B). This was also found insufficient due to the poor calibration technique employed and was superseded by TEST C.

The transducers calibrations were converted from volts/division to Newtons (Force) or kN/m^2 (Pressure) and computerised for subsequent calculations.

3(a) Calibration Procedure

As mentioned in FIG. 17 TEST B was modified to TEST C (FIG. 15) by calibrating/

INITIAL PROCEDURE FOR DYNAMIC FORCE GENERATION.

TEST A.

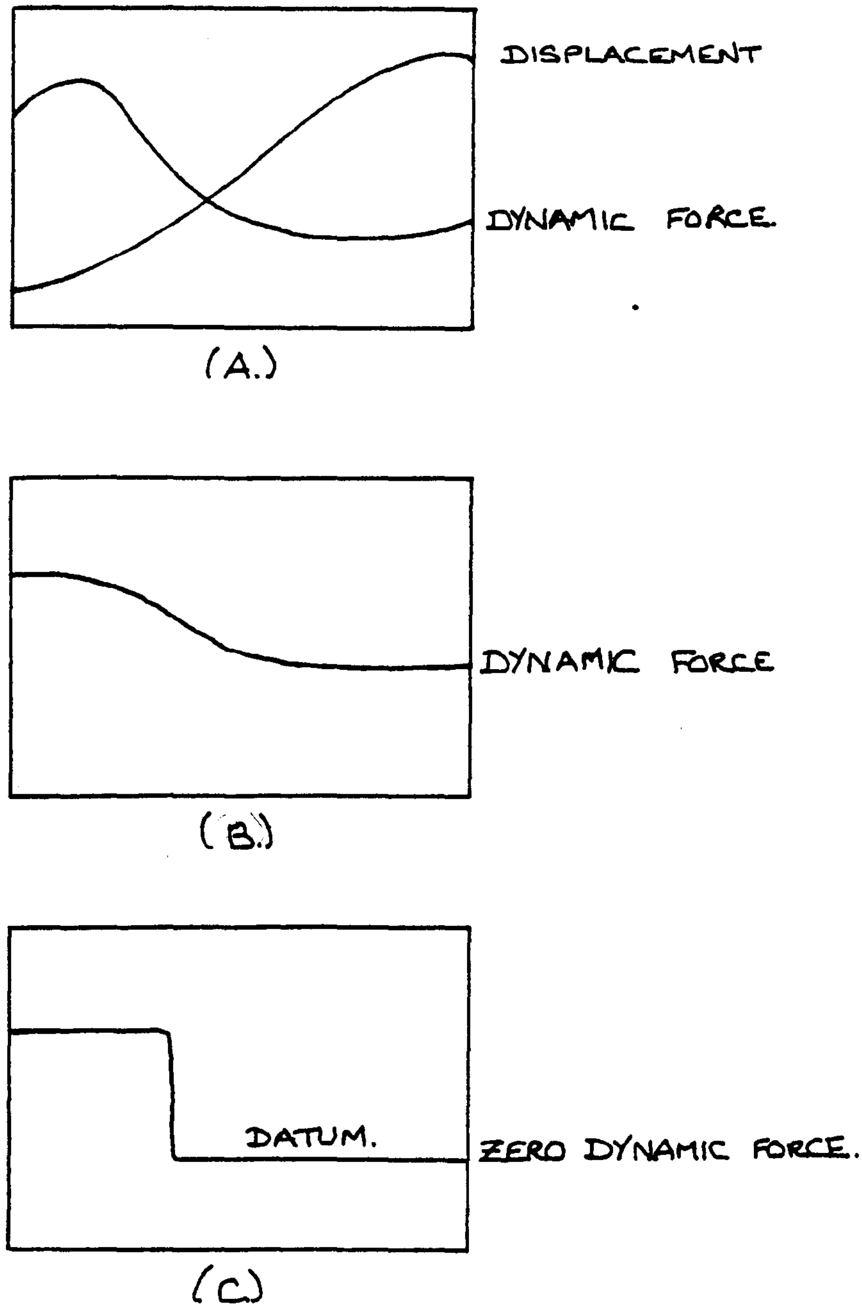

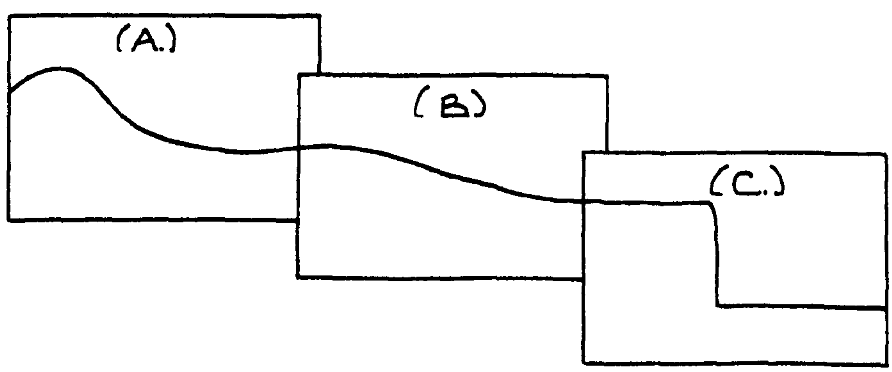

FIGURE 17

calibrating the pressure transducer against the pressure gauge before <u>and</u> after each individual test. This was found necessary since the pressure displayed on the oscilloscope was not always consistent at the beginning and end of a <u>sequence</u> of tests. Calibration of the pressure transducer against the pressure gauge was by mercury manometer. With the cylinder down (valve closed), a pressure was set on the manometer and checked with the pressure displayed on the gauge. Transducer pressure was displayed on the oscilloscope and compared. Results are as shown in TABLE 2

The force transducers were also calibrated. This was done by putting a known weight on the end face of the transducers and noting the resultant displacement on the oscilloscope. The force tests gave consistent results and were therefore only repeated after a full sequence of tests. It cannot be emphasised enough that although Kistler piezo-electric pressure and force transducers are perhaps the best obtainable, the measurements made in these tests were close to the limit of their sensitivities.

It was only by exercising the greatest possible care in ensuring that the transducers were clean, dry and free from temperature changes that it was possible to obtain consistent results.

(b) <u>Static Procedure</u>

The time constants of the charge amplifiers used during the dynamic tests were sufficiently long that steady-state measurements could be made using the same equipment. The time taken to complete one steady-state test was of the order 7 - 10 secs. This ensured the compatibility of the static test results with the dynamic results.

The/

TABLE 2

Calibration Results for Acceleration Compensated Pressure Transducer

GAUGE PRESSURE kN/m^2	MANOMETER PRESSURE kN/m^2	TRANSDUCER PRESSURE kN/m^2
13.79 (2 psig)	15.24	15.44
20.69 (3 psig)	23.79	23.51
27.58 (4 psig)	29.79	29.44
34.48 (5 psig)	37.30	37.71
41.37 (6 psig)	44.61	44.13
48.27 (7 psig)	52.40	52.00
55.16 (8 psig)	61.43	60.81
62.06 (9 psig)	67.43	67.64
68.95 (10 psig)	74.12	74.54
68.95 (10 psig)	74.26	75.50
68.95 (10 psig)	74.81	75.50
82.74 (12 psig)	88.74	89.22
82.74 (12 psig)	90.12	90.19
89.64 (13 psig)	95.84	96.12

NOTE As can be seen from above, agreement appears to exist between the pressure transducer and the manometer pressures over the range considered and hence, any further reference throughout this work to transducer pressure implies coincidence between these two sets of data.

The sequence of events to carry out these experiments began with the valve and valve seat being centralised using a circular disc as a template. This disc had, on one side, a recess which fitted over the valve face and on the other side, a protuberance which fitted the seat. The cylinder and seat could be adjusted by means of the three bottom bearings so as to enable the valve and the valve seat centres to be made co-axial. The valve and valve seat were then checked for parallelism by shining a light between the valve and the valve seat and adjusting accordingly. This adjustment was achieved by either raising or lowering the bottom plate by means of the bottom nuts.

Accurate displacement of the cylinder from the valve was achieved by incorporating two stops into the top plate (FIG. 18). For large displacements, 0.127 mm - 1.524 mm (5 - 60 thou) it was a reasonably simple matter to set the required gap. To do this, the stops were used in conjunction with the Wayne Kerr displacement meter. The valve was first closed by screwing down the stops. This displacement on the meter was then noted. The seat was then withdrawn to the required displacement by screwing back the stops, the opening process being spring assisted. This value was further checked by using feeler gauges between the valve and valve seat. It was then a simple matter to set intermediate values of displacement as required using this meter. Once the further check had been made, the stops were locked into position and rechecked.

For smaller displacements, 0.025 mm - 0.127 mm (1 - 5 thou) feeler gauges were difficult to use but since a displacement signal from the Wayne Kerr displacement meter could be displayed on the oscilloscope screen, it was possible to increase the oscilloscope gain/

ARRGT. FOR SETTING DISPLACEMENT DURING STATIC TESTS.

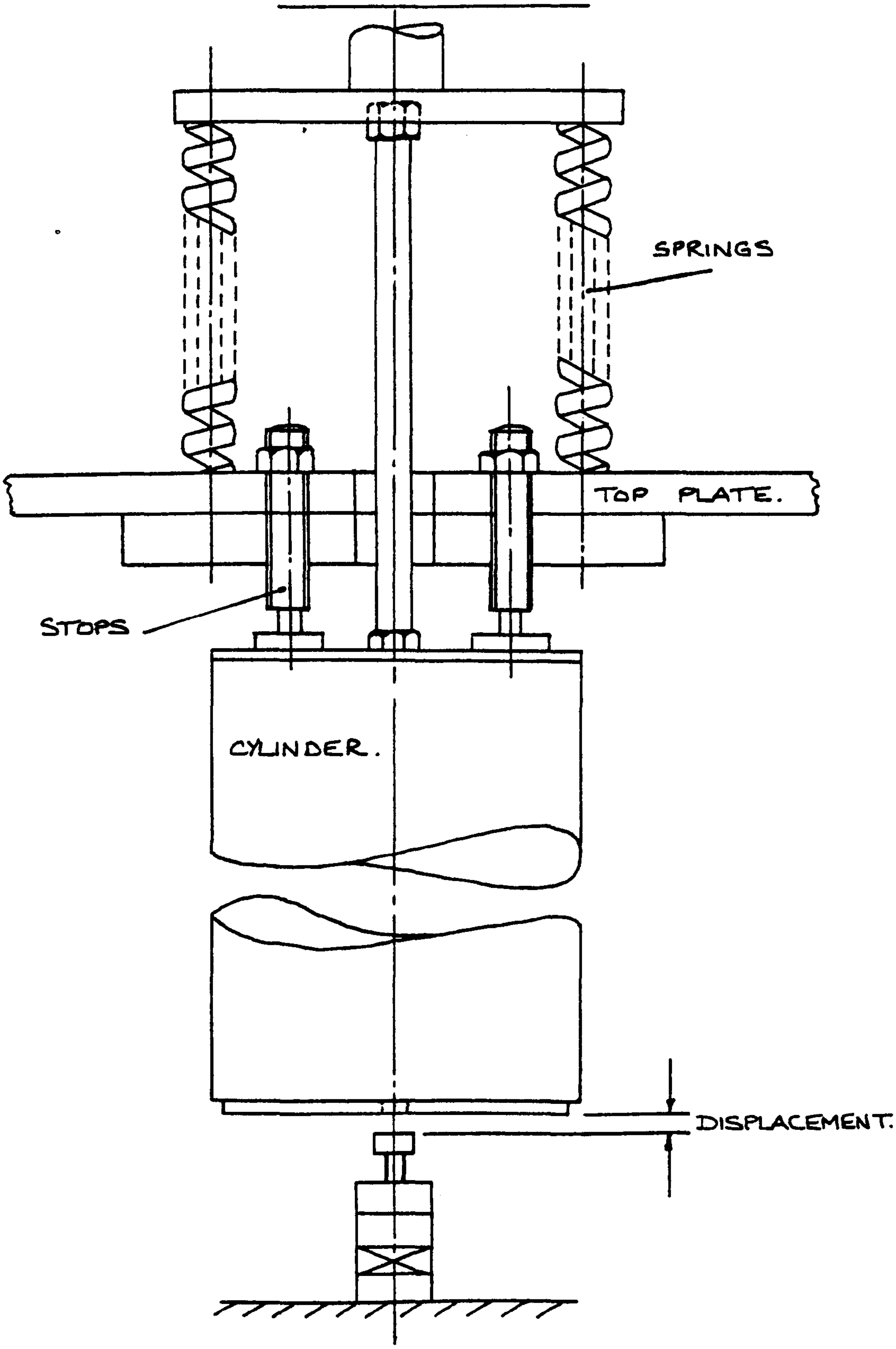

FIGURE 18

gain to enable a measure of small displacements to be seen.

The sensitivities of the transducers were then set on their respective charge amplifiers and sufficient time was allowed for them to become drift free (see CHAPTER I, Section 3b). Having ensured the required displacement was set, the test sequence was now ready to commence. The range of displacements being 0.025 mm (1 thou), 0.051 (2 thou), 0.076 (3 thou), 0.102 (4 thou), 0.127 (5 thou), 0.178 (7 thou), 0.254 (10 thou), 0.0381 (15 thou), 0.508 (20 thou), 0.762 (30 thou), 1.016 (40 thou), 1.27 (50 thou), 1.524 (60 thou).

In general, a displacement was set and maintained for a range of pressures in the cylinder. To set pressures, the solenoid valve was opened enabling air to flow through the valve. The cylinder was brought to the required pressure using the reducing valve in the air supply. The range of pressures used during these static tests were 6.895 - 82.74 kN/m^2 (1 - 12 psi) generally in steps of 13.79 kN/m^2 (2 psi).

The signal from the acceleration compensated pressure transducer was displayed on the oscilloscope screen with the force trace below it. A low speed was set on the oscilloscope time-base and the scope controls set to single shot and store. When the signals had approximately reached the centre of the screen and a steady response being achieved, the air flow was interrupted by closing the solenoid valve causing these signals to fall to zero (PHOTOGRAPH 8). The drop in pressure and force was then tabulated as in CHAPTER IV, Section 1a, using the appropriate combination of charge amplifier and oscilloscope gains and conversion terms as previously computed. During this test the oscilloscope gains for pressure and force/

force were found by trial and error to enable a suitable deflection to be shown on the screen. It should be noted that, effectively, we were calibrating the pressure gauge against the pressure transducer.

Since two different valve sizes were used, two different sets of results were obtained and are as shown graphically in CHAPTER IV, Section 1a.

(c) Dynamic Procedure

The dynamic test procedure was fairly complicated and sections of it had to be carried out extremely quickly to eliminate amplifier and transducer drift. To overcome this problem, the procedure was recorded on cassette tape and played back during the test as a check list. Accuracy of measurement was ensured by superimposing a datum force line on the stored record before and after each dynamic test as described in "Back-Off Circuit", CHAPTER I, Section 3d. The coincidence of these datum force lines demonstrated that no time-constant or other movement in the datum force signal had occurred.

As in the case of the static tests, the procedure begins with the setting of the displacement. This is done by removing the stops used during the static tests and setting the gap between the top plate and the top of the plenum chamber to 1.524 mm (60 thou) in conjunction with the Wayne Kerr displacement meter. This, as before, being checked using feeler gauges between the valve and the valve seat. The valve was then checked for parallelism and concentricity.

Prior to the actual dynamic test, a calibration test of transducer pressure was done to enable the initial value of pressure to/

to be determined. With the valve closed, air was then supplied to the plenum chamber by operating the solenoid valve. Cylinder pressure was adjusted by means of the pressure gauge and reducing valve in the air supply. Four different traces were simultaneously positioned on the oscilloscope screen these being:

a. Plenum chamber pressure.

b. Displacement of cylinder.

c. Dynamic force.

d. Pre-load (low-gain force).

As before, trial and error was required to obtain satisfactory gains to enable an adequate record for (a), (b) and (c) to be displayed on the screen. In the case of the low gain force (d) (pre-load) the main conditions to be met were that a sufficient seal was available between the valve and the valve seat to ensure impulsive start conditions and that adequate triggering of the oscilloscope on removal of the seat from the valve could be achieved. This was done by varying the rheostats A and B of the lift-off circuit till the pre-load signal was zero (i.e. leakage occurred), then increasing the pre-load sufficiently to enable adequate triggering of the oscilloscope without flooding of the oscilloscope amplifier. This was interpreted as the force line on the oscilloscope rising "X" grids from the level at which leakage was first encountered. This was found to satisfy the previously mentioned points.

The switches in the back-off circuit A, B and C were switched to "off", "normal" and "normal" positions respectively. With the valve closed, air was then pressurised within the cylinder and the charge amplifiers reset using the remote switches. The battery in the back-off voltage was inserted (switch B). This resulted/

resulted in a datum value of force being displayed and stored on the oscilloscope screen (PHOTOGRAPH 9). The next portion of the test had to be done quickly to overcome drift problems. This was the actual recording of the dynamic test. Firstly, the back-off was removed and the valve closed and with pressurised air in the cylinder, the electro-mechanical actuator was operated, thus triggering the oscilloscope. To ensure accuracy of these results a second datum-force line was applied by reinserting the back-off. The coincidence of the two datum lines indicated that no time constant effects etc were present. This completed this stage of the dynamic test. The composite oscillograph thus obtained was recorded for analysis by use of a Tektronix oscilloscope camera.

To obtain a measure of the back-off, the "measure back-off" switch was applied and the battery switch operated in an on/off mode. This resulted in a step like configuration as shown in PHOTOGRAPH 10.

To complete the dynamic test a "zero air" test as mentioned in CHAPTER I, Section 3b, was carried out to show that no "visible" acceleration was displayed on the oscilloscope before the cylinder struck the top plate (PHOTOGRAPH 6).

Finally, the calibration test for the pressure transducer was repeated to ensure initial pressure value had not varied. Further dynamic tests were then carried out to complete a range of pressures and opening times as listed in CHAPTER IV, Section 2.

Using these photographic results in conjunction was the method used in analysing these results, as outlined in Section 4 of this Chapter, graphs were drawn and are as shown in CHAPTER IV, Section/

Section 4.

4. Method of Analysing Experimental Results

In order to obtain graphs of dynamic force, pressure and displacement in their respective units, a computer program was set up to analyse the photographic results obtained in the previous tests.

From these results, graphs were drawn and are as shown in CHAPTER IV, "Experimental Results". These graphs also include static force results for direct comparison.

CHAPTER IV

EXPERIMENTAL RESULTS

CHAPTER IV

EXPERIMENTAL RESULTS

1. Static Results
    - (a) Tabulated Results
    - (b) Graphs
2. Dynamic Results
    - (a) Tabulated Results
3. Method of Comparison Between Static and Dynamic Results
4. Comparison Curves (Dynamic and Static)
5. Comments

This chapter contains the results obtained during the static and dynamic force tests. Firstly, the static results are tabulated, followed by static curves drawn for the two different sizes of valves. Next, the dynamic results are tabulated followed by an explanation of the method used in comparing static and dynamic results. Finally, using this method, overall static and dynamic curves are presented.

Along with early experimental work, tests were carried out to obtain throat pressures during dynamic operation of the 9.525 mm O/D valve. These results are not included in this chapter since it is more appropriate that they be included in CHAPTER VI.

After leaving University, similar tests were carried out on the 8.410 mm O/D valve and these too are included in CHAPTER VI.

It should be noted that this work was initiated before the change at Strathclyde from Imperial to SI units and the valve dimensions, pressures etc., are therefore in preferred Imperial sizes, but are quoted in SI units with Imperial sizes in brackets where appropriate.

1. Static Results*

(a) Tabulated Results

TABLE NO.	VALVE SEAT BORE mm	VALVE O/D mm
1.1	6.35 (¼")	9.525 (⅜")
1.2	6.35 (¼")	8.410 (0.331")

(b) Graphs

GRAPH NO.	VALVE SEAT BORE mm	VALVE O/D mm
1	6.35 (¼")	9.525 (⅜")
2	6.35 (¼")	8.410 (0.331")

TABLE 1.1/

* These results are obtained in conjunction with Transducer Calibrations

TABLE 1.1

TRANSDUCER PRESSURE		DISPLACEMENT		TRANSDUCER FORCE (MEAN)
kN/m^2	PSI	mm	thous	NEWTONS
72.54	10.52	1.524	60	1.86
64.68	9.38	"	"	1.76
64.68	9.38	"	"	1.72
56.88	8.25	"	"	1.52
49.02	7.11	"	"	1.31
43.16	6.26	"	"	1.18
35.30	5.12	"	"	0.96
28.41	4.12	"	"	0.78
20.69	3.00	"	"	0.57
14.69	2.13	"	"	0.38
6.34	0.92	"	"	0.17
72.54	10.52	1.27	50	1.96
56.88	8.25	"	"	1.57
43.16	6.26	"	"	1.13
29.44	4.27	"	"	0.78
13.79	2.00	"	"	0.39
6.34	0.92	"	"	0.15
74.47	10.80	1.016	40	1.77
64.68	9.38	"	"	1.62
56.88	8.25	"	"	1.42
50.95	7.39	"	"	1.23
45.09	6.54	"	"	1.13
35.30	5.12	"	"	0.90
27.44	3.98	"	"	0.69
23.51	3.41	"	"	0.59
12.76	1.85	"	"	0.31
7.38	1.07	"	"	0.19
72.40	10.50	0.762	30	1.57
56.81	8.24	"	"	1.27
43.16	6.26	"	"	0.98
27.44	3.98	"	"	0.64
13.79	2.00	"	"	0.31
72.40	10.50	0.508	20	1.42
62.74	9.10	"	"	1.18
55.85	8.10	"	"	0.93
50.95	7.39	"	"	0.83
43.16	6.26	"	"	0.67
35.30	5.12	"	"	0.57
29.44	4.27	"	"	0.43
21.58	3.13	"	"	0.33
14.69	2.13	"	"	0.25
10.41	1.51	"	"	0.10
74.47	10.80	"	"	1.47
58.81	8.53	"	"	0.98

TABLE 1.1 cont

TRANSDUCER PRESSURE		DISPLACEMENT		TRANSDUCER FORCE (MEAN)
kN/m^2	PSI	mm	thous	NEWTONS
88.26	12.80	0.508	20	1.96
78.60	11.40	"	"	1.67
66.68	9.67	"	"	1.23
88.26	12.80	0.381	15	2.06
72.40	10.50	"	"	1.57
50.47	7.32	"	"	0.90
28.41	4.12	"	"	0.45
72.54	10.52	0.254	10	2.01
66.68	9.67	"	"	1.77
56.88	8.25	"	"	1.52
52.95	7.68	"	"	1.42
45.09	6.54	"	"	1.18
35.30	5.12	"	"	0.93
21.58	3.13	"	"	0.59
6.90	1.00	"	"	0.20
88.26	12.80	0.178	7	2.60
75.50	10.95	"	"	2.16
52.95	7.68	"	"	1.47
29.44	4.27	"	"	0.72
74.47	10.80	0.127	5	2.20
58.81	8.53	"	"	1.81
45.09	6.54	"	"	1.32
28.41	4.12	"	"	0.84
15.65	2.27	"	"	0.47
6.07	0.88	"	"	0.19
89.22	12.94	0.102	4	3.14
75.50	10.95	"	"	2.55
51.92	7.53	"	"	1.72
29.44	4.27	"	"	0.98
88.26	12.80	0.076	3.0	3.43
73.57	10.67	"	"	2.80
60.81	8.82	"	"	2.26
45.30	6.57	"	"	1.68
31.37	4.55	"	"	1.12
74.47	10.80	0.051	2	2.80
62.74	9.10	"	"	2.26
46.06	6.68	"	"	1.72
32.38	4.69	"	"	1.18
15.65	2.27	"	"	0.57
4.90	0.71	"	"	0.20

TABLE 1.1 cont

TRANSDUCER PRESSURE		DISPLACEMENT		TRANSDUCER FORCE (MEAN)
kN/m^2	PSI	mm	thous	NEWTONS
88.26	12.80	0.038	1.5	3.73
74.47	10.80	"	"	3.24
60.68	8.80	"	"	2.45
46.06	6.68	"	"	1.91
31.37	4.55	"	"	1.28
76.53	11.10	0.025	1.0	3.82
60.81	8.82	"	"	2.94
47.09	6.83	"	"	2.25
29.44	4.27	"	"	1.42
14.69	2.13	"	"	0.74

TABLE 1.2

TRANSDUCER PRESSURE		DISPLACEMENT		TRANSDUCER FORCE (MEAN)
kN/m^2	PSI	mm	thous	NEWTONS
93.15	13.51	1.524	60	2.60
79.43	11.52	"	"	2.16
60.81	8.82	"	"	1.69
46.06	6.68	"	"	1.27
29.79	4.32	"	"	0.84
95.08	13.79	"	"	2.70
76.47	11.09	"	"	2.21
61.71	8.95	"	"	1.77
47.02	6.82	"	"	1.32
30.34	4.40	"	"	0.85
91.15	13.22	1.27	50	2.50
76.47	11.09	"	"	2.06
61.30	8.89	"	"	1.67
46.54	6.75	"	"	1.25
31.03	4.50	"	"	0.85
92.19	13.37	1.016	40	2.45
76.47	11.09	"	"	2.06
61.30	8.89	"	"	1.62
46.54	6.75	"	"	1.23
30.41	4.41	"	"	0.81
92.19	13.37	0.762	30	2.4
76.47	11.09	"	"	2.06
60.81	8.82	"	"	1.67
46.13	6.69	"	"	1.23
30.41	4.41	"	"	0.80
90.19	13.08	0.508	20	2.4
76.47	11.09	"	"	2.06
60.81	8.82	"	"	1.67
45.09	6.54	"	"	1.23
30.41	4.41	"	"	0.80
90.19	13.08	0.381	15	2.55
76.47	11.09	"	"	2.06
60.81	8.82	"	"	1.67
45.09	6.54	"	"	1.23
30.89	4.48	"	"	0.82
90.19	13.08	0.254	10	2.55
78.47	11.38	"	"	2.06
59.78	8.67	"	"	1.52
49.02	7.11	"	"	1.23
29.79	4.32	"	"	0.69

TABLE 1.2 cont

TRANSDUCER PRESSURE		DISPLACEMENT		TRANSDUCER FORCE (MEAN)
kN/m^2	PSI	mm	thous	NEWTONS
92.19	13.37	0.178	7	2.60
76.47	11.09	"	"	2.16
60.81	8.82	"	"	1.59
45.09	6.54	"	"	1.13
29.79	4.32	"	"	0.77
90.19	13.08	0.127	5	2.84
76.47	11.09	"	"	2.30
60.81	8.82	"	"	1.84
45.09	6.54	"	"	1.30
31.37	4.55	"	"	0.85
92.19	13.37	0.102	4	2.89
77.43	11.23	"	"	2.45
62.74	9.10	"	"	1.96
46.54	6.75	"	"	1.42
31.10	4.51	"	"	0.94
91.15	13.22	0.076	3	2.94
76.47	11.09	"	"	2.40
60.33	8.75	"	"	1.86
46.54	6.75	"	"	1.42
31.10	4.51	"	"	0.94
91.15	13.22	0.051	2	3.09
75.43	10.94	"	"	2.60
60.33	8.75	"	"	1.99
45.58	6.61	"	"	1.52
31.10	4.51	"	"	1.03
84.33	12.23	0.025	1	3.34
65.71	9.53	"	"	2.45
54.88	7.96	"	"	2.01
42.13	6.11	"	"	1.57
30.89	4.48	"	"	1.20

6·35mm BORE / 9·525mm O/D VALVE.
(1/4" BORE / 3/8" O/D.)

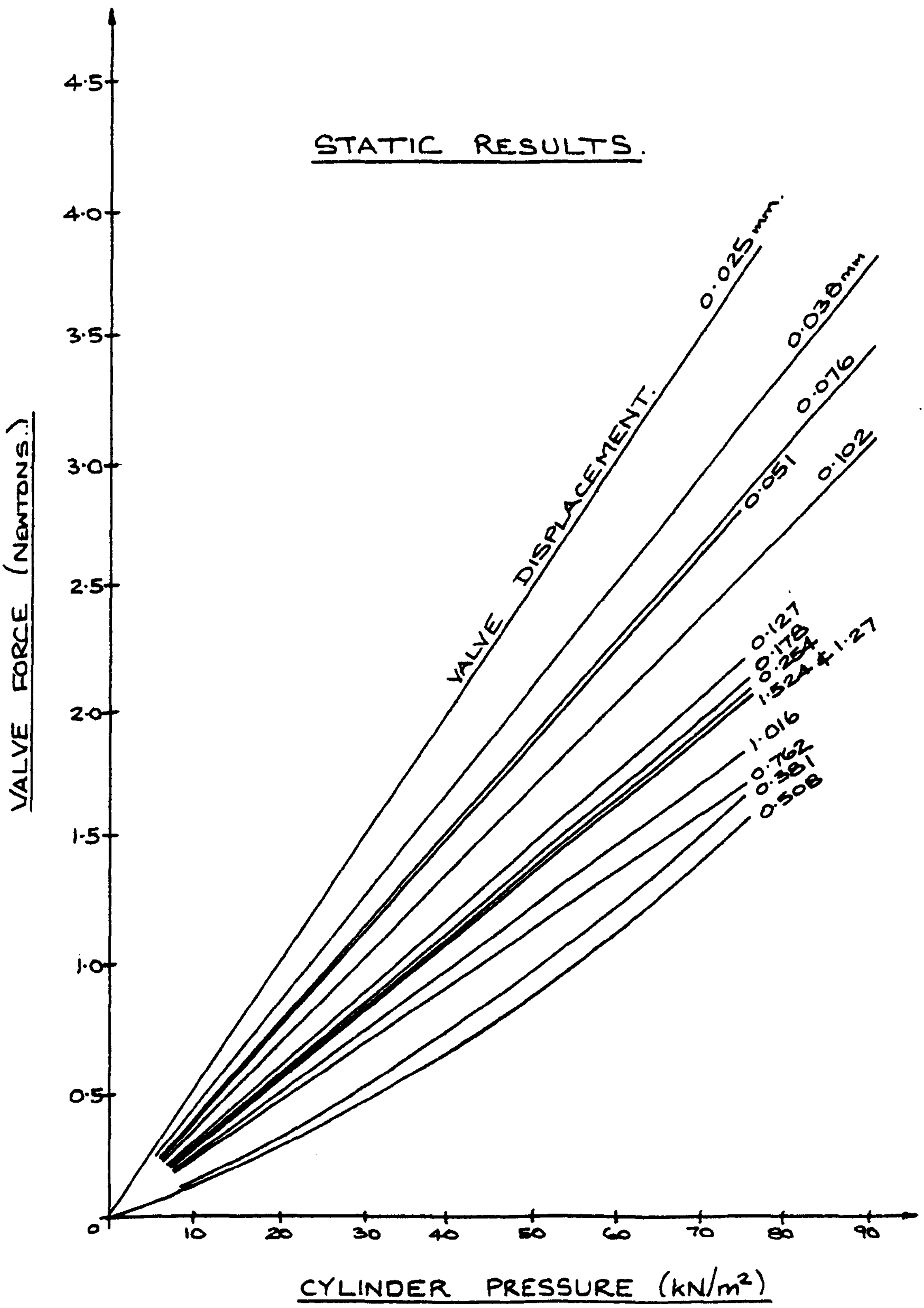

GRAPH 1.

6·35 mm BORE / 8·410 mm O/D VALVE.

($\frac{1}{4}$" BORE / 0·331" O/D)

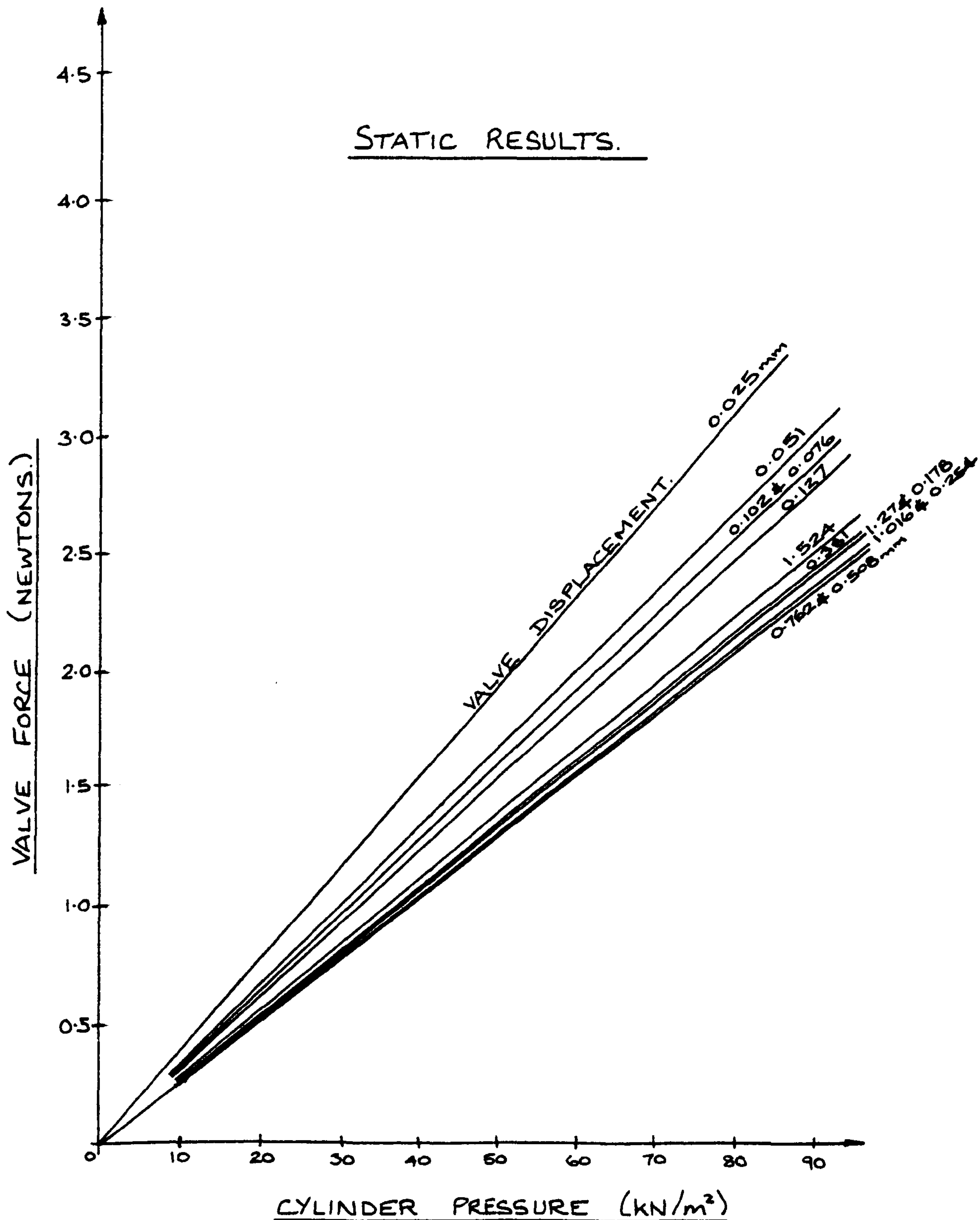

GRAPH 2.

2. Dynamic Results

(a) Tabulated Results

TABLE NO.	VALVE O/D mm	GRAPH NO.	STARTING PRESSURE kN/m^2	STARTING PRESSURE PSI	VALVE OPENING TIME msecs
2.1	9.525 ($\frac{3}{8}$")	3	31.03	4.50	15
2.2	"	4	50.00	7.25	"
2.3	"	5	76.88	11.15	"
2.4	"	6	29.64	4.30	35
2.5	"	7	53.44	7.75	"
2.6	"	8	77.92	11.30	"
2.7	"	9	25.58	3.71	45+
2.8	"	10	54.00	7.83	45+
2.9	"	11	76.40	11.08	45+
2.10	8.410 (0.331")	12	29.64	4.30	8
2.11	"	13	55.16	8.0	"
2.12	"	14	69.29	10.05	"

TABLE 2.1

TIME	TRANSDUCER PRESSURE IN CYLINDER	VALVE DISPLACEMENT	TRANSDUCER DYNAMIC FORCE (NEWTONS)	
msecs	kN/m^2	mm	MAXIMUM	MINIMUM
0	31.03	0.00	1.53	1.53
2	30.72	0.05	1.11	1.11
4	30.50	0.16	0.80	0.80
6	30.28	0.33	0.49	0.47
8	29.70	0.57	0.47	0.32
10	29.04	0.87	0.71	0.47
12	28.61	1.21	0.76	0.47
14	27.94	1.58	0.91	0.41
16	27.42	1.66	0.84	0.46
18	26.49	1.50	0.78	0.45

TABLE 2.2

TIME	TRANSDUCER PRESSURE IN CYLINDER	VALVE DISPLACEMENT	TRANSDUCER DYNAMIC FORCE (NEWTONS)	
msecs	kN/m^2	mm	MAXIMUM	MINIMUM
0	50.00	0.00	2.56	2.56
2	49.97	0.06	1.84	1.84
4	49.46	0.18	1.33	1.33
6	49.11	0.34	0.91	0.78
8	48.45	0.58	0.82	0.58
10	47.78	0.91	1.17	0.89
12	46.68	1.26	1.29	0.95
14	46.02	1.63	1.34	0.95
16	45.14	1.64	1.29	0.95
18	44.70	1.49	1.26	0.95

TABLE 2.3

TIME	TRANSDUCER PRESSURE IN CYLINDER	VALVE DISPLACEMENT	TRANSDUCER DYNAMIC FORCE (NEWTONS)	
msecs	kN/m^2	mm	MAXIMUM	MINIMUM
0	76.88	0.00	3.82	3.82
1	76.88	0.03	3.38	3.38
3	76.44	0.10	2.44	2.44
5	76.00	0.26	1.85	1.81
7	75.34	0.48	1.58	1.27
9	74.25	0.76	1.72	0.99
11	73.37	1.10	1.88	1.41
13	72.49	1.46	2.04	1.52
15	71.62	1.69	2.04	1.56
17	70.31	1.55	1.93	1.56
19	69.43	1.46	1.84	1.58

TABLE 2.4

TIME	TRANSDUCER PRESSURE IN CYLINDER	VALVE DISPLACEMENT	TRANSDUCER DYNAMIC FORCE (NEWTONS)	
msecs	kN/m^2	mm	MAXIMUM	MINIMUM
0	29.64	0.00	1.54	1.54
2	29.64	0.02	1.37	1.37
7	29.21	0.12	0.93	0.93
12	28.77	0.26	0.62	0.57
17	27.66	0.55	0.53	0.35
22	26.34	0.84	0.75	0.46
27	25.24	1.15	0.77	0.51
32	23.69	1.50	0.82	0.46
37	22.15	1.52	0.75	0.51
42	20.61	1.45	0.64	0.48
47	19.52	1.42	0.57	0.44

TABLE 2.5

TIME	TRANSDUCER PRESSURE IN CYLINDER	VALVE DISPLACEMENT	TRANSDUCER DYNAMIC FORCE (NEWTONS)	
msecs	kN/m^2	mm	MAXIMUM	MINIMUM
0	53.44	0.00	2.67	2.67
2	53.44	0.02	2.29	2.29
7	53.00	0.15	1.58	1.58
12	52.12	0.33	1.12	0.97
17	50.58	0.60	0.97	0.57
22	49.04	0.91	1.32	0.88
27	47.29	1.23	1.45	0.96
32	45.08	1.57	1.44	0.98
37	42.89	1.53	1.38	0.98
42	40.70	1.46	1.24	0.95
47	38.93	1.43	1.12	0.91

TABLE 2.6

TIME	TRANSDUCER PRESSURE IN CYLINDER	VALVE DISPLACEMENT	TRANSDUCER DYNAMIC FORCE (NEWTONS)	
msecs	kN/m^2	mm	MAXIMUM	MINIMUM
0	77.92	0.00	3.82	3.82
2.5	77.89	0.02	3.23	3.23
7.5	77.25	0.15	2.24	2.24
12.5	76.16	0.36	1.69	1.56
17.5	74.40	0.62	1.57	1.09
22.5	72.64	0.93	1.86	1.34
27.5	70.44	1.28	2.05	1.50
32.5	68.02	1.62	2.03	1.52
37.5	65.17	1.51	1.95	1.51
42.5	62.97	1.44	1.80	1.51
47.5	60.33	1.43	1.64	1.49

TABLE 2.7

TIME	TRANSDUCER PRESSURE IN CYLINDER	VALVE DISPLACEMENT	TRANSDUCER DYNAMIC FORCE (NEWTONS)	
msecs	kN/m^2	mm	MAXIMUM	MINIMUM
0	25.58	0.00	1.46	1.46
1.5	25.58	0.01	1.38	1.38
6.5	25.32	0.07	1.04	1.04
11.5	25.05	0.17	0.82	0.82
16.5	24.26	0.29	0.65	0.61
21.5	23.33	0.43	0.46	0.38
26.5	22.41	0.59	0.50	0.35
31.5	21.18	0.75	0.59	0.43
36.5	20.11	0.91	0.59	0.46
41.5	18.84	1.07	0.59	0.47
46.5	17.42	1.34	0.56	0.46

TABLE 2.8

TIME	TRANSDUCER PRESSURE IN CYLINDER	VALVE DISPLACEMENT	TRANSDUCER DYNAMIC FORCE (NEWTONS)	
msecs	kN/m^2	mm	MAXIMUM	MINIMUM
0	54.00	0.00	2.67	2.67
2	54.00	0.01	2.45	2.45
7	53.50	0.08	1.85	1.85
12	52.84	0.18	1.45	1.45
17	51.87	0.32	1.13	1.05
22	50.85	0.48	0.95	0.69
27	49.35	0.64	0.97	0.74
32	47.98	0.82	1.15	0.89
37	46.09	0.98	1.20	0.93
42	44.54	1.15	1.20	1.02
47	42.78	1.30	1.16	1.01

TABLE 2.9

TIME	TRANSDUCER PRESSURE IN CYLINDER	VALVE DISPLACEMENT	TRANSDUCER DYNAMIC FORCE (NEWTONS)	
msecs	kN/m^2	mm	MAXIMUM	MINIMUM
0	76.40	0.00	3.83	3.83
2	76.40	0.01	3.41	3.41
7	76.00	0.07	2.59	2.59
12	75.07	0.19	2.07	2.01
17	74.23	0.33	1.72	1.51
22	72.92	0.50	1.59	1.14
27	71.28	0.68	1.74	0.99
32	69.47	0.87	1.81	1.26
37	67.35	1.06	1.91	1.30
42	65.15	1.23	1.89	1.32
47	63.16	1.39	1.85	1.33

TABLE 2.10

TIME	TRANSDUCER PRESSURE IN CYLINDER	VALVE DISPLACEMENT	TRANSDUCER DYNAMIC FORCE (NEWTONS)	
msecs	kN/m^2	mm	MAXIMUM	MINIMUM
0	29.64	0.00	1.32	1.32
0.8	29.64	0.02	1.08	1.08
1.8	29.64	0.10	0.84	0.84
2.8	29.43	0.23	0.77	0.66
3.8	29.00	0.41	0.82	0.72
4.8	27.88	0.66	0.79	0.67
5.8	27.00	1.01	0.77	0.65
6.8	25.47	1.46	0.79	0.63
7.8	24.77	1.76	1.09	0.34
8.8	24.58	1.57	1.00	0.43

TABLE 2.11

TIME	TRANSDUCER PRESSURE IN CYLINDER	VALVE DISPLACEMENT	TRANSDUCER DYNAMIC FORCE (NEWTONS)	
msecs	kN/m^2	mm	MAXIMUM	MINIMUM
0	55.16	0.00	2.18	2.18
0.7	54.94	0.02	1.93	1.93
1.7	54.50	0.08	1.62	1.62
2.7	54.27	0.20	1.48	1.38
3.7	53.62	0.38	1.49	1.42
4.7	52.73	0.60	1.45	1.34
5.7	51.19	0.88	1.45	1.28
6.7	49.88	1.27	1.43	1.25
7.7	47.45	1.69	1.64	1.07
8.7	46.34	1.69	1.66	0.99

TABLE 2.12

TIME	TRANSDUCER PRESSURE IN CYLINDER	VALVE DISPLACEMENT	TRANSDUCER DYNAMIC FORCE (NEWTONS)	
msecs	kN/m^2	mm	MAXIMUM	MINIMUM
0	69.29	0.00	2.65	2.65
0.65	68.85	0.02	2.34	2.34
1.65	68.42	0.08	1.84	1.84
2.65	67.97	0.20	1.82	1.64
3.65	67.09	0.37	1.77	1.61
4.65	66.00	0.61	1.69	1.53
5.65	64.45	0.91	1.69	1.43
6.65	62.69	1.35	1.70	1.38
7.65	61.45	1.62	2.03	1.17
8.65	59.16	1.52	1.87	1.22

3. Method of Comparison Between Static and Dynamic Results

The method of comparison between dynamic and static results begins by drawing the dynamic curves.

As can be seen from FIG. 19 , a maximum and minimum value of dynamic force has been shown. These maximum and minimum values are averages, since high frequency vibrations were present during the dynamic opening of the valve. This effect being probably due to forcing of turbulence or self-excited eddies. A typical dynamic test showing these transients can be seen in PHOTOGRAPH 9.

The comparable static force value (e.g. ZZ) is then determined, in conjunction with GRAPHS 1 or 2, at a particular corresponding displacement (X) and pressure (Y) and plotted on these dynamic curves. This procedure is repeated at a range of displacements and corresponding pressures, thereby enabling a static force curve to be drawn.

The resultant graphs are shown in Section 4 of this chapter.

4. Comparison Curves (Dynamic and Static)

Attached are comparison curves 3 to 18 as noted in Section 2a of this chapter.

COMPARISON METHOD USED TO COMPARE STATIC AND DYNAMIC CURVES.

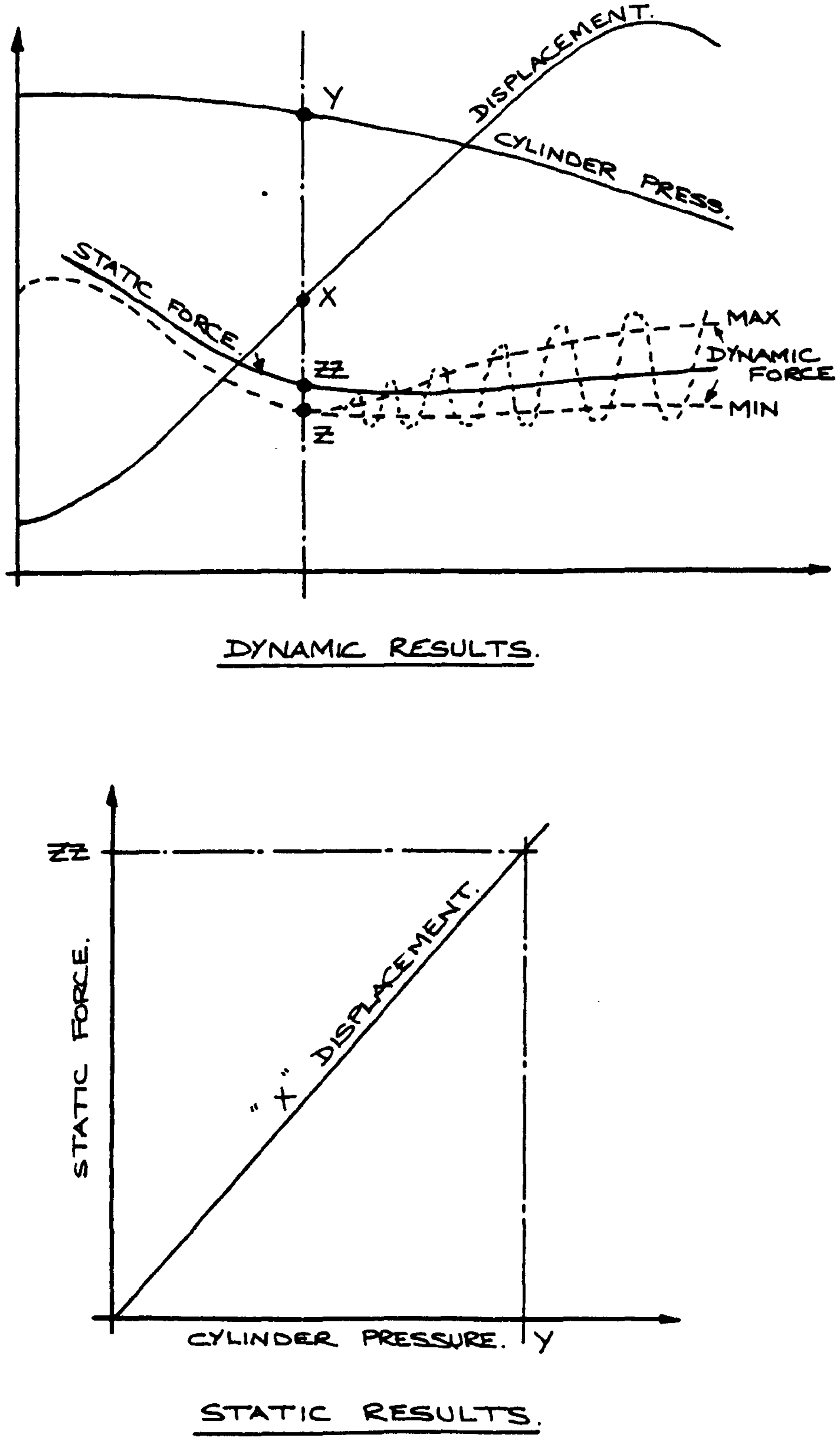

FIGURE 19

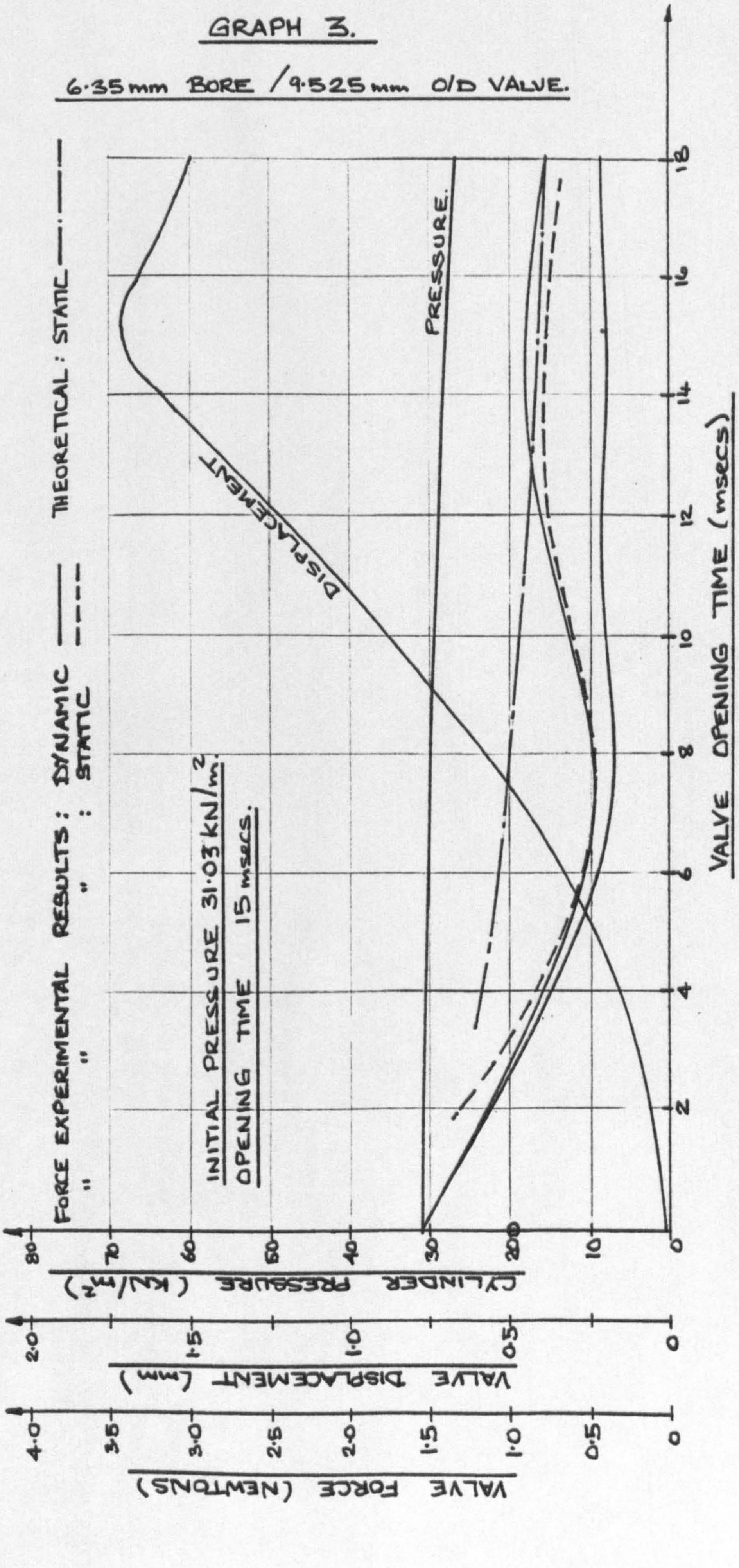
GRAPH 3.
6·35 mm BORE / 9·525 mm O/D VALVE.
FORCE EXPERIMENTAL RESULTS : DYNAMIC
" " " : STATIC
THEORETICAL : STATIC
INITIAL PRESSURE 31·03 KN/m²
OPENING TIME 15 msecs.
PRESSURE.
DISPLACEMENT
VALVE OPENING TIME (msecs)
CYLINDER PRESSURE (KN/m²)
VALVE DISPLACEMENT (mm)
VALVE FORCE (NEWTONS)
0
2
4
6
8
10
12
14
16
18
10
20
30
40
50
60
70
80
0·5
1·0
1·5
2·0
2·5
3·0
3·5
4·0

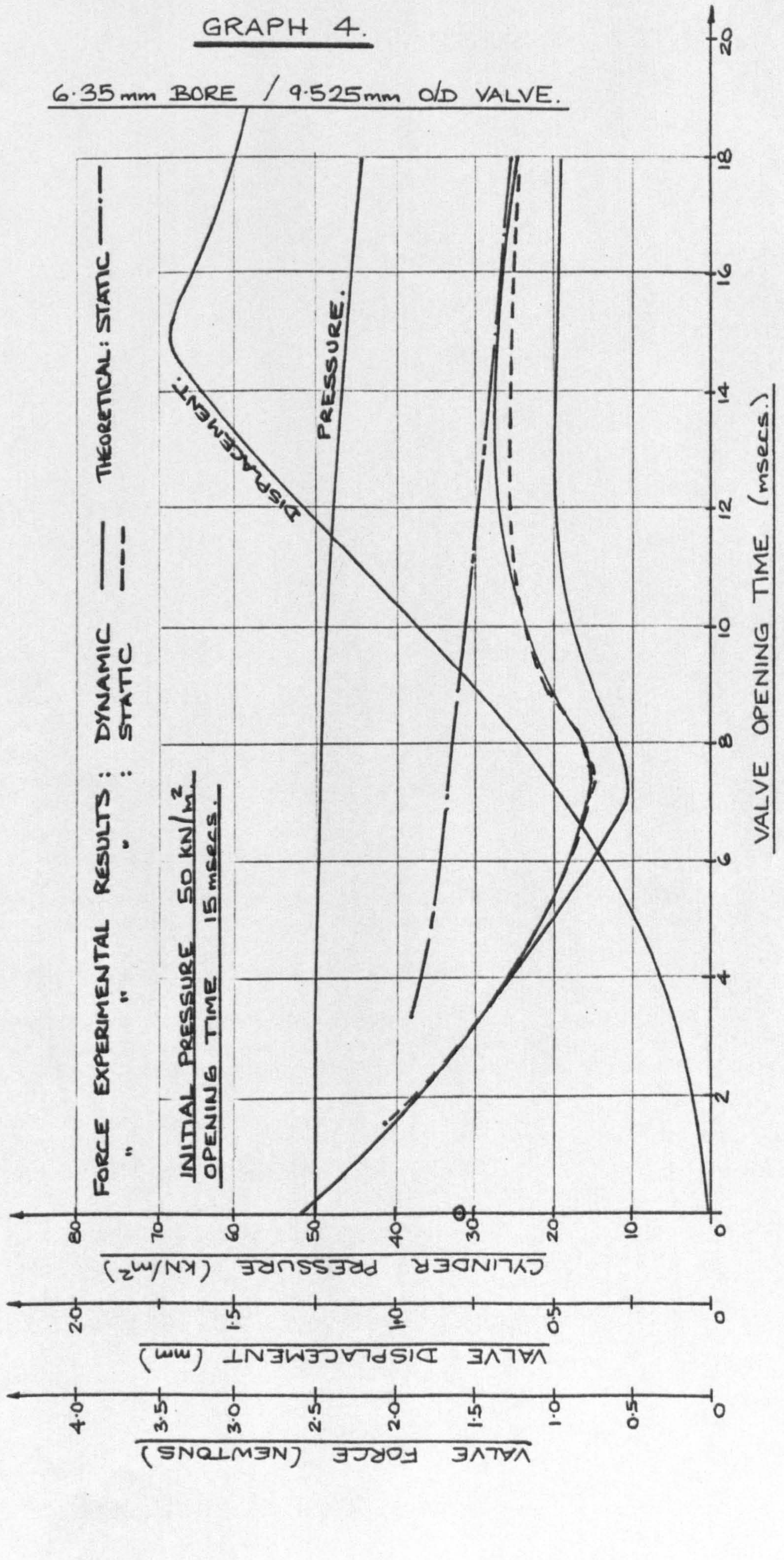
GRAPH 4.
6·35 mm BORE / 9·525 mm O/D VALVE.
FORCE EXPERIMENTAL RESULTS : DYNAMIC
" " : STATIC
THEORETICAL : STATIC
INITIAL PRESSURE 50 KN/m²
OPENING TIME 15 msecs.
DISPLACEMENT.
PRESSURE.
VALVE OPENING TIME (msecs.)
CYLINDER PRESSURE (KN/m²)
VALVE DISPLACEMENT (mm)
VALVE FORCE (NEWTONS)

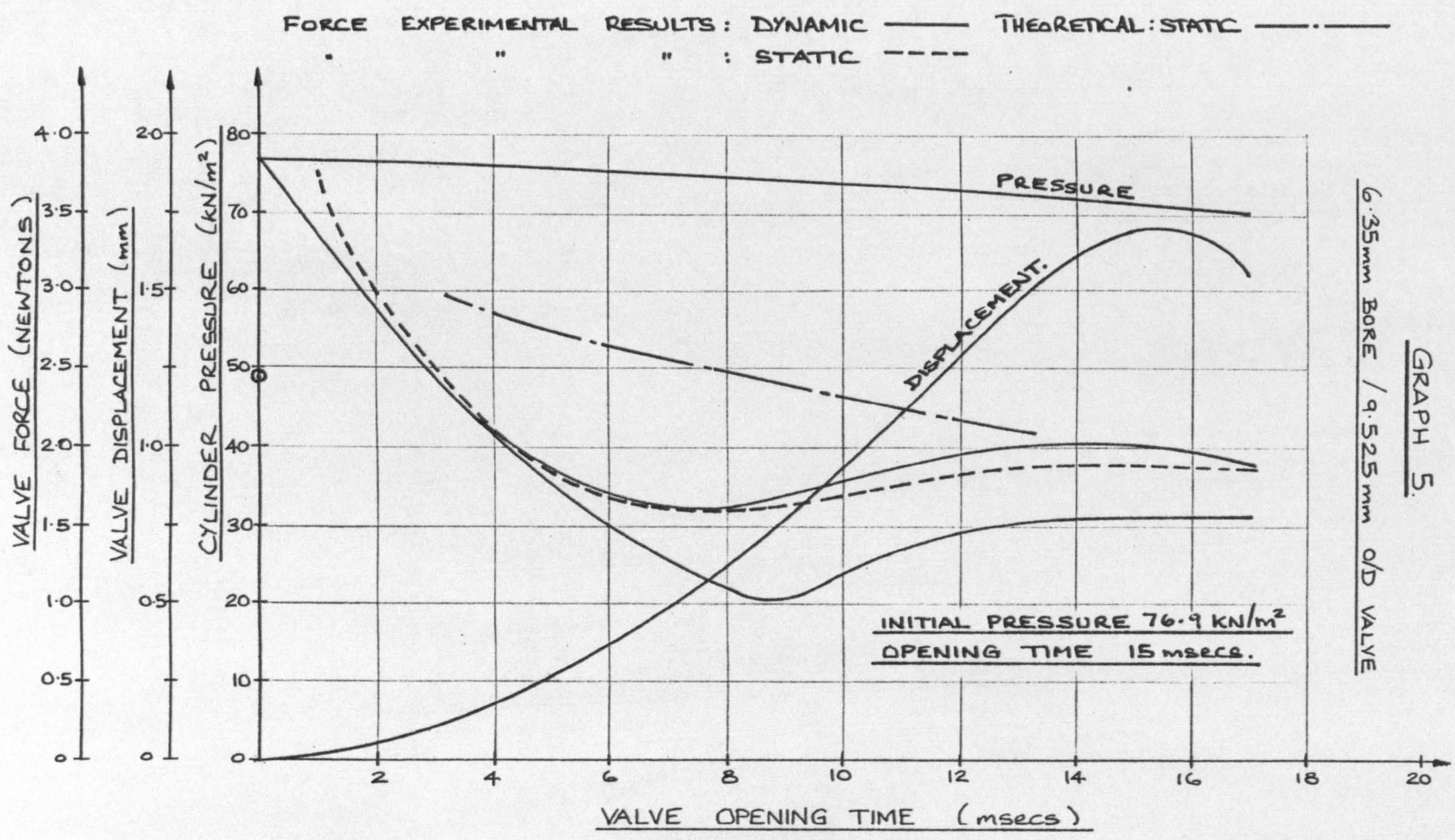
GRAPH 5.
6·35mm BORE / 9·525mm O/D VALVE
FORCE EXPERIMENTAL RESULTS : DYNAMIC
" " " : STATIC
THEORETICAL : STATIC
PRESSURE
DISPLACEMENT.
INITIAL PRESSURE 76·9 KN/m²
OPENING TIME 15 msecs.
VALVE FORCE (NEWTONS)
VALVE DISPLACEMENT (mm)
CYLINDER PRESSURE (KN/m²)
VALVE OPENING TIME (msecs)
0
0.5
1.0
1.5
2.0
2.5
3.0
3.5
4.0
10
20
30
40
50
60
70
80
2
4
6
8
10
12
14
16
18
20

GRAPH 6.

6·35mm BORE / 9·525mm O/D VALVE.

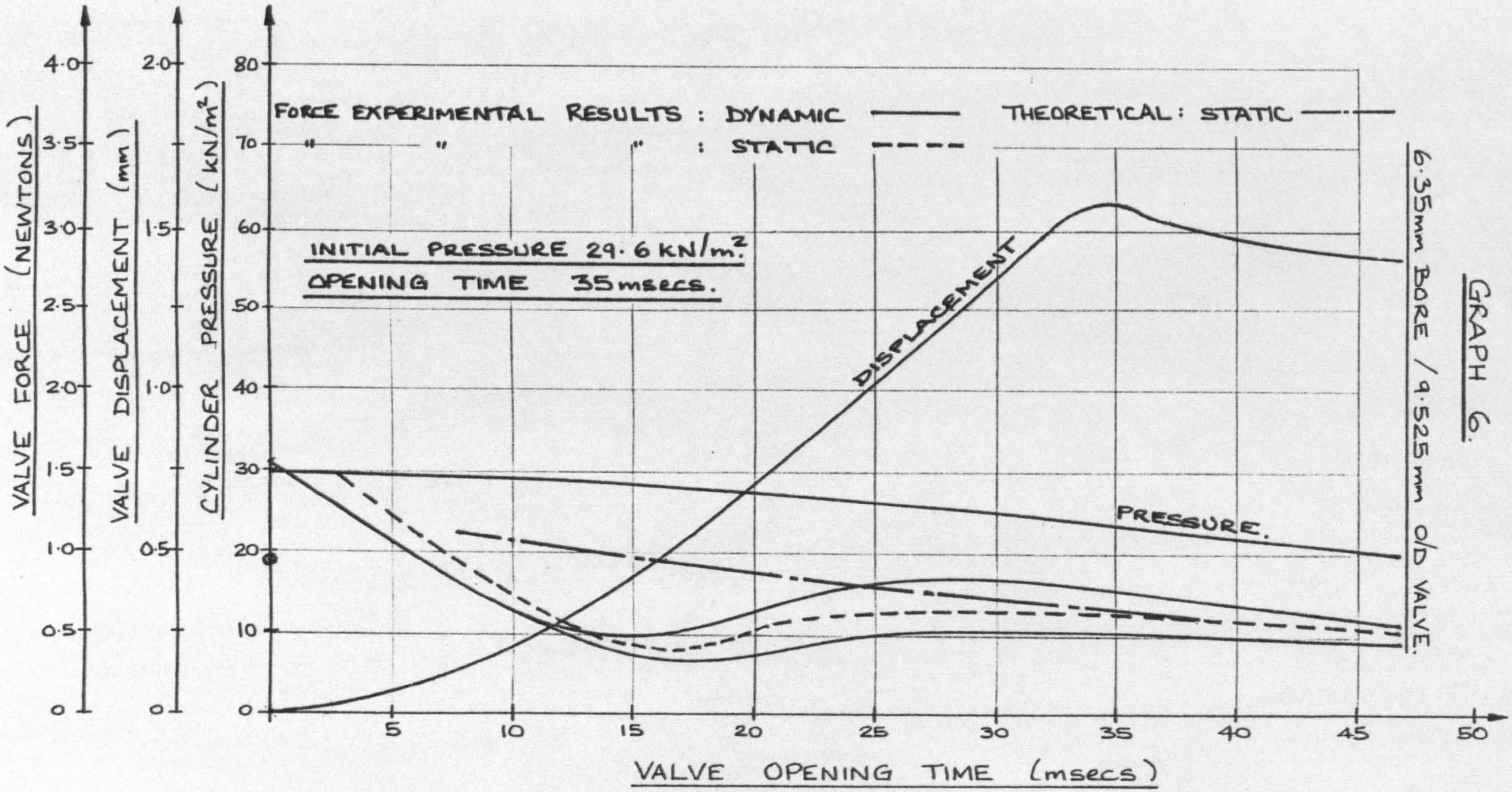

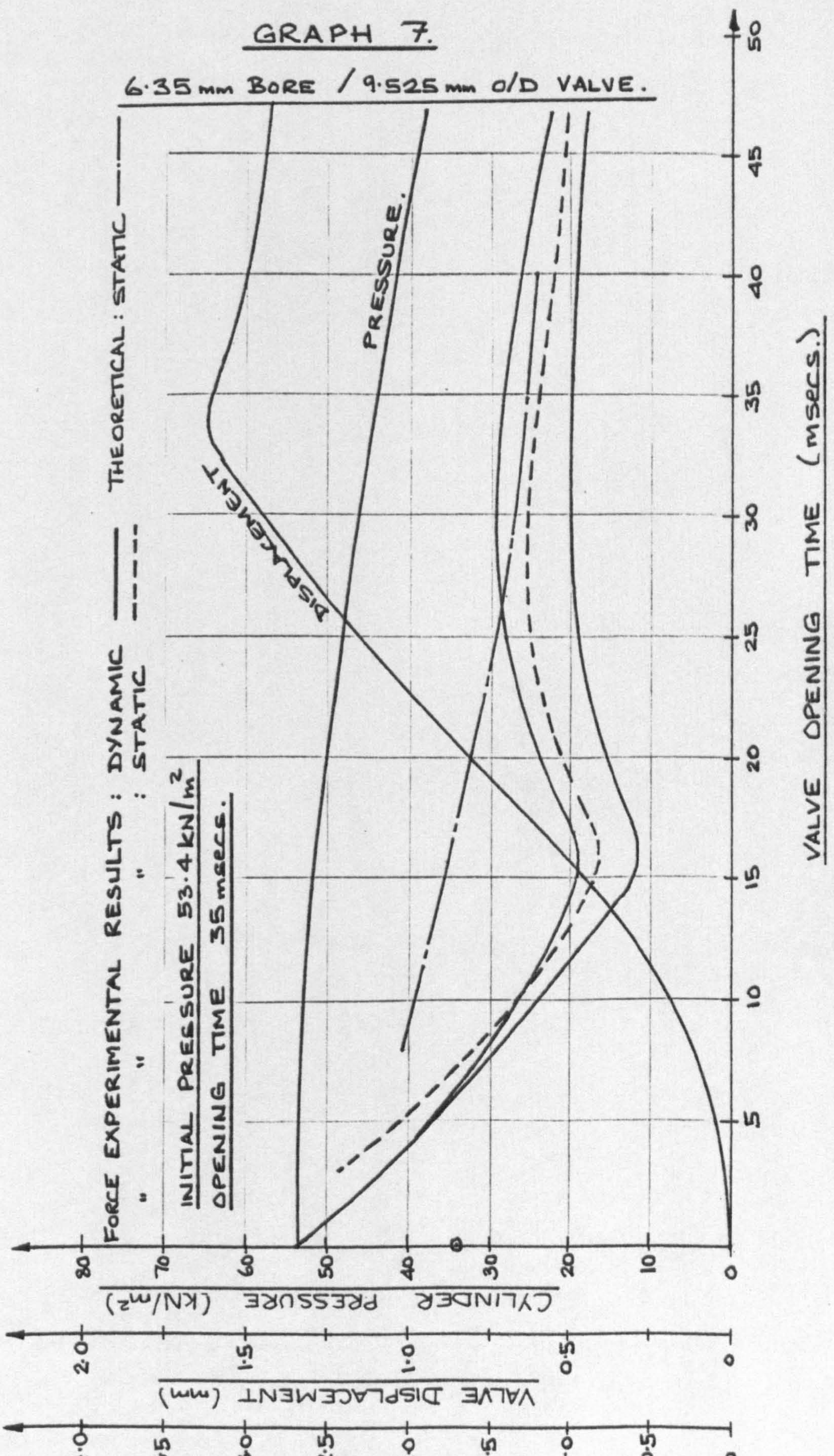
GRAPH 7.
6·35 mm BORE / 9·525 mm O/D VALVE.
FORCE EXPERIMENTAL RESULTS : DYNAMIC
" " : STATIC
THEORETICAL : STATIC
INITIAL PRESSURE 53·4 kN/m²
OPENING TIME 35 msecs.
PRESSURE.
DISPLACEMENT
VALVE OPENING TIME (msecs.)
CYLINDER PRESSURE (kN/m²)
VALVE DISPLACEMENT (mm)
VALVE FORCE (NEWTONS.)
0
5
10
15
20
25
30
35
40
45
50
60
70
80
0·5
1·0
1·5
2·0
2·5
3·0
3·5
4·0

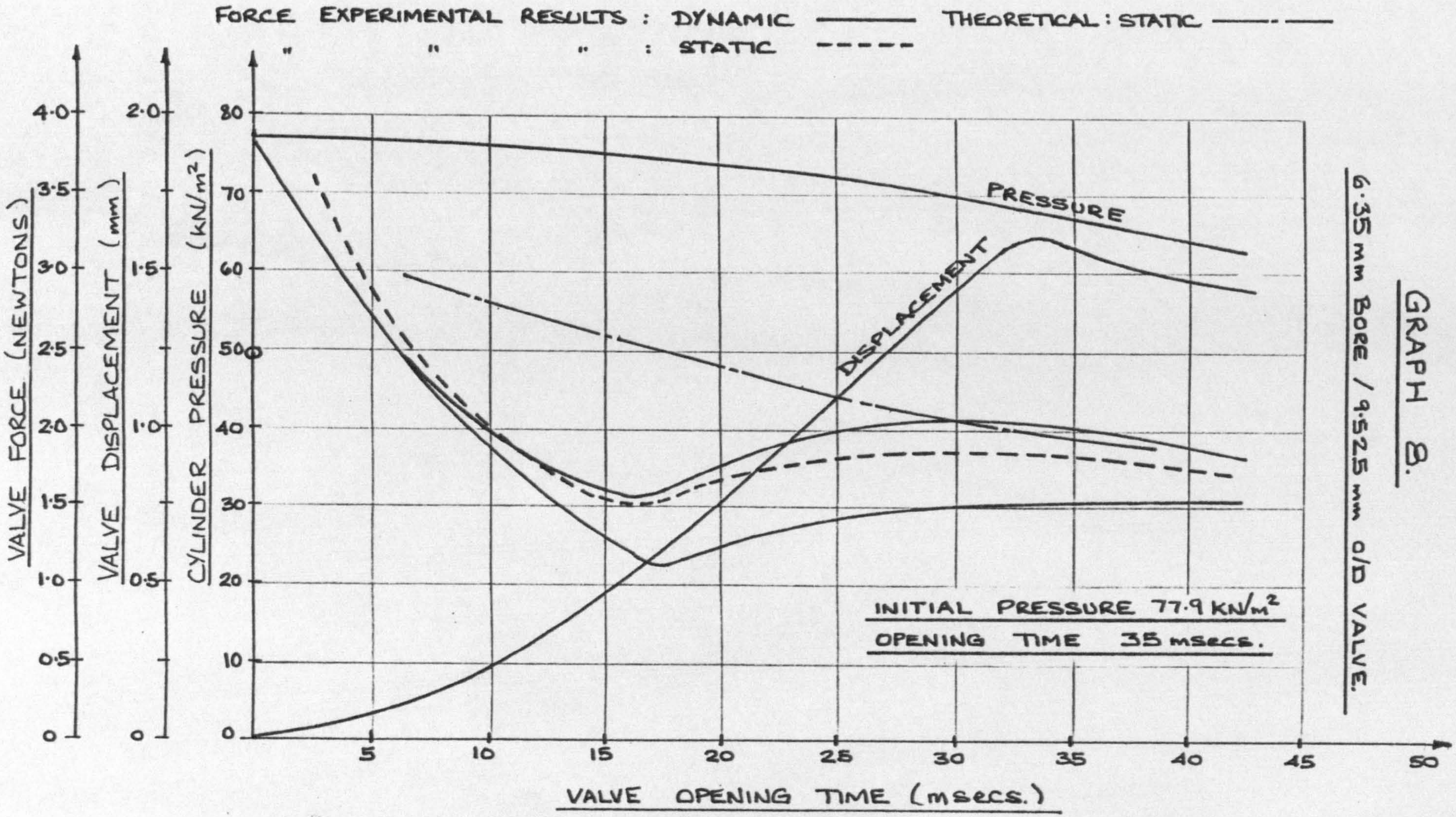
GRAPH 8.
6·35 mm BORE / 9·525 mm O/D VALVE.
FORCE EXPERIMENTAL RESULTS : DYNAMIC
" " " : STATIC
THEORETICAL : STATIC
INITIAL PRESSURE 77·9 KN/m²
OPENING TIME 35 msecs.
PRESSURE
DISPLACEMENT
VALVE OPENING TIME (msecs.)
CYLINDER PRESSURE (KN/m²)
VALVE DISPLACEMENT (mm)
VALVE FORCE (NEWTONS)
0
5
10
15
20
25
30
35
40
45
50
60
70
80
0·5
1·0
1·5
2·0
2·5
3·0
3·5
4·0

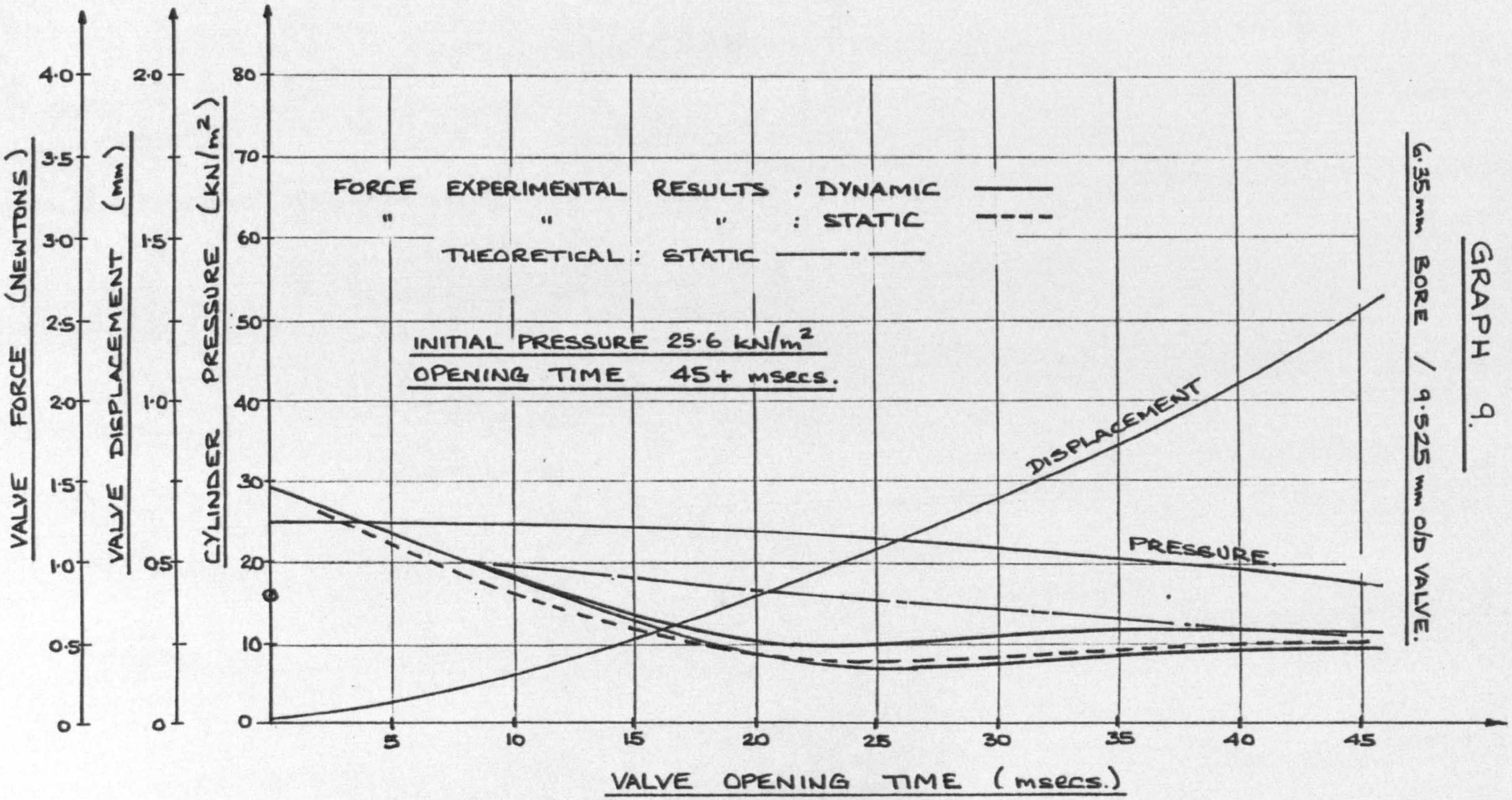

GRAPH 9.

6.35 mm BORE / 9.525 mm O/D VALVE.

GRAPH 10.

6·35mm BORE / 9·525 mm O/D VALVE.

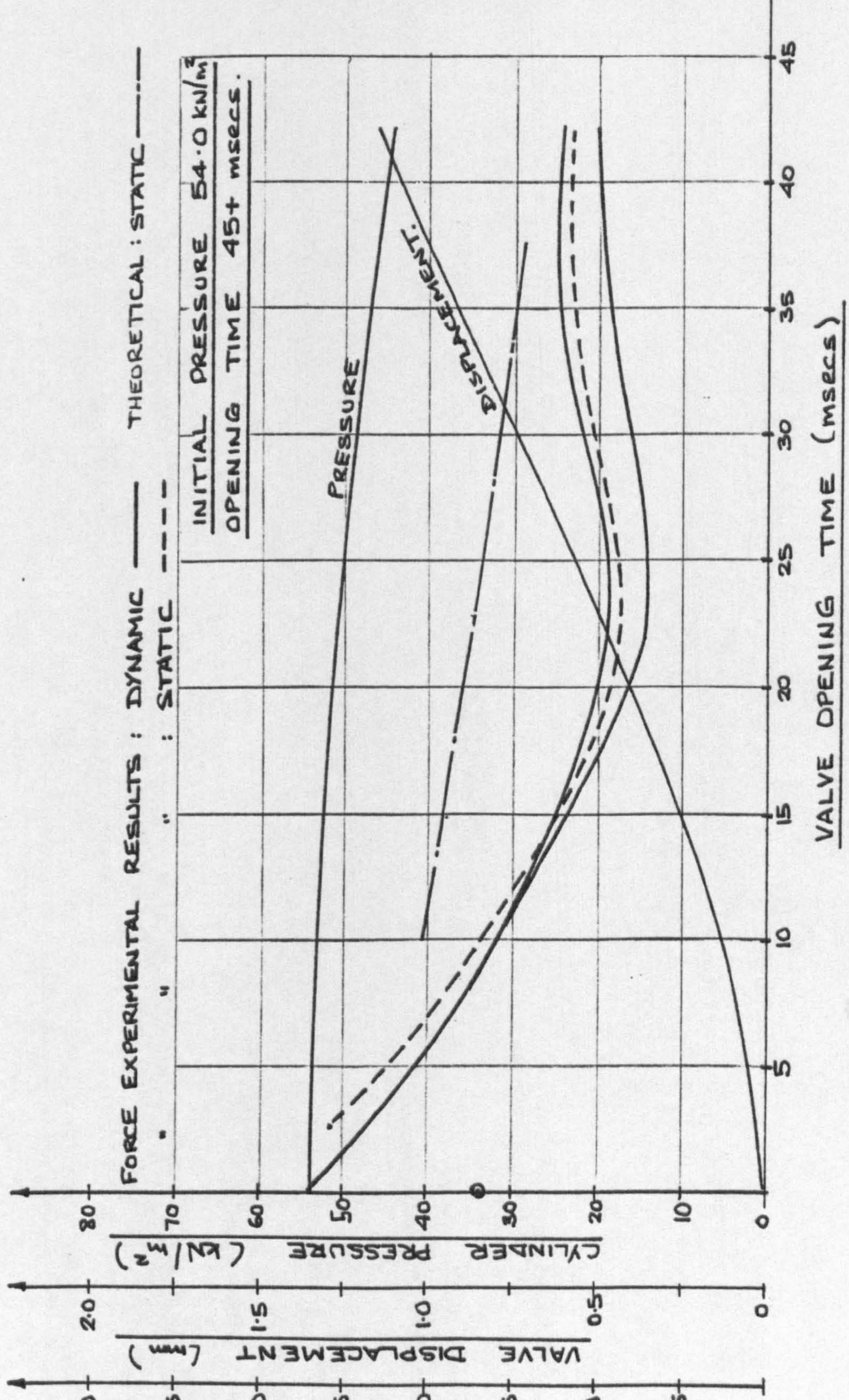

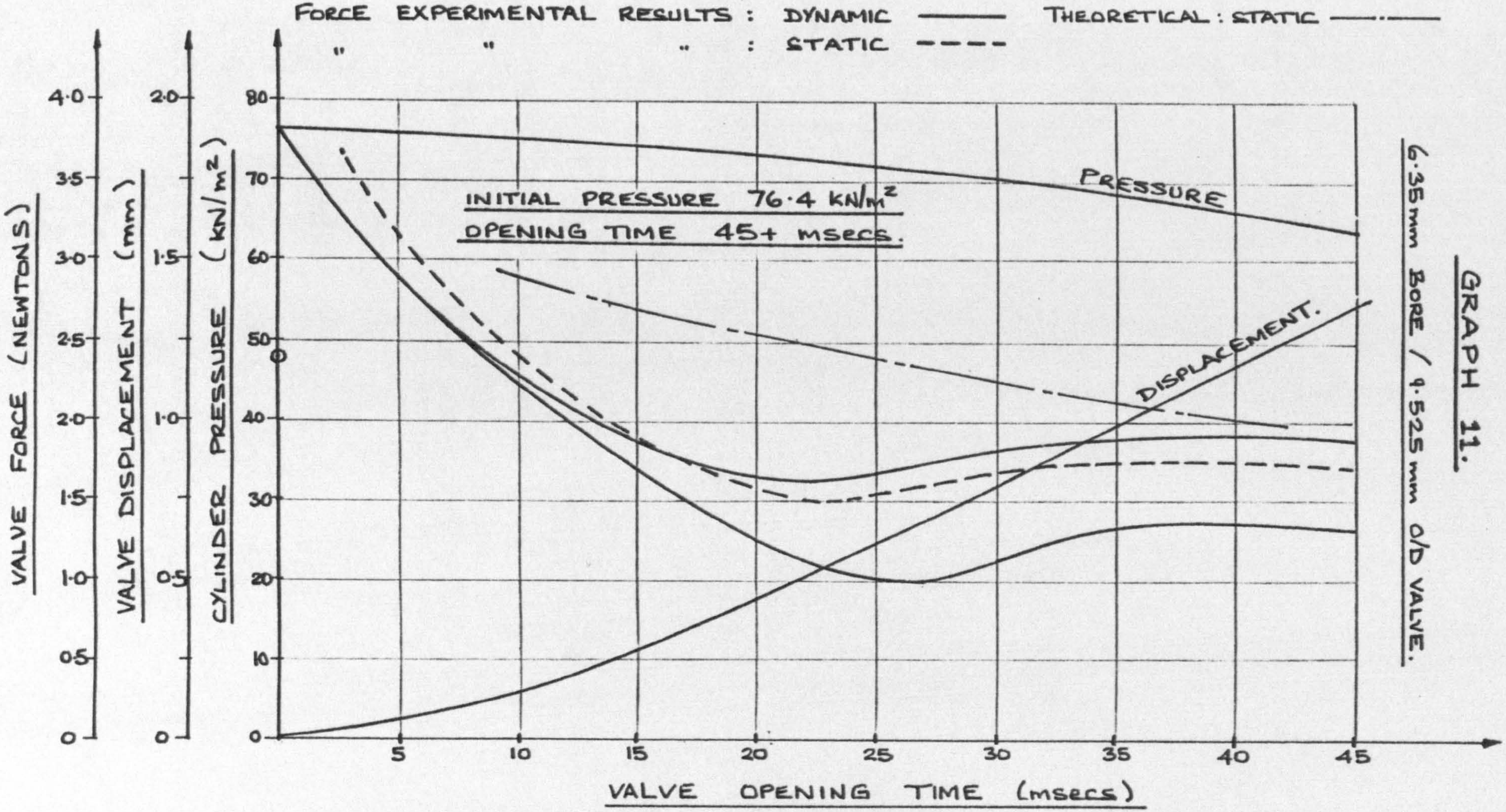

FORCE EXPERIMENTAL RESULTS : DYNAMIC
THEORETICAL : STATIC
" " " : STATIC
INITIAL PRESSURE 76·4 kN/m²
OPENING TIME 45+ msecs.
PRESSURE
DISPLACEMENT.
VALVE FORCE (NEWTONS)
VALVE DISPLACEMENT (mm)
CYLINDER PRESSURE (kN/m²)
VALVE OPENING TIME (msecs)
GRAPH 11.
6·35 mm BORE / 9·525 mm O/D VALVE.

GRAPH 12.

6·35 mm BORE / 8·410 mm O/D VALVE.

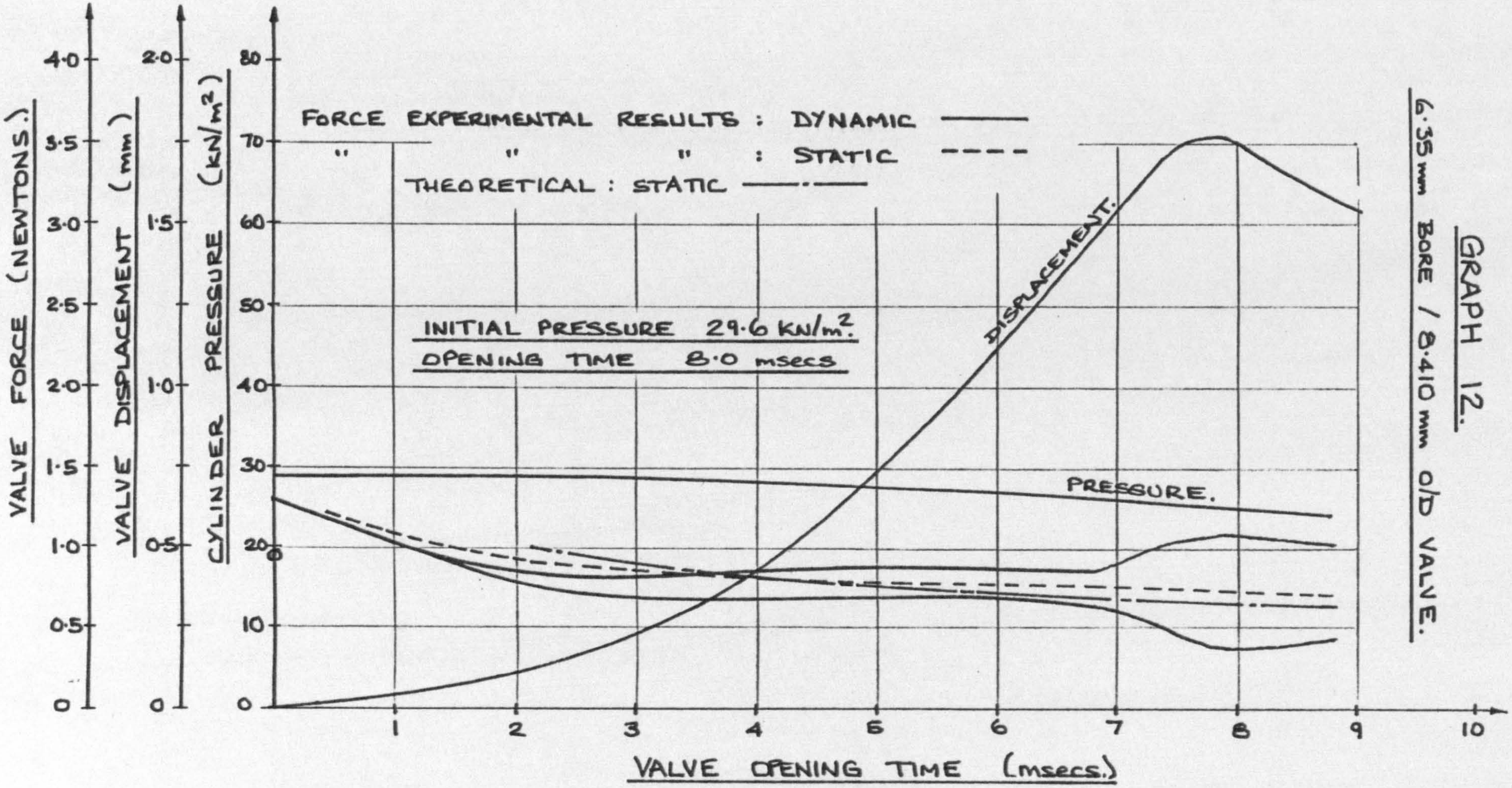

GRAPH 13.

6·35mm BORE / 8·410 mm O/D VALVE.

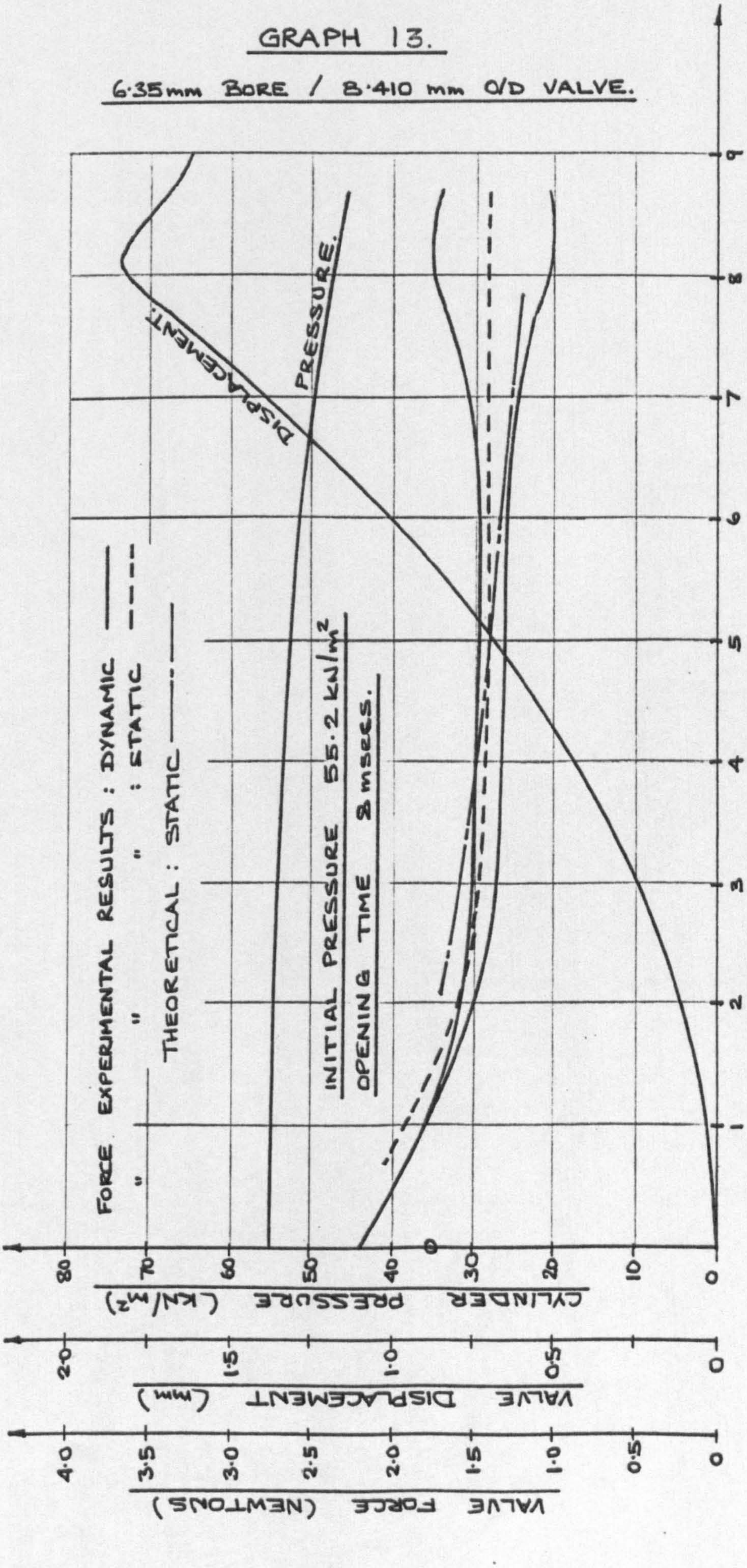

GRAPH 14.

6·35 mm BORE / 8·410 mm O/D VALVE.

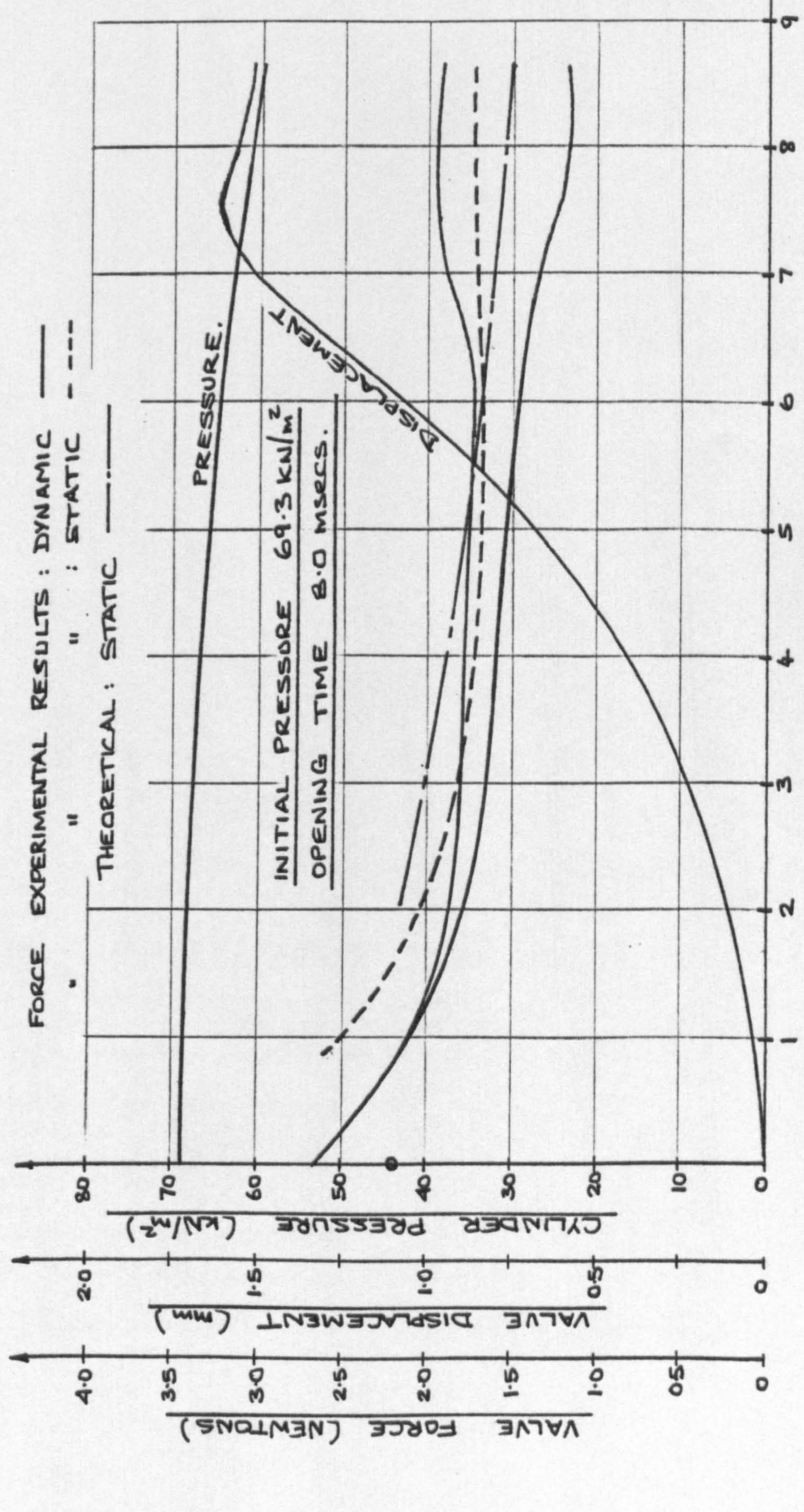

5. COMMENTS

This section contains the salient points arising from dynamic and static experimental tests carried out on a 9.525mm O/D valve (Graphs 3-11), and a 8.410mm O/D valve (Graphs 12-14), both having a bore of 6.35mm diameter.

9.525mm O/D VALVE (GRAPHS 3-11)

Let us focus our attention firstly on the 9.525mm O/D valve, where Graphs 3, 4 and 5 show the fastest valve opening rate which achieved the fully overshot position in approximately 15ms. Graphs 6, 7 and 8 show an intermediate rate of opening taking approximately 35ms, and finally Graphs 9, 10 and 11 show a very slow rate of valve opening in which the fully open position is not achieved after 45ms. The valve stops in each case were set to 1.524mm (0.060"), the overshoot arising from elastic deflection of the stops.

Within these sets, three pressure conditions are recorded, representing approximate initial closed cylinder pressures of 30, 50 and 75 kN/m^2. In each case, the pressure falls off during the opening phase, and in particular, in the condition of higher pressure and slow valve movement.

Dynamic force curves are directly transcribed from oscilloscope records of tests. Except in the early stages of opening, there was considerable fluctuation in dynamic force. Upper and lower limits of this fluctuation are shown. The static curve is built up from experiments at fixed valve openings, and represents at every point, the static force at the valve displacement and cylinder pressure pertaining at that instant in the dynamic experiment.

Upon observing all the curves, they clearly show a force minimum in all cases, and since this appears also in the static curves, it is clearly not a function of valve opening time.

The minimum does, however, appear at about the same valve displacement for the corresponding initial pressure condition in each set of graphs, as follows,

Initial pressure (kN/m^2)	Valve displ. (mm)	Min. force (N)
30	0.5	0.35
50	0.5	0.60
75	0.7	1.00

This indicates that the minimum is a function of valve displacement and cylinder pressure. Schrenk [45] found a change of flow regime at a critical valve opening, at which the flow detached from the valve seat and became a free jet. It seems likely that the minimum described is the force manifestation of this change in regime.

In all dynamic curves, separation of upper and lower limits builds up from a start some milliseconds after inception of valve opening. This separation represents the limits of growing high frequency undulation, as may be seen in Photograph 9. Now the cylinder charge is subjected to an impulsive start from rest, and therefore, begins to flow in laminar conditions. The build up of signal oscillations thus follows a pattern which might be anticipated from eddy growth within the flow, finally achieving full turbulence. Eddy growth of this kind is mentioned in later work. [49].

On this basis, it seems unlikely that viscous effects have much influence on the minimum force previously described, since turbulence appears to be well established before the minimum force point is achieved.

On each of these graphs, a force point is indicated by a ⊙ at zero time. This is the experimentally found gas force on the valve before activation of the opening mechanism.

Immediately on inception of opening, however, the force increased to the initial value shown for the curve. This is merely the spread of pressure across the whole valve surface, indicating that the seal was initially satisfactory.

Finally, differences between static and dynamic forces are not large. However, before the point identified above as the onset of turbulence, the static force is consistently higher than the dynamic force. It was unfortunately impossible to set the extremely small valve lifts required to extend the static force curve towards zero lift, but in the region recorded, static force exceeded dynamic force by something of the order of 10%, with the curves coming together generally in the region of developing turbulence. This would be consistent with laminar flow in the early stages of dynamic lift, while static flow is, of course, always fully turbulent. These differences are not large, but valve characteristics in real compressors are so critical that an allowance for this effect might be a useful modification in computer models.

At later times and larger valve lifts, some measure of this difference between static and mean dynamic forces persists but on a very long time base the curves, as they must, eventually come together.

Graph 9, showing very slow opening at low initial pressure is an exception to the above discussion. Here, static force appears slightly lower than dynamic in the early stages. With the low pressure and very slow opening involved, however, static and dynamic conditions are not radically different. The difference here may therefore be an indication of general curve accuracy, since there is no obvious explanation of the low static curve. In this case, differences between static and dynamic reported for other curves may be subject to this degree of inaccuracy. However, this consistent finding of a higher static force indicates that a difference does exist.

8.410mm O/D VALVE (GRAPHS 12-14)

In these experiments, the 9.525 valve was replaced by a valve of 8.410mm dia, the new valve having a gasket ratio to the valve bore in line with compressor automatic reed valves as fitted by a particular compressor manufacturer. This was part of a general redesign of the rig, which also included replacement of a brass cylinder by a lightweight plastic cylinder, with the aim of bringing valve rise times nearer to those experienced in a compressor. By this means, the rise time was reduced to about seven milliseconds. This is still considerably higher than that to be anticipated in a compressor (less than 3 ms) but was as fast as could be obtained under the necessary condition of pulling the cylinder off the valve seat. Graphs 12, 13 and 14 show the behaviour of valve gas force at this shorter rise time, with initial cylinder pressures as before of approximately 30, 50 and 75kN/m^2 respectively.

In Graphs 12-14, the limits of dynamic force beyond impact at around 8ms increase suddenly. This is due to acceleration effects transmitted through the rig following impact on the stops, has nothing to do with valve gas forces and should therefore be discounted. (Photographs 2 and 3).

It should be noted that no comparable acceleration effects were encountered for the 9.525mm O/D Valve case, the indications being that this effect was attributable to the speed of valve opening.

At this gasket ratio, the clear minimum in force found using the larger valve does not appear. This suggests that, at low gasket ratios, detachment of the flow from the valve seat occurs so early as to be lost in the early force gradients. Since this valve has a gasket ratio similar to those used in compressor practise, the indications are that the flow may generally in compressor practise be regarded as being in the free jet detached mode, and not in the mode of attached flow along the valve seat.

The difference between static and dynamic gas force during the early stages of valve opening, as found for the 9.525mm O/D valve is again apparent in graphs 12-14, particularly at the highest initial cylinder pressure (Graph 14).

Theoretical Curves

Theoretical curves of gas force on the valve obtained from a finite element model of continuous flow through the valve at various valve openings and pressures are also shown on these graphs. These will be discussed following development of the finite element model in Chapter VI. The discussion of these curves appears on pages 144 etc.

CHAPTER V

THEORETICAL ANALYSIS FOR TWO-DIMENSIONAL AND AXI-SYMMETRIC FLOWS

CHAPTER V

THEORETICAL ANALYSIS FOR TWO-DIMENSIONAL AND AXI-SYMMETRIC FLOWS

1. Introduction

The analysis of two-dimensional and axi-symmetric flows has attracted the attention of engineers over a very long time. Flow characteristics of interest include velocity distribution and pressure distribution over the entire flow field and also the forces produced and the free-surface location for free-surface problems. Although two-dimensional flow analysis has been well developed and extended to axi-symmetric flows, most of the existing methods can solve only problems with simple geometric boundaries and the popular finite difference method sometimes is susceptible to accuracy problems (irregular stars). There could also be good value in tackling this problem using the finite difference technique, but a large degree of sophistication and advanced knowledge would be required. Therefore, the finite element technique was chosen to enable results to be obtained in a reasonably defined period of time.

In this chapter, the formulation of the general two-dimensional irrotational flow of an ideal fluid by finite element analysis will be presented. This will be followed by an extension of this method to cover axi-symmetric flow. When the free-surface problem is encountered as in the axi-symmetric flow case, it has only to be treated in almost exactly the same manner as in treating a two-dimensional problem.

2. Problem Formulation

(a) Problem Formulation for Two-Dimensional Flow

Both a velocity potential ϕ and a stream function ψ exist to aid the present study of a steady, two-dimensional, irrotational/

irrotational flow of an ideal fluid. As the method of formulation for ϕ and ψ are very similar in practice, only the formulation for ϕ will be developed and presented in this section since this is applicable in this study.

In variational form the velocity potential problem to be solved is that of minimising the functional (equation 2.19a):

$$I(\phi) = \frac{\rho}{2} \iint_A \left[(\phi,_x)^2 + (\phi,_y)^2 \right] dx.dy - \rho \oint_c \phi.(\phi,_n)^a . ds \qquad (5.1)$$

over the flow domain A enclosed by a boundary curve B. The first term is to be integrated over the entire flow region, giving the kinetic energy of the flow and the second term is to be evaluated over the boundary portion c, where non-zero normal velocity $q_n = (\phi,_n)^a$ is specified, representing twice the work done by the impulsive pressure in starting motion from rest.

A general flow domain is shown in FIG. 20

As pointed out earlier, minimisation of $I(\phi)$ is equivalent to solving the Laplace equation:

$$\phi,_{xx} + \phi,_{yy} = 0 \qquad \text{in A}$$

with

$$\phi,_n = (\phi,_n)^a \qquad \text{on C.}$$

In the finite element formulation, the region to be analysed is divided into N' sub-regions or finite elements and equation (5.1) can be replaced by:

$$I(\phi^e) = \sum_{e=1}^{N'} I^e. (\phi^e) \qquad (5.2a)$$

where

$I^e (\phi^e)$ =/

GENERAL FLOW DOMAIN.

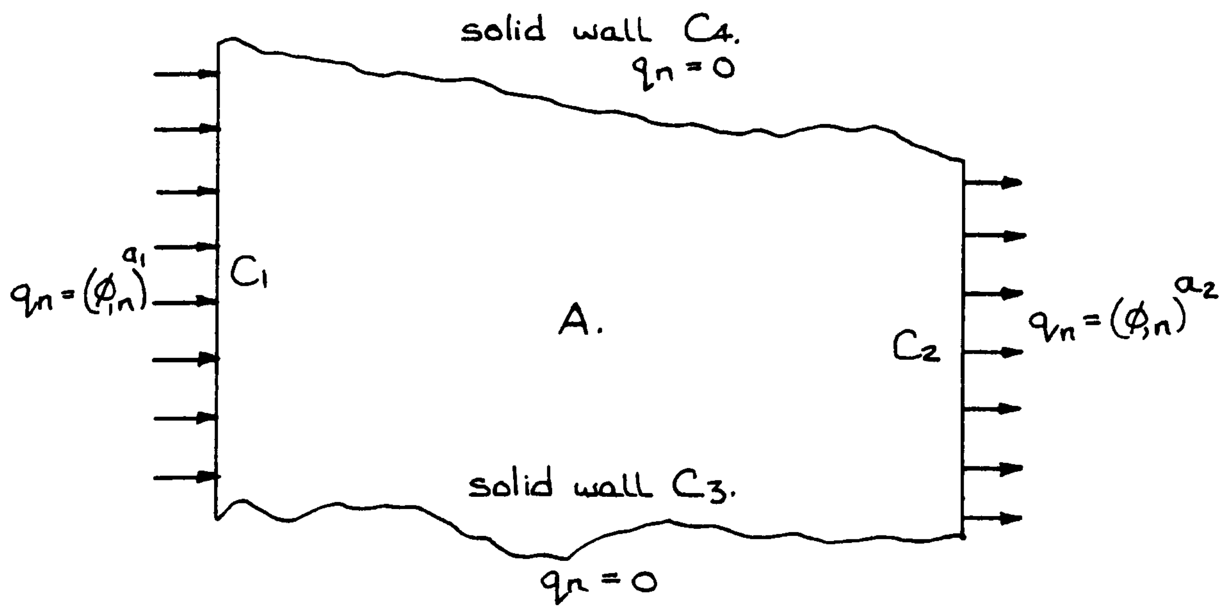

$$C = C_1 + C_2$$

$$B = C_1 + C_2 + C_3 + C_4$$

FIGURE 20

$$I^e \cdot (\phi^e) = \frac{\rho^e}{2} \iint_{A^e} \left(\left[\phi,_x{}^e \right]^2 + \left[\phi,_y{}^e \right]^2 \right) dx . dy - \rho^e \oint_{c^e} \phi^e \cdot (\phi,_n)^a \, ds \tag{5.2b}$$

is a measure of the energy of a representative element e, which may, in turn, consist of several sub-elements. In the present study, it was decided to chose quadrilateral elements to approximate the flow region under consideration.

Each element is composed of four triangular elements, as shown in FIG. 21. Within each triangle $\phi^{(m)}$ is approximated by a second order polynomial, so that the velocity components $u = \phi,_x{}^{(m)}$ and $v = \phi,_y{}^{(m)}$ in the x and y directions respectively, can vary linearly throughout each triangular region. Since the prediction of boundary velocities or pressures is often an important result of the analysis, this velocity representation is needed if solutions are to be accurate.

Each triangular element has three corner nodes and three side nodes, one at the mid-point of each side. FIG. 21 gives the triangular or area co-ordinates:

$$L_i = \frac{A_i}{A^{(m)}}$$

where $A^{(m)}$ = area of entire triangle and

A_i = area of one sub-triangle.

Thus, the side connecting nodes 1 and 2 is described by:

$$L_3 = 0 \quad \text{and also} \quad L_1 + L_2 + L_3 = 1$$

For these conditions the representation of ϕ in triangle (m), in terms of the six nodal values $\phi_i{}^{(m)}$ where i = 1 to 6 when written/

QUADRILATERAL ELEMENT AND ITS SUBELEMENT.

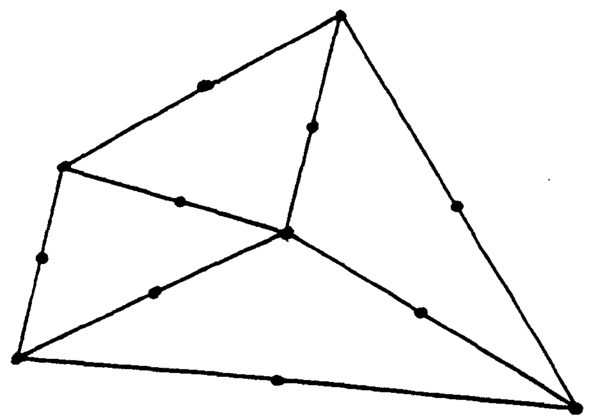

(a) QUADRILATERAL ELEMENT.

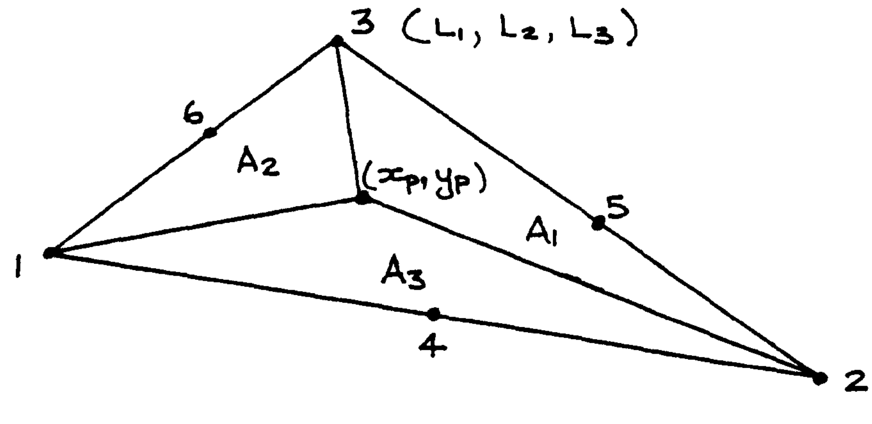

(b) TRIANGULAR SUBELEMENT. (TWO DIMENSIONAL)

FIGURE 21

written in a simplified form by using the summation convention, is:

$$\phi^{(m)} = \phi_i^{(m)} . N_i \qquad (i = 1, 6) \qquad (5.3a)$$

where repeated subscript implies summation from one to the number indicated, where:

$$N_i = \langle L_1 (2 L_1 - 1), L_2 (2 L_2 - 1), L_3 (2 L_3 - 1), 4 L_1 L_2, 4 L_2 L_3, 4 L_3 L_1 \rangle \qquad (5.3b)$$

According to equation (2.3a), the velocity components are then:

$$u^{(m)} = \phi,_x^{(m)} = \phi_i^{(m)} . T_i^{(m)} \qquad (i = 1 \text{ to } 6) \quad (5.4a)$$

and

$$v^{(m)} = \phi,_y^{(m)} = \phi_i^{(m)} . \hat{T}_i^{(m)} \qquad (i = 1 \text{ to } 6) \quad (5.4b)$$

where

$$T_i^{(m)} = (4 L_i - 1) b_i/2A^{(m)} \qquad (\text{no summation on } i) \quad (5.5a)$$

$$T_{i+3}^{(m)} = 4 (b_i L_j + b_j L_i) 2A^{(m)} \qquad (\text{no summation on } i) \quad (5.5b)$$

$$a_k = x_j - x_i, \; b_k = y_i - y_j, \; 2A^{(m)} = a_k.b_j - a_j.b_k \qquad (5.5c)$$

and

$$i = (1, 2, 3), \; j = (2, 3, 1), \; k = (3, 1, 2) \qquad (5.5d)$$

The array $\hat{T}_i^{(m)}$ is found by replacing the b's with a's in the expressions for $T_i^{(m)}$.

Upon substituting equations (5.3), (5.4) and (5.5) into equation (5.2b) (where subscript (m) is used instead of e to denote triangular sub-element), followed by computing the partial derivation of $I^{(m)} (\phi)$ with respect to $\phi_i^{(m)}$ and interchanging sub-scripts i and j, one similarly obtains equations as (A.13), (A.14) and (A.15) as shown in APPENDIX A:

i.e./

$$\text{i.e.}\quad \frac{\partial I^{(m)}(\phi)}{\partial \phi_i^{(m)}} = \rho^m \iint_{A^{(m)}} (T_i^{(m)} \cdot T_j^{(m)} + \hat{T}_i^{(m)} \cdot \hat{T}_j^{(m)})\, \phi_j^{(m)}\, dA$$

$$- \rho^{(m)} \cdot \oint_{c^{(m)}} N_i\, (\phi,_n)^a\, ds \tag{5.6a}$$

$$\text{or}\quad \frac{\partial I^{(m)}(\phi)}{\partial \phi_i^{(m)}} = S_{ij}^{(m)} \cdot \phi_j^{(m)} - SL_i^{(m)} \tag{5.6b}$$

$$= \left[S\right]^{(m)} \left\{\phi\right\}^{(m)} + \left\{SL\right\}^{(m)} \tag{5.6c}$$

It will be noticed that in equation (5.6c) the last term is +ve. This is dependent on the convention used for the defining of the direction of the boundary velocity.

In the terminology of structural mechanics, $S_{ij}^{(m)}$ is the element stiffness matrix and $SL_i^{(m)}$ is the corresponding load matrix for a triangular sub-element, which are derived and listed in (APPENDIX A, Derivation of Element Matrices). The contribution from each triangle in a quadrilateral element to the terms in equation (5.6) is first evaluated, followed by appropriately adding up all the contributions to the 13 nodal points. The equations for the five interior points of the quadrilateral are then eliminated at the element level to obtain the element stiffness matrix S_{ij}^{e} and its load matrix SL_i^{e} for a quadrilateral element. The expressions for each quadrilateral are then added together appropriately to form the system matrices, which is identical to the direct stiffness method of structural mechanics [39].

The resulting system of equations is linear, symmetric and in band form. The total number of equations is equal to the total number/

number of nodal points and the semi band width is equal to one plus the difference between the largest and the smallest nodal numbers in a quadrilateral element. This system of equations is then solved for the ϕ_i's by Gaussian elimination. Once the ϕ_i's are known, the velocity components at any point are calculated by equations (5.4). After that the pressure and force distributions can be evaluated by applying equations (2.15).

(b) Problem Formulation for Axi-Symmetric Flow

Like the analysis of two-dimensional flows, both a velocity potential ϕ and a stream function ψ exist to aid the present study of a steady, axi-symmetric, irrotational flow of an ideal fluid. However, formulation in terms of the velocity potential function appears to be much simpler, because it bears a close resemblance to the formulation for two-dimensional flows. In this study, the velocity potential function was chosen to be the primary unknown.

In variational form the velocity potential problem to be solved is that of minimising the functional (equation 2.19b):

$$I(\phi) = \rho\pi \iint_A \left[(\phi,_x)^2 + (\phi,_r)^2 \right] r.\,dr.\,dx - 2.\rho\pi \oint_c \phi.(\phi,_n)^a.\, r.\,ds \tag{5.7}$$

The first term on the right hand side is the kinetic energy in the entire flow region and the second term, with the integration carried out on the portion of surface boundary where the normal velocity component is specified, represents twice the work done by the impulsive force in starting the flow to move from rest. This equation resembles the one for two-dimensional flow except that in place of y, the radius r has been used. As a direct result of axial/

axial symmetry r appears inside both integrals. Once again, the minimisation of $I(\phi)$ is equivalent to solving the Laplace equation:

$$\phi,_{xx} + \frac{1}{r}\phi,_r + \phi,_{rr} = 0 \qquad \text{in } A$$

with

$$\phi,_n = (\phi,_n)^a \qquad \text{on } C$$

Since the procedures to be followed in the finite element formulation are exactly the same for two-dimensional and axisymmetric flows, only a brief description of the development and the resulting equations will be presented.

Upon dividing the flow region into N' quadrilateral elements (NOTE: Each quadrilateral element is now a cross-section of an annular region through which flow occurs), equation (5.7) is approximated by:

$$I(\phi) = \sum_{e=1}^{N'} I^e\ (\phi) \tag{5.8a}$$

where

$$I^e\ (\phi) = \rho^e \cdot \pi \int\int_{A^e} \left[(\phi,_x{}^e)^2 + (\phi,_r{}^e)^2\right] r\ dr\ dx - 2\rho^e \pi \oint_{c^e} \phi^e\ (\phi,_n)^a\ r\ ds \tag{5.8b}$$

represents the energy of a typical element e, which may, in turn, consist of several sub-elements. The quadrilateral element, composed of four triangular elements, will again be used as in the two-dimensional analysis. In each triangular element, $\phi^{(m)}$, is approximated by a second order polynomial in the form:

$$\phi^{(m)} = \phi_i{}^{(m)}\ N_i{}^{(m)} \qquad (i = 1 \text{ to } 6) \tag{5.9a}$$

where/

where

$$N_i = \langle L_1 (2 L_1 - 1), L_2 (2 L_2 - 1), L_3 (2 L_3 - 1), 4 L_1 . L_2,$$

$$4 L_2 . L_3, 4 L_3 . L_1 \rangle \quad (5.9b)$$

The velocity components are, according to equation (2.3b):

$$V_x^{(m)} = \phi,_x^{(m)} = \phi_i^{(m)} . T_i^{(m)} \qquad (i = 1 \text{ to } 6) \quad (5.10a)$$

$$V_r^{(m)} = \phi,_r^{(m)} = \phi_i^{(m)} \hat{T}_i^{(m)} \qquad (i = 1 \text{ to } 6) \quad (5.10b)$$

with

$$T_i^{(m)} = (4 L_i - 1) b_i/2 A^{(m)} \qquad \text{(no summation on i)} \quad (5.11a)$$

$$T_{i+3}^{(m)} = 4 (b_i . L_j + b_j . L_i)/2 A^{(m)} \qquad \text{(no summation on i)} \quad (5.11b)$$

$$a_k = x_j - x_i, \ b_k = r_i - r_j, \ 2 A^{(m)} = a_k b_j - a_j b_k \quad (5.11c)$$

$$i = (1, 2, 3), \ j = (2, 3, 1) \text{ and } k = (3, 1, 2) \quad (5.11d)$$

As before the array $\hat{T}_i^{(m)}$ is found by replacing the b's with a's in the expressions for $T_i^{(m)}$.

In addition to the above equations, the variable r is introduced as:

$$r = r_1 . L_1 + r_2 . L_2 + r_3 . L_3 \quad (5.12)$$

where r_1, r_2 and r_3 are radial co-ordinates of the corner nodes 1, 2 and 3 respectively, and L_1, L_2 and L_3 are again the area co-ordinates of a point in the triangular element.

Upon substituting equations (5.9), (5.10) and (5.11) into equation (5.8b) (NOTE: Subscript (m) must be used in place of e to designate/

designate calculations for a triangular element) followed by computing the partial derivatives of $I^{(m)}\ \phi$ with respect to $\phi_j^{(m)}$ and interchanging subscripts i and j, one similarly obtains equations as (A.37) and (A.38) as shown in APPENDIX A:

$$\frac{\partial I^{(m)}(\phi)}{\partial \phi_i^{(m)}} = 2\,\rho^{(m)}\pi \iint_{A^{(m)}} \left(T_i^{(m)}\, T_j^{(m)} + \hat{T}_i^{(m)}\, \hat{T}_j^{(m)}\right) r \cdot \phi_j^{(m)}\, dA$$

$$- 2\,\rho^{(m)}\pi \oint_{c^{(m)}} N_i \cdot (\phi,_n)^a\, r \cdot ds \tag{5.13}$$

or

$$\frac{\partial I^{(m)}(\phi)}{\partial \phi_i^{(m)}} = SA_{ij}^{(m)}\ \phi_j^{(m)} - SLA_i^{(m)} \tag{5.14a}$$

$$= \left[SA\right]^{(m)} \left\{\phi\right\}^{(m)} + \left\{SLA\right\}^{(m)} \tag{5.14b}$$

Here $SA_{ij}^{(m)}$ and $SLA_i^{(m)}$ are the element stiffness matrix and the corresponding load matrix for a triangular element, which are derived and listed in APPENDIX A, Derivation of Element Matrices.

The element stiffness matrix SA_{ij}^{e} and its associated load matrix SLA_i^{e} for a quadrilateral element can then be formed by adding up the contributions from the four triangular sub-elements and then eliminating the equations for the five interior points. Next, the system matrices are formed in a process identical to the direct stiffness method [39]. These matrices constitute a system of equations which is linear, symmetric and in band form as in the case for two-dimensional flow.

Solution is then done, to obtain the $\phi_i^{(m)}$ values and then secondary unknowns are obtained in the same manner as for two-dimensional/

dimensional flow.

For a more complete explanation of the derivation of the element matrices and the subsequent overall program produced, see APPENDICES A and C respectively.

CHAPTER VI

THEORETICAL - PROCEDURE AND RESULTS

CHAPTER VI

THEORETICAL - PROCEDURE AND RESULTS

1. Introduction

2. Theoretical Assumptions

3. Mathematical Static-Force Procedure

4. Tabulated Results

5. Comments

1. Introduction

The theoretical procedure adopted in this thesis, for determining the quasi-static forces on a disc valve for various displacements, is based on the finite element technique. This determines the velocity profile throughout the discretised flow domain from whence pressure distribution and subsequently quasi-static force distribution can be determined over the valve face.

CHAPTER V detailed the procedure used in obtaining the velocity distribution throughout the flow domain and in particular, over the valve face, from which point this chapter will describe the further modifications required to enable quasi-static force values over the valve face to be obtained.

Velocity potentials throughout the flow domain for a particular valve O/D and displacement case (nominal upstream velocity equal to 1 m/s) is shown in FIG. 25.

2. Theoretical Assumptions

The predominant aspect of this analysis is that Laplace's equation has been used in determining the quasi-static force on the valve. This implies that the approach momentum force is negligible in comparison to the pressure force on the valve. This assumption can be justified in this case since:

$$F_{momentum} = \rho A.V^2 = \underline{0.03\ N}$$

where ρ = density of fluid, kg/m^3

A = area of throat, m^2

and V = velocity at throat, m/s

whereas the <u>minimum</u> resulting pressure force from GRAPHS 3 - 14 = $\underline{0.5\ N}$.

Further/

Further to this prior assumption, no forces were considered on the back of the valve since a fully stalled condition was considered to be applicable. Experimental work showed the flow to be almost in the form of a disc with a boundary very little above valve level and only downward entrained flow appeared above the valve (REFERENCE 49).

In conclusion, the overall assumption made in obtaining the theoretical quasi-static force was that Laplace's equations were used up to the valve perimeter, then jet theory was considered with downward air entrainment from behind the valve.

The flow domain used for the theoretical determination of quasi-static valve forces is shown in FIG. 22.

This figure shows half of the physical plane of flow where the x-axis is chosen to coincide with the axis of symmetry and the y-axis chosen to pass through points J and A, the upstream portion of the domain.

The flow region under consideration is then divided into 123 quadrilateral elements as shown in FIG. 23, with elements of smaller size near the valve to accommodate more accurately the larger velocity gradients in this region (see APPENDIX C). FIG. 24 shows in detail the nodes and dimensions across the valve face.

In arriving at the amount of elements chosen, the following two major points should be borne in mind. Firstly the limitation of core space available for any particular computer and secondly, that monotonic convergence should prevail.

Having finally decided the number of elements suitable without reasonable loss of accuracy the work can continue.

To ensure the program was correctly developed, it was applied/

VALVE BORE	6·35mm
VALVE O/D. A	9·525 "
" " B	8·410 "

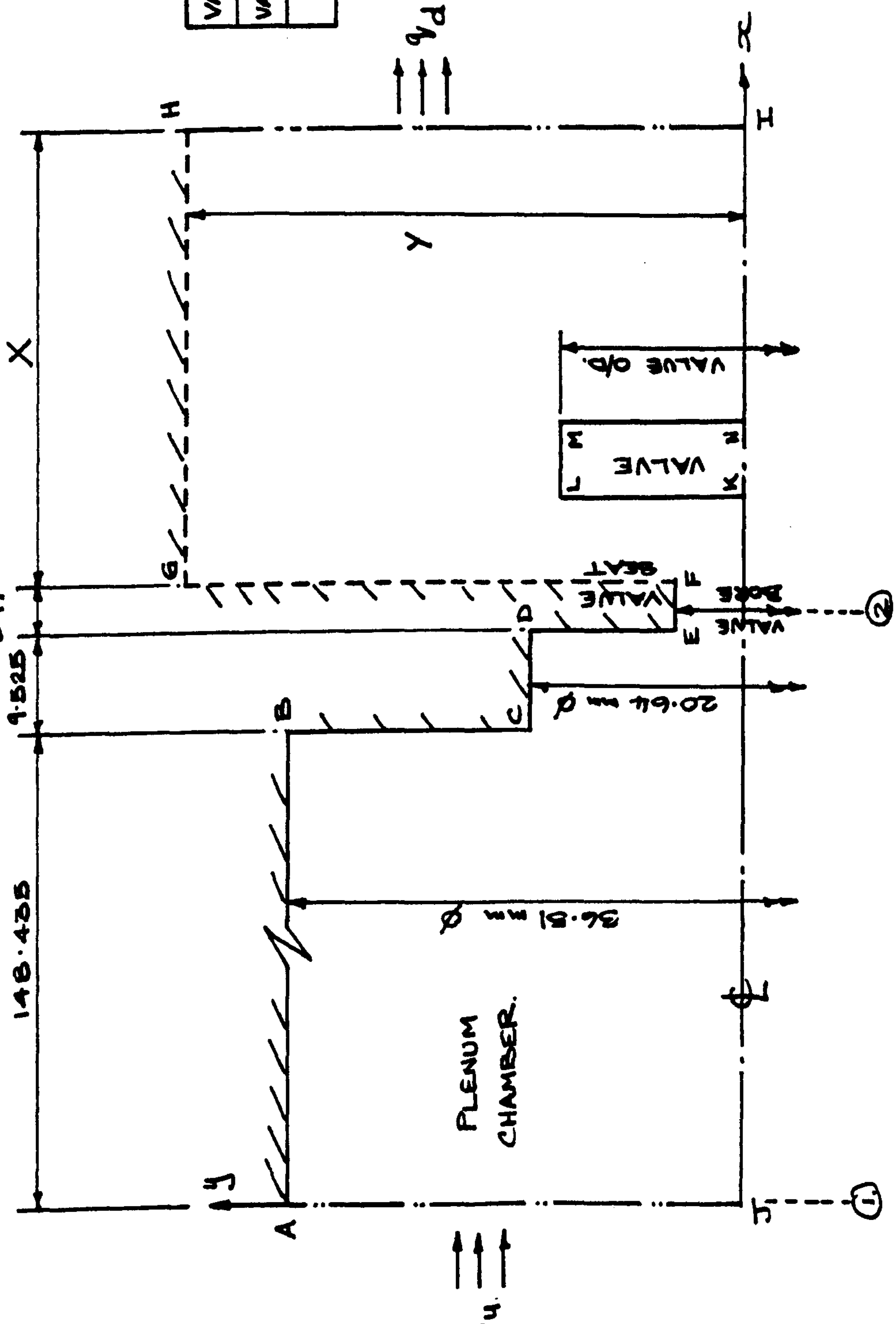

THEORETICAL FLOW DOMAIN (AXISYMMETRIC CASE)

FIGURE 22.(N.T.S)

GRID DISCRETIZATION (N.T. S)

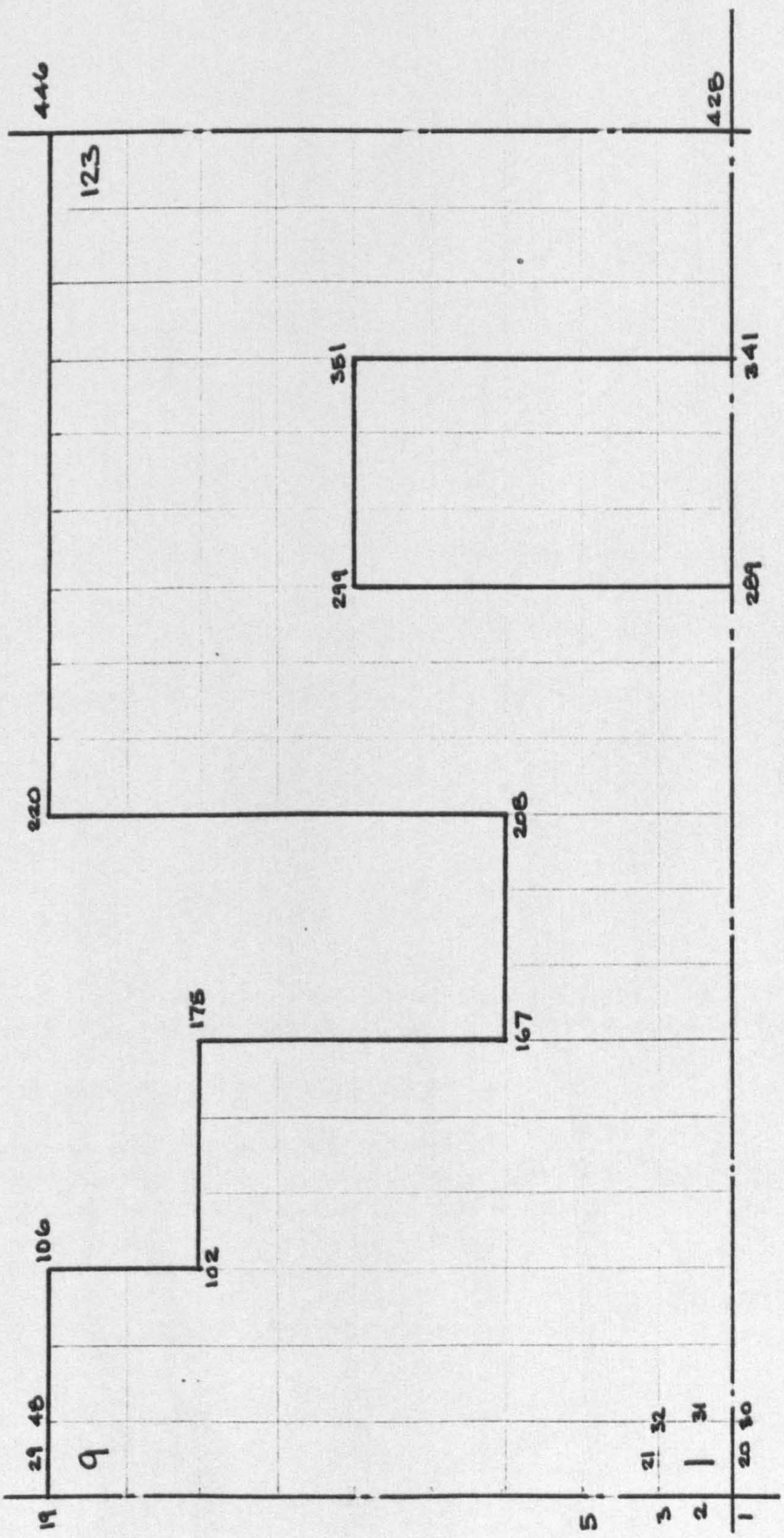

FIGURE 23.

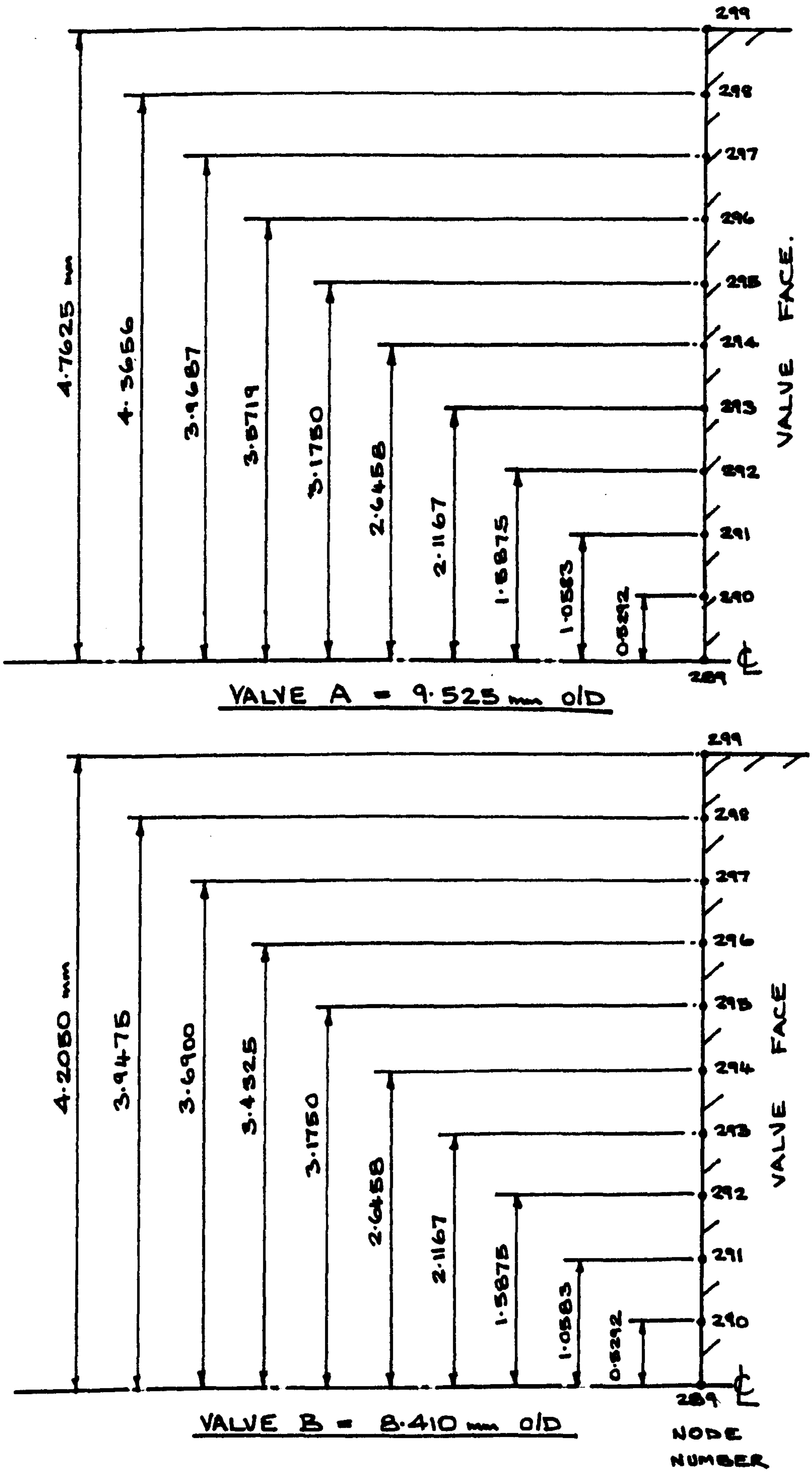

NODE DIMENSIONS.

FIGURE 24.

applied to calculate steady and free surface flow from a nozzle. The results obtained when compared with other experimenters showed agreement and the program was therefore modified to encompass the valve problem.

For flow chart, listing and description of program see APPENDIX C.

The boundary conditions imposed by this problem are as follows; normal velocity components along ABCDEFGH and IJ are zero, i.e. $(\phi,_{n})^{a} = \phi$, but the upstream face has a normal velocity of $(\phi,_{n})^{a} = -q_{u}$, which is determined using equation 6.1:

$$q_{u} = \sqrt{\frac{2A_{2}^{2}\ (P_{1} - P_{2})}{(A_{1}^{2} - A_{2}^{2})}} \tag{6.1}$$

where subscripts 1 and 2 refer to the upstream and throat conditions respectively.

The downstream velocity is obtained from the mass continuity equation:

$$A_{1}\ q_{u} = A_{2}\ q_{d} = \text{const} \tag{6.2}$$

and in turn is equivalent to $(\phi,_{n})^{a} = q_{d}$.

It should be noted that the velocities obtained from the computer program are firstly calculated on the basis of $q_{u} = 1$ m/s and then using equation 6.1, as the appropriate scaling factor, the correct velocities with respect to the chosen pressure and displacement are obtained.

These calculations are based on the non-viscous assumption and that therefore, similar streamlines are applicable at all speeds.

3. <u>Mathematical Static-Force Procedure</u>/

3. Mathematical Static-Force Procedure

Having obtained the velocity distribution throughout the discretised flow domain based on an upstream velocity $q_u = 1$ m/s and in particular over the valve face for the various displacements, the following equations are required to enable the quasi-static force over the valve face to be determined.

As previously obtained from Bernoulli's equation:

$$q_u = \text{scaling factor} = \sqrt{\frac{2A_2^2 (P_1 - P_2)}{(A_1^2 - A_2^2)}} \qquad (6.1)$$

where subscripts 1 and 2 refer to upstream and throat conditions respectively and for a particular displacement and node the actual velocity on the valve face equals:

$$q_{\text{valve face}} = q_u * (q_{\text{valve}}) \qquad (6.3)$$

where q_{valve} = velocity on valve face based on $q_u = 1$ m/s. Hence, having obtained $q_{\text{valve face}}$ and once more using Bernoulli's equation:

$$P_{\text{valve face}} = \left[\frac{(q_u^2 - q_{\text{valve face}}^2)}{2}\right] + \frac{P_1}{\rho} \qquad (6.4)$$

or $$P_{\text{valve face}} = q_u^2\left[\frac{(1 - q_{\text{valve}}^2)}{2}\right] + \frac{P_1}{\rho} \qquad (6.5)$$

If now all nodes on valve face are considered, a pressure curve over this surface would result and upon integration using equation 6.6, a quasi-static force would result.

$$F = \int_0^{2\pi} \int_0^{R} P \, . \, dr \, . \, r \, . \, d\theta$$

A program has been written to enable these calculations to be carried out. This incorporates a best curve fit routine which, when using the pressure distribution data, generally yields a 7th order polynomial fit.

4. Tabulated Results

VELOCITY PROFILES FOR VARYING DISPLACEMENTS

TABLE NO.	VALVE O/D mm (inches)
4.1	9.525 (0.375)
4.2	8.410 (0.331)

VALVE BORE 6.35 mm (0.25") IN BOTH CASES

THEORETICAL QUASI-STATIC FORCE RESULTS

TABLE NO.	VALVE O/D mm	GRAPH NO.	UPSTREAM PRESSURE P_1	
			kN/m^2	PSI
4.3	9.525	3	31.03	4.50
4.4	"	4	50.00	7.25
4.5	"	5	76.88	11.15
4.6	"	6	29.64	4.30
4.7	"	7	53.44	7.75
4.8	"	8	77.92	11.30
4.9	"	9	25.58	3.71
4.10	"	10	54.00	7.83
4.11	"	11	76.40	11.08
4.12	8.410	12	29.64	4.30
4.13	"	13	55.16	8.0
4.14	"	14	69.29	10.05

Comparison curves between experimental and theoretical results can be found in GRAPHS 3 - 14, CHAPTER IV.

TABLE 4.1 VALVE O/D = 9.525 mm

NODE NO. → ↓mm DISPL	289	290	291	292	293	294	295	296	297	298	299
0.25	0.4243	5.0164	9.4173	19.0530	21.8569	66.2927	153.7119	181.2951	165.3841	155.9951	82.4331
0.50	0.2755	4.8597	9.5386	17.7239	24.5641	49.6307	82.0258	87.9474	81.8047	82.6918	54.3045
0.75	0.2284	4.6429	9.2511	16.3523	23.7016	38.5902	54.6272	56.9366	53.6913	58.0193	41.8212
1.00	0.1705	4.3800	8.7961	14.9133	21.5437	30.9688	40.1963	41.6337	39.7660	45.2279	34.2618
1.25	0.1142	4.0801	8.2281	13.4476	19.0898	25.4435	31.3362	32.5128	31.4513	37.1591	29.0498
1.50	0.0685	3.7616	7.5955	12.0360	16.7518	21.2983	25.3832	26.4572	25.9202	31.5206	25.1962

ALL RESULTS BASED ON NOMINAL UPSTREAM VELOCITY = 1 m/s

TABLE 4.2 VALVE O/D = 8.410 mm

NODE NO. → / ↓ mm DISPL	289	290	291	292	293	294	295	296	297	298	299
0.25	0.4396	5.0337	9.4029	19.1749	21.4798	67.3128	151.3107	185.3133	178.3628	175.6562	93.7601
0.50	0.2716	4.8680	9.5560	17.7725	24.5707	50.0604	80.7433	88.8096	87.0373	95.3116	62.3760
0.75	0.2291	4.6534	9.2735	16.4041	23.7890	38.8494	54.2492	57.7581	57.1295	67.5740	48.0990
1.00	0.1725	4.3911	8.8177	14.9689	21.6269	31.2118	40.3258	42.6126	42.6240	52.8098	39.2221
1.25	0.1165	4.0941	8.2548	13.5155	19.1827	25.7332	31.7708	33.5913	34.0413	43.3993	33.0317
1.50	0.0707	3.7795	7.6300	12.1187	16.8660	21.6374	25.9908	27.5728	38.3235	36.7953	28.4334

ALL RESULTS BASED ON NOMINAL UPSTREAM VELOCITY = 1 m/s

TABLE 4.3

UPSTREAM PRESSURE P_1		THROAT PRESSURE P_2		VALVE DISPLACEMENT		THEORETICAL STATIC FORCE	
kN/m^2	PSI	kN/m^2	PSI	mm	thous	N	lbf
30.57	4.46	29.31	4.28	0.125	5	1.17	0.26
30.38	4.44	28.41	4.15	0.25	10	1.09	0.25
29.87	4.36	26.56	3.88	0.50	20	1.03	0.23
29.30	4.28	23.62	3.45	0.75	30	0.96	0.22
28.88	4.22	21.06	3.08	1.00	40	0.91	0.21
28.54	4.17	18.78	2.74	1.25	50	0.86	0.19
26.49	3.87	16.24	2.37	1.50	60	0.76	0.17

TABLE 4.4

UPSTREAM PRESSURE P_1		THROAT PRESSURE P_2		VALVE DISPLACEMENT		THEORETICAL STATIC FORCE	
kN/m^2	PSI	kN/m^2	PSI	mm	thous	N	lbf
49.69	7.25	47.64	6.96	0.125	5	1.89	0.43
49.31	7.20	46.10	6.73	0.25	10	1.77	0.40
48.67	7.11	43.29	6.32	0.50	20	1.67	0.38
48.10	7.02	38.78	5.66	0.75	30	1.58	0.36
47.50	6.93	34.65	5.06	1.00	40	1.50	0.34
46.71	6.82	30.74	4.49	1.25	50	1.40	0.32
44.73	6.53	27.43	4.00	1.50	60	1.29	0.29

TABLE 4.5

UPSTREAM PRESSURE P_1		THROAT PRESSURE P_2		VALVE DISPLACEMENT		THEORETICAL STATIC FORCE	
kN/m^2	PSI	kN/m^2	PSI	mm	thous	N	lbf
76.37	11.15	73.22	10.69	0.125	5	2.91	0.66
76.03	11.10	71.09	10.38	0.25	10	2.73	0.62
75.26	10.99	66.93	9.77	0.50	20	2.59	0.58
74.29	10.85	59.90	8.74	0.75	30	2.42	0.54
73.63	10.75	53.70	7.84	1.00	40	2.32	0.52
73.00	10.66	48.04	7.01	1.25	50	2.19	0.49
72.33	10.56	44.34	6.47	1.50	60	2.08	0.47

TABLE 4.6

UPSTREAM PRESSURE P_1		THROAT PRESSURE P_2		VALVE DISPLACEMENT		THEORETICAL STATIC FORCE	
kN/m^2	PSI	kN/m^2	PSI	mm	thous	N	lbf
29.19	4.26	27.99	4.09	0.125	5	1.11	0.25
28.80	4.20	26.93	3.93	0.25	10	1.04	0.23
27.85	4.07	24.77	3.62	0.50	20	0.96	0.22
26.75	3.91	21.57	3.15	0.75	30	0.88	0.20
25.77	3.76	18.80	2.74	1.00	40	0.81	0.18
24.80	3.62	16.32	2.38	1.25	50	0.74	0.17
21.71	3.17	13.31	1.94	1.50	60	0.62	0.14

TABLE 4.7

UPSTREAM PRESSURE P_1		THROAT PRESSURE P_2		VALVE DISPLACEMENT		THEORETICAL STATIC FORCE	
kN/m^2	PSI	kN/m^2	PSI	mm	thous	N	lbf
53.00	7.75	50.8	7.42	0.125	5	2.02	0.46
52.50	7.67	49.09	7.17	0.25	10	1.89	0.43
51.15	7.47	45.49	6.64	0.50	20	1.76	0.40
49.83	7.28	40.18	5.87	0.75	30	1.64	0.37
48.55	7.09	35.41	5.17	1.00	40	1.53	0.35
47.16	6.89	31.04	4.53	1.25	50	1.42	0.32
41.95	6.12	25.72	3.75	1.50	60	1.21	0.27

TABLE 4.8

UPSTREAM PRESSURE P_1		THROAT PRESSURE P_2		VALVE DISPLACEMENT		THEORETICAL STATIC FORCE	
kN/m^2	PSI	kN/m^2	PSI	mm	thous	N	lbf
77.37	11.30	74.18	10.83	0.125	5	2.95	0.66
76.73	11.21	71.74	10.47	0.25	10	2.76	0.62
75.21	10.98	66.89	9.77	0.50	20	2.59	0.58
73.66	10.75	59.39	8.67	0.75	30	2.42	0.54
72.20	10.54	52.66	7.69	1.00	40	2.28	0.51
70.63	10.31	46.48	6.79	1.25	50	2.12	0.48
64.86	9.47	39.77	5.81	1.50	60	1.87	0.42

TABLE 4.9

UPSTREAM PRESSURE P_1		THROAT PRESSURE P_2		VALVE DISPLACEMENT		THEORETICAL STATIC FORCE	
kN/m^2	PSI	kN/m^2	PSI	mm	thous	N	lbf
25.17	3.68	24.13	3.52	0.125	5	0.96	0.22
24.52	3.58	22.93	3.35	0.25	10	0.88	0.20
22.93	3.35	20.39	2.98	0.50	20	0.79	0.18
21.18	3.09	17.08	2.49	0.75	30	0.70	0.16
19.40	2.83	14.15	2.07	1.00	40	0.61	0.14
17.90	2.61	11.78	1.72	1.25	50	0.54	0.12
-	-	-	-	1.50	60	-	-

TABLE 4.10

UPSTREAM PRESSURE P_1		THROAT PRESSURE P_2		VALVE DISPLACEMENT		THEORETICAL STATIC FORCE	
kN/m^2	PSI	kN/m^2	PSI	mm	thous	N	lbf
53.65	7.83	51.44	7.51	0.125	5	2.05	0.46
52.36	7.64	48.96	7.15	0.25	10	1.88	0.42
50.66	7.40	45.06	6.58	0.50	20	1.74	0.39
48.51	7.08	39.11	5.71	0.75	30	1.59	0.36
45.91	6.70	33.49	4.89	1.00	40	1.45	0.33
-	-	-	-	1.25	50	-	-
-	-	-	-	1.50	60	-	-

TABLE 4.11

UPSTREAM PRESSURE P_1		THROAT PRESSURE P_2		VALVE DISPLACEMENT		THEORETICAL STATIC FORCE	
kN/m^2	PSI	kN/m^2	PSI	mm	thous	N	lbf
76.00	11.09	72.87	10.64	0.125	5	2.90	0.65
74.71	10.91	69.85	10.20	0.25	10	2.68	0.60
72.92	10.65	64.85	9.47	0.50	20	2.51	0.56
70.61	10.31	56.93	8.31	0.75	30	2.32	0.52
68.02	9.93	49.61	7.25	1.00	40	2.15	0.48
64.90	9.48	42.71	6.24	1.25	50	1.95	0.44
-	-	-	-	1.50	60	-	-

TABLE 4.12

UPSTREAM PRESSURE P_1		THROAT PRESSURE P_2		VALVE DISPLACEMENT		THEORETICAL STATIC FORCE	
kN/m^2	PSI	kN/m^2	PSI	mm	thous	N	lbf
29.60	4.32	28.38	4.14	0.125	5	0.93	0.21
29.38	4.28	27.47	4.01	0.25	10	0.87	0.20
28.60	4.18	25.44	3.71	0.50	20	0.80	0.18
27.65	4.04	22.29	3.25	0.75	30	0.76	0.17
27.03	3.95	19.72	2.88	1.00	40	0.71	0.16
26.18	3.82	17.23	2.52	1.25	50	0.66	0.15
25.91	3.78	15.89	2.32	1.50	60	0.62	0.14

TABLE 4.13

UPSTREAM PRESSURE P_1		THROAT PRESSURE P_2		VALVE DISPLACEMENT		THEORETICAL STATIC FORCE	
kN/m^2	PSI	kN/m^2	PSI	mm	thous	N	lbf
54.41	7.94	52.17	7.62	0.125	5	1.71	0.39
54.09	7.90	50.57	7.38	0.25	10	1.60	0.36
53.13	7.76	47.25	6.90	0.50	20	1.49	0.34
51.91	7.58	41.85	6.11	0.75	30	1.43	0.32
50.79	7.41	37.04	5.41	1.00	40	1.33	0.30
49.95	7.29	32.87	4.80	1.25	50	1.27	0.29
48.55	7.09	29.77	4.35	1.50	60	1.17	0.26

TABLE 4.14

UPSTREAM PRESSURE P_1		THROAT PRESSURE P_2		VALVE DISPLACEMENT		THEORETICAL STATIC FORCE	
kN/m^2	PSI	kN/m^2	PSI	mm	thous	N	lbf
68.25	9.96	65.43	9.55	0.125	5	2.15	0.48
67.71	9.88	63.30	9.24	0.25	10	2.01	0.45
66.50	9.71	59.14	8.63	0.50	20	1.87	0.42
65.28	9.53	52.63	7.68	0.75	30	1.80	0.40
64.09	9.36	46.75	6.82	1.00	40	1.68	0.38
63.09	9.21	41.52	6.06	1.25	50	1.60	0.36
62.00	9.05	38.01	5.55	1.50	60	1.49	0.33

TABLE 4.13

UPSTREAM VERSUS THROAT PRESSURES

DISPLACEMENT (mm)	UPSTREAM PRESSURE P_1 (kN/m^2)	THROAT PRESSURE P_2 (kN/m^2)	
		9.525 mm O/D VALVE	8.410 mm O/D VALVE
0.125	80	77.30	76.10
"	50	48.70	49.30
"	20	19.40	19.60
0.25	80	74.60	75.00
"	50	45.90	46.20
"	20	18.60	18.90
0.50	80	71.00	71.30
"	50	42.50	45.00
"	20	16.90	18.00
0.75	80	65.20	63.80
"	50	39.90	41.40
"	20	17.10	17.00
1.00	80	58.90	57.80
"	50	36.60	39.20
"	20	14.90	15.10
1.25	80	53.60	51.70
"	50	33.50	32.60
"	20	13.70	15.10
1.50	80	49.20	48.90
"	50	30.70	31.20
"	20	12.30	11.80

5. COMMENTS

This section includes the main points arising from the theoretical analysis used to determine the quasi-static forces on a disc type valve.

Adopting the technique outlined in Section 3 of this chapter, velocity profiles over the valve face for various valve displacements, with a nominal upstream velocity of 1 m/s are tabulated in Tables 4.1 - 4.2, and represented graphically in Graphs 15 and 16. From these graphs very little velocity difference exists between the two different valve sizes from the axis of symmetry (node point 289) to the throat outside diameter. (Node point 295). Over the area of overhang, for the larger valve case, the velocity profile drops off more quickly due to radial flow, hence a corresponding increase in valve face pressure and quasi-static force would result.

Graph 17 shows the variation in upstream pressure P_1 with the throat pressure P_2 (both obtained experimentally) for various displacements. The 1st set of results were carried out on the 9.525 mm O/D valve at Strathclyde University early in the research phase, and the 2nd set carried out on the 8.410 mm O/D valve since leaving Strathclyde. Since no discernable differences existed between P_1 and P_2, the results were combined and are hence applicable to both O/D valve cases.

These pressures were subsequently required in the determination of the upstream velocity qu, which led to the theoretical quasi-static force values being obtained as described in Section 3. Tables of these results are shown in Tables 4.3 - 4.14 and graphically in Graphs 18 and 19.

Finally, Table 4.15 includes values of experimental upstream versus throat pressures.

VELOCITY PROFILE FOR 9·525 mm O/D VALVE.

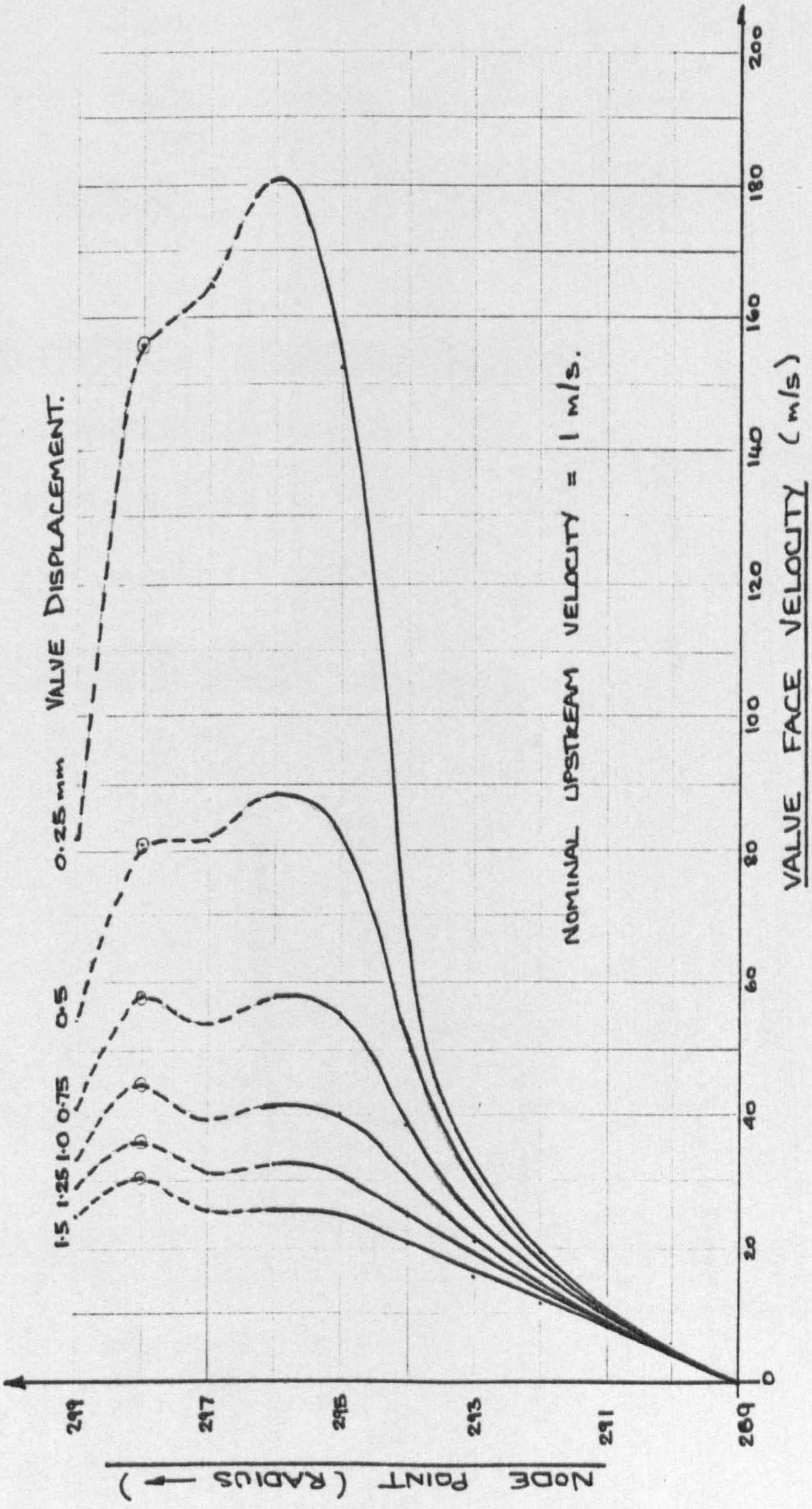

GRAPH 15.

VELOCITY PROFILE FOR 8·410 mm O/D VALVE

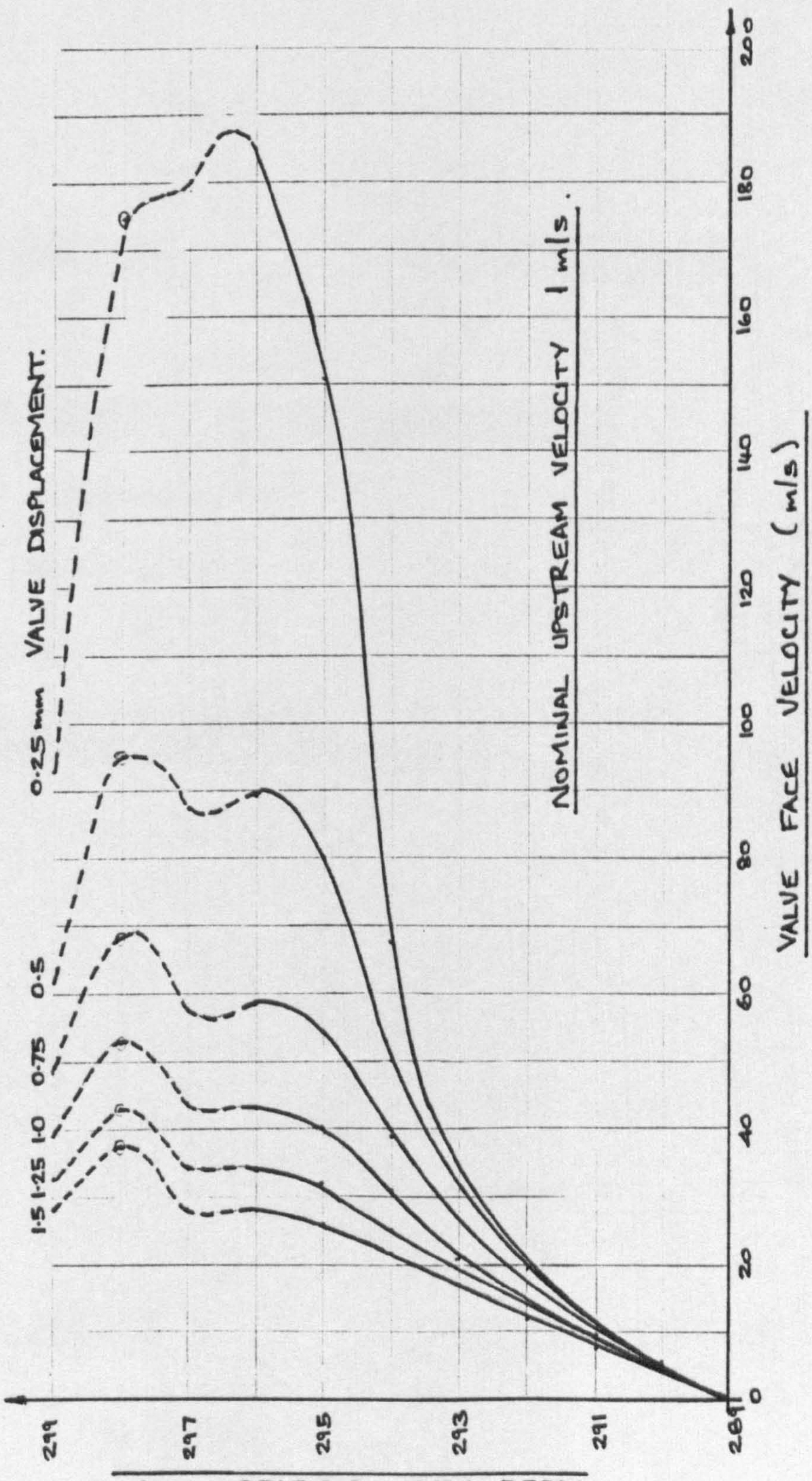

GRAPH 16.

THROAT PRESSURE VERSUS UPSTREAM PRESSURE

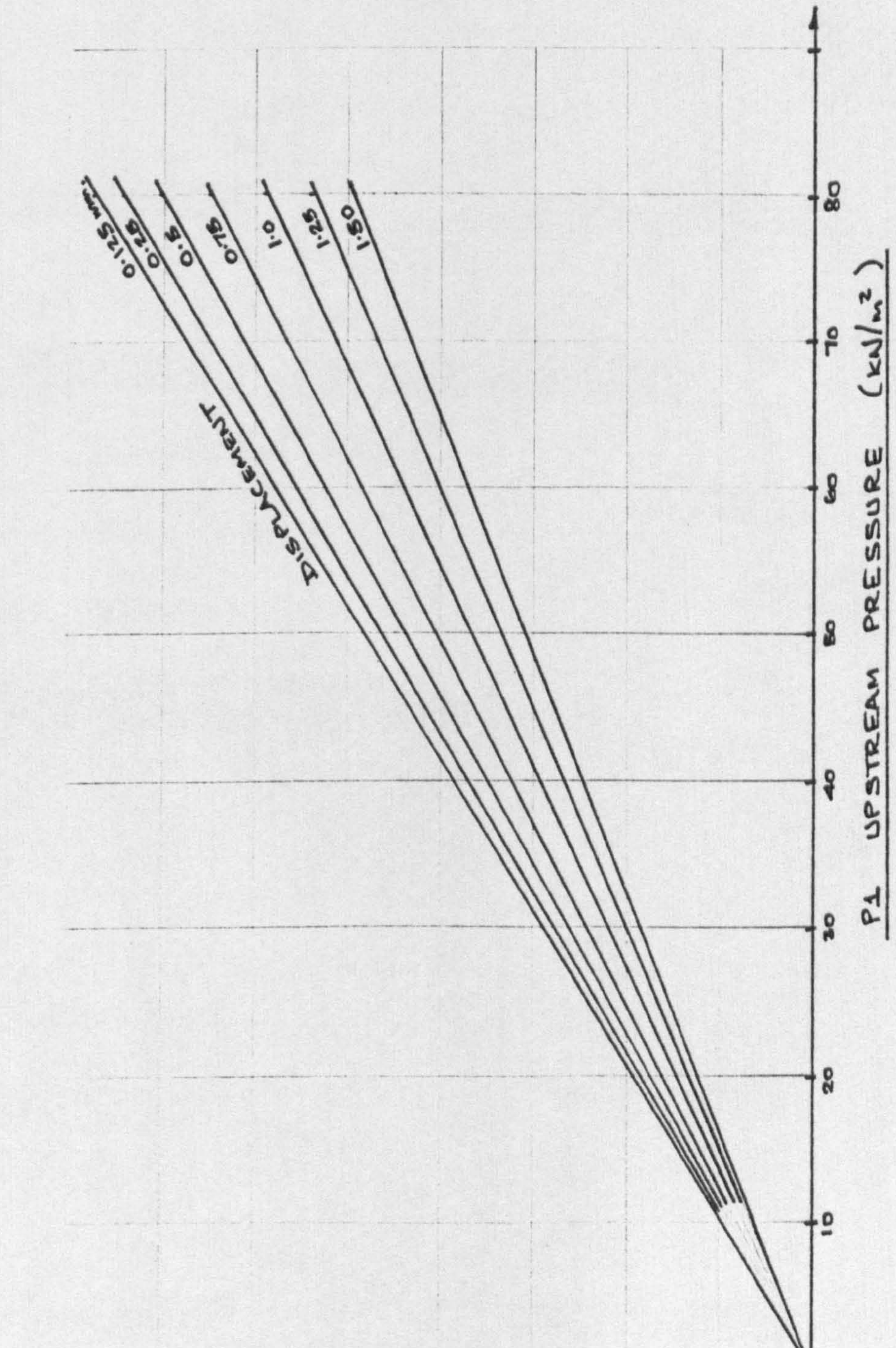

GRAPH 17.

THEORETICAL STATIC FORCE RESULTS.

9·525 mm O/D VALVE.

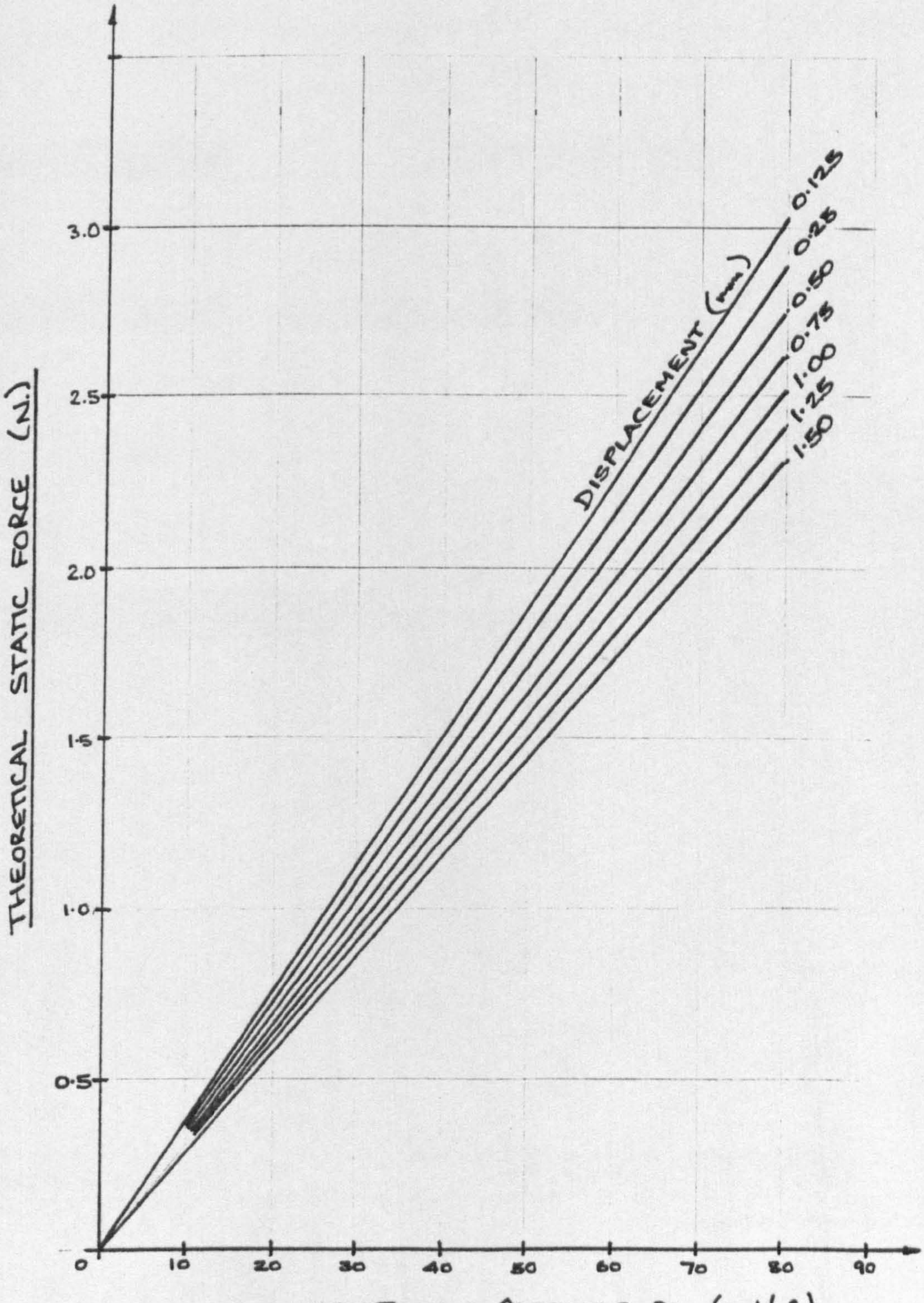

GRAPH 18.

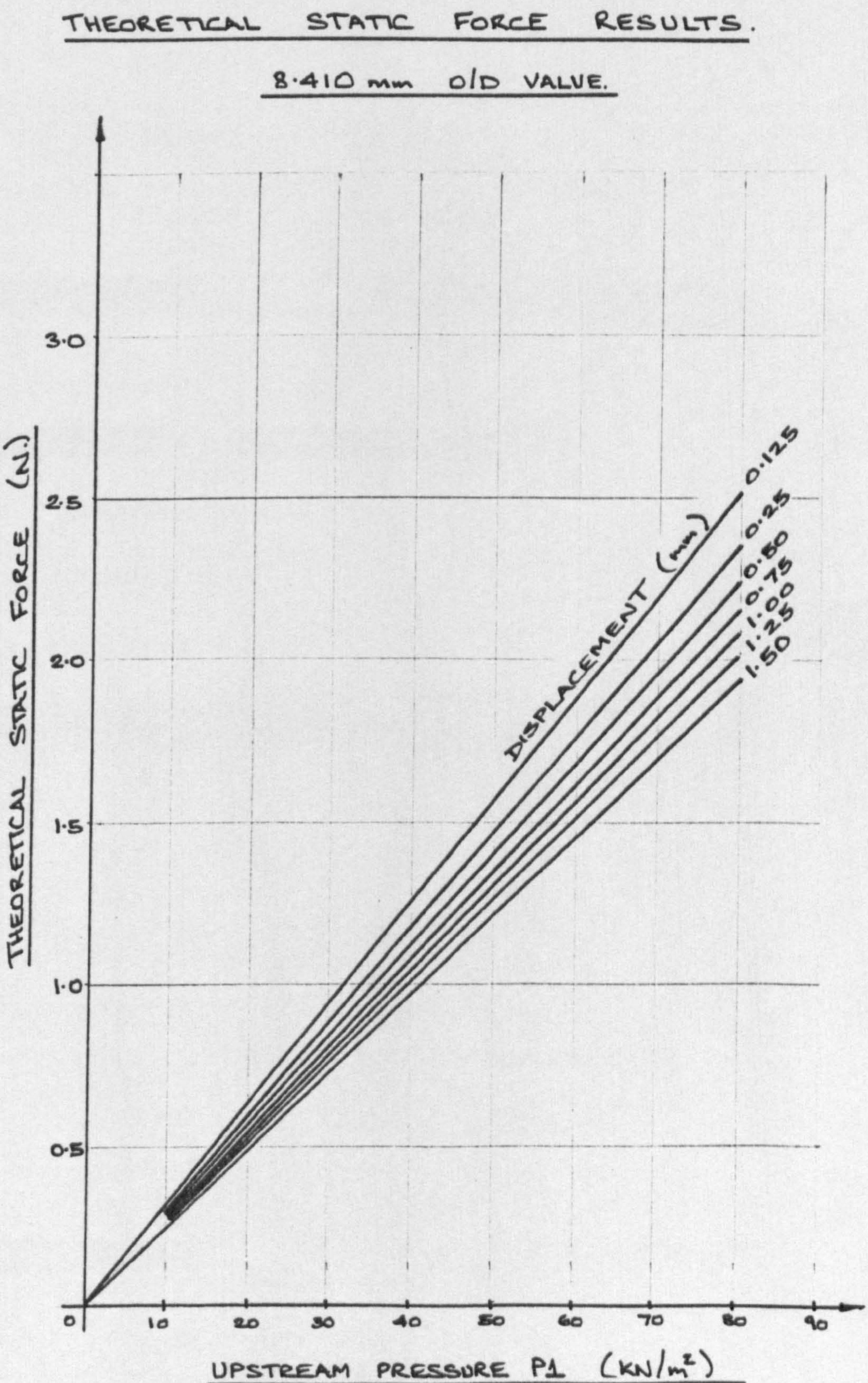
THEORETICAL STATIC FORCE RESULTS.
8·410 mm O/D VALVE.
THEORETICAL STATIC FORCE (N.)
3·0
2·5
2·0
1·5
1·0
0·5
0
10
20
30
40
50
60
70
80
90
DISPLACEMENT (mm)
0·125
0·25
0·50
0·75
1·00
1·25
1·50
UPSTREAM PRESSURE P1 (KN/m²)

GRAPH 19.

5. COMMENTS (Cont)

Theoretical quasi-static forces, on the assumption of a steady non-viscous flow, fully attached to (a) the valve seat, (b) the valve face, and (c) the valve circumferential surface, are shown with experimental results in graphs 3-14 of Chapter IV (pp 94).

As mentioned previously in this Chapter, the main theoretical assumptions made in obtaining these theoretical quasi-static forces were, firstly, that Laplace's equation was used up to the valve perimeter, and secondly, that jet theory was considered with downward air entrainment from behind the valve, therefore, the flow domain section of most relevant interest was the 'area' enclosed by the throat inlet to circumferential surface of valve (Figure 25).

Further to this, upon closer examination of the theoretical flow domain, as presently configured (Figure 22), and the flow profile thereby produced, it may be postulated that since flow is constrained in the x direction due to solid boundaries, that the theoretical model is more symptomatic of an upwards flow across the valve surface, and is therefore representative of the latter stages of valve opening.

From the present experimental work carried out it was concluded that two regimes of flow existed, these being:-

a) During the initial stages of valve opening a fully attached flow condition

and b) During the latter stages of valve opening a fully detached condition

The model referred to above is therefore deemed to be more in keeping with the detached flow condition.

It should be noted however, that the theoretical 'detached' mode implied above does not mean that full turbulence was modelled, only that the flow was more representative of this type.

The reader will no doubt be aware, that to model the fully attached or detached flow conditions in particular, the model would be more appropriate if an algorithm for predicting a free surface profile were present, but at the instigation of this study, the more basic flow domain was considered more practical in the time span available, although a pilot study using this algorithm was carried out concurrently. (Appendix B)

The model as presently configured appears to have credence since when comparison was drawn between theoretical and experimental results, closer agreement existed during the 'detached' mode regime. This can be seen in particular for the case of the 8.410mm O/D valve and to a lesser extent during the latter stages of opening of the 9.525mm O/D valve.

In conclusion, regarding the modelling technique used, it appears that as the flow domain is presently configured, an upwards flow profile across the valve is present, and hence, on this basis it is thought to be a suitable method for predicting detached flow quasi-static forces.

VELOCITY POTENTIALS.

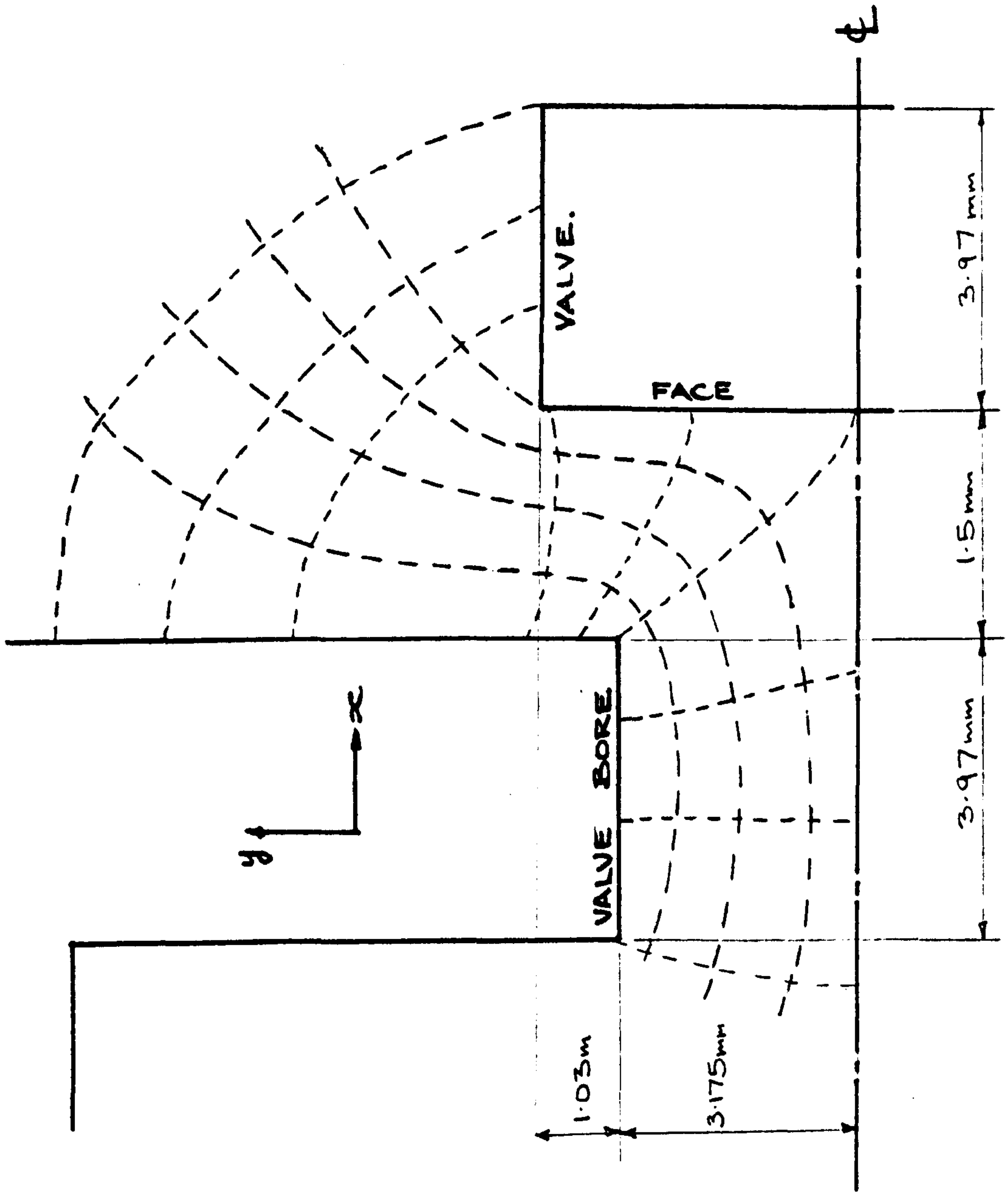

FIGURE 25. (N.T.S)

5. COMMENTS (Cont)

Graphs 20 and 21 show for an arbitrarily chosen upstream pressure of $70kN/m^2$, (a) a cross curve of experimentally determined curves of steady flow, or 'static' force, and (b) the corresponding curve determined from the theoretical model. Graph 20 is for the 9.525mm valve case and graph 21 for the 8.410mm.

When referring to Graph 20 the maximum error between the theoretical and experimental results during the valve opening range of 0.125-0.75mm was of the order of 75%, but during the latter stages of valve opening, this error was reduced to 11%.

Similarly, Graph 21 shows the relationship between theoretical and experimental results for the 8.410mm O/D valve case. Here, the average error is of the order of 10%.

Since both the experimental and theoretical results are considered to be that for the detached mode, this agreement is encouraging and these 10% differences may be accounted by viscosity and compressibility effects, and/or domain differences.

Generally speaking, the model as presently configured appears to give fair comparison between experimental and theoretical results for small gasket ratios and in particular where the detached mode of flow is predominant.

DERIVED CURVE FROM EXPERIMENTAL & THEORETICAL STATIC FORCE RESULTS.

9·525 mm O/D VALVE.

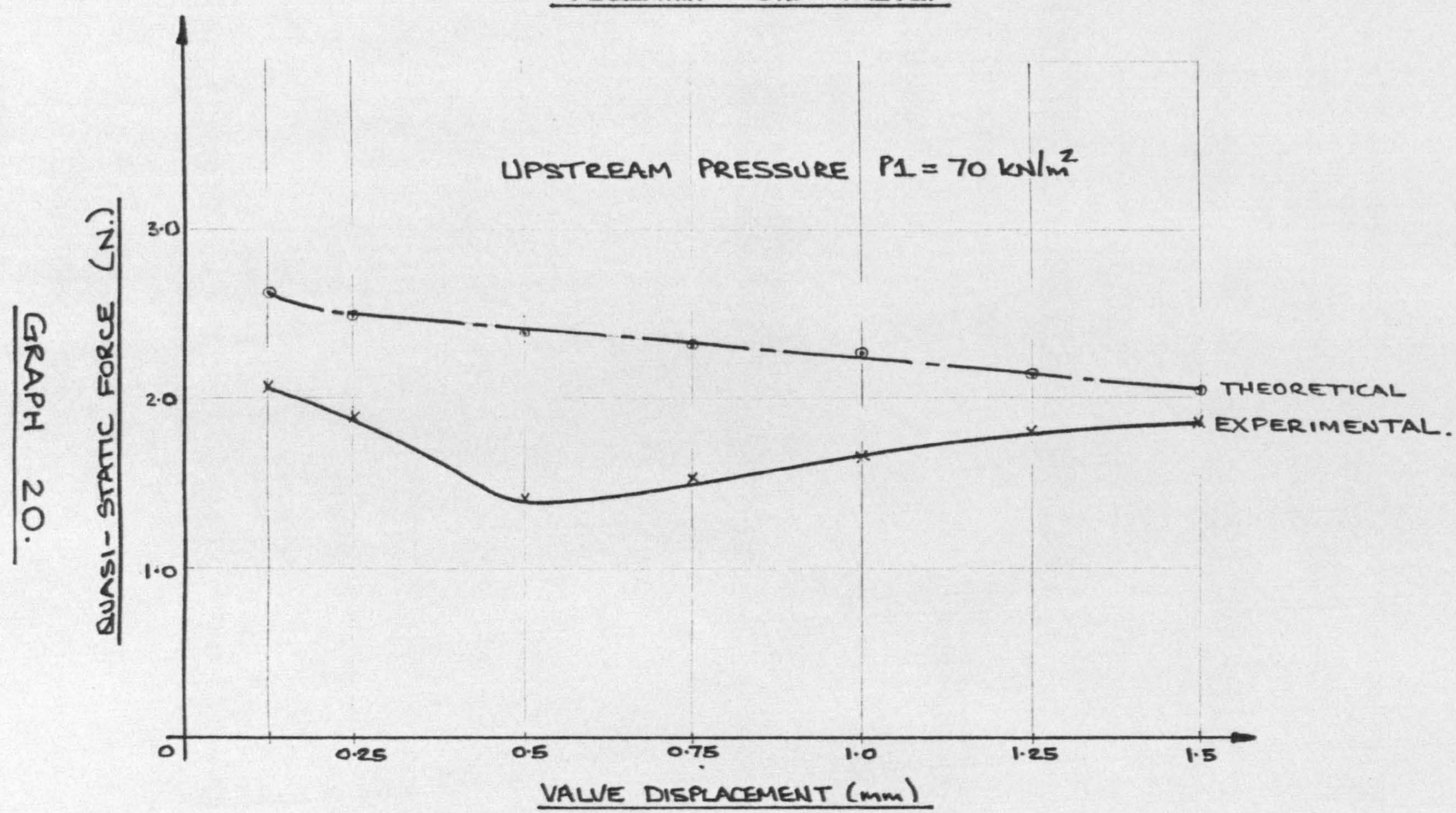

GRAPH 20.

DERIVED CURVE FROM EXPERIMENTAL & THEORETICAL STATIC FORCE RESULTS.

8·410 mm O/D VALVE.

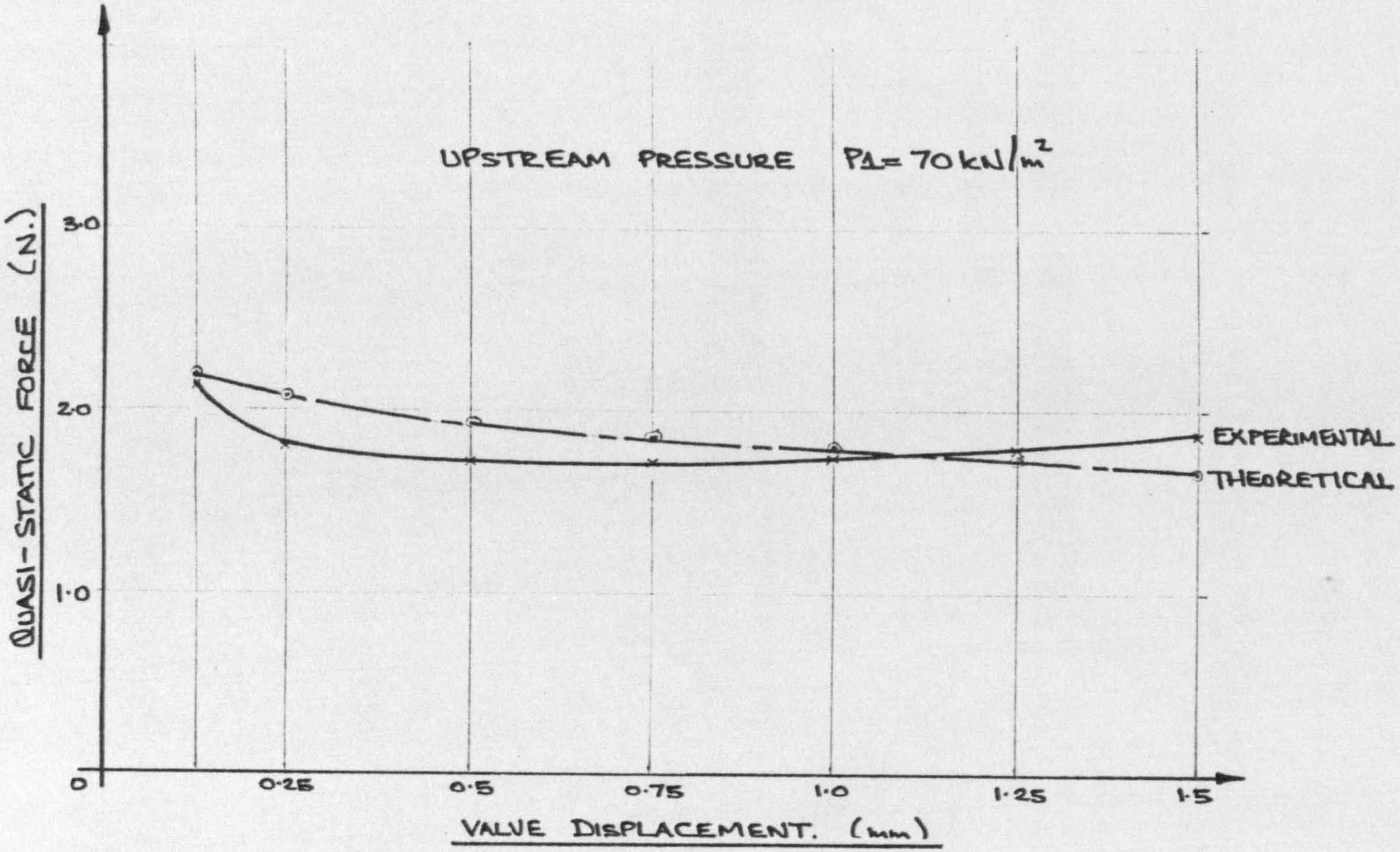

GRAPH 21.

CONCLUSIONS

The main conclusions drawn from this study are noted below. For detailed discussion of experimental findings see pp 106, and for theoretical see pp 144.

1. The minimum experimental static and dynamic forces occurred for the higher gasket ratio investigated (e.g. 1.5).

2. No minimum forces were observed for the lower gasket ratio investigated (e.g. 1.32).

3. From the previous conclusions, it seems likely that for the higher gasket ratio, the attached mode of flow along the valve seat was applicable up to the minimum force value, where upon, the flow condition changed to that of free-jet detached flow.

   For the lower gasket ratio free jet detached mode of flow was found applicable throughout the valve opening, since detachment of flow from the valve seat appears to have occurred so early as to be lost in early force gradients.

   It is therefore felt that this observed minimum is the manifestation of this change of regime, and is predominantly a function of gasket ratio.

4. There is evidence of a difference between static and dynamic experimental force results during the early stages of valve opening (the former being greater) before full development of turbulence.

   Below is an estimate of the degree of difference for pressure versus rise time for each valve diameter.

Valve O/D (mm)	Upstream Pressure (kN/m^2)	Rise Time (ms)	% Diff $\left[\frac{\text{Static-Dynamic}}{\text{Dynamic}}\right]$
8.410	30	8	4.2
8.410	50	8	7.9
8.410	75	8	18.2
9.525	30	15	17.4
9.525	50	15	15.4
9.525	75	15	-
9.525	30	35	5.0
9.525	50	35	9.0
9.525	75	35	8.3
9.525	30	45+	11.9
9.525	50	45+	10.8
9.525	75	45+	12.1

5. The applicability of the theoretical model as presently configured in determining the valve forces appears to give fair comparison between experimental and theoretical results for small gasket ratios and in particular, where the detached mode of flow is predominant. This appears to be borne out in the case of the 8.410mm O/D valve case (10% error) and to a lesser degree in the latter stages of the 9.525mm O/D valve case (10-30% error).

Further Work

A few brief points outlining the possible modifications which could be carried out on the model are noted below.

It is felt that the theoretical model as presently configured, although appearing to be satisfactory when modelling detached laminar flow for low gasket ratio cases, requires further development. A useful addition, it is believed, would be that of incorporating a free surface algorithm which would be useful to enable the flow domain chosen to be more representative of radial free-jet detached flow, and should lead to even better correlation.

A certain amount of this free-surface modelling, all be it for a simple nozzle, has been carried out by the author (App B.), to obtain a feel for the algorithm involved.

The confined boundary analysis developed for this thesis is currently being used with success by the author in solving similar problems in Industry e.g.

(a) Electrical Actuation Valve Forces
(b) Jet Efflux flow of an Underwater Projectile

In addition to this major modification to the program, viscosity and compressibility effects where felt appropriate could be implemented, using suitable functionals as available.

APPENDIX A

DERIVATION OF ELEMENT MATRICES

APPENDIX A

DERIVATION OF ELEMENT MATRICES

1. Introduction

2. Matrices for Two-Dimensional Flow

3. Matrices for Axi-symmetric Flow

1. Introduction

Derivation of the element matrices for both two-dimensional and axi-symmetric flow will be discussed in this appendix. These matrices are derived for a general triangular sub-element as shown in FIG. A1.1. Further reference throughout this appendix made to triangular element implies triangular sub-element.

The matrices for the quadrilateral element used in this study are then formed by adding up the contributions from the four triangular elements and eliminating the equations for the five interior points. The computer program is written so that these additions and eliminations are performed by the computer.

To derive these matrices, a suitable element had to be chosen. In this study, a six node triangular element was chosen to enable a quadratic variation of the interpolation function to be obtained.

For this six node triangular element, the quadratic variation of ϕ can be written in the following polynomial form:

$$\phi(x,y) = \alpha_1 + \alpha_2.x + \alpha_3.y + \alpha_4.x.y + \alpha_5.x^2 + \alpha_6.y^2 \quad (A.1)$$

or fully in matrix form as:

$$\left\{\phi\right\} = \left[G\right]\left\{\alpha\right\} \quad (A.2)$$

where

$$\left\{\phi\right\} = \begin{bmatrix} \phi_1 \\ \phi_2 \\ \phi_3 \\ \phi_4 \\ \phi_5 \\ \phi_6 \end{bmatrix}$$

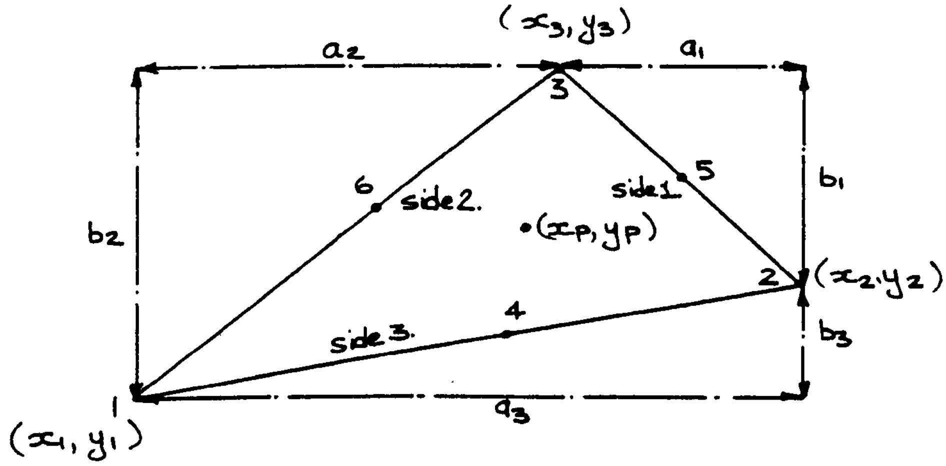

Triangular Sub-Element

This notation is used in this appendix unless otherwise stated.

FIG. A1.1

$$[G] = \begin{bmatrix} 1 & x_1 & y_1 & x_1y_1 & x_1^2 & y_1^2 \\ 1 & x_2 & y_2 & x_2y_2 & x_2^2 & y_2^2 \\ 1 & x_3 & y_3 & x_3y_3 & x_3^2 & y_3^2 \\ 1 & x_4 & y_4 & x_4y_4 & x_4^2 & y_4^2 \\ 1 & x_5 & y_5 & x_5y_5 & x_5^2 & y_5^2 \\ 1 & x_6 & y_6 & x_6y_6 & x_6^2 & y_6^2 \end{bmatrix}$$

and

$$\{\alpha\} = \begin{bmatrix} \alpha_1 \\ \alpha_2 \\ \alpha_3 \\ \alpha_4 \\ \alpha_5 \\ \alpha_6 \end{bmatrix}$$

therefore/

therefore, we can express the generalised co-ordinates (α) as the solution of equation (A.2), that is:

$$\{\alpha\} = [G]^{-1}\{\phi\} \qquad (A.3)$$

where $[G]^{-1}$ is an inverse matrix.

Expressing the terms of the interpolation polynomial equation (A.1) as a product of a row vector and a column vector, we obtain:

$$\phi = [P]\{\alpha\} \qquad (A.4)$$

where $[P] = [1 \; x \; y \; xy \; x^2 \; y^2]$

Thus, by substituting equation (A.3) into equation (A.4) we obtain:

$$\phi = [P][G]^{-1}\{\phi\} = [N]\{\phi\} \qquad (A.5)$$

where $[N] = [P][G]^{-1}$ (A.6)

where $[N]$ is known as the interpolation function (<u>NOTE</u>: this avoids using inverse matrix methods).

Suppose the solution domain A is divided into M elements of r nodes each, then from above, for each element:

$$\phi^{(m)} = \sum_{i=1}^{r} N_i \cdot \phi_i = [N]\{\phi\}^{(m)} \qquad (A.7)$$

where ϕ_i is the nodal value of ϕ at node i.

To demonstrate the method of solution for two dimensional cases, the functional to be solved is obtained from the overall Quasi-Harmonic Equation (steady state) and is:

$$I(\phi) = A' \int_A \left[\left(\frac{\partial \phi}{\partial x}\right)^2 + \left(\frac{\partial \phi}{\partial y}\right)^2 \right] dA + A'' \int_{S_2} (g \cdot \phi) \cdot dS_2 \qquad (A.8)$$

where/

where A' and A'' are constants their values being

$$A' = \frac{\rho}{2}$$

and $A'' = -\rho$ where ρ = density

and g = boundary velocity = $(\phi,n)^a$

and also S_2 = portion of boundary where non-zero boundary conditions arise

This equation (A.8) is now identical to equation (2.19a)

$$I(\phi) = \frac{\rho}{2} \iint_A \left[(\phi,x)^2 + (\phi,y)^2 \right] dx.dy - \oint_c \phi.(\phi,n)^a ds \quad (2.19a)$$

Since the functional $I(\phi)$ contains only first order derivatives, we have a C^o problem and the interpolation functions (Ni) must be chosen to preserve continuity of ϕ at element interfaces (compatibility requirement).

It will later be ensured that interpolation functions chosen guarantee C^o continuity as this must be so to ensure monotonic convergence.

Assuming C^o continuity has been met, we can focus our attention on one element only, because the integral $I(\phi)$ can be represented as the sum of integrals over all the elements, that is:

$$I(\phi) = \sum_{m=1}^{M} I.(\phi^{(m)}) \quad (A.9)$$

The discretised form of the functional for one element is obtained by substituting equation (A.7) into equation (A.8). Then the minimum condition $\delta I(\phi) = 0$ for one element becomes:

$$\frac{\partial I(\phi^{(m)})}{\partial \phi_i} = 0, \quad i = 1, 2, 3 \ldots\ldots r \quad (A.10)$$

For/

For a node i on boundary S_2, from equation (A.8) we have:

$$\frac{\partial I(\phi^{(m)})}{\partial \phi_i} = 0$$

$$= \int_{A^{(m)}} \left[\frac{\partial \phi^{(m)}}{\partial x} \cdot \frac{\partial}{\partial \phi_i} \cdot \left(\frac{\partial \phi^{(m)}}{\partial x}\right) + \frac{\partial \phi^{(m)}}{\partial y} \cdot \frac{\partial}{\partial \phi_i} \cdot \left(\frac{\partial \phi^{(m)}}{\partial y}\right) \right] dA^{(m)}$$

$$+ \int_{S_2^{(m)}} g \cdot \frac{\partial \phi^{(m)}}{\partial \phi_i} \cdot dS_2^{(m)} \qquad \text{(A.11)}$$

If node i does not lie on S_2, the second integral does not appear. Now referring to equation (A.7), we may evaluate each of the derivatives in (A.11). These become:

$$\frac{\partial \phi^{(m)}}{\partial x} = \sum_{i=1}^{r} \frac{\partial N_i}{\partial x} \cdot \phi_i = \left[\frac{\partial N}{\partial x}\right] \left\{\phi\right\}^{(m)}$$

$$\frac{\partial}{\partial \phi_i} \left(\frac{\partial \phi^{(m)}}{\partial x}\right) = \frac{\partial N_i}{\partial x}$$

$$\frac{\partial \phi^{(m)}}{\partial \phi_i} = N_i$$

Thus we obtain

$$\frac{\partial I(\phi^{(m)})}{\partial \phi_i} = 0$$

$$= \int_{A^{(m)}} \left(\left[\frac{\partial N}{\partial x}\right] \left\{\phi\right\} \frac{\partial N_i}{\partial x} + \left[\frac{\partial N}{\partial y}\right] \left\{\phi\right\} \frac{\partial N_i}{\partial y} \right) dA^{(m)}$$

$$+ \int_{S_2^{(m)}} g \cdot N_i \cdot dS_2^{(m)} \quad \text{on surface} \quad S_2 \qquad \text{(A.12)}$$

Combining/

Combining all such equations as (A.12) for all the nodes of the element gives the following set of element equations:

$$\left\{\frac{\partial I}{\partial \phi^{(m)}}\right\}^{(m)} = \left\{\begin{array}{c} \dfrac{\partial I(\phi^{(m)})}{\partial \phi_1} \\ \dfrac{\partial I(\phi^{(m)})}{\partial \phi_2} \\ \vdots \\ \dfrac{\partial I(\phi^{(m)})}{\partial \phi_r} \end{array}\right\} = \left[S \right]^{(m)} \left\{ \phi \right\}^{(m)} + \left\{ SL \right\}^{(m)} \qquad \text{(A.13)}$$

where $\left[S \right]$ is an r x r matrix

$\left\{ \phi \right\}$ is an r x 1 matrix

and $\left\{ SL \right\}$ is an r x 1 matrix

and are defined as:

$$S_{ij}^{(m)} = \int_{A^{(m)}} \left(\frac{\partial N_i}{\partial x} \cdot \frac{\partial N_j}{\partial x} + \frac{\partial N_i}{\partial y} \cdot \frac{\partial N_j}{\partial y}\right) \; dA^{(m)}$$

$$= \int_{A^{(m)}} \left(T_i^{(m)} \; T_j^{(m)} + \hat{T}_i^{(m)} \; \hat{T}_j^{(m)}\right) \; dA^{(m)} \qquad \text{(A.14)}$$

and

$$SL_i^{(m)} = \int_{S_2^{(m)}} g \cdot N_i \cdot dS_2^{(m)} = \oint_{C^{(m)}} N_i \cdot (\phi,_n)^a \; dS \qquad \text{(A.15)}$$

It is again emphasised that the equation (A.15) only appears if element (m) contributes to the definition of the boundary portion S_2.

Assembly of these element equations to obtain the system equations then follows the standard procedure.

It/

It can be readily seen that these equations (A.13), (A.14) and (A.15) are similar to those obtained in CHAPTER V (equations 5.6).

The derivation of the interpolation functions, N, will now be discussed.

In order to ensure C^0 continuity for the interpolation functions, we require that the number of nodes along a side of an element, and hence the number of nodal values of ϕ along that side, shall be sufficient to determine uniquely the variation of ϕ along that side. For example, in this study where ϕ is assumed to have a quadratic variation within an element and to retain its quadratic behaviour along the element sides, three values of ϕ or three external nodes must lie along each side.

For C^0 problems, elements that require polynomials of order greater than three are rarely used because little additional accuracy is gained. Also, if we model a complicated boundary, it is advantageous to use a large number of simple elements rather than a few complex ones.

To derive the quadratic interpolation functions, we begin by obtaining interpolation functions for a linear triangle (three nodes) and subsequently derive the interpolation functions for this higher order triangle by means of the natural co-ordinates and recurrence formulae. In the formulation of the linear interpolation functions we obtain $N_i = L_i$ where L_i are the natural co-ordinates of a linear triangle.

The development of natural co-ordinates for triangular elements now follows.

The goal is to choose co-ordinates L_1, L_2 and L_3 to describe/

describe the location of any point x_p, y_p within the element or on its boundary (FIG. A1.1). The original co-ordinates of a point in the element should be linearly related to the new co-ordinates by the following equations:

$$x = L_1.x_1 + L_2.x_2 + L_3.x_3$$

$$y = L_1.y_1 + L_2.y_2 + L_3.y_3 \qquad (A.16)$$

In addition to these equations, we impose a third condition requiring that the weighting functions sum to unity, that is:

$$L_1 + L_2 + L_3 = 1 \qquad (A.17)$$

From equation (A.17) it is clear that only two of the natural co-ordinates can be independent, just as in the original co-ordinate system, where there are only two independent co-ordinates (x_p, y_p).

Inversion of equations (A.16) and (A.17) gives the natural co-ordinates in terms of the Cartesian co-ordinates. Thus:

$$L_1\ (x, y) = \frac{1}{2\Delta}\ (a_1' + b_1'.x + c_1'.y)$$

$$L_2\ (x, y) = \frac{1}{2\Delta}\ (a_2' + b_2'.x + c_2'.y)$$

$$L_3\ (x, y) = \frac{1}{2\Delta}\ (a_3' + b_3'.x + c_3'.y) \qquad (A.18)$$

where

$$2\Delta = 2\ (\text{area of triangle 1-2-3}) \qquad (A.19)$$

and

$$a_1' = x_2.y_3 - x_3\,y_2$$

$$b_1' = y_2 - y_3$$

$$c_1' = x_3 - x_2 \qquad (A.20)$$

The other coefficients are obtained by cyclically permutating the subscripts.

As/

As shown in FIG. 20, when the point (x_p, y_p) is located on the boundary of the element, one of the area segments vanish and appropriate natural co-ordinate (area co-ordinate) along the boundary is zero. For example, if (x_p, y_p) is on line 1-3 then:

$$L_2 = \frac{A_2}{\Delta} = 0 \quad \text{since } A_2 = 0$$

If we interpret the field variable ϕ as a function of L_1, L_2 and L_3 instead of x, y, differentiation becomes:

$$\frac{d\phi}{dx} = \frac{\partial\phi}{\partial L_1} \cdot \frac{\partial L_1}{\partial x} + \frac{\partial\phi}{\partial L_2} \cdot \frac{\partial L_2}{\partial x} + \frac{\partial\phi}{\partial L_3} \cdot \frac{\partial L_3}{\partial x} \tag{A.21}$$

and

$$\frac{d\phi}{dy} = \frac{\partial\phi}{\partial L_1} \cdot \frac{\partial L_1}{\partial y} + \frac{\partial\phi}{\partial L_2} \cdot \frac{\partial L_2}{\partial y} + \frac{\partial\phi}{\partial L_3} \cdot \frac{\partial L_3}{\partial y}$$

where

$$\frac{\partial L_i}{\partial x} = \frac{b_i'}{2\Delta} \quad , \quad \frac{\partial L_i}{\partial y} = \frac{c_i'}{2\Delta} \quad , \quad i = 1, 2, 3 \tag{A.22}$$

There is also a convenient formula for integrating area co-ordinates over the area of a triangle this being:

$$\int_{A^{(m)}} L_1^{\alpha} \cdot L_2^{\beta} \cdot L_3^{\gamma} \, dA^{(m)} = \frac{\alpha! \cdot \beta! \cdot \gamma!}{(\alpha + \beta + \gamma + 2)!} \tag{A.23}$$

TABLE A.1 gives the values of equation (A.23) and use of it is made later in obtaining the $[S]$ matrix terms.

Now the method used in obtaining interpolation functions for higher order triangles is based on a procedure advanced by Silvester [38].

Silvester introduced a triple index numbering scheme.

The/

The nodes of the elements in FIG. (A1.2) can be given the three-digit label $\alpha\beta\gamma$, where α , β and γ are integers satisfying $\alpha + \beta + \gamma = n$, where n is the order of the interpolation polynomial for the triangle. These integers designate constant co-ordinate lines in the area co-ordinate system. We may use the same digit notation for the interpolation functions for the element. Employing a triple subscript, we may write $N_{\alpha\beta\gamma}(L_1, L_2, L_3)$ to denote the interpolation function for node $\alpha\beta\gamma$ as a function of the area co ordinates L_1, L_2 and L_3.

Silvester has shown that the interpolation functions for an nth order triangular element may be expressed by the following simple and convenient formula:

$$N_{\alpha\beta\gamma}(L_1, L_2, L_3) = N_{\alpha}(L_1).N_{\beta}(L_2).N_{\gamma}(L_3)$$

where

$$N_{\alpha}(L_1) = \prod_{i=1}^{\alpha} \left(\frac{n.L_1 - i + 1}{i}\right) , \quad \alpha \geqslant 1 \qquad (A.24)$$

$$= 1 \qquad \alpha = 0 \qquad (A.25)$$

For $N_{\beta}(L_2)$ and $N_{\gamma}(L_3)$ the formula has the same form. The symbol Π signifies the product of all the terms. For example:

$$\prod_{i=1}^{4} (i^2 + 1) = (1^2 + 1)(2^2 + 1)(3^2 + 1)(4^2 + 1) = 1700$$

Equations (A.24) and (A.25) now provide the means for constructing the interpolation functions for a quadratic triangle (n = 2) thereby requiring N_{200}, N_{020}, N_{002} and N_{101}, N_{110} and N_{011} to be determined.

These can be shown to be:

$$N_{200} =/$$

LINEAR AND HIGHER-ORDER TRIANGULAR ELEMENTS WITH Ø SPECIFIED AT THE NODES

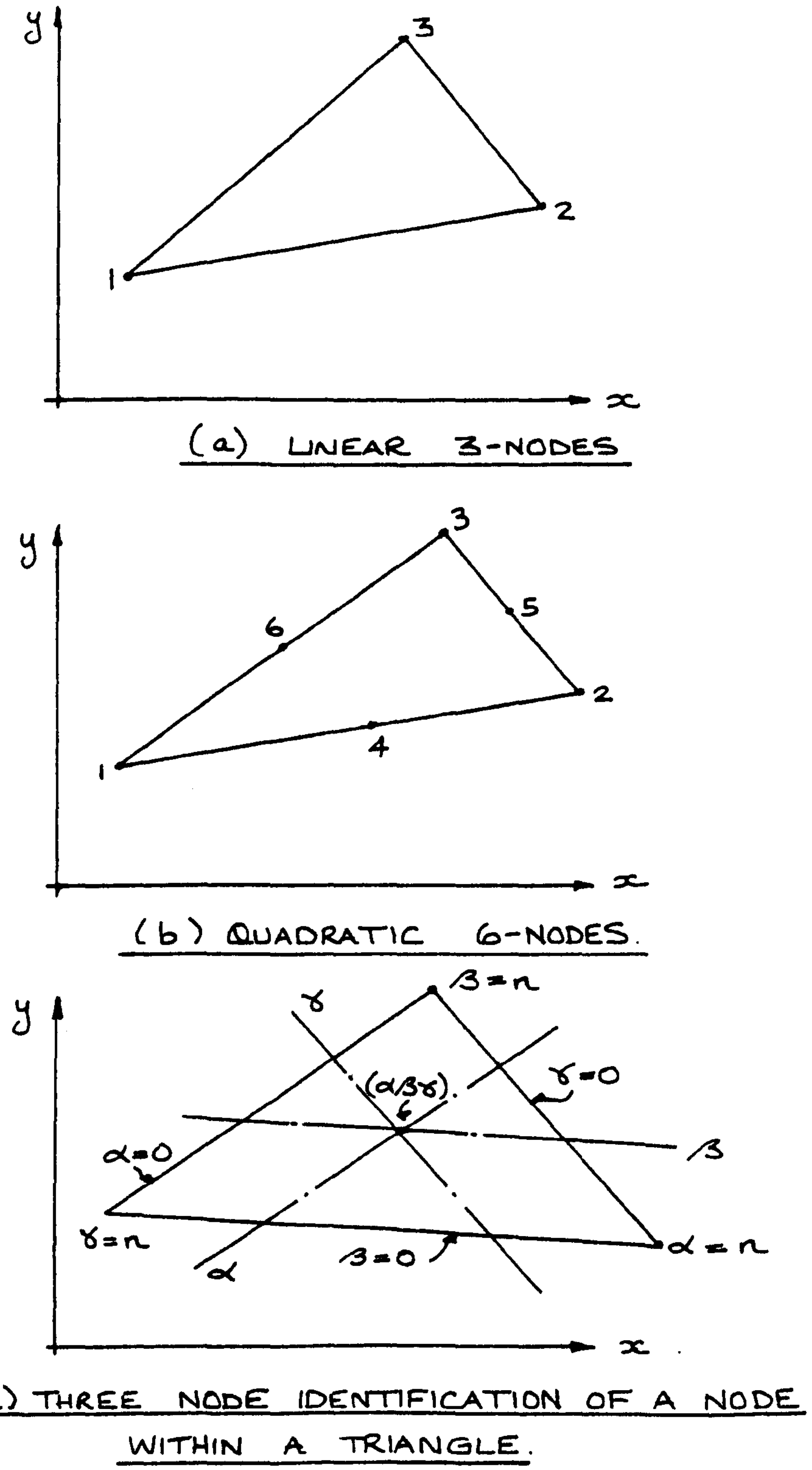

FIGURE A.1.2.

$$N_{200} = L_1\ (2 \cdot L_1 - 1)$$

$$N_{020} = L_2\ (2 \cdot L_2 - 1)$$

$$N_{002} = L_3\ (2 \cdot L_3 - 1)$$

$$N_{101} = 4 \cdot L_3 \cdot L_1$$

$$N_{110} = 4 \cdot L_1 \cdot L_2$$

$$N_{011} = 4 \cdot L_2 \cdot L_3 \qquad (A.26)$$

These are similar to equation (5.3b) as shown in CHAPTER V.

Now, to obtain the partial differential $\frac{\partial N}{\partial x}$ to substitute into equation (A.14) use is made of the following equation:

$$\frac{\partial N_i}{\partial x} = \frac{\partial N_i}{\partial L_i} \cdot \frac{\partial L_i}{\partial x} \quad \text{etc.} \qquad (A.27)$$

Having now the means to obtain all the terms in solution of equation (A.13), the specific matrix components must be derived.

2. Matrices for Two-Dimensional Flow

From CHAPTER V:

$$S_{ij}^{(m)} = \rho^{(m)} \int_{A^{(m)}} (T_i^{(m)} \cdot T_j^{(m)} + \hat{T}_i^{(m)} \cdot \hat{T}_j^{(m)})\ dA^{(m)}$$

$$(i,\ j\ =\ 1,\ 6) \qquad (A.28)$$

$$SL_i^{(m)} = \rho^{(m)} \oint_{c^{(m)}} N_i \cdot (\phi,_n)^a\ dS \qquad (A.29)$$

with $< N_1, \ldots\ldots N_6 > = < L_1\ (2\ L_1 - 1),\ L_2\ (2\ L_2 - 1),\ L_3\ (2\ L_3 - 1),$

$$4 \cdot L_1 \cdot L_2,\ 4 \cdot L_2 \cdot L_3,\ 4 \cdot L_3 \cdot L_1 > \qquad (A.30)$$

$T_1^{(m)}$,/

$$<T_1^{(m)}, \ldots T_6^{(m)}> = <(4\,L_1 - 1)\,b_1/2\,A^{(m)},\ (4\,L_2 - 1)\,b_2/2\,A^{(m)},$$

$$(4\,L_3 - 1)\,b_3/2\,A^{(m)},\ 2\,(L_2\,b_1 + L_1\,b_2)/A^{(m)},$$

$$2\,(L_3\,b_2 + L_2\,b_3)/A^{(m)},\ 2\,(L_1\,b_3 + L_3\,b_1)/A^{(m)} \qquad \text{(A.31)}$$

$$< a_1, a_2, a_3 > \; = \; <(x_3 - x_2), (x_1 - x_3), (x_2 - x_1)> \qquad \text{(A.32)}$$

$$< b_1, b_2, b_3 > \; = \; <(y_2 - y_3), (y_3 - y_1), (y_1 - y_2)> \qquad \text{(A.33)}$$

and $A^{(m)} = (a_k . b_j - a_j . b_k)/2$ where $j = 2, 3, 1$ and $k = 3, 1, 2$ (A.34)

The array $\hat{T}_i^{(m)}$ is found by replacing the b's with a's in the expression for $T_i^{(m)}$.

An explicit expression for any element matrix is now obtained by a straightforward substitution of the appropriate quantities into equation (A.28) and making use of TABLE (A.1). For example, to evaluate $S_{11}^{(m)}$, both i and j are set equal to 1 and the following expression is obtained:

$$S_{11}^{(m)} = \rho^{(m)} \int_{A^{(m)}} (T_1^{(m)} . T_1^{(m)} + \hat{T}_1^{(m)} . \hat{T}_1^{(m)})\, dA$$

The constant is included although it does not contribute to the overall solution.

$$\therefore\ S_{11}^{(m)} = \frac{\rho^{(m)}}{(2\,A^{(m)})^2} \cdot \int_{A^{(m)}} \cdot \left[(4\,L_1 - 1)^2\, b_1^2 \right.$$

$$\left. + (4\,L_2 - 1)^2 . a_1^2 \right] dA^{(m)} = \frac{(a_1^2 + b_1^2)}{(2\,A^{(m)})^2}\ \rho^{(m)} \int_{A^{(m)}}$$

$$(16\,L_1^2 - 8\,L_1 + 1)\ dA^{(m)}$$

Now/

Now upon using TABLE (A.1) and simplifying, one obtains:

$$S_{11}^{(m)} = \frac{(a_1^{\,2} + b_1^{\,2})}{4\ A^{(m)}} \cdot \rho^{(m)}$$

The remaining elements can be found in the same manner. Letting $S_{ij} = (a_i\ a_j + b_i\ b_j) \cdot \rho^{(m)}/12\ A^{(m)}$, the element matrix for the chosen triangle is as listed below:

$$S_{11}^{(m)} = 3\ S_{11}$$

$$S_{12}^{(m)} = S_{21}^{(m)} = -\ S_{12}$$

$$S_{13}^{(m)} = S_{31}^{(m)} = -\ S_{13}$$

$$S_{14}^{(m)} = S_{41}^{(m)} = 4\ S_{12}$$

$$S_{15}^{(m)} = S_{51}^{(m)} = 0$$

$$S_{16}^{(m)} = S_{61}^{(m)} = 4\ S_{13}$$

$$S_{22}^{(m)} = 3\ S_{22}$$

$$S_{23}^{(m)} = S_{32}^{(m)} = -\ S_{23}$$

$$S_{24}^{(m)} = S_{42}^{(m)} = 4\ S_{12}$$

$$S_{25}^{(m)} = S_{52}^{(m)} = 4\ S_{23}$$

$$S_{26}^{(m)} = S_{62}^{(m)} = 0$$

$$S_{33}^{(m)} = 3\ S_{33}$$

$$S_{34}^{(m)} = S_{43}^{(m)} = 0$$

$$S_{35}^{(m)} = S_{53}^{(m)} = 4\ S_{23}$$

$$S_{36}^{(m)} =/ \qquad \text{(A.35)}$$

cont./

$$S_{36}^{(m)} = S_{63}^{(m)} = 4\ S_{13}$$

$$S_{44}^{(m)} = 8\ (S_{33} - S_{12})$$

$$S_{45}^{(m)} = S_{54}^{(m)} = 8\ S_{13}$$

$$S_{46}^{(m)} = S_{64}^{(m)} = 8\ S_{23}$$

$$S_{55}^{(m)} = 8\ (S_{11} - S_{23})$$

$$S_{56}^{(m)} = S_{65}^{(m)} = 8\ S_{12}$$

$$S_{66}^{(m)} = 8\ (S_{22} - S_{31}) \tag{A.35}$$

Now boundary conditions are considered in order to obtain the load matrix. For a triangular element, one has:

$$\oint_{c^{(m)}} \phi\,.(\phi,_n)^a\, ds = \oint_{l_1} \phi\,(\phi,_n)^{a_1}\, ds + \oint_{l_2} \phi(\phi,_n)^{a_2}\, ds$$

$$+ \oint_{l_3} \phi\,(\phi,_n)^a\, ds$$

The symbols $(\phi,_n)^{a_1}$, $(\phi,_n)^{a_2}$ and $(\phi,_n)^{a_3}$ represent the specified normal velocity components on sides l_1, l_2 and l_3, respectively and these components are assumed to be constants (or to be approximated as constants).

The integrals on the right hand side can be evaluated by straightforward substitutions. For instance, the first integral may be written as:

$$\oint_{l_1} \phi\,(\phi,_n)^{a_1}\, ds = (\phi,_n)^{a_1} \oint_{l_1} \phi_i\, N_i\, ds \quad (i = 1 \text{ to } 6 \text{ as required})$$

Since/

Since $L_1 = 0$ on side 1, $L_2 + L_3 = 1$ or $L_2 = 1 - L_3$.

Using these relationships, the following equations are obtained:

$$\oint_{l_1} \phi .(\phi,_n)^{a_1} ds = (\phi,_n)^{a_1} \oint_{l_1} \Big[L_2 \,(2\, L_2 - 1). \phi_2 + L_3 \,(2\, L_3 - 1). \phi_3$$

$$+ 4. L_2. L_3. \phi_5 \Big] ds = (\phi,_n)^{a_1} . l_1 \int_0^1 \Big[(1 - L_3)(1 - 2\, L_3). \phi_2$$

$$+ L_3 .(2\, L_3 - 1). \phi_3 + 4.(1 - L_3). L_3\, \phi_5 \Big] d\, L_3$$

Taking the partial derivatives of the above integral with respect to ϕ_2, ϕ_3 and ϕ_5, respectively and using TABLE A.2:

$$\frac{\partial}{\partial \phi_2}\Big[\oint_{l_1} \phi .(\phi,_n)^{a_1} ds \Big] = (\phi,_n)^{a_1} . l_1 \int_0^1 (1 - L_3)(1 - 2\, L_3)\, d\, L_3$$

$$= \frac{(\phi,_n)^{a_1} . l_1}{6}$$

Similarly:

$$\frac{\partial}{\partial \phi_3}\Big[\oint_{l_1} \phi .(\phi,_n)^{a_1} . ds \Big] = \frac{(\phi,_n)^{a_1} . l_1}{6}$$

and

$$\frac{\partial}{\partial \phi_5}\Big[\oint_{l_1} \phi .(\phi,_n)^{a_1} ds \Big] = \frac{4 .(\phi,_n)^{a_1} . l_1}{6}$$

Similar results can be obtained by considering the other two integrals. In this way, the corresponding load matrix may be derived as:

$SL_1^{(m)} =/$

$$SL_1^{(m)} = \left[(\phi,_n)^{a_2}.\,l_2 + (\phi,_n)^{a_3}.\,l_3\right] \frac{\rho\, m}{6}$$

$$SL_2^{(m)} = \left[(\phi,_n)^{a_3}.\,l_3 + (\phi,_n)^{a_1}.\,l_1\right] \frac{\rho\, m}{6}$$

$$SL_3^{(m)} = \left[(\phi,_n)^{a_1}.\,l_1 + (\phi,_n)^{a_2}.\,l_2\right] \frac{\rho\, m}{6}$$

$$SL_4^{(m)} = 2\,(\phi,_n)^{a_3}.\,l_3 \,.\, \frac{\rho\, m}{3}$$

$$SL_5^{(m)} = 2\,(\phi,_n)^{a_1}.\,l_1 \,.\, \frac{\rho\, m}{3}$$

$$SL_6^{(m)} = 2\,(\phi,_n)^{a_2}.\,l_2 \,.\, \frac{\rho\, m}{3} \qquad (A.36)$$

3. <u>Matrices for Axi-symmetric Flow</u>

From CHAPTER V:

$$SA_{ij}^{(m)} = 2.\rho^{(m)}.\pi \iint_{A^{(m)}} (T_i^{(m)}.\,T_j^{(m)} + \hat{T}_i^{(m)}\,\hat{T}_j^{(m)})\; r\,dA \quad (i,\ j = 1 \text{ to } 6)$$

(A.37)

and
$$SLA_i^{(m)} = 2.\rho^{(m)}.\pi \oint_{c^{(m)}} N_i.(\phi,_n)^a\; r\,ds \qquad (A.38)$$

with

$$<T_1^{(m)} \ldots, T_6^{(m)}> = \langle (4.L_1 - 1).\,b_1/2\,A^{(m)},\ (4\,L_2 - 1).\,b_2/2\,A^{(m)},$$

$$(4.L_3 - 1).\,b_3/2\,A^{(m)},\ 2\,(L_2.\,b_1 + L_1.\,b_2)/A^{(m)},$$

$$2\,(L_3.\,b_2 + L_3.\,b_3)/A^{(m)},\ 2\,(L_1.\,b_3 + L_3.\,b_1)/A^{(m)}$$

(A.39)

$N_1 \ldots N_6 \quad =/$

$$< N_1 \ldots, N_6 > \; = \; < L_1 (2 L_1 - 1), L_2 (2 L_2 - 1), L_3 (2 L_3 - 1),$$

$$4 L_1 L_2, 4 L_2 L_3, 4 L_3 L_1 > \qquad (A.40)$$

$$< a_1, a_2, a_3 > \; = \; < (x_3 - x_2), (x_1 - x_3), (x_2 - x_1) > \qquad (A.40a)$$

$$< b_1, b_2, b_3 > \; = \; < (y_2 - y_3), (y_3 - y_1), (y_1 - y_2) > \qquad (A.40b)$$

and $A^{(m)} = a_k \cdot b_j - a_j \cdot b_k$ where $j = 2,3,1$ and $k = 3,1,2$. (A.40c)

To obtain the element matrices, equation (5.12) is used in conjunction with the procedure used for the two-dimensional case.

S_{ij} is used to represent: $= (a_i \cdot a_j + b_i \cdot b_j)\, \varrho\, {}^{m}/60 . A^{(m)}$ because a constant factor, 2π appears in every term of the matrices. This cancels out for the problem studied and is therefore omitted.

$$SA_{11}^{(m)} = 3\, S_{11} (3 r_1 + r_2 + r_3)$$

$$SA_{12}^{(m)} = SA_{21}^{(m)} = - S_{12} (2 r_1 + 2 r_2 + r_3)$$

$$SA_{13}^{(m)} = SA_{31}^{(m)} = - S_{13} (2 r_1 + r_2 + 2 r_3)$$

$$SA_{14}^{(m)} = SA_{41}^{(m)} = S_{11} (3 r_1 - 2 r_2 - r_3) + S_{12} (14 r_1 + 3 r_2 + 3 r_3)$$

$$SA_{15}^{(m)} = SA_{51}^{(m)} = S_{12} (3 r_1 - r_2 - 2 r_3) + S_{13} (3 r_1 - 2 r_2 - r_3)$$

$$SA_{16}^{(m)} = SA_{61}^{(m)} = S_{11} (3 r_1 - r_2 - 2 r_3) + S_{13} (14 r_1 + 3 r_2 + 3 r_3)$$

$$SA_{22}^{(m)} = 3\, S_{22} (r_1 + 3 r_2 + r_3)$$

$$SA_{23}^{(m)} = SA_{32}^{(m)} = - S_{23} (r_1 + 2 r_2 + 2 r_3)$$

$$SA_{24}^{(m)} = /$$

$$SA_{24}^{(m)} = SA_{42}^{(m)} = S_{12}\,(3\,r_1 - 14\,r_2 + 3\,r_3) + S_{22}\,(-2\,r_1 + 3\,r_2 - r_3)$$

$$SA_{25}^{(m)} = SA_{52}^{(m)} = S_{22}\,(-r_1 + 3\,r_2 - 2\,r_3) + S_{23}\,(3.r_1 + 14.r_2\ 3.r_3)$$

$$SA_{26}^{(m)} = SA_{62}^{(m)} = S_{12}\,(-r_1 + 3.r_2 - 2\,r_3) + S_{23}\,(-2\,r_1 + 3\,r_2 - r_3)$$

$$SA_{33}^{(m)} = 3\,S_{33}\,(r_1 + r_2 + 3\,r_3)$$

$$SA_{34}^{(m)} = SA_{43}^{(m)} = S_{13}\,(-r_1 - 2\,r_2 + 3\,r_3) + S_{23}\,(-2\,r_1 - r_2 + 3\,r_3)$$

$$SA_{35}^{(m)} = SA_{53}^{(m)} = S_{23}\,(3\,r_1 + 3\,r_2 + 14\,r_3) + S_{33}\,(-r_1 - 2\,r_2 + 3\,r_3)$$

$$SA_{36}^{(m)} = SA_{63}^{(m)} = S_{13}\,(3\,r_1 + 3\,r_2 + 14\,r_3) + S_{33}\,(-2\,r_1 - r_2 + 3\,r_3)$$

$$SA_{44}^{(m)} = 8\Big[S_{11}\,(r_1 + 3\,r_2 + r_3) + S_{12}\,(2\,r_1 + 2\,r_2 + r_3) + S_{22}\,(3\,r_1 + r_2 + r_3)\Big]$$

$$SA_{45}^{(m)} = SA_{54}^{(m)} = 8\,S_{13}\,(r_1 + 3\,r_2 + r_3) - 4\,(S_{12}\,r_1 + S_{22}\,r_2 + S_{23}\,r_3)$$

$$SA_{46}^{(m)} = SA_{64}^{(m)} = 8\,S_{23}\,(3\,r_1 + r_2 + r_3) + 4\,(S_{11}\,r_1 + S_{12}\,r_2 + S_{13}\,r_3)$$

$$SA_{55}^{(m)} = 8\Big[S_{22}\,(r_1 + r_2 + 3\,r_3) + S_{23}\,(r_1 + 2\,r_2 + 2\,r_3) + S_{33}\,(r_1 + 3\,r_2 + r_3)\Big]$$

$$SA_{56}^{(m)} = SA_{65}^{(m)} = 8\,S_{12}\,(r_1 + r_2 + 3\,r_3) - 4\,(S_{13}\,r_1 + S_{23}\,r_2 + S_{33}\,r_3)$$

$$SA_{66}^{(m)} = 8\Big[S_{11}\,(r_1 + r_2 + 3\,r_3) + S_{13}\,(2\,r_1 + r_2 + 2\,r_3) + S_{33}\,(3\,r_1 + r_2 + r_3)\Big] \quad (A.41)$$

In/

In the load matrix terms, l_i = length of side i of a triangular element. Thus:

$$SAL_1^{(m)} = r_1 \left[(\phi,_n)^{a_2} . l_2 + (\phi,_n)^{a_3} . l_3 \right] \frac{\rho^m}{6}$$

$$SAL_2^{(m)} = r_2 \left[(\phi,_n)^{a_1} . l_1 + (\phi,_n)^{a_3} . l_3 \right] \frac{\rho^m}{6}$$

$$SAL_3^{(m)} = r_3 \left[(\phi,_n)^{a_1} . l_1 + (\phi,_n)^{a_2} . l_2 \right] \frac{\rho^m}{6}$$

$$SAL_4^{(m)} = (r_1 + r_2)(\phi,_n)^{a_3} . l_3 . \frac{\rho^m}{3}$$

$$SAL_5^{(m)} = (r_2 + r_3)(\phi,_n)^{a_1} . l_1 . \frac{\rho^m}{3}$$

$$SAL_6^{(m)} = (r_3 + r_1)(\phi,_n)^{a_2} . l_2 . \frac{\rho^m}{3} \qquad (A.42)$$

TABLE A.1

Coefficients (α) for Area Integrals in Area Co-ordinate System

Order: $n = p_i + p_j + p_k$	p_i	p_j	p_k	α
0	0	0	0	1
1	1	0	0	1/3
2	2	0	0	1/6
	1	1	0	1/12
3	3	0	0	1/10
	2	1	0	1/30
	1	1	1	1/60

Remarks: $\iint_{A^{(m)}} L_i^{p_i} \cdot L_2^{p_j} \cdot L_3^{p_k} \cdot dA$

$= \alpha A^{(m)}$ and i, j and k represent any permutation of 1, 2 and 3

TABLE A.2

Coefficients (α) for Length Integrals in Length Co-ordinate System

Order: $n = p_i + p_j$	p_i	p_j	α
0	0	0	1
1	1	0	1/2
2	2	0	1/3
	1	1	1/6
3	3	0	1/4
	2	1	1/12

Remarks: $\frac{1}{(x_2-x_1)} \int_{x_1}^{x_2} L_i^{p_i} \cdot L_2^{p_j} = \alpha$ and i and j represent any permutation of 1, 2 and 3

APPENDIX B

FREE-SURFACE PROBLEM

The finite element techniques developed in this study can not only handle problems involving solid boundaries of arbitrary shapes, but are also quite efficient in locating "simple" free surface profiles, when such a problem is encountered, regardless of whether or not gravity effects are considered. To demonstrate these features, flow from a finite-width slot with a 45^{o} inclination will be investigated, both with and without considering gravitational effects and results are also given for flow from an axisymmetric profile (i.e. nozzle with 45^{o} shaped outlet).

Results consisting of velocity and/or pressure distributions, free surface profile and contraction coefficient were obtained by Larock [9, 43], Von Mises [7] and Chan [3], by other methods. It is found that good agreement exists among the results predicted by these different methods.

FIG. B.1.1 shows half of the physical plane of the flow from a 45^{o} slot together with an initially assumed free surface. The X-axis is chosen to coincide with the axis of symmetry and the Y-axis chosen to pass through point A, the lip of the slot. Far upstream the channel is of unvarying half-width y_u and conveys a flow at uniform speed q_u. Flow passes along the slot, then separates smoothly at the lip A and eventually contracts to a jet half-width y_d with uniform speed q_d far downstream. Here the x-axis may present either a solid wall or an axis of symmetry. For practical computation, uniform flows can be assumed to exist at finite distances from the lip. Based on Chan's [3], criteria, uniform flow is assumed to occur at 2.4 times the slot half-width at the downstream end and 2.0 times the slot half-width at the upstream end respectively. Based on these assumptions, a flow region was well/

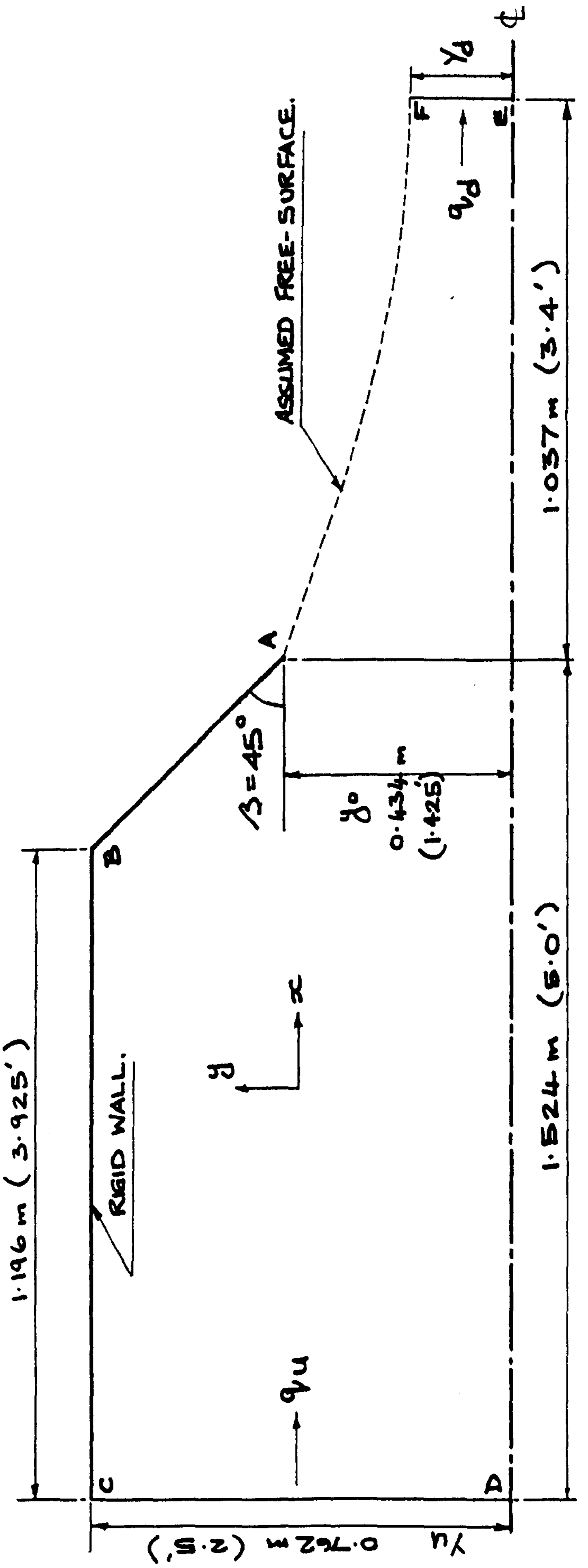

FLOW REGION OF A 2D OR AXI-SYMMETRIC 45° NOZZLE.

FIGURE B.1.1

well defined and analysis could proceed.

The flow region under consideration is divided into 72 quadri-lateral elements as shown in FIG. B.1.2, with elements of smaller size near the lip to accommodate more accurately the large velocity gradients in this region. Also narrow bands of elements have been used near the "guessed" free surface to obtain a more accurate prediction of the velocity components for the nodal points on this boundary, this step is important because these values are to be used in locating a better free surface profile for the next iteration.

The boundary conditions imposed on the problem are as follows: normal velocity component is zero, i.e. $(\phi,_n)^a = \phi$, along ABC and DE, the upstream face has a normal velocity of $(\phi,_n)^a = -q_u$, while at the far downstream boundary $(\phi,_n)^a = +q_d$, which is in turn, equal to the total flow rate divided by the assumed downstream cross-sectional area.

On the assumed free surface AF, the constant-pressure condition is imposed first, which leads to the specification of values of the velocity potential function at all the nodes on this surface. The requirement of zero normal velocity is not to be imposed until after the whole system of equations has been solved and a "better" free surface profile has been located as described in CHAPTER II, Section 4.

The results from the 45^o 2-D slot are shown in FIGS. B.1.3 - B.1.8. Depicted in FIG. B.1.3 are two free surface profiles, one computed with and one without gravitational effects. Comparing the cases with Larock's complex variable solution, it is noted that no significant difference exists between the answers obtained by the two/

two completely different techniques. For the case g = 0 the present method predicted a contraction coefficient (C_c = 0.7589) compared with 0.7562 by Von Mises [7], 0.7559 by Larock [9] and 0.7643 by Chan [3].

When gravitational effects are considered for the case under study (e.g. total head = 0.840 m (2.755 ft)), g = 9.81 m/s (32.2 ft/s) acting transversely, the present approach predicts a coefficient of contraction 0.7083, which compares well with 0.7009 by Larock [43] for flow under the same total head but for a slightly altered slot shape ($\beta = 45.325^{\circ}$, y_0/y_u = 0.571) and 0.7113 by Chan [3], who uses (β = 45°, y_0/y_u = 0.570) as used in this study.

From these results it appears that the finite element method, in general, appears to predict a slightly higher free surface location.

Since the present method produces a speed variation on the free surface which is substantially less than 1.5%, which is considered to be tolerable [8], no further attempt has been made to achieve higher accuracy. However, results could be improved by using a finer grid of elements to represent the flow region if a more accurate solution is required.

With the free surface location determined, the velocity distribution and pressure distribution can be subsequently calculated. FIGS. B.1.4 and B.1.5 show such distributions along the solid boundaries of the flow domain. For brevity, only those plots for the case where g = 0 are presented.

It is seen in FIG. B.1.4 that along the rigid wall the velocity decreases towards the stagnation point, reaches a minimum there and then increases towards the lip as the flow is accelerating in/

in that zone. Along the centre line the velocity increases monotonically in the downstream direction, finally reaching an asymptotic speed q_d of about 2.3 times the inflow speed q_u.

FIG. B.1.5 represents the corresponding pressure distribution which, in contrast to the velocity distribution, increases towards the stagnation point, reaching a maximum then decreasing towards the lip. Along the centre line the pressure decreases monotonically towards the downstream end and finally reaches a value of "almost" zero.

As seen in these figures, the values predicted are poorest at the singular stagnation point, while results are better at the lip. However, these results could be improved by increasing the number of elements near these regions.

FIGS. B.1.6 and B.1.7 show the velocity and pressure distributions for the axisymmetric 45^o nozzle flow case respectively and FIG. B.1.8 shows the convergence procedure in operation.

FIGURE B.1.2.

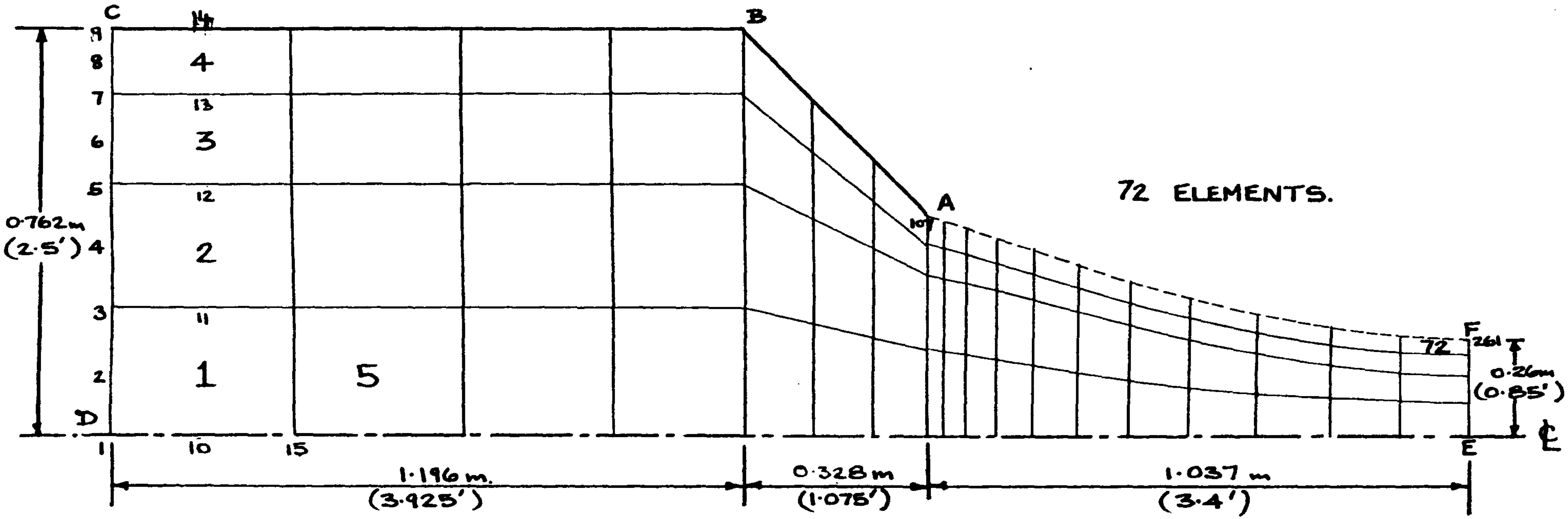

FINITE ELEMENT REPRESENTATION OF A 45° NOZZLE. (OR SLOT)

FREE SURFACE LOCATIONS OF FLOW FROM A 45° TWO-DIMENSIONAL NOZZLE.

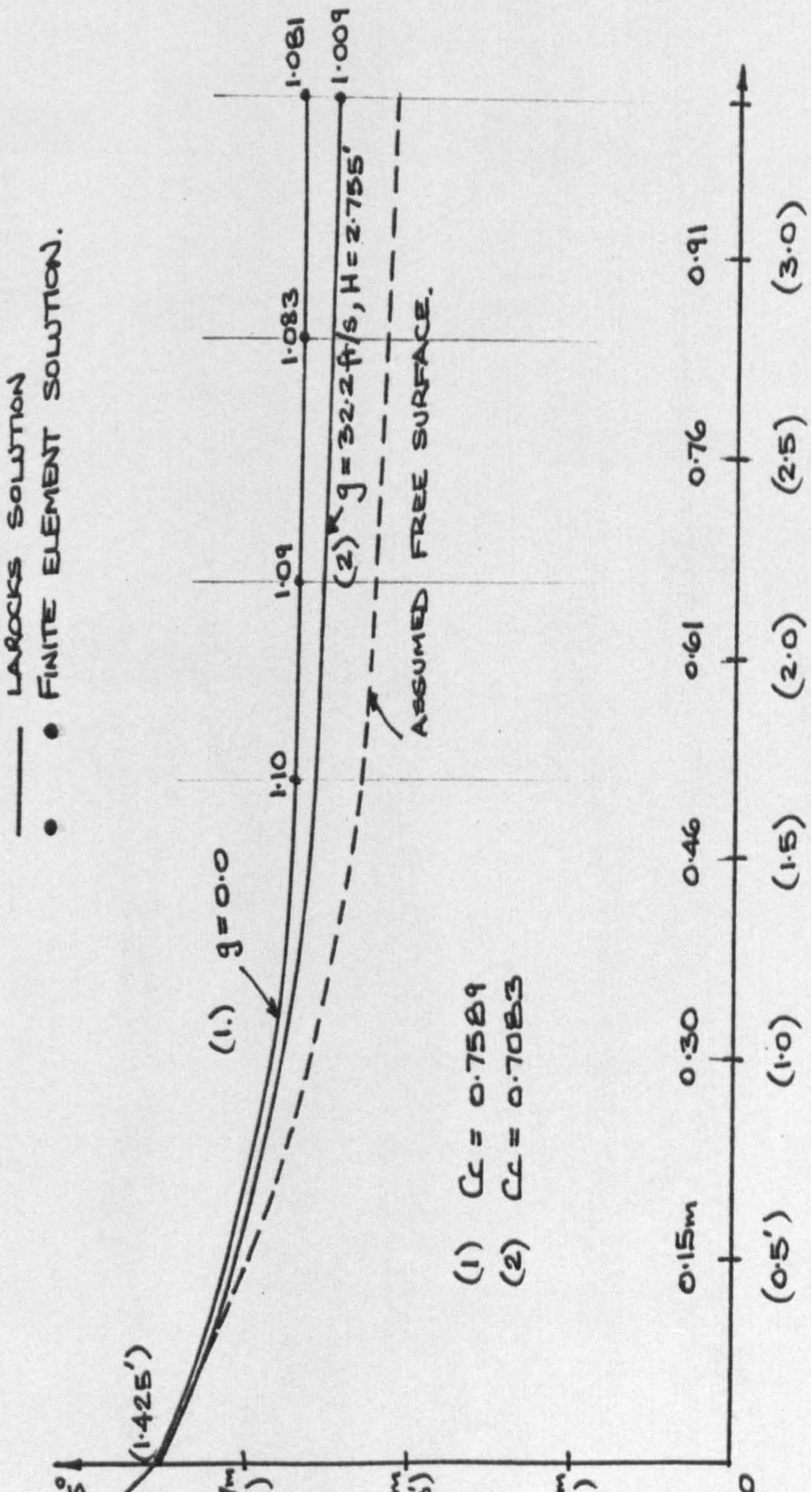

FIGURE B. 1. 3

NORMALIZED VELOCITY DISTRIBUTION (q/q_u) ALONG BOUNDARIES OF A 45° TWO-DIMENSIONAL SLOT. ($g = 0.0$)

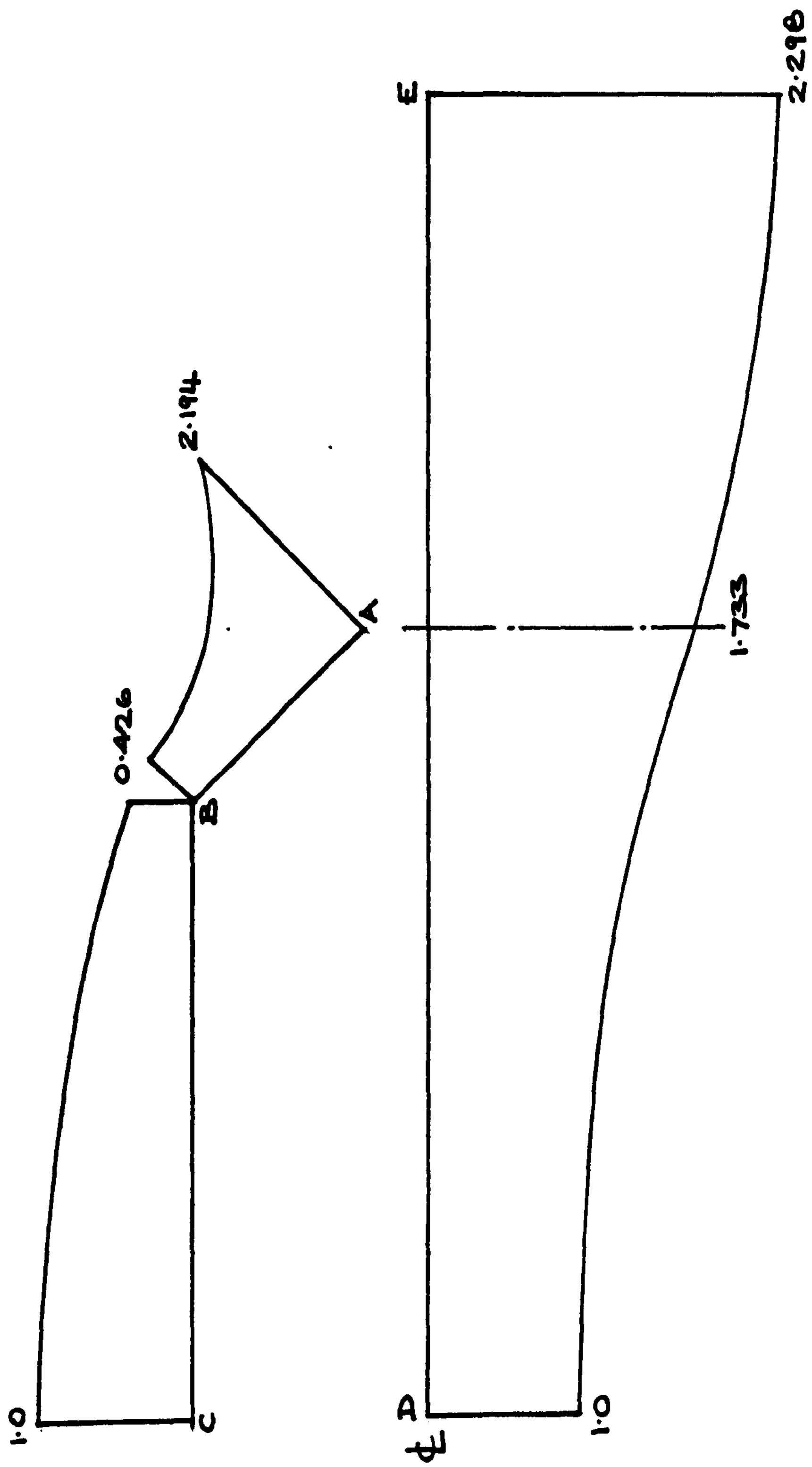

FIGURE B.1.4

PRESSURE DISTRIBUTION (Cp) ALONG BOUNDARIES OF A 45° TWO-DIMENSIONAL SLOT. (g= 0.0)

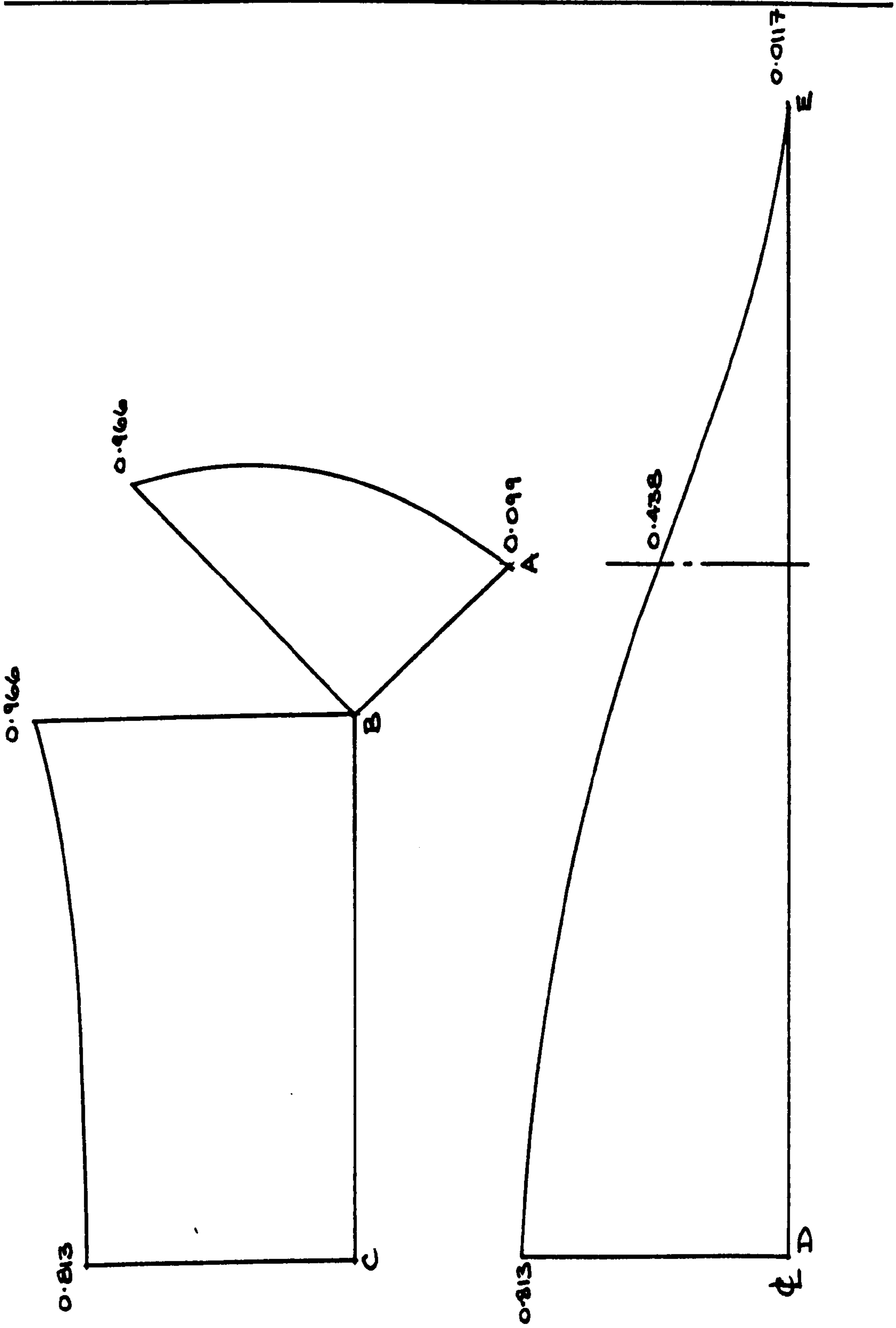

FIGURE B.1.5

NORMALIZED VELOCITY DISTRIBUTION (q/qu) ALONG BOUNDARIES OF A 45° AXI-SYMMETRIC NOZZLE (45°)
(g = 0.0)

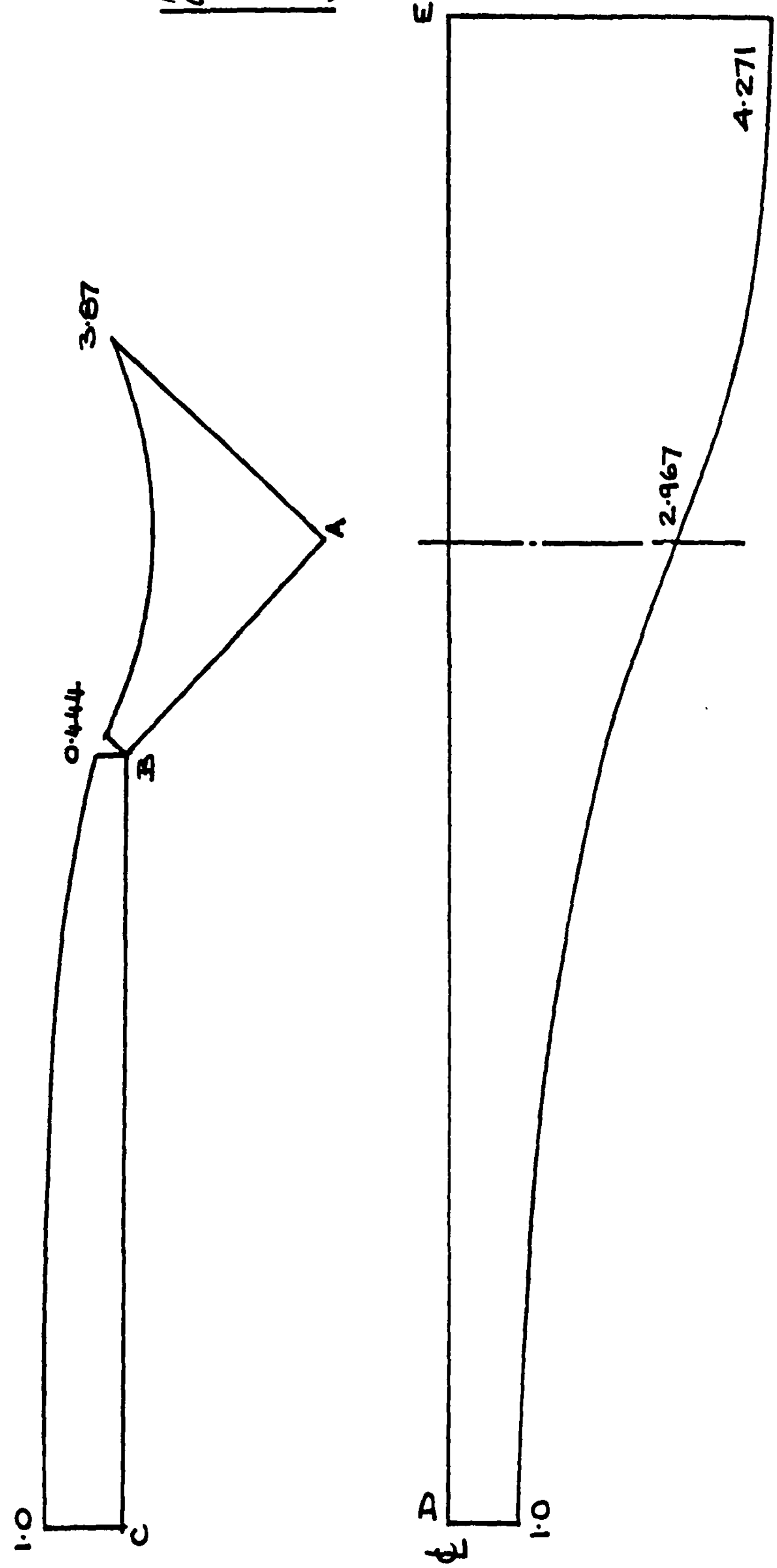

FIGURE B.1.6

PRESSURE DISTRIBUTION (Cp) ALONG BOUNDARIES OF A 45° AXI-SYMMETRIC NOZZLE (g = 0.0)

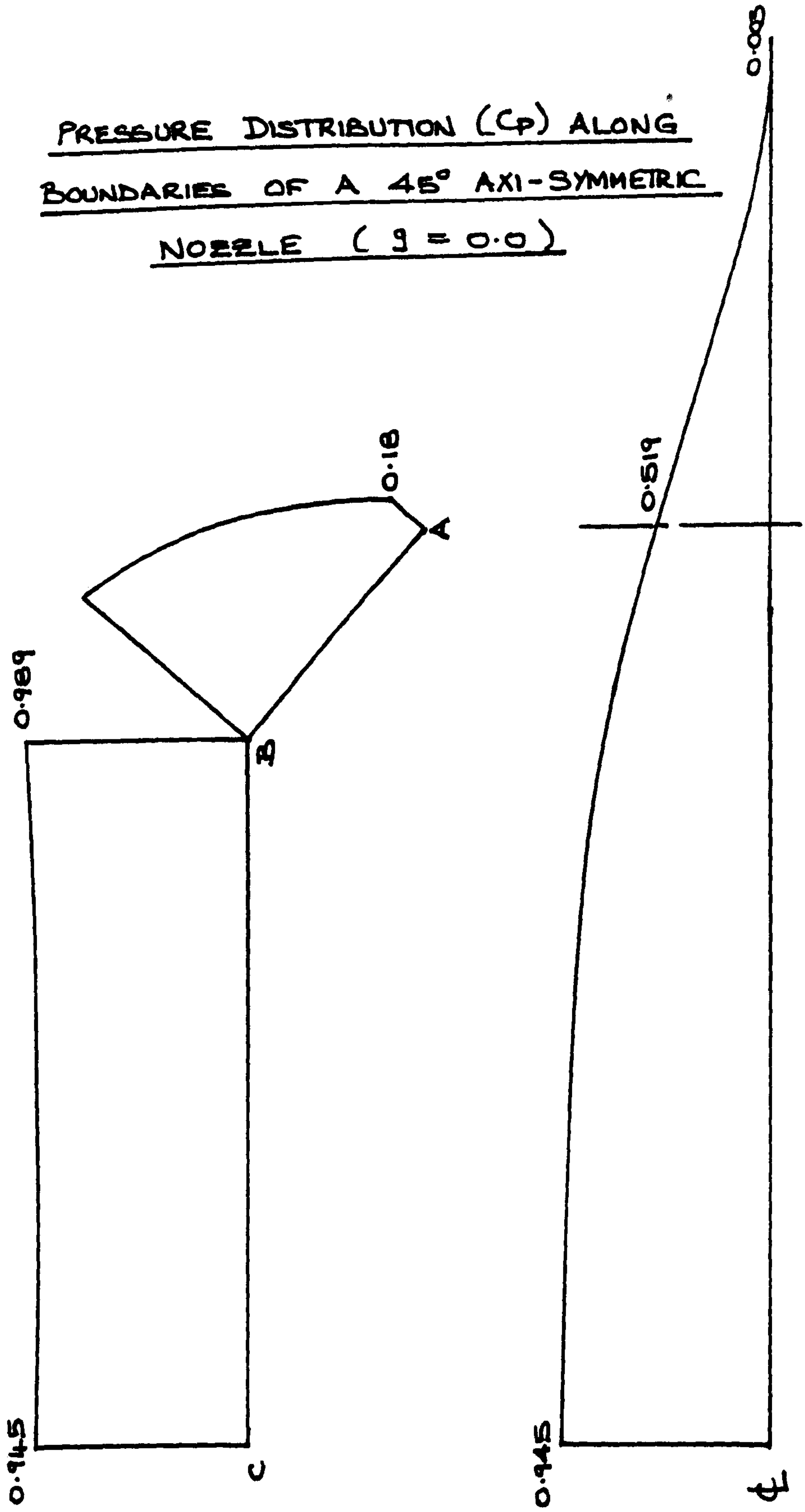

FIGURE B.1.7

CONVERGENCE OF CONTRACTION COEFF'S FOR 2-D AND AXI-SY. FLOW CASES.

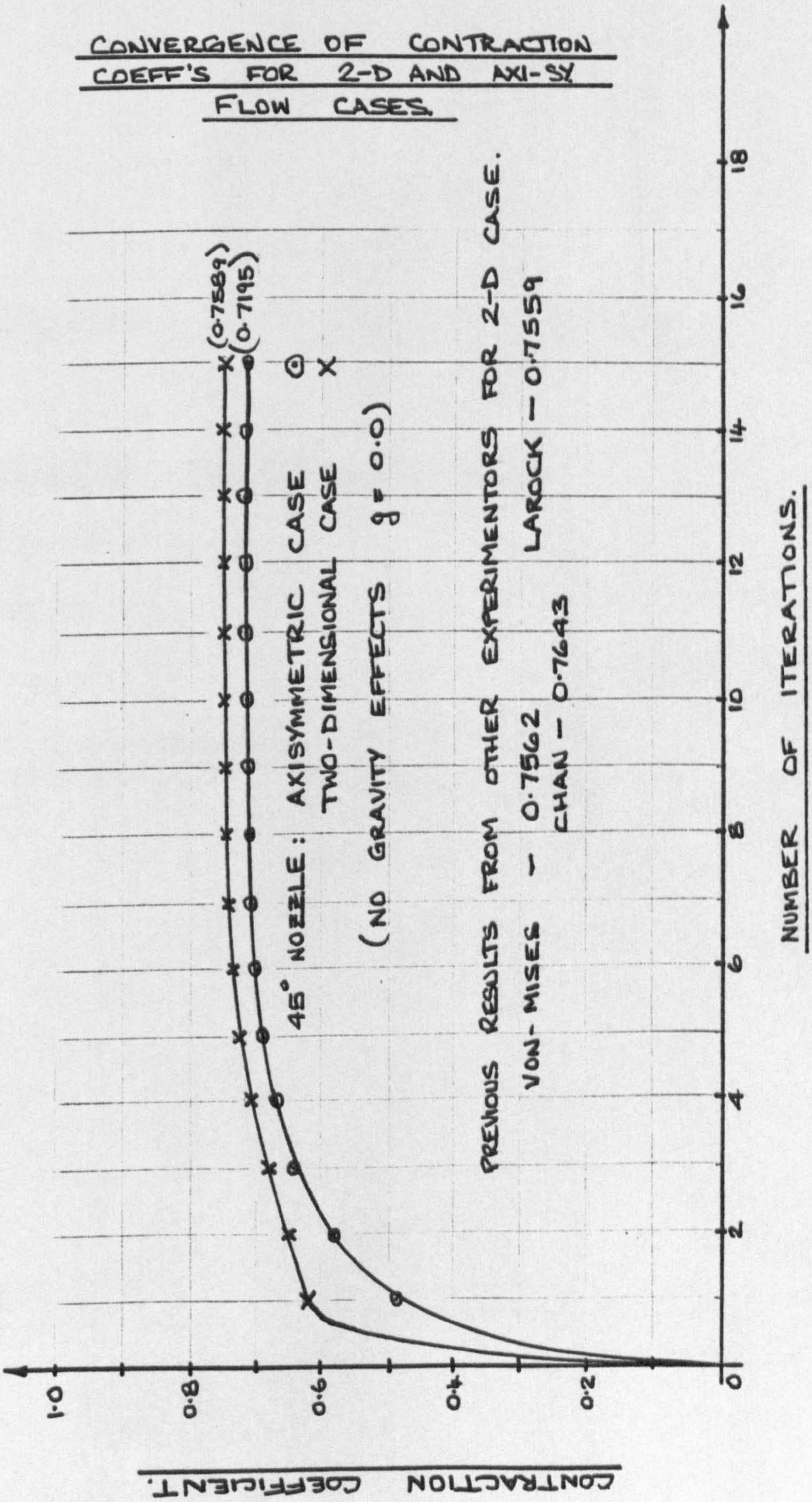

FIGURE B.1.8.

APPENDIX C

COMPUTER PROGRAM

This program carries out the calculations for the analysis of two-dimensional and axisymmetric flow problems. The flow may be either confined or involving a free surface. Gravity acting in the longitudinal direction can be taken into account for both two-dimensional and axisymmetric flows. For two-dimensional flows, a transverse gravity field can also be considered.

The program, as presently coded is in FORTRAN IV language and can analyse a problem with a maximum number of 150 elements together with 500 nodal points, nevertheless, this program can be modified quite easily by using temporary files to handle a problem beyond this limit. The computer used in this study was initially an ICL 1300 series (Strathclyde) and latterly a UNIVAC 1100 series (Sperry, Bracknell). In the present program a temporary file is set up only to store the unchanged part of the system matrix for use in later iterations.

The following is a detailed description of the inputs required and the outputs obtained during the running of this program, for a) confined boundary case and b) free surface boundary problem.

INPUT

a) CONFINED DATA

Confined boundary problems conform generally to the type shown in FIG. 20 or in particular to FIG. C.1.1 a) and b) (as used in this report), and hence two methods of application are available.

The flow region which is being studied is firstly defined, followed by setting up of the co-ordinate axes. The location of the origin of these axes, in general, is arbitrary except that for a problem involving axial symmetry the x-axis must coincide with the axis/

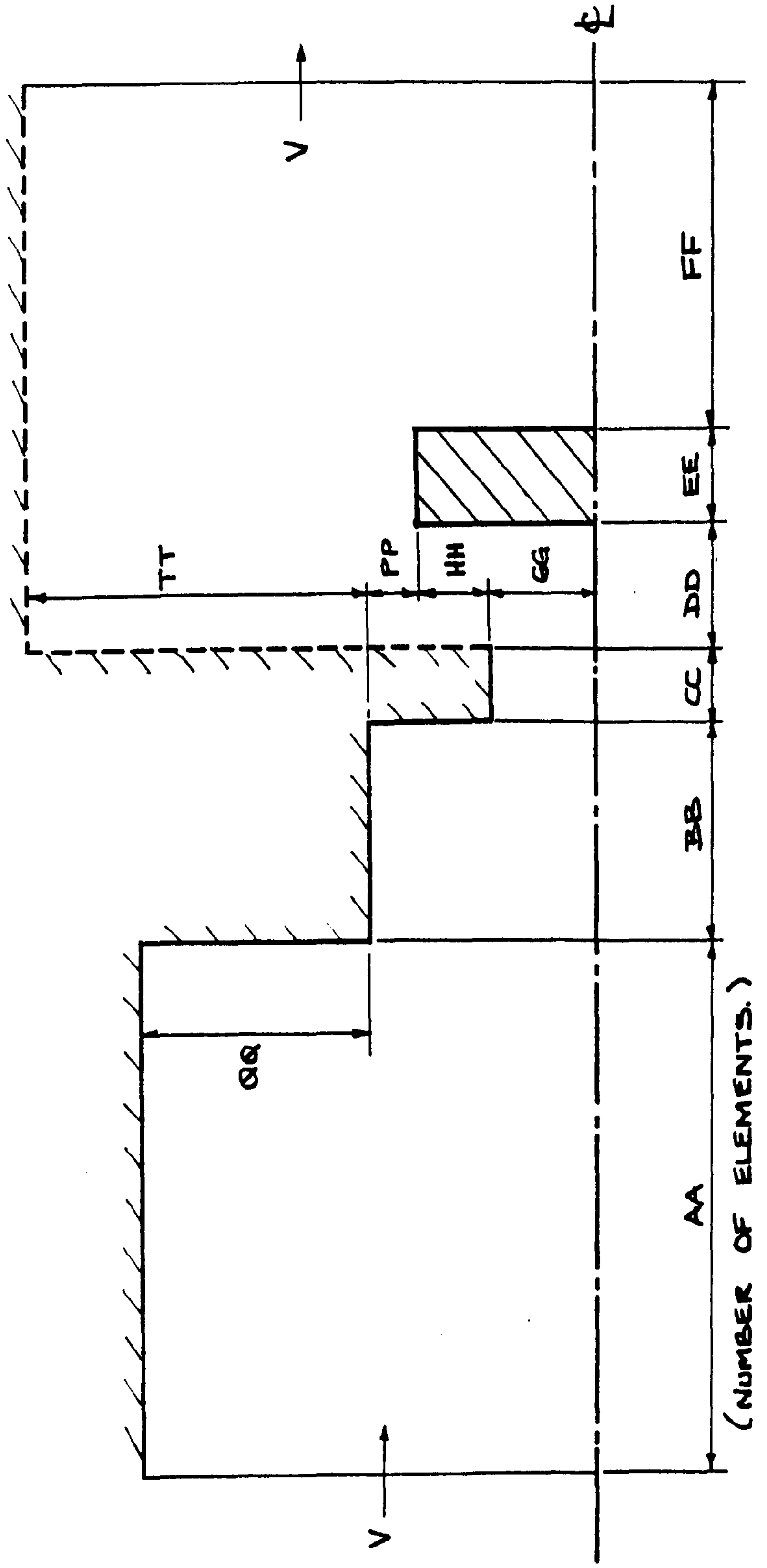

FLOW PROFILE. (DISPLAYING DATA REQUIRED.)

FIGURE C.1.1.(a)

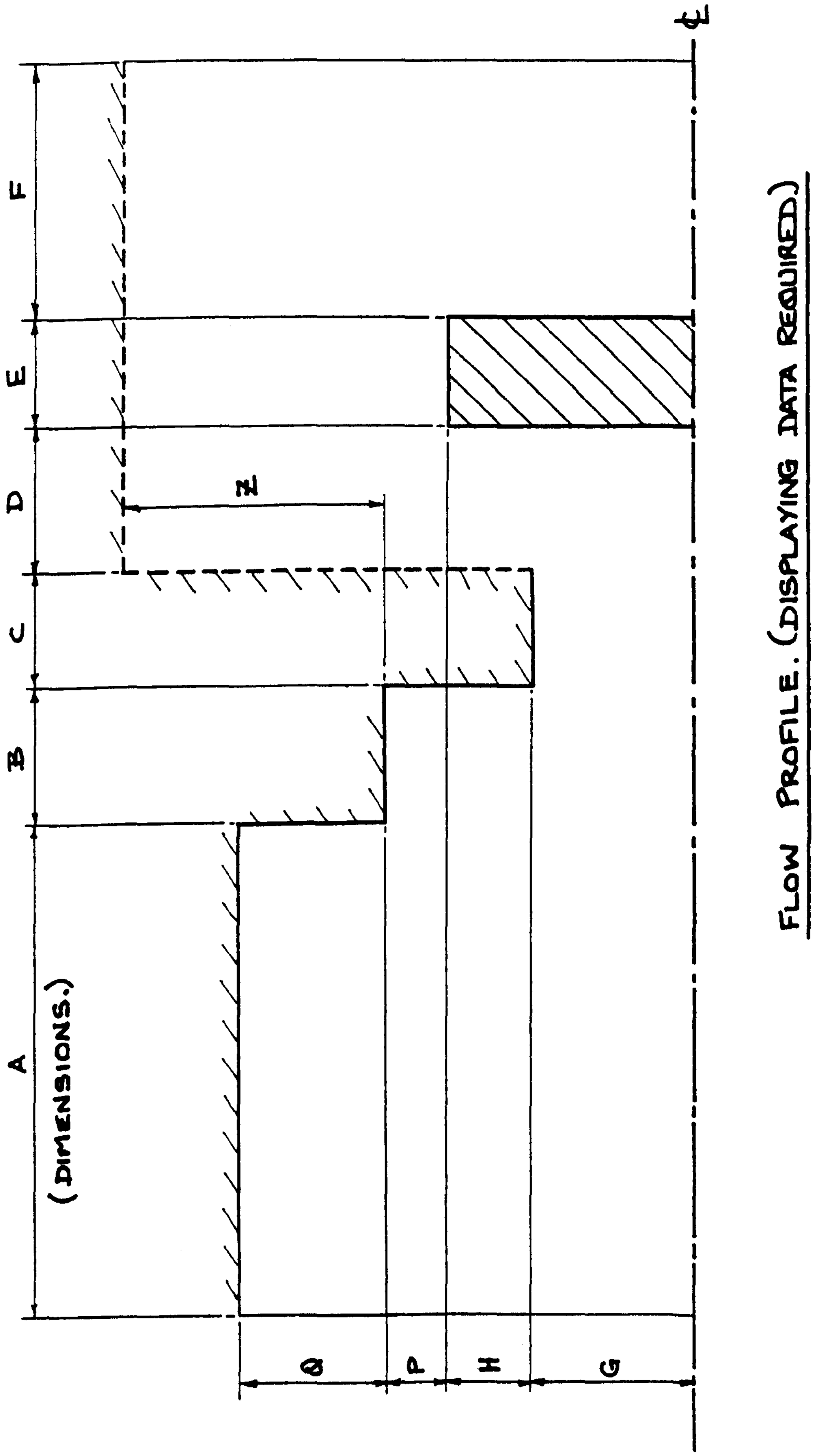
FLOW PROFILE. (DISPLAYING DATA REQUIRED)
A
(DIMENSIONS.)
B
C
D
E
F
Z
Q
P
H
G

FIGURE C.1.1 (b).

axis of symmetry. The flow region is then divided into a mesh of quadrilateral elements and the nodal points are numbered in a numerical sequence starting with the number 1. For convenience the starting point is chosen to be the lower-left corder node. Also in order to obtain a smaller 'band' width to save computational time in solving the system of equations, the nodal points should be numbered in the shorter direction [44].

To save effort in preparing data, the case used in this report has been developed to include two options, one for generating node point co-ordinates and one for generating noide point numbers of an array. In this way only a limited amount of data is required.

A CONTROL CARD (2I3, 2F10.4)

COLUMNS	1-3	NTYPE	Use 1 for automatic generation procedures. Use 2 for flow domain which does not conform to FIG. C.1.1
	4-6	NDIMEN	Use 2 to designate two-dimensional problems. Use Ø for axisymmetric problem.
	7-16	DENS	Density of Fluid.
	17-26	D	Valve Lift.

If NTYPE = 2 further data required is fed in from b) section A etc. (free surface) with appropriate zero's.

If NTYPE = 1 continue.

B DOMAIN DATA CARD (12F5.0)

COLUMNS	1-5	AA	
	6-10	BB	
	11-15	CC	See FIG. C.1.1
	16-20	DD	
	21-25	EE	
	26/		

COLUMNS	26-30	FF	
	31-35	GG	
	36-40	HH	
	41-45	PP	See FIG. C.1.1
	46-50	QQ	
	51-55	TT	
	56-60	Z	

C BOUNDARY CARD (I3)

COLUMNS	1-3	NPBOC	The number of boundary value cards which specify the non-zero values of normal velocity components along the boundaries.

D ELEMENT CARD (8I5, I10)

COLUMNS	1-5	NOD(1,1)	Number of nodal point 1 for element 1.
	6-10	NOD(1,2)	Number of nodal point 2 for element 1.
	11-15	NOD(1,3)	Number of nodal point 3 for element 1.
	16-20	NOD(1,4)	Number of nodal point 4 for element 1.
	21-25	NOD(1,5)	Number of nodal point 5 for element 1.
	26-30	NOD(1,6)	Number of nodal point 6 for element 1.
	31-35	NOD(1,7)	Number of nodal point 7 for element 1.
	36-40	NOD(1,8)	Number of nodal point 8 for element 1.
	41-50	NMIS	Number of the succeeding elements whose nodal numbers are not provided and generation option has to be used to obtain such information.

As/

As the program is now coded, to use the generation options the node point numbers of an element must be arranged such that the starting point is the lower-left hand corner node and followed by other nodes in a counter-clockwise direction.

b) FREE SURFACE DATA

As the program is coded at present, only "simple" free surface problems can be analysed (FIG. C.1.2). "Simple" implies no "bodies" are present under the free surface boundary as shown dotted in FIG. C.1.2.

If bodies were present (e.g. valve etc.) new algorithms would be required to tackle this type of problem and since these would require quite extensive modifications to the program and would hence be time consuming, this has not been implemented.

As before the flow region is defined, followed by the setting up of co-ordinate axes as described for case a).

A CONTROL CARD (5I10, F10.0, I5)

COLUMNS	1-10	NNPC	The number of corner nodes at which co-ordinate values will be supplied so that co-ordinates of the remaining nodes can be generated.
	11-20	NELEMC	The number of elements for which nodal numbers will be provided so as to generate the nodal numbers for the rest of the elements.
	21-30	NPBOC	The number of boundary cards which specify the non-zero values of normal velocity component along the boundaries.
	31-40	NPFS	The number of corner nodes on the free surface including the one at the lip.

41-50/

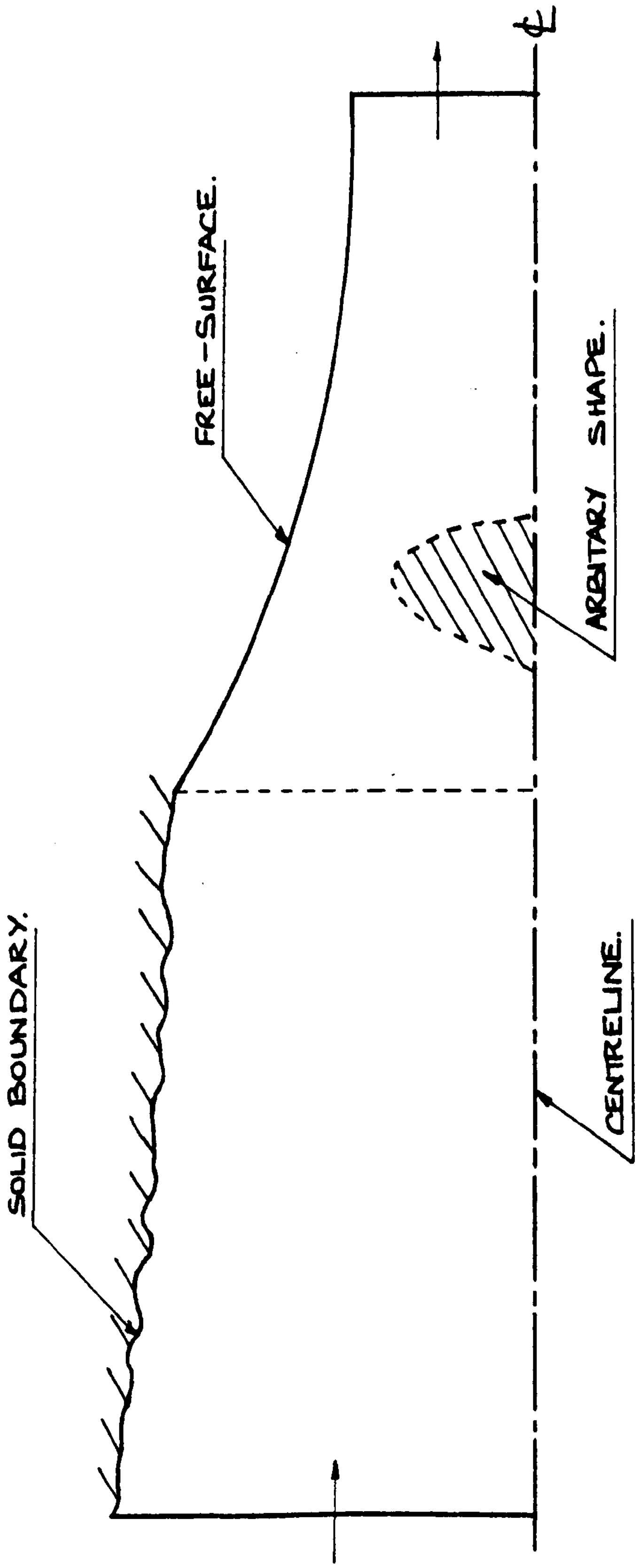

FREE-SURFACE FLOW DOMAIN.

FIGURE C.1.2.

COLUMNS	41-50	ITGIV	Estimated number of iterations necessary to complete the solution for a free surface problem, which is usually set between 10 and 20.
	51-60	GR	The constant of gravitational acceleration if gravity is to be considered.
	61-65	INDGR	Number indicating the direction of gravity. Use 2 if gravity acts transversely; otherwise leave it blank.

B <u>CORNER NODE CARDS</u> (I10, 2F10.0, I10)

Without using the generation option, one card will be required for each corner node. If the option is used, only those cards for the controlling corner nodes will be needed. In that case, the program generates the omitted information automatically, including the co-ordinates of omitted corner node points by linear interpolation and also the associated corner node numbers.

COLUMNS	1-10	N	The corner node number.
	11-20	X(N)	X-co-ordinate.
	21-30	Y(N)	Y-co-ordinate or radial co-ordinate.
	31-40	NPMIS	Use 1 if there is at least one corner node omitted between the present and the succeeding corner node cards and hence generation option is to be used.

C <u>ELEMENT CARDS</u> (8I5, I10)

One card for each element unless the generation option is used.

COLUMNS	1-5	NOD(N,1)	Number of nodal point 1.
	6-10/		

COLUMNS	6-10	NOD(N,2)	Number of nodal point 2.
	11-15	NOD(N,3)	Number of nodal point 3.
	16-20	NOD(N,4)	Number of nodal point 4.
	21-25	NOD(N,5)	Number of nodal point 5.
	26-30	NOD(N,6)	Number of nodal point 6.
	31-35	NOD(N,7)	Number of nodal point 7.
	36-40	NOD(N,8)	Number of nodal point 8.
	41-50	NMIS	Number of the succeeding elements whose nodal numbers are not provided and generation option has to be used to obtain such information.

As the program is now coded, to use the generation option the node point numbers of an element must be arranged such that the starting point is the lower-left hand corner node and followed by other nodes in a counter-clockwise direction. It must be so for all the controlling element cards.

D BOUNDARY VALUE CARDS (I10, F10.0, 2I10)

One card is required for each portion of the boundary on which a constant non-zero value of the normal velocity component exists. The far downstream face is not considered to be such a boundary. On that face a constant velocity potential will instead be specified for all nodes to impose the condition of uniform flow.

COLUMNS	1-10	NSTART	Node point number at which the specified boundary value is to begin.
	11-20	BVAL	The specified value of non-zero normal velocity component.
	21-30	NBSAME	Number of the sides of elements over which the same boundary value is to be specified.
	31-40/		

COLUMNS	31-40	NINC	The algebraic difference between two adjacent corner node numbers on this portion of the boundary.

E CARDS FOR FREE SURFACE

The following set of cards is needed only for a problem involving a free surface which requires the iteration scheme to locate its profile.

NPFSA, NPBOT — i) Array of corner node numbers on the free surface and the array of corner node number on the x-axis (16I5).

These two arrays of corner node numbers are arranged in pairs, starting with that pair of numbers which describe the far two nodes downstream and continuing up to and including that pair at the lip.

NPSFM — ii) Array of mid-point node numbers on the free surface (16I5).

This array also starts far downstream and ends with the mid-point next to the lip.

iii) Information needed for the adjustment of free surface location (2F10.0, 3I10, F10.0).

COLUMNS	1-10	SPDDW	Assumed downstream speed.
	11-20	SMAS	Total flow rate.
	21-30	NELB	The number of the element on the free surface which has the lip as one of its nodes. The element numbers are in a numerical sequence starting with number one, counting from bottom to top and from left to right.
	31-40	NELT	The element number of the last element on the free surface.

41-50/

COLUMNS	41-50	NELMIS	Difference of the element numbers of two adjacent elements on the free surface.
	51-60	ALPHA	The acute angle between the rigid wall and the vertical axis.

<u>OUTPUT</u>

The following information is developed and printed by the program in the order listed below and is similar for either confined or free surface problems.

<u>A</u>

All input data, co-ordinates of corner nodes, element numbers with their node point numbers, the specified normal velocity components, node point numbers on the free surface etc., are printed.

<u>B</u>

For free surface flow problems, the adjusted free surface location with its associated contraction or discharge coefficient and the velocity components for the corner nodes on the free surface are printed after each iteration. For gravity-affected flows, the total head for each of these nodes is also calculated and printed out.

<u>C</u>

Finally, the computed results for the entire flow field under consideration are printed. These results include the velocity potential, the distributions of velocity, pressure and valve forces, and for free surface flow problems, the predicted free surface profile and its corresponding contraction or discharge coefficient.

COMPUTER PROGRAM.

```
427A01*E44...(1).FLOT
      C
      C     ****************************************************************
      C             FINITE ELEMENT ANALYSIS OF POTENTIAL FLOWS
      C          THE FLOW MAY BE TWO DIMENSIONAL OR AXISYMMETRIC
      C          CONFINED OR WITH A FREE SURFACE. WITH OR WITHOUT
      C             CONSIDERATION OF GRAVITATIONAL EFFECTS
      C     ****************************************************************
      C
      C
      C
            IMPLICIT DOUBLE PRECISION (A-H,O-Z)
            DIMENSION IND(1000),PHI(50)
            COMMON NPNOD(300,8),X(1000),Y(1000),N1,N2,N3,AN,INDEX,T(6,6),
           1,SL3,NI,NNIS
            COMMON /A/ CSL(13),CS(13,13),NPBC,NPBOA(100),BOV(100),ND(4,6)
            COMMON /SYMS/ SL(1000),S(1000,41),NNP,NCOL
            COMMON /FSS/ U(1000),V(1000),NPFSA(25),NPBOT(25),NPFSM(24),
           1         NPFS,ALPHA
            INTEGER SA,SS
            FGAVX(QO,XI,XJ,XO,GR)=0.5*(SQRT(QO*QO-2.*GR*(XO-XI))
           1                    +SQRT(QO*QO-2.*GR*(XO-XJ)))
            FGAVY(QO,YI,YJ,YO,GR) =0.5*(SQRT(QO*QO-2.*GR*(YI-YO))
           1                    +SQRT(QO*QO-2.*GR*(YJ-YO)))
            READ(5,3102) NTYPE,NDIMEN,DENS,D
       3102 FORMAT(I3,I3,2F10.0)
      C
      C
      C     ****************************************************************
      C     IF NTYPE=1 THIS IS A CONFINED BOUNDARY PROBLEM.
      C     IF NTYPE=2 THIS IS A FREE SURFACE BOUNDARY PROBLEM.
      C     ****************************************************************
      C
      C
            IF(NTYPE.EQ.1) GO TO 3100
            GO TO 100
       3100 CONTINUE
            WRITE(6,711) NTYPE,NDIMEN,DENS,D
        711 FORMAT(7H NTYPE=,I3,3X,8H NDIMEN=,I3,3X,6H DENS=,F10.4,
           1         3X,3H D=,F10.4)
            READ(5,3111)AA,BB,CC,DD,EE,FF,GG,HH,PP,QQ,TT,Z
       3111 FORMAT(12F5.0)
            A=10.0
            B=9.525
            C=3.97
            E=3.97
            F=10.0
            G=3.175
            H=1.03
            P=8.10
            Q=7.94
            READ(5,3103) NPBOC
       3103 FORMAT(I3)
            N=1
            X(N)=0.0
      C
      C
      C
```

```
C
C     ******************************************************************
C                        GENERATE NODE CO-ORDINATES.
C     ******************************************************************
C
      Y(N)=0.0
      NPMIS=1
      WRITE(6,3200) N,X(N),Y(N)
 3200 FORMAT(1H ,13X,4HNODE,I4,5X,4HX = ,F10.6,5X,4HY = ,F10.6)
      NI=N
      N=N+(2*GG)
      X(N)=0.0
      Y(N)=G
      NPMIS=1
      CALL RNUM
      NI=N
      N=N+(2*HH)
      X(N)=0.0
      Y(N)=H+G
      NPMIS=1
      CALL RNUM
      NI=N
      N=N+(2*PP)
      X(N)=0.0
      Y(N)=H+G+P
      NPMIS=1
      CALL RNUM
      NI=N
      N=N+(2*GG)
      X(N)=0.0
      Y(N)=H+G+P+G
      NPMIS=0.0
      CALL RNUM
      NN=AA
      DO 211 J=1,NN
      N=N+GG+HH+PP+GG+2
      X(N)=J*(A/AA)
      Y(N)=0.0
      NPMIS=1
      WRITE(6,3200) N,X(N),Y(N)
      NI=N
      N=N+(2*GG)
      X(N)=J*(A/AA)
      Y(N)=G
      NPMIS=1
      CALL RNUM
      NI=N
      N=N+(2*HH)
      X(N)=J*(A/AA)
      Y(N)=H+G
      NPMIS=1
      CALL RNUM
      NI=N
      N=N+(2*PP)
      X(N)=J*(A/AA)
      Y(N)=P+H+G
      NPMIS=1
```

```
      CALL RNUM
      NI=N
      N=N+(2*GG)
      X(N)=J*(A/AA)
      Y(N)=G+P+H+G
      NPMIS=0
      CALL RNUM
211   CONTINUE
      NN=BB
      DO 212 J=1,NN
      N=N+GG+HH+PP+2
      X(N)=J*(B/BB)+A
      Y(N)=0.0
      NPMIS=1
      WRITE(6,3200)N,X(N),Y(N)
      NI=N
      N=N+(2*GG)
      X(N)=A+(B/BB)*J
      Y(N)=G
      NPMIS=1
      CALL RNUM
      NI=N
      N=N+(2*HH)
      X(N)=A+(B/BB)*J
      Y(N)=H+G
      NPMIS=1
      CALL RNUM
      NI=N
      N=N+(2*PP)
      X(N)=A+(B/BB)*J
      Y(N)=G+P+H
      NPMIS=0
      CALL RNUM
212   CONTINUE
      NN=CC-1
      DO 213 J=1,NN
      N=N+GG+2
      X(N)=A+B+(C/CC)*J
      Y(N)=0
      NPMIS=1
      WRITE(6,3200) N,X(N),Y(N)
      NI=N
      N=N+(2*GG)
      X(N)=A+B+(C/CC)*J
      Y(N)=G
      NPMIS=0
      CALL RNUM
213   CONTINUE
      NN=DD+1
      DO 2133 J=1,NN
      IF(J.EQ.1) GO TO 3500
      GO TO 3501
3500  N=N+GG+2
      GO TO 3502
3501  N=N+GG+HH+PP+TT+2
3502  X(N)=A+B+C+(D/DD)*(J-1)
      Y(N)=0
```

```
      NPMIS=1
      WRITE(6,3200) N,X(N),Y(N)
      NI=N
      N=N+(2*GG)
      X(N)=(J-1)*(D/DD)+A+B+C
      Y(N)=G
      NPMIS=1
      CALL RNUM
      NI=N
      N=N+(2*HH)
      X(N)=(J-1)*(D/DD)+A+B+C
      Y(N)=H+G
      NPMIS=1
      CALL RNUM
      NI=N
      N=N+(2*PP)
      X(N)=(J-1)*(D/DD)+A+B+C
      Y(N)=P+H+G
      NPMIS=1
      CALL RNUM
      NI=N
      N=N+(2*TT)
      X(N)=A+B+C+(J-1)*(D/DD)
      Y(N)=G+H+P+Z
      NPMIS=1
      CALL RNUM
 2133 CONTINUE
      NN=EE-1
      DO 2144 J=1,NN
      N=N+PP+TT+2
      X(N)=A+B+C+D+J*(E/EE)
      Y(N)=G+H
      NPMIS=1
      WRITE(6,3200) N,X(N),Y(N)
      NI=N
      N=N+2*PP
      X(N)=A+B+C+D+(J*(E/EE))
      Y(N)=G+H+P
      NPMIS=1
      CALL RNUM
      NI=N
      N=N+(2*TT)
      X(N)=A+B+C+D+J*(E/EE)
      Y(N)=G+H+P+Z
      NPMIS=1
      CALL RNUM
 2144 CONTINUE
      NN=FF+1
      DO 2122 J=1,NN
      IF(J.EQ.1) GO TO 3510
      GO TO 511
 3510 N=N+PP+TT+2
      GO TO 3512
  511 N=N+PP+TT+GG+HH+2
 3512 CONTINUE
      X(N)=A+B+C+D+E+(J-1)*(F/FF)
      Y(N)=0
```

```
      NPMIS=1
      WRITE(6,3200) N,X(N),Y(N)
      NI=N
      N=N+2*GG
      X(N)=A+B+C+D+E+(J-1)*(F/FF)
      Y(N)=G
      NPMIS=1
      CALL RNUM
      NI=N
      N=N+2*HH
      X(N)=A+B+C+D+E+(J-1)*(F/FF)
      Y(N)=G+H
      NPMIS=1
      CALL RNUM
      NI=N
      N=N+2*PP
      X(N)=A+B+C+D+E+(J-1)*(F/FF)
      Y(N)=G+H+P
      NPMIS=1
      CALL RNUM
      NI=N
      N=N+2*TT
      X(N)=A+B+C+D+E+(J-1)*(F/FF)
      Y(N)=G+H+P+Z
      NPMIS=1
      CALL RNUM
 2122 CONTINUE
      NNP=N
      N=0
      N=N+1
      READ(5,3101)(NOD(N,I),I=1,8),NMIS
C
C     ******************************************************************
C                         GENERATE NODE NUMBERS.
C     ******************************************************************
C
 3101 FORMAT(8I5,I10)
      NMIS=GG+HH+PP+QQ-1
      CALL RSEG
      SA=GG+HH+QQ+PP
      SS=(SA*3)+2
      NN=AA-1
      DO 201 J=1,NN
      N=N+1
      DO 3310 I=1,8
      NOD(N,I)=NOD(N-SA,I)+SS
 3310 CONTINUE
      NMIS=SA-1
      CALL RSEG
  201 CONTINUE
      N=N+1
      DO 311 I=1,8
      IF(I.EQ.3) GO TO 504
      CONTINUE
      IF(I.EQ.4) GO TO 504
      CONTINUE
      IF(I.EQ.5) GO TO 504
```

```
      CONTINUE
      GO TO 506
504   NOD(N,I)=NOD(N-SA,I)+SS-QQ
      GO TO 506
505   NOD(N,I)=NOD(N-SA,I)+SS
506   CONTINUE
311   CONTINUE
      NMIS=GG+HH+PP-1
      CALL RSEQ
      SA=GG+HH+PP
      SS=(SA*3)+2
      NN=GG-1
      DO 202 J=1,NN
      N=N+1
      DO 312 I=1,8
      IF(J.NE.1) GO TO 600
      IF(I.EQ.1) GO TO 515
      CONTINUE
      IF(I.EQ.7) GO TO 515
      CONTINUE
      IF(I.EQ.8) GO TO 515
      GO TO 516
515   CONTINUE
      NOD(N,I)=NOD(N-SA,I)+SS+2*QQ
      GO TO 517
516   NOD(N,I)=NOD(N-SA,I)+SS
      GO TO 517
600   NOD(N,I)=NOD(N-SA,I)+SS
517   CONTINUE
312   CONTINUE
      NMIS=SA-1
      CALL RSEQ
202   CONTINUE
      N=N+1
      DO 313 I=1,8
      IF(I.EQ.3) GO TO 518
      CONTINUE
      IF(I.EQ.4) GO TO 518
      CONTINUE
      IF(I.EQ.5) GO TO 518
      CONTINUE
      GO TO 519
518   NOD(N,I)=NOD(N-SA,I)+SS-(HH+PP)
      GO TO 520
519   NOD(N,I)=NOD(N-SA,I)+SS
520   CONTINUE
313   CONTINUE
      NMIS=GG-1
      CALL RSEQ
      SA=GG
      SS=(GG*3)+2
      NN=CC-1
      DO 203 J=1,NN
      N=N+1
      DO 314  I=1,8
      IF(J.NE.1) GO TO 522
      IF(I.EQ.1) GO TO 521
```

```
      CONTINUE
      IF(I.EQ.7) GO TO 521
      CONTINUE
      IF(I.EQ.8) GO TO 521
      CONTINUE
      GO TO 522
521   NOD(N,I)=NOD(N-SA,I)+SS+2*(HH+PP)
      GO TO 523
522   NOD(N,I)=NOD(N-SA,I)+SS
523   CONTINUE
314   CONTINUE
      CALL RSEG
203   CONTINUE
      N=N+1
      DO 3315 I=1,8
      IF(I.EQ.1) GO TO 524
      IF(I.EQ.7) GO TO 524
      IF(I.EQ.8) GO TO 524
      IF(I.EQ.2) GO TO 525
      IF(I.EQ.6) GO TO 525
      NOD(N,I)=NOD(N-SA,I)+SS+3*(HH+PP+TT)
      GO TO 526
524   NOD(N,I)=NOD(N-SA,I)+SS
      GO TO 526
525   NOD(N,I)=NOD(N-SA,I)+SS+2*(HH+PP+TT)
526   CONTINUE
3315  CONTINUE
      NMIS=GG+HH+PP+TT-1
      CALL RSEG
      NN=DD-1
      SA=(GG+HH+PP+TT)
      SS=(GG+HH+PP+TT)*2+2
      DO 204 J=1,NN
      N=N+1
      DO 316 I=1,8
      NOD(N,I)=NOD(N-SA,I)+SS
316   CONTINUE
      CALL RSEG
204   CONTINUE
      N=N+1
      SA=PP+TT+GG+HH
      SS=(3*SA)+2
      DO 317 I=1,8
      IF(I.EQ.1) GO TO 527
      IF(I.EQ.7) GO TO 527
      IF(I.EQ.8) GO TO 527
      IF(I.EQ.2) GO TO 528
      IF(I.EQ.6) GO TO 528
      NOD(N,I)=NOD(N-SA,I)+SS-(GG+HH)
      GO TO 317
527   NOD(N,I)=NOD(N-SA,I)+SS+2*(GG+HH)
      GO TO 317
528   NOD(N,I)=NOD(N-SA,I)+SS
317   CONTINUE
      NMIS=PP+TT-1
      CALL RSEG
      NN=EE-1
```

```
      SA=PP+TT
      SS=(3*SA)+2
      DO 205 J=1,NN
      N=N+1
      DO 318 I=1,8
      IF(J.NE.NN) GO TO 801
      IF(I.EQ.3) GO TO 529
      IF(I.EQ.4) GO TO 529
      IF(I.EQ.5) GO TO 529
      NOD(N,I)=NOD(N-SA,I)+SS
      GO TO 318
  529 NOD(N,I)=NOD(N-SA,I)+SS+2*(GG+HH)
      GO TO 318
  801 NOD(N,I)=NOD(N-SA,I)+SS
  318 CONTINUE
      CALL RSEQ
  205 CONTINUE
      N=N+1
      SA=PP+TT
      SS=(3*SA)+2
      DO 319 I=1,8
      IF(I.EQ.1) GO TO 530
      IF(I.EQ.7) GO TO 530
      IF(I.EQ.8) GO TO 530
      IF(I.EQ.2) GO TO 531
      IF(I.EQ.6) GO TO 531
      NOD(N,I)=NOD(N-SA,I)+SS+GG+HH
      GO TO 319
  530 NOD(N,I)=NOD(N-SA,I)+SS
      GO TO 319
  531 NOD(N,I)=NOD(N-SA,I)+SS+2*(GG+HH)
  319 CONTINUE
      NMIS=GG+HH+PP+TT-1
      CALL RSEQ
      NN=FF-1
      SA=GG+HH+PP+TT
      SS=(3*SA)+2
      DO 206 J=1,NN
      N=N+1
      DO 3320 I=1,8
      NOD(N,I)=NOD(N-SA,I)+SS
 3320 CONTINUE
      CALL RSEQ
  206 CONTINUE
      NELEM=N
 3224 WRITE (6,103)NNP,NELEM
  103 FORMAT(5H NNP=,I5/7H NELEM=,I5)
      DO 3229 N=1,NELEM
 3229 WRITE(6,3230)N,(NOD(N,I),I=1,8)
 3230 FORMAT (1H ,11X,9I5)
      CONTINUE
      GO TO 3231
C
C     ***************************************************************
C                      READ AND PRINT CONTROL DATA
C     ***************************************************************
C
```

```
  160 WRITE(6,711) NTYPE,NDIMEN,DENS,D
      READ(5,170) NNPC,NELEMC,NPBOC,NPFS,ITGIV,GR,INDGR
  170 FORMAT(5I10,F10.0,I5)
      WRITE(6,130) NNPC,NELEMC,NPBOC,NPFS,ITGIV,GR,INDGR
  130 FORMAT(6H NNPC=,I5/8H NELEMC=,I5/7H NPBOC=,I5/6H NPFS=,
     -       I5/7H ITGIV=,I5/4H GR=,F10.4/7H INDGR=,I5)
C
C     ****************************************************************
C     READ AND/OR GENERATE CORNER POINT COORDINATES FOR NTYPE=2 MODELS
C     ****************************************************************
C
      NCC=0
  180 NCC=NCC+1
      IF (NCC .GT. NNPC) GO TO 215
      READ (5,190) N,X(N),Y(N),NPMIS
  190 FORMAT (I10,2F10.0,I10)
      WRITE (6,200) N,X(N),Y(N)
  200 FORMAT (1H+,13X,4HNODE,I4,5X,4HX = ,F8.4,5X,4HY = ,F8.4)
      NI=N
      IF (NPMIS. NE . 0) GO TO 210
      GO TO 180
  210 NCC=NCC+1
      IF (NCC .GT. NNPC) GO TO 215
      READ (5,190) N,X(N),Y(N),NPMIS
      NE=N
      NPG=(NE-NI)/2
      DX=(X(NE)-X(NI))/FLOAT(NPG)
      DY=(Y(NE)-Y(NI))/FLOAT(NPG)
      DO 214 I=1,NPG
      NG=NI+2*I
      X(NG)=X(NI)+FLOAT(I)*DX
      Y(NG)=Y(NI)+FLOAT(I)*DY
  214 WRITE (6,200) NG,X(NG),Y(NG)
      IF (NPMIS .EQ. 0) GO TO 180
      NI=N
      GO TO 210
  215 NNP=N
C
C     ****************************************************************
C     READ AND/OR GENERATE ELEMENT NODAL POINTS FOR NTYPE=2 MODELS
C     ****************************************************************
C
  219 N=0
      DO 222 M=1,NELEMC
      N=N+1
      READ (5,220) (NOD(N,I),I=1,8),NMIS
  220 FORMAT (8I5,I10)
      IF(NMIS.EQ.0) GO TO 222
      DO 221 K=1,NMIS
      N=N+1
      DO 221 J=1,8
      NOD(N,J)=NOD(N-1,J)+2
      IF (J.EQ.2.OR.J.EQ.6) NOD(N,J)=NOD(N,J)-1
  221 CONTINUE
  222 CONTINUE
      NELEM=N
      WRITE(6,225) NNP,NELEM
```

```
 225  FORMAT(1H1,10X,25HNUMBER OF NODAL POINTS....,I4//11X,
     -                25HNUMBER OF ELEMENTS.......,I4//11X,
     -                   8HELE.NO.,5X,12HNODAL POINTS//)
      DO 229 N=1,NELE
 229  WRITE (6,230) N, (NOD(N,I),I=1,8)
 230  FORMAT (1H ,11X,9I5)
      WRITE(6,444) NNP,NELEM
 444  FORMAT(5H NNP=,I5/7H NELEM=,I5)
C
C     ***********************************************************
C                  READ AND/OR GENERATE BOUNDARY VALUES
C
C     FOR THE BOUNDARY WHERE NON-ZERO NORMAL VELOCITY IS SPECIFIED,
C        THIS SECTION GENERATES THE VALUE AT EACH CORNER NODE.
C     ***********************************************************
C
3231  CONTINUE
      WRITE(6,2231)
2231  FORMAT(1H1,29HNORMAL VELOCITIES ON BOUNDARY//1H0,
     -          5HNODES,5X,15HNORMAL VELOCITY//)
      I=0
      DO 235 J=1,NPBOC
      READ(5,232) NSTART,BVAL,NBSAME,NINC
 232  FORMAT (I10,F10.0,2I10)
      DO 234 K=1,NBSAME
      I=I+1
      NPBOA(I)=NSTART+NINC*(K-1)
      NB=NPBOA(I)
      NE=NB+NINC
      BOV(I)=BVAL
      WRITE (6,233) NB,NE,BOV(I)
 233  FORMAT (1H ,I3,1H-,I3,5X,F10.4)
 234  CONTINUE
      I=I+1
      NPBOA(I)=NE
      BOV(I)=BVAL
      SPLDN=BVAL
 235  CONTINUE
      NPBO=I
      WRITE(6,630) NSTART,BVAL,NBSAME,NINC
 630  FORMAT(8H0NSTART=,I5/6H BVAL=,F10.4/8H NBSAME=,
     -       I5/6H NINC=,I5)
      WRITE(6,150) I,NPBOA(I),NPBO
 150  FORMAT(4H0I =,I5/10H NPBOA(I)=,I5/6H NPBO=,I5)
C
C     ***********************************************************
C                  INFORMATION FOR THE FREE SURFACE
C     ***********************************************************
C
      NOE=NPFS-1
      IF (NOE .LT. 0) GO TO 2000
      READ (5,236) (NPFSA(I),NPBOT(I),I=1,NPFS)
 236  FORMAT (12I5)
      IF (NOE.EQ.0) GO TO 2000
      READ (5,236) (NPFSM(I),I=1,NOE)
      WRITE (6,237) (NPFSA(I),NPFSM(I),I=1,NPFS)
 237  FORMAT (1H0///23H NODAL POINTS ON FREE SURFACE//(20I5))
```

```
      READ (5,238) SPDOW,SMAS,NELB,NELT,NELMIS,ALPHA
  238 FORMAT (2F10.0,3I10,F10.0)
      WRITE (6,239) SPDOW,SMAS
  239 FORMAT (1H1,13HMASS. F.S. SPEED=,F10.4,5X,12HTOTAL MASS =,
     -              F12.4)
      WRITE(6,180) NELB,NELT,NELMIS,ALPHA
  180 FORMAT(6H NELB=,I5/6H NELT=,I5/8H NELMIS=,
     -       I5/7H ALPHA=,F10.4)
      NELSTP=NELB-NELMIS
      NPSTP=NPFSA(NPFS)
      PI=3.14159265
      ALPHA=ALPHA*PI/180
      WRITE(6,241) NELSTP,NPSTP,ALPHA
  241 FORMAT(9H NELSTP =,I5/7H NPSTP=,I5/7H ALPHA=,F10.4)
C
C     ******************************************************************
C            COMPUTE THE MATRIX BAND WIDTH AND CHECK TO SEE IF IT
C                                EXCEEDS 29.
C     ******************************************************************
C
 2000 NCOL=1
      DO 240 N=1,NELEM
      DO 240 I=1,3
      DO 240 J=1,3
      NN=NOD(N,I)-NOD(N,J)+1
  240 IF (NCOL-NN.LT.0) NCOL=NN
      WRITE(6,729) NCOL
  729 FORMAT(1H ,6H NCOL=,I5)
      IF (NCOL .GT. 41) GO TO 4001
C
C     ******************************************************************
C                 ZERO OUT THE STIFFNESS AND LOAD MATRICES
C     ******************************************************************
C
      ITER=0
 1000 IF (ITGIV .NE. 0)   CALL CLOSE(2,1)
      DO 290 I=1,NNP
      SL(I)=0.0
      DO 290 J=1,NCOL
  290 S(I,J)=0.0
      WRITE(6,181)NCOL
  181 FORMAT(7H NCOL =,I5)
C
C     ******************************************************************
C      DEVELOP THE STIFFNESS AND LOAD MATRICES FOR ELEMENT N AND
C                     ELIMINATE THE INTERIOR POINTS
C     ******************************************************************
C
      N3=NNP+1
      WRITE(6,243) N3
  243 FORMAT(5H0N3 =,I5)
      INDEX=0
      IF (ITGIV .EQ. 0 .OR. ITER .EQ. 0) GO TO 291
      NELSTR=NELB-NELMIS+1
      WRITE(6,244) NELSTR
  244 FORMAT(9H NELSTR =,I5)
      READ (2) (SL(I),(S(I,J),J=1,NCOL),I=1,NPSTP)
```

```
                GO TO 292
      291       NELSTR=1
      292       DO 320 M=NELSTR,NELEM
                N=M
                IF (NDIMEN .EQ. 2) GO TO 293
                CALL QUADAK
                GO TO 294
      293       CALL QUAD2D
      294       DO 300 I=1,5
                IM=13-I
                IP=IM+1
                DO 300 J=1,IM
                CSL(J)=CSL(J)-CS(J,IP)*CSL(IP)/CS(IP,IP)
                DO 300 K=1,IM
      300       CS(J,K)=CS(J,K)-CS(J,IP)*CS(IP,K)/CS(IP,IP)
      C
      C         **********************************************************
      C         ADD CONTRIBUTION FROM ELEMENT N INTO TOTAL STIFFNESS MATRIX
      C         **********************************************************
      C
                DO 315 J=1,8
                NOROW=NOD(N,J)
                DO 310 K=1,8
                NOCOL=NOD(N,K)-NOROW+1
      310       IF(NOCOL.GT.0) S(NOROW,NOCOL)=S(NOROW,NOCOL)+CS(J,K)
      315       SL(NOROW)=SL(NOROW)+CSL(J)
                IF (ITGIV .EQ. 0) GO TO 320
                IF (ITER .EQ. 0 .AND. N .EQ. NELSTP) WRITE (2) (SL(K),
               -     (S(K,L),L=1,NCOL),K=1,NPSTP)
      320       CONTINUE
      C
      C         **********************************************************
      C            SOLVE FOR THE V-POTENTIAL FUNCTION AT THE NODAL POINTS
      C          WHILE VALUES FOR THE NODES ON THE FREE SURFACE ARE PROPERLY
      C                                ASSIGNED
      C         **********************************************************
      C
                IF (NDE.LT.0) GO TO 329
                PHI(1)=100.
                NPTE=NPFSA(1)
                NPBE=NPBOT(1)
                XO=X(NPTE)
                YO=Y(NPTE)
                NI=NPTE-NPBE+1
                DO 327 I=1,NI
                M=NPBE+I-1
                SL(M)=PHI(1)*10.**25
      327       S(M,1)=10.**25
                IF (NDE.EQ.0) GO TO 331
                DO 324 I=1,NDE
                K=2*I-1
                M=2*I
                J=2*I+1
                NP=NPFSA(I)
                NPF=NPFSA(I+1)
                NPM=NPFSM(I)
                DX=X(NP)-X(NPF)
```

```
      DY=Y(NPF)-Y(NP)
      DSFS=0.5*SQRT(DX*DX+DY*DY)
      IF (INDGR.EQ.2) GO TO 321
      XI=X(NP)
      XJ=X(NPM)
      QAV1=FQAVX(SPDDW,XI,XJ,X0,GR)
      PHI(M)=PHI(K)-QAV1*DSFS
      XJJ=X(NPF)
      QAV2=FQAVX(SPDDW,XJ,XJJ,X0,GR)
  324 PHI(J)=PHI(M)-QAV2*DSFS
      GO TO 322
  321 YI=Y(NP)
      YJ=Y(NPM)
      QAV1=FQAVY(SPDDW,YI,YJ,Y0,GR)
      PHI(M)=PHI(K)-QAV1*DSFS
      YJJ=Y(NPF)
      QAV2=FQAVY(SPDDW,YJ,YJJ,Y0,GR)
      PHI(J)=PHI(M)-QAV2*DSFS
  322 DO 325 I=1,NPFS
      K=2*I-1
      NR=NPFSA(I)
      SL(NR)=PHI(K)*10.**25
  325 S(NR,1)=10.**25
      DO 326 I=1,NDE
      K=2*I
      NR=NPFSM(I)
      SL(NR)=PHI(K)*10.**25
  326 S(NR,1)=10.**25
      GO TO 331
  329 S(1,1)=1.0
      SL(1)=0.0
      DO 330 I=2,NCOL
  330 S(1,I)=0.0
  331 CALL SYMSOL
C
C     ******************************************************************
C     PRINT THE VALUES OF V-POTENTIAL FCN AND CALCULATE THE VELOCITIES
C     ******************************************************************
C
      NN1=NPFSA(NPFS)
      NN2=NPBOT(NPFS)
      IF (ITER.EQ.ITGIV) NN1=1
      DO 341 I=NN1,NNP
      U(I)=0.0
      V(I)=0.0
  341 IND(I)=0
      INDEX=1
      IF (ITER.NE.ITGIV) GO TO 342
      NELB=1
      NELT=NELEM
      NELMIS=1
  342 DO 370 M=NELB,NELT,NELMIS
      N=M
      IF (NDIMEN.EQ.2) GO TO 343
      CALL QUADAX
      GO TO 344
  343 CALL QUAD2D
```

```
344   DO 353 J=1,8
      NOROW=NOD(N,J)
      CSL(J)=SL(NOROW)
      DO 353 I=9,13
353   CSL(I)=CSL(I)-CS(I,J)*CSL(J)
      DO 346 K=9,12
      KP=K+1
      DO 348 I=KP,13
      CSL(I)=CSL(I)-CS(I,K)*CSL(K)/CS(K,K)
      DO 348 J=KP,13
348   CS(I,J)=CS(I,J)-CS(I,K)*CS(K,J)/CS(K,K)
346   CONTINUE
      DO 351 J=1,5
      I=14-J
      II=J-1
      IF(II.EQ.0) GO TO 351
      DO 352 KK=1,II
      K=14-KK
352   CSL(I)=CSL(I)-CS(I,K)*CSL(K)
351   CSL(I)=CSL(I)/CS(I,I)
      DO 365 KT=1,4
      I=KT
      IF (ITER.NE.ITGIV) I=3
      N1=NOD(N,2*I-1)
      N2=NOD(N,1)
      IF (I.NE.4) N2=NOD(N,2*I+1)
      A1=X(N3)-X(N2)
      A2=X(N1)-X(N3)
      A3=X(N2)-X(N1)
      B1=Y(N2)-Y(N3)
      B2=Y(N3)-Y(N1)
      B3=Y(N1)-Y(N2)
      AN=.5*(A3*B2-A2*B3)
      N4=NOD(N,2*I)
      AI=1./AN
      I1=ND(I,1)
      I2=ND(I,2)
      I3=ND(I,3)
      I4=ND(I,4)
      I5=ND(I,5)
      I6=ND(I,6)
      F1=CSL(I1)
      F2=CSL(I2)
      F3=CSL(I3)
      F4=CSL(I4)
      F5=CSL(I5)
      F6=CSL(I6)
      UAD1=AI*(1.5*B1*F1-.5*B2*F2-.5*B3*F3+2.*B2*F4+2.*B3*F6)
      VAD1=AI*(1.5*A1*F1-.5*A2*F2-.5*A3*F3+2.*A2*F4+2.*A3*F6)
      UAD2=AI*(-.5*B1*F1+1.5*B2*F2-.5*B3*F3+2.*B1*F4+2.*B3*F5)
      VAD2=AI*(-.5*A1*F1+1.5*A2*F2-.5*A3*F3+2.*A1*F4+2.*A3*F5)
      UAD4=AI*(.5*B1*F1+.5*B2*F2+B3*(F5+F6-F4-.5*F3))
      VAD4=AI*(.5*A1*F1+.5*A2*F2+A3*(F5+F6-F4-.5*F3))
      U(N1)=U(N1)+UAD1
      V(N1)=V(N1)+VAD1
      U(N2)=U(N2)+UAD2
      V(N2)=V(N2)+VAD2
```

```
      U(N4)=U(N4)+UAD
      V(N4)=V(N4)+VAD
      IND(N1)=IND(N1)+1
      IND(N2)=IND(N2)+1
      IND(N4)=IND(N4)+1
      IF (ITER.NE.ITGIV) GO TO 370
  365 CONTINUE
  370 CONTINUE
      DO 375 I=NN1,NNP
      IF (IND(I).EQ.0) GO TO 375
      RIND=1./FLOAT(IND(I))
      U(I)=U(I)*RIND
      V(I)=V(I)*RIND
  375 CONTINUE
      IF (ITER.NE.ITGIV) GO TO 500
      WRITE (6,380)
  380 FORMAT (1H0,4HNODE,3X,12HX COORDINATE,3X,12HY COORDINATE,
     -       5X,11HV-POTENTIAL,5X,10HX-VELOCITY,
     -     5X,10HY-VELOCITY,5X,11HTOTAL VELO.,
     -       4X,11HPRES. COFF./)
      DO 390 I=1,NNP
      VEL=SQRT(U(I)*U(I)+V(I)*V(I))
      IF (GR.NE.0) GO TO 404
      CP=1.-(VEL/SPDDW)**2
      PRG=CP*0.5*DENS*(SPDDW**2)
      WRITE(6,1112) PRG
 1112 FORMAT(1H F10.4)
  390 WRITE (6,400) I,X(I),Y(I),SL(I),U(I),V(I),VEL,CP
  400 FORMAT (1H ,I4,2F15.4,5X,F11.4,4F15.4)
      GO TO 405
  404 WRITE (6,400) I,X(I),Y(I),SL(I),U(I),V(I),VEL
  405 GO TO 4000
  500 WRITE (6,501)
  501 FORMAT (1H0,4HNODE,3X,12HX COORDINATE,3X,12HY COORDINATE,
     -         5X,11HV-POTENTIAL,5X,10HX-VELOCITY,
     -      5X,10HY-VELOCITY,5X,10HTOTAL VEL.,
     -        5X,10HTOTAL HEAD/)
      DO 510 J=1,NPFS
      K=NPFS-J+1
      I=NPFSA(K)
      VEL=SQRT(U(I)*U(I)+V(I)*V(I))
      IF (GR.EQ.0.0) GO TO 512
      IF (INDGR.EQ.0) THEAD=X0-X(I)+0.5*VEL*VEL/GR
      IF (INDGR.EQ.2) THEAD=Y(I)-Y0+0.5*VEL*VEL/GR
      GO TO 513
  512 WRITE (6,400) I,X(I),Y(I),SL(I),U(I),V(I),VEL
      GO TO 510
  513 WRITE (6,400) I,X(I),Y(I),SL(I),U(I),V(I),VEL,THEAD
  510 CONTINUE
C
C     ***************************************************************
C           ADJUST THE CORNER NODES ON THE FREE SURFACE
C     ***************************************************************
C
      ITER=ITER+1
      WRITE (6,610) ITER
  610 FORMAT (1H1,21HADJUSTED FREE SURFACE,5X,11HITERATION =,I3/)
```

```
      CALL YFSSL
      IF (NOLDEN.EQ.2) GO TO 615
      RDW=Y(NPTE)-Y(NPBE)
      AREADW=PI*RDW*RDW
      SPDDW=SMAS/AREADW
      RORF=Y(NN1)-Y(NN2)
      CCOLD=CCNEW
      CCNEW=(RDW/RORF)**2
      GO TO 616
 615  SPDDW=SMAS/(Y(NPTE)-Y(NPBE))
      CCOLD=CCNEW
      WRITE(6,617) NN1,Y(NN1)
 617  FORMAT(1H ,I5,1F10.6)
      CCNEW=(Y(NPTE)-Y(NPBE))/(Y(NN1)-Y(NN2))
 616  WRITE (6,620) SPDDW,CCNEW
 620  FORMAT (1H0,17HDOWNSTREAM SPEED=,F9.4,8X,
     -        20HCONTRACTION COEFF. =,F7.4/)
      CCERR=ABS(CCNEW-CCOLD)
      WRITE(6,640) CCERR
 640  FORMAT(8H0CCERR=,F12.6)
      IF (CCERR.LT.0.00005)  ITGIV=ITER
      GO TO 1000
4000  CONTINUE
4001  STOP
      END
C
C     ******************************************************************
C                               BLOCK DATA
C     ******************************************************************
C
      BLOCK DATA
C     IMPLICIT DOUBLE PRECISION (A-H,O-Z)
      COMMON /G/ CSL(13),CS(13,13),NPBO,NPBOA(100),BOV(100),ND(4,6)
      DATA ND/1,3,5,7,3,5,7,1,4*13,2,4,6,8,10,11,12,9,9,10,11,12/
      END
C
C     ******************************************************************
C          SUBROUTINE TO DETERMINE THE CENTER OF ELEMENT N
C     ******************************************************************
C
      SUBROUTINE CENTER
C     IMPLICIT DOUBLE PRECISION (A-H,O-Z)
      COMMON N,NOD(300,8),X(1000),Y(1000),N1,N2,N3,AN,INDEX,T(6,6),
     -       I,SL3,NI,NMIS
      M1=NOD(N,1)
      M2=NOD(N,3)
      M3=NOD(N,5)
      M4=NOD(N,7)
      X(N3)=0.25*(X(M1)+X(M2)+X(M3)+X(M4))
      Y(N3)=0.25*(Y(M1)+Y(M2)+Y(M3)+Y(M4))
      RETURN
      END
C
C     ******************************************************************
C     SUBROUTINE TO DEVELOP ELEMENT MATRICES FOR AXISYMMETRIC FLOW
C     ******************************************************************
C
```

```
      SUBROUTINE QUADAX
C     IMPLICIT DOUBLE PRECISION (A-H,O-Z)
      COMMON N,NOD(300,8),X(1000),Y(1000),N1,N2,N3,AN,INDEX,T(6,6),
     - I,SL3,NI,NMIS
      COMMON /G/ CSL(13),CS(13,13),NPBO,NPBOA(100),BOV(100),ND(4,6)
      DO 100 J=1,13
      CSL(J)=0.0
      DO 100 K=1,13
  100 CS(J,K)=0.0
      CALL CENTER
      DO 200 KT=1,4
      I=KT
      CALL TMATAX
      DO 200 J=1,6
      NR=ND(KT,J)
      IF (INDEX.EQ.1) GO TO 190
      IF (J.NE.1) GO TO 190
      DO 150 KR=1,NPBO
      K=NPBO+1-KR
      IF (N1.NE.NPBOA(K)) GO TO 150
      DO 160 JR=1,NPBO
      JJ=NPBO+1-JR
      IF (N2.NE.NPBOA(JJ)) GO TO 160
      DSL=SL3*BOV(K)/6.
      CSL(NR)=CSL(NR)+DSL*Y(N1)
      NRF=ND(KT,4)
      CSL(NRF)=CSL(NRF)+2.*DSL*(Y(N1)+Y(N2))
      NRFF=ND(KT,2)
      CSL(NRFF)=CSL(NRFF)+DSL*Y(N2)
      GO TO 190
  160 CONTINUE
  150 CONTINUE
  190 DO 200 K=1,6
      NC=ND(KT,K)
  200 CS(NR,NC)=CS(NR,NC)+T(J,K)
      RETURN
      END
C
C     ****************************************************************
C         SUBROUTINE TO DETERMINE THE GEOMETRIC PROPERTIES OF A
C               TRIANGULAR SUB-ELEMENT FOR AXISYMMETRIC FLOW
C     ****************************************************************
C
      SUBROUTINE TMATAX
C     IMPLICIT DOUBLE PRECICION (A-H,O-Z)
      COMMON N,NOD(300,8),X(1000),Y(1000),N1,N2,N3,AN,INDEX,T(6,6),I,
     -          SL3,NI,NMIS
      N1=NOD(N,2*I-1)
      N2=NOD(N,1)
      IF (I.NE.4) N2=NOD(N,2*I+1)
      N4=NOD(N,2*I)
      X(N4)=0.5*(X(N1)+X(N2))
      Y(N4)=0.5*(Y(N1)+Y(N2))
      A1=X(N3)-X(N2)
      A2=X(N1)-X(N3)
      A3=X(N2)-X(N1)
      B1=Y(N2)-Y(N3)
```

```
      B2=Y(N3)-Y(N1)
      B3=Y(N1)-Y(N2)
      AN=.5*(A3*B2-A2*B3)
      R1=Y(N1)
      R2=Y(N2)
      R3=Y(N3)
      S11=A1*A1+B1*B1
      S12=A1*A2+B1*B2
      S13=A1*A3+B1*B3
      S22=A2*A2+B2*B2
      S23=A2*A3+B2*B3
      S33=A3*A3+B3*B3
      S33=SQRT(S33)
      R311=3.*R1+R2+R3
      R131=R1+3.*R2+R3
      R113=R1+R2+3.*R3
      R221=2.*(R1+R2)+R3
      R212=2.*(R1+R3)+R2
      R122=2.*(R2+R3)+R1
      T(1,1)=3.*S11*R311
      T(2,2)=3.*S22*R131
      T(3,3)=3.*S33*R113
      T(1,2)=-S12*R221
      T(1,3)=-S13*R212
      T(2,3)=-S23*R122
      R321=4.*R1-2.*R2-R3
      R312=3.*R1-R2-2.*R3
      R433=14.*R1+3.*(R2+R3)
      T(1,4)=S11*R321+S12*R433
      T(1,5)=S12*R312+S13*R321
      T(1,6)=S11*R312+S13*R433
      R343=14.*R2+3.*(R1+R3)
      R231=-2.*R1+3.*R2-R3
      R132=-R1+3.*R2-2.*R3
      T(2,4)=S12*R3+3+S22*R231
      T(2,5)=S22*R132+S23*R343
      T(2,6)=S12*R132+S23*R231
      R123=-R1-2.*R2+3.*R3
      R213=-2.*R1-R2+3.*R3
      R334=3.*(R1+R2)+14.*R3
      T(3,4)=S13*R123+S23*R213
      T(3,5)=S23*R334+S33*R123
      T(3,6)=S13*R334+S33*R213
      T(4,4)=8.*(S11*R131+S12*R221+S22*R311)
      T(5,5)=8.*(S22*R113+S23*R122+S33*R131)
      T(6,6)=8.*(S11*R113+S13*R212+S33*R311)
      T(4,5)=8.*S13*R131-4.*(S12*R1+S22*R2+S23*R3)
      T(4,6)=8.*S23*R311-4.*(S11*R1+S12*R2+S13*R3)
      T(5,6)=8.*S12*R113-4.*(S13*R1+S23*R2+S33*R3)
      DO 100 J=1,5
      JJ=J+1
      DO 100 K=JJ,6
  100 T(K,J)=T(J,K)
      A60=1./(60.*AN)
      DO 110 J=1,6
      DO 110 K=1,6
      T(J,K)=T(J,K)*A60
```

```
  110 CONTINUE
      RETURN
      END
C
C     ******************************************************************
C          SUBROUTINE TO DEVELOP ELEMENT MATRICES FOR 2-D FLOW
C     ******************************************************************
C
      SUBROUTINE QUAD2D
      IMPLICIT DOUBLE PRECISION (A-H,O-Z)
C
      COMMON NN,NOD(300,8),X(1000),Y(1000),N1,N2,N3,AN,INDEX,T(6,6),I,
     -         SL3,NI,NMIS
      COMMON /B/ CSL(13),CS(13,13),NPBO,NPBOA(100),BOV(100),ND(4,6)
      DO 100 J=1,13
      CSL(J)=0.0
      DO 100 K=1,13
      CS(J,K)=0.0
  100 CONTINUE
      CALL CENTER
      DO 200 KT=1,4
      I=KT
      CALL TMAT2D
      DO 200 J=1,6
      NR=ND(KT,J)
      IF (INDEX.EQ.1) GO TO 190
      IF (J.NE.1) GO TO 190
      DO 150 KR=1,NPBO
      K=NPBO+1-KR
      IF (N1.NE.NPBOA(K)) GO TO 150
      DO 160 JR=1,NPBO
      JJ=NPBO+1-JR
      IF (N2.NE.NPBOA(JJ)) GO TO 160
      DSL=SL3*BOV(K)/6.
      CSL(NR)=CSL(NR)+DSL
      NRF=ND(KT,4)
      CSL(NRF)=CSL(NRF)+4.*DSL
      NRFF=ND(KT,2)
      CSL(NRFF)=CSL(NRFF)+DSL
      GO TO 190
  160 CONTINUE
  150 CONTINUE
  190 DO 200 K=1,6
      NC=ND(KT,K)
      CS(NR,NC)=CS(NR,NC)+T(J,K)
  200 CONTINUE
      RETURN
      END
C
C     ******************************************************************
C        SUBROUTINE TO DETERMINE THE GEOMETRIC PROPERTIES OF A
C                TRIANGULAR SUB-ELEMENT FOR 2-D FLOW
C     ******************************************************************
C
      SUBROUTINE TMAT2D
      IMPLICIT DOUBLE PRECISION (A-H,O-Z)
C
      COMMON NN,NOD(300,8),X(1000),Y(1000),N1,N2,N3,AN,INDEX,T(6,6),I,
     -         SL3,NI,NMIS
```

```
      N1=MOD(N,2*I-1)
      N2=MOD(N,I)
      IF (I.NE.4) N2=MOD(N,2*I+1)
      N4=MOD(N,2*I)
      X(N4)=0.5*(X(N1)+X(N2))
      Y(N4)=0.5*(Y(N1)+Y(N2))
      A1=X(N3)-X(N2)
      A2=X(N1)-X(N3)
      A3=X(N2)-X(N1)
      B1=Y(N2)-Y(N3)
      B2=Y(N3)-Y(N1)
      B3=Y(N1)-Y(N2)
      AN=.5*(A3*B2-A2*B3)
      SL1=SQRT(A1*A1+B1*B1)
      SL2=SQRT(A2*A2+B2*B2)
      SL3=SQRT(A3*A3+B3*B3)
      T(1,1)=3.*SL1*SL1
      T(1,2)=-(A1*A2+B1*B2)
      T(1,3)=-(A1*A3+B1*B3)
      T(1,4)=4.*(A1*A2+B1*B2)
      T(1,5)=0.
      T(1,6)=4.*(A1*A3+B1*B3)
      T(2,2)=3.*SL2*SL2
      T(2,3)=-(A2*A3+B2*B3)
      T(2,4)=T(1,4)
      T(2,5)=4.*(A2*A3+B2*B3)
      T(2,6)=0.
      T(3,3)=3.*SL3*SL3
      T(3,4)=0.
      T(3,5)=T(2,5)
      T(3,6)=T(1,6)
      T(4,4)=8.*(SL3*SL3-A1*A2-B1*B2)
      T(4,5)=8.*(A1*A3+B1*B3)
      T(4,6)=8.*(A2*A3+B2*B3)
      T(5,5)=T(4,4)
      T(5,6)=8.*(A1*A2+B1*B2)
      T(6,6)=T(4,4)
      DO 100 J=1,5
      JJ=J+1
      DO 100 K=JJ,6
100   T(K,J)=T(J,K)
      A12=1./(12.*AN)
      DO 110 J=1,6
      DO 110 K=1,6
      T(J,K)=T(J,K)*A12
110   CONTINUE
      RETURN
      END
C
C     ***************************************************************
C     SUBROUTINE TO SOLVE A SET OF LINEAR ALGEBRAIC SIMULTANEOUS
C     EQUATIONS WITH A COEFFICIENT MATRIX WHICH IS BOTH SYMMETRIC
C                        AND IN BAND FORM.
C     ***************************************************************
C
      SUBROUTINE SYMSOL
      IMPLICIT DOUBLE PRECISION (A-H,O-Z)
```

```
      COMMON /SYMS/ SL(1000),S(1000,41),NROW,NCOL
      DIMENSION ST(1000)
      WRITE(6,700)NROW,NCOL,NOE
  700 FORMAT(1H ,20X,3I10)
      N=0
  100 N=N+1
C     ******************************
C          REDUCE PIVOT EQUATION
C     ******************************
      SL(N)=SL(N)/S(N,1)
      IF (N-NROW) 150,300, 150
  150 DO 200 K=2,NCOL
      ST(K)=S(N,K)
  200 S(N,K)=S(N,K)/S(N,1)
C     *************************************
C     REDUCE REMAINING EQUATIONS WITHIN SPAN
C     *************************************
      DO 260 L=2,NCOL
      I=N+L-1
      IF (NROW -I) 260,240,240
  240 J=0
      DO 250 K=L,NCOL
      J=J+1
  250 S(I,J)=S(I,J)-ST(L)*S(N,K)
      SL(I)=SL(I)-ST(L)*SL(N)
  260 CONTINUE
      GO TO 100
C     *****************
C     BACK SUBSTITUTION
C     *****************
  300 N=N-1
      IF (N) 350,500,350
  350 DO 400 K=2,NCOL
      L=N+K-1
      IF (NROW-L) 400,370,370
  370 SL(N)=SL(N)-S(N,K)*SL(L)
  400 CONTINUE
      GO TO 300
  500 RETURN
      END
C
C     ***************************************************************
C          THIS SUBROUTINE ADJUSTS THE FREE SURFACE LOCATION
C             BY ELIMINATING NORMAL VELOCITY COMPONENT
C     ***************************************************************
C
      SUBROUTINE YFSSL
      IMPLICIT DOUBLE PRECISION (A-H,O-Z)
      COMMON N,NOD(300,8),X(1000),Y(1000),N1,N2,N3,AN,INDEX,T(6,6),I,
     -       SL3,NI,NMIS
      COMMON /FSS/ U(1000),V(1000),NPFSA(25),NPBOT(25),NPFSM(24),NPFS
     -       ALPHA
      DYT=0.0
      NM1=NPFSA(NPFS)
      NOE=NPFS-1
      DO 100 K=1,NOE
      J=NPFS-K
```

```
      II=J+1
      NPR=NPFSA(II)
      NPF=NPFSA(J)
      NPM=NPFSM(J)
      IF (K.NE.1) GO TO 120
      WRITE(6,150) SLP1,ALPHA
      SLP1=0.0-TAN(ALPHA)
      WRITE(6,150) SLP1,ALPHA
  150 FORMAT(//1H ,2F15.10)
      SLP2=U(NPM)/V(NPM)
      SLP3=U(NPF)/V(NPF)
      DXM=2.*(X(NPF)-X(NPR))
      DYT=DXM/(SLP1+4.*SLP2+SLP3)
      GO TO 130
  120 SLP1=V(NPR)/U(NPR)
      SLP2=V(NPM)/U(NPM)
      SLP3=V(NPF)/U(NPF)
      DXM=(X(NPF)-X(NPR))/6.
      DYT=DYT+DXM*(SLP1+4.*SLP2+SLP3)
  130 DYNET=Y(NN1)+DYT-Y(NPF)
      NPFB=NPBOT(J)
      NI=(NPF-NPFB)/2
      DO 110 L=1,NI
      M=NPFB+2*L
      RATIO=(Y(M)-Y(NPFB))/(Y(NPF)-Y(NPFB))
  110 Y(M)=Y(M)+DYNET*RATIO
  100 WRITE (6,200) NPF,X(NPF),Y(NPF)
  200 FORMAT (1H ,5HNODE=,I3,5X,3HX =,F8.4,5X,3HY =,F8.4)
      RETURN
      END
C
C     ****************************************************************
C                  NODE CO-ORDINATE AUTOMATIC GENERATION
C     ****************************************************************
C
      SUBROUTINE RSEQ
C     IMPLICIT DOUBLE PRECISION (A-H,O-Z)
      COMMON N,NOD(300,8),X(1000),Y(1000),N1,N2,N3,AN,INDEX,
     -       T(6,6),I,SL3,NI,NMIS
      DO 221 K=1,NMIS
      N=N+1
      DO 221 J=1,8
      NOD(N,J)=NOD(N-1,J)+2
      IF (J.EQ.2.OR.J.EQ.6) NOD(N,J)=NOD(N,J)-1
  221 CONTINUE
      RETURN
      END
C
C     ****************************************************************
C                  ELEMENT NUMBER AUTOMATIC GENERATION
C     ****************************************************************
C
      SUBROUTINE RNUM
C     IMPLICIT DOUBLE PRECISION (A-H,O-Z)
      COMMON N,NOD(300,8),X(1000),Y(1000),N1,N2,N3,AN,INDEX,
     -       T(6,6),I,SL3,NI,NMIS
      NE=N
```

```
      NPG=(N2-N1)/2
      DX=(X(N2)-X(N1))/FLOAT(NPG)
      DY=(Y(N2)-Y(N1))/FLOAT(NPG)
      DO 214 I=1,NPG
      NG=NT+I
      X(NG)=X(N1)+FLOAT(I)*DX
      Y(NG)=Y(N1)+FLOAT(I)*DY
  214 WRITE(6,200) NG,X(NG),Y(NG)
  200 FORMAT(1H ,I3,6HNODE,I4,5X,4HX = ,F10.6,5X,4HY = ,F10.6)
      RETURN
      END
```

REFERENCES

1. WAMBSGANSS, M.W. — PhD THESIS, Purdue University, 1966. Mathematical Modelling and Design Evaluation of High-Speed Reciprocating Compressors.

2. MacLAREN, J.F.T. and KERR, S.V. — An Analytical and Experimental Study of Self-Acting Valves in a Reciprocating Air Compressor. Proc. Inst. Mech. Engs., 1969-70.

3. CHAN, S.T.K. and LAROCK, B.E. — Fluid Flows From Axisymmetric Orifices and Valves. Journal Hydraulics Division, Proc. A.S.C.E., Jan 1973.

4. JEPPSON, R.W. — Numerical Solutions to Free Surface Axisymmetric Flows. Journal Eng. Mech. Div. Proc. A.S.C.E., Feb 1969.

5. SOUTHWELL, R.V. and VAISEY, G. — Relaxation Methods Applied to Engineering Problems. XII Fluid Motions Characterised by 'Free' stream-lines. Phil. Trans. Roy. Soc. London, Ser. A., Vol. 240, 1948, p 117-161.

6. ROUSE, H. and FETOUH, A. — Characteristics of Irrotational Flow Through Axially Symmetric Orifices. Journal of Applied Mechanics, Vol. 17, No. 4, 1950, p 421-426.

7. VON-MISES — Rouse, H. (ed.) Engineering Hydraulics. John Wiley and Sons Inc., New York, 1950, p 32-36.

8. HUNT, B.W. — Numerical Solution of An Integral Equation for Flow From A Circular Orifice. Journal of Fluid Mechanics, Vol. 31, part 2, 1968, p 361-377.

9. LAROCK, B.E. — Jets from Two-Dimensional Symmetric Nozzles of Arbitrary Shape. Journal of Fluid Mechanics, Vol. 37, part 3, 1969, p 479-489.

10. GARABEDIAN, P. — Calculation of Axially Symmetric Cavities and Jets. Pacific Journal Maths, Vol. 6, 1956, p 611-684.

11./

11. TREFFTZ, E. — Uber die Kontraktion Kreisformiger Flussigkeits-Stahlen. Z. Math. Phys., Vol. 64, 1917, p 34.

12. WILSON, E.L. and NICKELL, R.E. — Applications of the Finite Element Method to Heat Conduction Analysis. Nuclear Eng. and Design, Vol. 4, 1966, p 276.

13. MARTIN, H.C. — Finite Element Analysis of Fluid Flows. Proceedings, 2nd Conference on Matrix Methods in Structural Mechanics, Ohio, Oct 1968.

14. VALLENTINE, H.R. — Applied Hydrodynamics. 2nd Edition, Plenum Press, New York, 1967, p 87-93.

15. PRANDTL, L. — Essentials of Fluid Dynamics. Blackie, 1952.

16. BINDER, R.C. — Fluid Mechanics. 3rd Edition, Prentice Hall, 1955.

17. ROBERTSON, J.M. — Hydrodynamics in Theory and Application. Englewood Cliffs, Prentice Hall, N.J., 1965, p 55-56.

18. MILNE-THOMSON, L.M. — Theoretical Hydrodynamics. 4th Edition, The MacMillan Co., New York, 1960, p 92-93.

19. WANG, C.T. — Energy Principles and Variational Methods. Chp. 7 of Applied Elasticity, McGraw-Hill Book Co., 1953, p 144-170.

20. LANGHAAR, H.L. — Energy Methods in Applied Mechanics. John Wiley & Sons Inc., 1962.

21. SOKOLNIKOFF, I.S. — Variational Methods. Chp. 7 of Mathematical Theory of Elasticity, 2nd Edition, McGraw-Hill, 1956, p 377-465.

22. GARABEDIAN, P.R. and SPENCER, D.C. — Extremal Methods in Cavitational Flow. Jour. of Rational Mechanics and Analysis, Vol. 1, 1952, p 359-411.

23. WHALEN, P.J. — Survey of Variational Methods in Fluid Mechanics. Aero. Tech. Component Fundamentals Memo. ATFM 67-07, GEC, March 1967.

24. DELLEUR, J. and SOOKY, A. — Variational Methods in Fluid Dynamics. Jour. of Eng. Mech. Division, A.S.C.E., Vol. 87, No. EM6, Dec. 1961, p 57-77.

25. ECKART, C. — Variational Principles of Hydrodynamics. Physics of Fluid Journal, May - June, 1960.

26. BATEMAN, H. — Proc. Nat. Acad. Sci., Vol. 16, p 816.

27. LEMIEUX, P.F., UNNY, T.E. and DUBEY, R.N. — Variational Principles in Fluid Dynamics. Jour. of Eng. Mechanics Div., A.S.C.E., Vol. 96, No. EM6, Dec. 1970, p 1031-1037.

28. COURANT, R. and HILBERT, D. — The Calculus of Variations. Methods of Mathematical Physics, Vol. 1, Wiley-Interscience, New York, 1953, p 164-274.

29. HILDEBRAND, F.B. — Methods of Applied Mathematics. Prentice Hall, Englewood Cliffs, N.J., 1965.

30. TURNER, M.J., CLOUGH, R.W., MARTIN, H.C. and TOPP, L.I. — Stiffness and Deflection Analysis of Complex Structures. Jour. Aeronaut. Sci. 23, 1956, p 805-823.

31. ZIENKIEWICZ, O.C. and CHEUNG, Y.K. — The Finite Element Method in Structural and Continuum Mechanics. McGraw-Hill, London, 1967.

32. ZIENKIEWICZ, O.C. and CHEUNG, Y.K. — Finite Elements in the Solution of Field Problems. "The Engineer", London, 24th Sept., 1965, p 507-510.

33. ZIENKIEWICZ, O.C., MAYER, P. and CHEUNG, Y.K. — Solution of Anisotropic Seepage by Finite Elements. Jour. of Engineering Mech. Div., A.S.C.E., Vol. 92, No. EM1, Feb. 1966, p 111-120.

34. FINN, W.D.L. — Finite Element Analysis of Seepage Through Dams. Jour. of Soil Mechanics and Foundation Div., A.S.C.E., Vol. 93, No. SM6, Nov. 1967, p 41-48.

35. BROWN, J. and LOUGH, A. — An Experimental Investigation Into the Response of Disc Valves to Rapid Pressure Changes. Purdue Compressor Technology Conference, Purdue University, USA, July 1972.

36. BROWN, J., DAVIDSON, R. and HALLAM, W.W. — Dynamic Measurement of Valve Lift Force. Purdue Compressor Technology Conference, USA, 1976.

37. HUEBNER, K.H. — The Finite Element Method for Engineers. John Wiley & Sons, 1975.

38. SILVESTER, P. — Higher Order Polynomial Triangular Finite Elements for Potential Problem. Int. J. Eng. Sci., Vol. 7, No. 8, p 849-861.

39. PIAN, T.H.H. — Derivation of Element Stiffness Matrices. AAIA Journal, Vol. 2, 1964, p 576-577.

40. ODEN, J.T. and SOMOGYI, D. — Finite Element Applications in Fluid Dynamics. Jour. of Engineering Mechanics Div., A.S.C.E., Vol. 95, No. EM3, June 1969, p 821-826.

41. ODEN, J.T. — Finite Element Analogue of Navier-Stokes Equations. J. of Engineering Mech. Div., A.S.C.E., No. EM4, Aug 1970, p 529-534.

42. MacLAREN, J.F.T. — A Review of Simple Mathematical Models of Valves in Reciprocating Compressors. Purdue University, Compressor Technology Conference, July 1972.

43. LAROCK, B.E. — Gravity-Affected Flow From Planer Sluice Gates. Jour. of Hydraulics Div., Proceedings A.S.C.E., No. HY4, July 1969, p 1211-1226.

44. MASON, W.E. and HERMANN, L.R. — Elastic Analysis of Irregular Shaped Prismatic Beams by the Method of Finite Elements. TR No. 67-1, U.C. Davis, July 1967, p 37-39.

45. SCHRENK, I.E. — Disc Valves; Flow Patterns, Resistance and Loading. Abbreviated Translation, The Britch Hydromechanics Research Assoc., Publ. No. T547, Jan 1957.

46. MOON and SPENCER — Field Theory for Engineers.

47. FELIPPA, C.A. and CLOUGH, R.W. — The Finite Element Method in Solid Mechanics. SIAM-AMS Proc., Vol. 2, American Mathematical Society, Providence, R.I., 1970, p 210-252.

48. HALLAM, W.W. — Finite Element Analysis of Fluid Flow Using Variational Approach. Purdue Compressor Technology Conference, USA, 1978.

49. BROWN, J., DAVIDSON, R. and FLEMING, J.S. — The Dynamic Performance of Automatic Compressor Valves. 15th International Conference of Refrigeration, Sept. 1979.

LIST OF FIGURES

FIG. NO.

FIG. NO.

LIST OF GRAPHS

GRAPH NO

LIST OF TABLES

TABLE NO.

PHOTOGRAPHS

1. Experimental Test Rig.

2. Acceleration Effects (Compensated/Uncompensated).

3. Acceleration Effects (Time Response).

4. Plenum Chamber.

5. Valve Assembly.

6. "No-Air" Test Responses.

7. Lift-Off Mechanism.

8. Typical Static Test Responses.

9. Typical Dynamic Test Responses.

10. Back-Off Response.

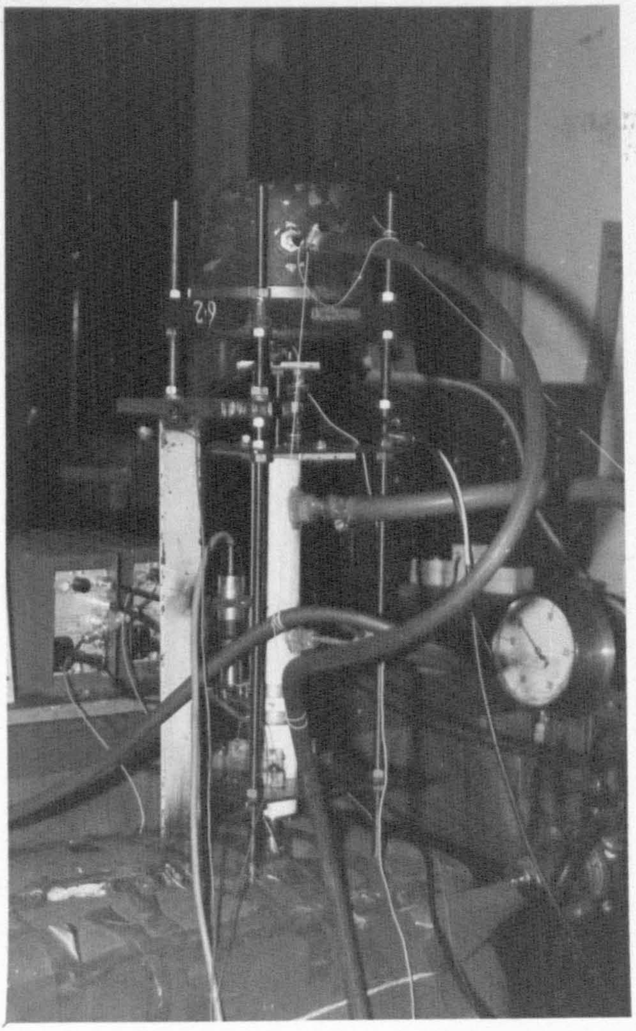

FIGURE 1 EXPERIMENTAL TEST RIG

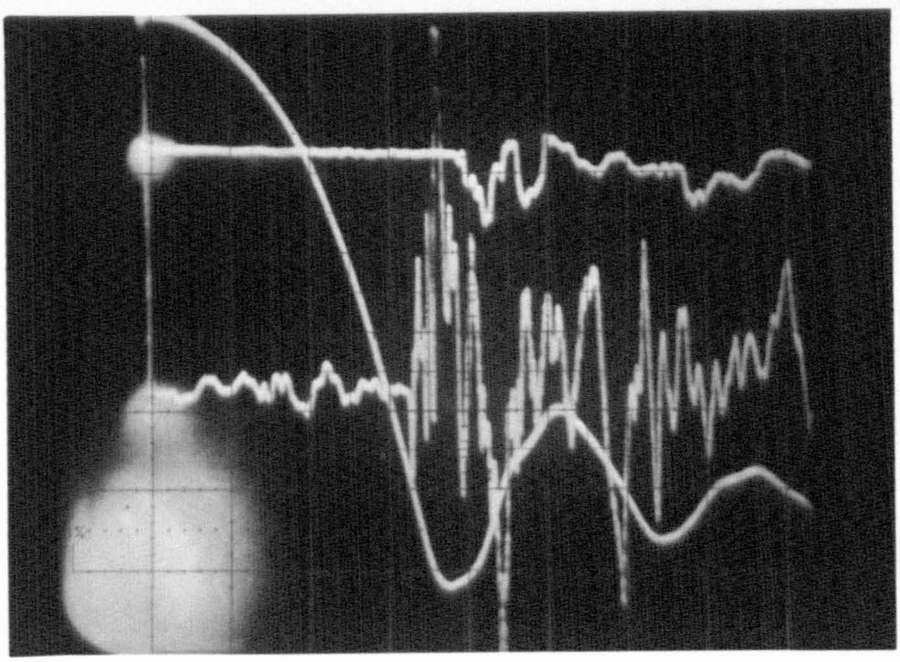

COMPENSATED

UNCOMPENSATED

DISPLACEMENT

FIGURE 2 ACCELERATION EFFECTS (COMPENSATED/UNCOMPENSATED)

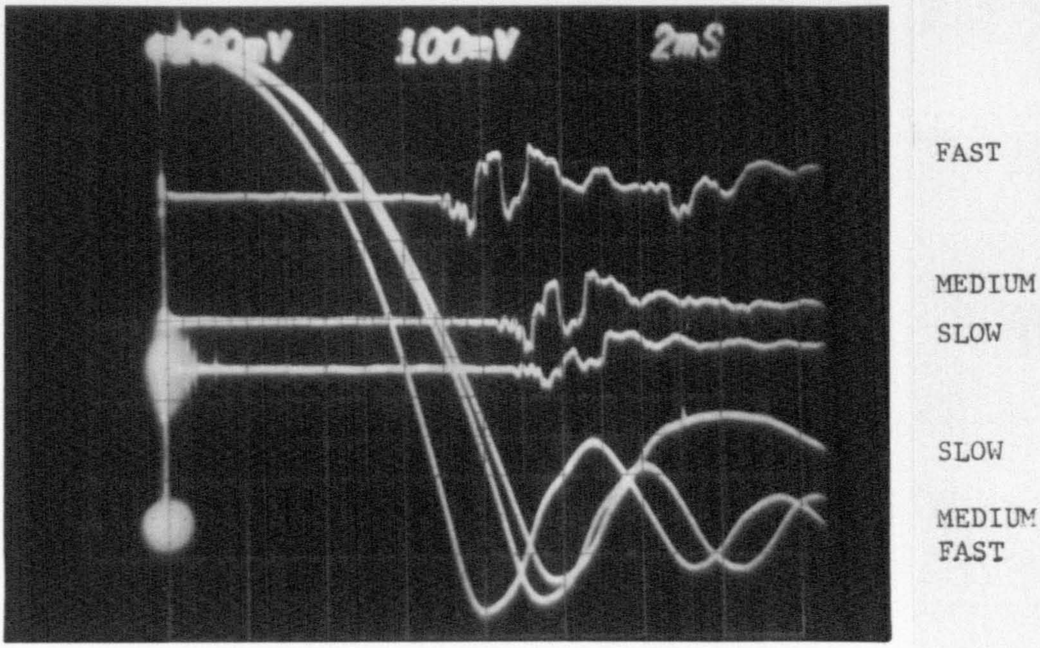

FIGURE 3 ACCELERATION EFFECTS (TIME RESPONSE)

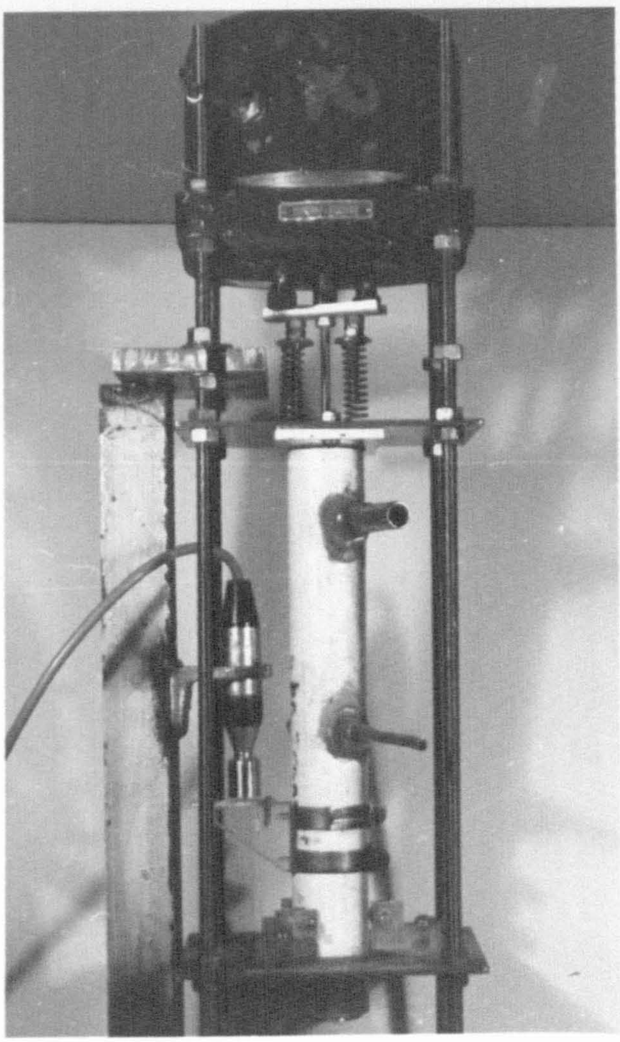

FIGURE 4 PLENUM CHAMBER

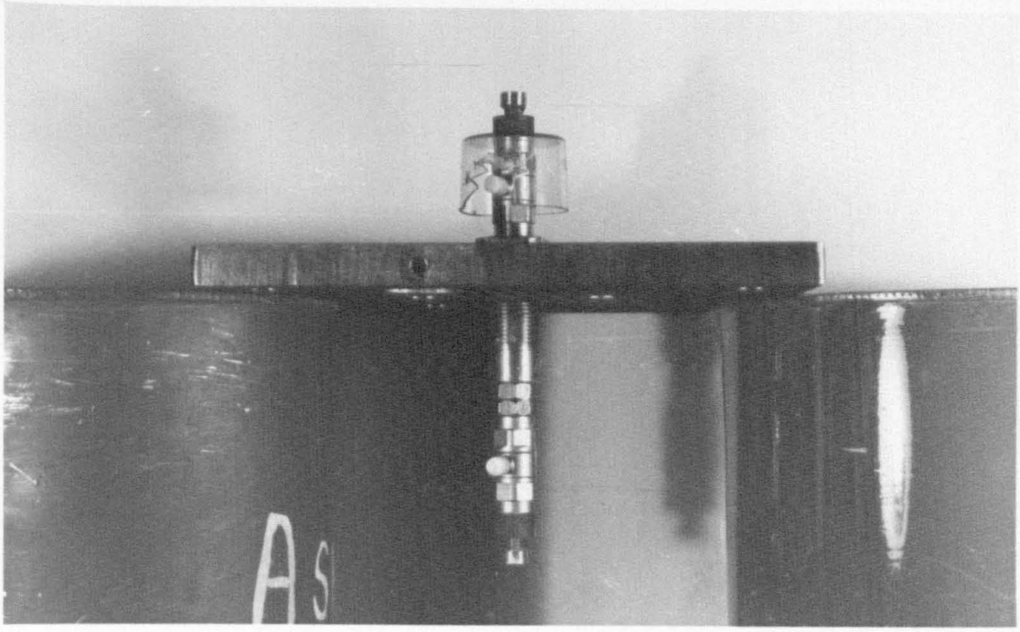

FIGURE 5 VALVE ASSEMBLY

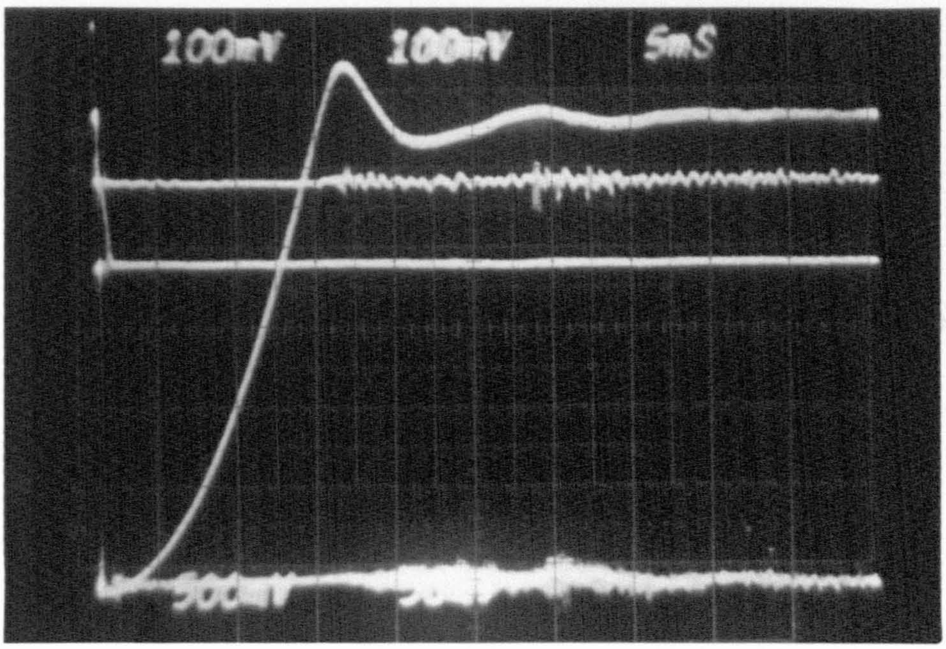

FIGURE 6 "NO-AIR" TEST RESPONSES

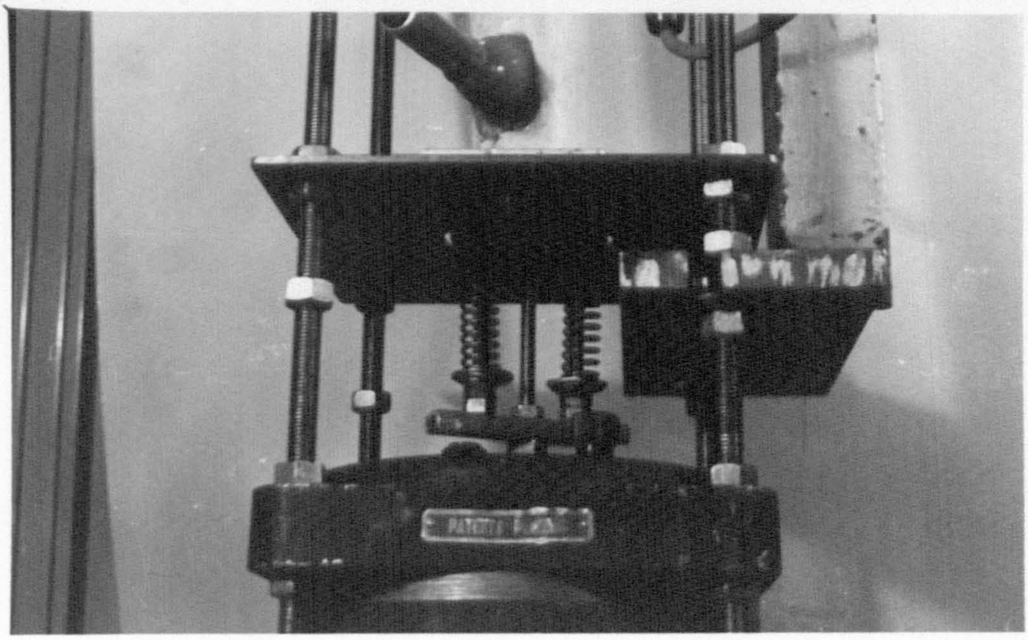

FIGURE 7 LIFT-OFF MECHANISM

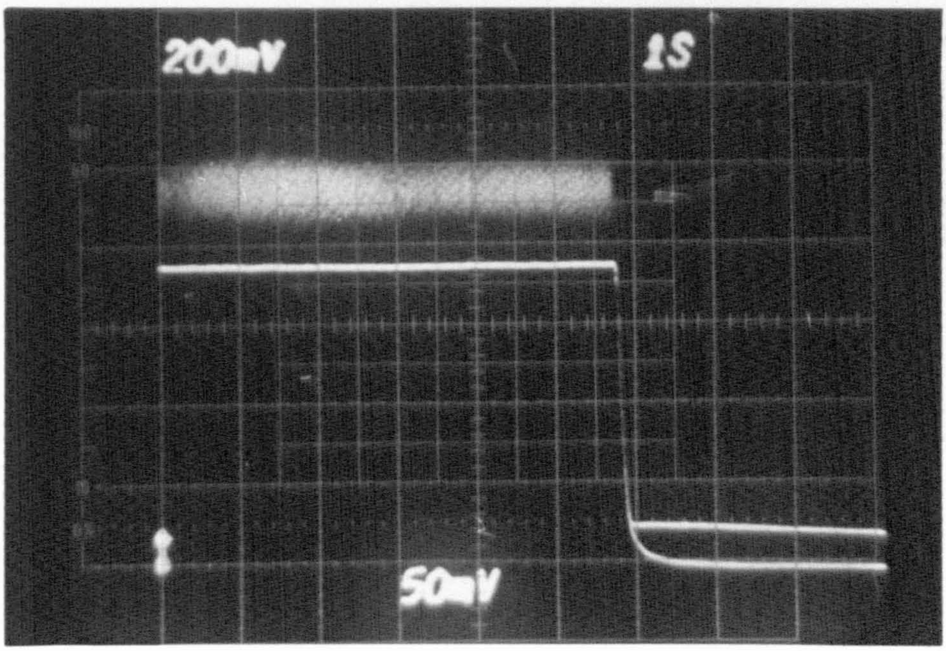

FIGURE 8 TYPICAL STATIC TEST RESPONSES

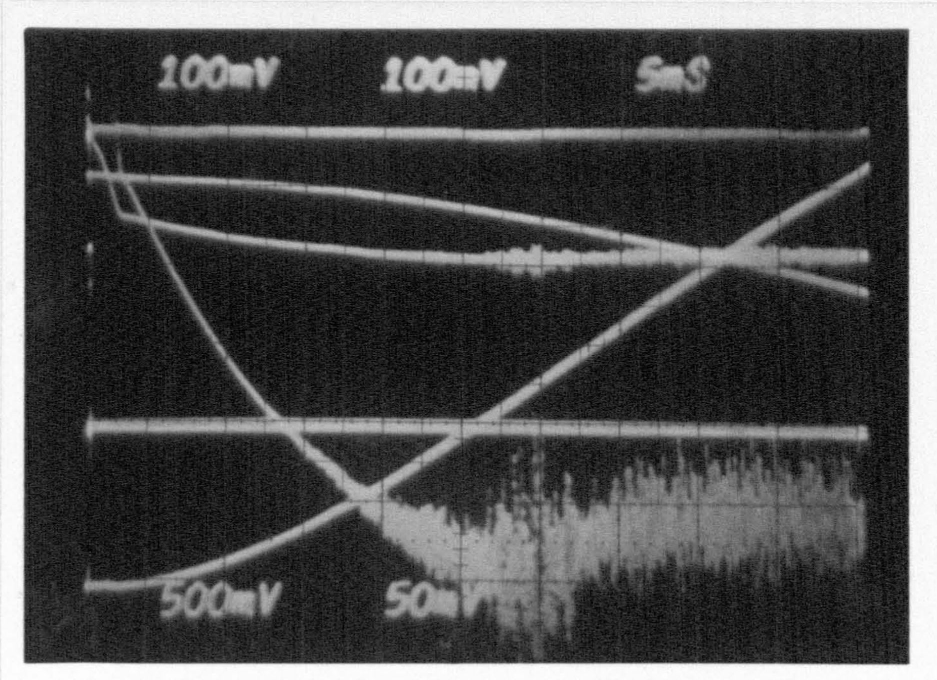

FIGURE 9 TYPICAL DYNAMIC TEST RESPONSES

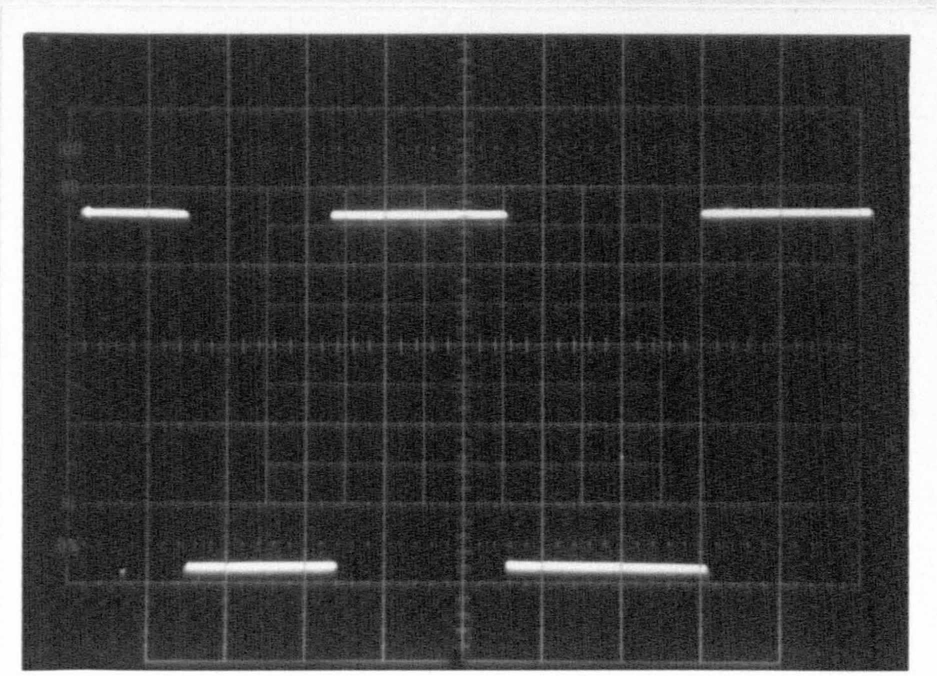

FIGURE 10 BACK-OFF RESPONSE

ACKNOWLEDGEMENTS

I wish to express my gratitude to the following: Professor W.B. McHutchison, BSc, ARCST, WhSch, MIEE, FIMechE, for the provision of research facilities and the opportunity to undertake this study:

Dr. R. Davidson, BSc, PhD, MRINA, and Dr. J. Brown, BSc, PhD, FIMechE, FInstR, for their assistance and encouragement:

Also I should like to thank Dr. D. McP. Sloan, MSc, PhD, FIMA, and Dr. R.F. McLean, MSc, PhD, ARCST, MIMechE, for their mathematical guidance:

Mr. C. Richardson and the technicians of the Department of Dynamics and Control for their help in the manufacture and assembly of the experimental apparatus:

Finally, to Ann for her excellent typing of this manuscript.